



**HAL**  
open science

# Les propriétés adhésives et rhéologie interfaciale de mortiers colles

Alessandra Fujii Yamagata

► **To cite this version:**

Alessandra Fujii Yamagata. Les propriétés adhésives et rhéologie interfaciale de mortiers colles. Génie civil. Université Paris Saclay (COMUE), 2018. Français. NNT : 2018SACLN035 . tel-01990594

**HAL Id: tel-01990594**

**<https://theses.hal.science/tel-01990594v1>**

Submitted on 23 Jan 2019

**HAL** is a multi-disciplinary open access archive for the deposit and dissemination of scientific research documents, whether they are published or not. The documents may come from teaching and research institutions in France or abroad, or from public or private research centers.

L'archive ouverte pluridisciplinaire **HAL**, est destinée au dépôt et à la diffusion de documents scientifiques de niveau recherche, publiés ou non, émanant des établissements d'enseignement et de recherche français ou étrangers, des laboratoires publics ou privés.

# Adhesive properties and interfacial rheology of adhesive mortars

*Les propriétés adhésives et rhéologie interfaciale de mortiers colles*

Thèse de doctorat de l'Université Paris-Saclay  
préparée à École Normale Supérieure Paris-Saclay

École doctorale n°579 Sciences mécaniques et énergétiques  
matériaux et géosciences  
Spécialité de doctorat: Génie Civil

Thèse présentée et soutenue à Cachan, le 17 décembre 2018, par

**Alessandra Lie Fujii Yamagata**

Composition du Jury :

M. Farid Benboudjema Professeur, Université Paris-Saclay	Président
M. Arnaud Perrot Maître de Conférences, Université de Bretagne-Sud	Rapporteur
M. Lazhar Benyahia Professeur, Université du Maine	Rapporteur
Evelyne Prat Directeur R&D, ParexGroup	Examinatrice
Mohend Chaouche Directeur de Recherche CNRS, Université Paris-Saclay	Directeur de thèse
Anne Daubresse Ingénieur R&D, ParexGroup	Co-encadrante
Laurent Frouin Directeur R&D, Ecocem Materials	Invité

## Acknowledgements

During this journey I believe I could finally understand the true meaning of becoming a Doctor of Philosophy. The term Doctor of Philosophy comes from the ancient Greek, and it means “lover of wisdom”. Through these years I feel that my relationship with knowledge has achieved a whole new level. I acquired the basis of critical thinking and the ability to apply the scientific method to various things in life. I am very thankful for that.

I acknowledge ParexGroup for trusting in me for this thesis, especially Anne Daubresse, Evelyne Prat and Marco Cappellari for their support, help and advices. Their knowledge, field experience and guidance were important to make this thesis more useful for real-world applications. I also hold great respect and admiration for all the professionals at the Centre d’innovation Parexgroup. They are very kind and nice people, caring for our safety and wellbeing.

I would like to thank my supervisor, Professor Mohend Chaouche, for giving me this unique opportunity. His creativity and vision were of great inspiration. Through these years I learned many important lessons about research and science from Professor Chaouche. I also would like to thank Fábio Alonso Cardoso for being a second unofficial supervisor, guiding me through difficulties and teaching me so much. His knowledge and patience were of huge inspiration to me to still desire to continue in the science path.

To all my colleagues and friends in LMT, I’m thankful for their friendship and help during my years in France. Living in a foreign country is much easier when you have friends to share happy moments with. These moments were important to make this process easier. I’d like to specially thank Rémy and Benjamin for their help with my thesis.

I’d like to also thank my family and Paulo, my life partner, for being a huge support in my life in all moments that I needed them. None of this have been possible without their love and support.

I’m also very thankful to my former supervisors at the University of Sao Paulo, Raphael Giuliano Pileggi and Roberto Cesar de Oliveira Romano, for introducing me to the world of research. Their passion will always be a great inspiration for me.

I like to think of Research as being a big project, which consists of expanding the frontiers of knowledge and human development. My thesis is perhaps one tiny grain of sand among many other grains at a seashore. All these tiny particles are important and necessary to expand our land into the ocean of knowledge. Therefore, I would like to thank the world research



community for contributing and being part of this. I feel truly honored to be part of this big project, even as a tiny grain of sand.

Finally, but not least, I'd like to thank God for all wonderful people and things he has brought to my life. I feel blessed for all opportunities I have gotten during my entire life.





# Contents

Chapter 1	– Context and objective.....	1
1.1	Context and relevance.....	1
1.2	Objective.....	2
1.3	Thesis structure.....	2
Chapter 2	– State of art review: Adhesive mortars, Cement hydration, mortar additives, skin formation and adhesion .....	5
2.1	Introduction.....	5
2.1.1	Adhesive mortars.....	5
2.2	Cement hydration.....	9
2.2.1	Portland cement.....	9
2.3	Mortars additives .....	13
2.3.1	General types of additives .....	13
2.3.2	Cellulose ether (CE) .....	14
2.3.3	Other polysaccharides admixtures: guar ether and starch ether .....	25
2.3.4	Latex.....	28
2.4	Skin formation .....	34
2.4.1	Skin formation mechanism.....	35
2.4.2	Polymer migration in adhesive mortars.....	36
2.4.3	Effect of skin formation on contact generation between mortar and tile .....	38
2.4.4	Skin rheological properties.....	39
2.5	Adhesion.....	41
2.5.1	Adhesion, cohesion and related forces .....	42
2.5.2	Capillary forces and surface tension .....	43
2.5.3	Brownian motion.....	44



2.5.4	Van der Waals forces .....	44
2.5.5	Particles agglomeration and surface charges.....	45
Chapter 3	– Bulk rheological properties of adhesive mortar with different cellulose ether contents	47
3.1	Introduction.....	47
3.2	Literature review.....	47
3.2.1	Rheology fundamentals, concepts of viscosity and yield stress.....	47
3.2.2	Measurement techniques .....	53
3.3	Experiments .....	74
3.3.1	Materials and formulations.....	74
3.3.2	Methods .....	77
3.4	Results and discussion of Chapter 3 .....	79
3.4.1	Bulk oscillatory properties .....	79
3.4.2	Effect of CE types .....	82
3.4.3	Flow rheological properties of mortars with different CE content .....	84
3.4.4	Squeeze flow of adhesive mortar with different cellulose ether (CE) content...	87
3.4.5	Tack test .....	90
3.5	Chapter conclusions.....	95
Chapter 4	– Skin formation evaluation .....	97
4.1	Introduction.....	97
4.2	Literature Review .....	98
4.2.1	Interfacial rheology .....	98
4.2.2	Magnetic Resonance Imaging (MRI).....	100
4.3	Experimental.....	102
4.3.1	Materials.....	102
4.3.2	Formulations.....	102
4.3.3	Methods.....	103



4.4	Results.....	105
4.4.1	MRI .....	105
4.4.2	Interfacial Rheology of skin .....	108
4.4.3	Effect of CE type.....	112
4.4.4	Wind effect for gray cement.....	113
4.5	Chapter conclusions.....	114
Chapter 5	– Microstructural evaluation with micro-tomography and adhesive stress.....	117
5.1	Chapter Introduction.....	117
5.2	Literature review.....	118
5.2.1	Fundamentals of tomography.....	118
5.2.2	Influence factors of micro-tomography.....	119
5.2.3	Micro-tomography applied in cementitious materials.....	121
5.3	Experimental.....	124
5.3.1	Materials.....	124
5.3.2	Methods.....	124
5.4	Results.....	127
5.4.1	CE content effect on adhesive stress .....	127
5.4.2	Concrete substrate-mortar-tile system micro-tomographic characterization ...	128
5.4.3	Ribs and flat application effect on a tile-mortar-substrate system at constant force	130
5.4.4	Pores distribution of mortar on a tile-mortar-tile system at constant gap .....	130
5.5	Chapter conclusions.....	135
Chapter 6	– Evaluation of mortar-substrate contact generation with optical microscopy	137
6.1	Introduction.....	137
6.2	State of art.....	137
6.2.1	Contact visualization .....	137
6.3	Experimental.....	139



6.3.1	Materials and formulations.....	139
6.3.2	Microscopical visualization method.....	140
6.3.3	Determination of wetting capability/transfer .....	141
6.4	Results and discussion of Optical microscopy .....	141
6.4.1	CE content effect on adhesive mortars contact generation .....	141
6.4.2	Impact of CE degree of substitution on contact generation .....	148
6.4.3	Transfer – effect of CE content .....	155
6.4.4	Transfer – effect of CE DS.....	158
6.5	Chapter conclusions.....	161
Chapter 7	– Final contributions.....	163
7.1	Conclusion and perspectives.....	163
Bibliography.....		165



## List of figures

Figure 1. Examples of use of adhesive mortar system (left to right): bathroom, swimming pool, facade.....	6
Figure 2. Simplest adhesive mortar system: Substrate-adhesive mortar-tile. ....	6
Figure 3. Flow diagram of the dry process for portland cement manufacture [7]. ....	10
Figure 4. Mechanism of air entrainment when an anionic surfactant with a nonpolar hydrocarbon.....	13
Figure 5. Cellulose [16].....	16
Figure 6. Production of MHEC [15]. ....	17
Figure 7. Structure of cellulose ethers: (a) HPMC, (b) MHEC, (c) HEC.[20].....	18
Figure 8. Representative architectures for polymers which undergo intermolecular association in aqueous solution [21]. ....	19
Figure 9. Representative chemical structures for polymers which undergo intermolecular association in aqueous solution. Note that for several of the structures (e.g. the polysaccharide) only part of the structure suggesting the attachment sites of the hydrophobes is indicated [21]. .....	20
Figure 10. Apparent Viscosity vs. Shear Rate, 2% aqueous solutions of an MHEC of different nominal viscosities [12].....	21
Figure 11. Apparent Viscosity vs. Shear Rate, for Aqueous Solutions of 4,000 mPa.s CE at different concentrations .....	22
Figure 12. Temperature-dependent viscosity and gelation of methylcellulose [15]. ....	23
Figure 13. Molecular structure of Guar gum [37]. ....	26
Figure 14. Molecular structure of HydroxyPropyl Guar [35]. ....	26
Figure 15. Amylose and amylopectin chemical structure [39]. ....	27
Figure 16. Representation of the successive stages in film formation as an aqueous dispersion of polymeric microspheres dries above the minimum film forming temperature (MFFT) [45]. .....	29
Figure 17. RPP production simplified model [52]. ....	31
Figure 18. Simplified model of formation of Polymer-cement cc-matrix [56].....	33
Figure 19. Simplified model of process of polymer film formation on cement hydrates [56].	34



Figure 20. Scheme for illustrating skinning mechanism. Abbreviations: $E$ - evaporation rate; $F$ - flow rate of mortar water [2].	36
Figure 21. Concentration profile of VC latex in the cement–polymer matrix sampled across the mortar bed on an xy section [1].	36
Figure 22. Concentration variations of CE and PVA in the cement–polymer matrix as a function of the distance from the substrate surface (along y axis in Fig. 2). (a, b) VC-modified mortar. (c, d) SA-modified mortar [1].	37
Figure 23. Schematic synthesis of the mortar evolution. The nonlinear horizontal time axis highlights the major stages of the mortar evolution [1].	38
Figure 24. (a–c) Deformation of fresh mortar including skin at the surface during tile	39
Figure 25. Dynamic in-situ micro-rheology with a Krüss tensiometer K-100 MK2 a cylindrical probe with a diameter of 2 mm is pushed with 1.2 mm/min from the mortar surface to a depth of 2.1 mm [2].	40
Figure 26. Micro-rheological intrusion-force diagram of an adhesive mortar for different open times (0-60 min) [59].	40
Figure 27. Plate/plate rheological response of a CE based mortar at 20min(a) and at 30min(b), Yield evaluation on shear stress response [19].	41
Figure 28. Definition of various energy terms associated with the adhesion of solid surfaces and the surface area changes of liquids. Note that $W$ and $g$ are idealized thermodynamic quantities, assuming reversibility and smooth surfaces. In practice, only with liquids can the area be changed gradually and reversibly, as in (c). For solids, their adhesion, cohesion, and debonding processes, as in (a) or (b), usually involve plastic deformations with the dissipation of irreversible energy as heat. Note the positive sign of $W$ (i.e., $W > 0$ ) for the work of adhesion/cohesion where, by convention, the reference state (of zero energy) is the contact state ( $D=0$ ), compared to the negative values for $W(D)$ and $w(r)$ where, again by convention, the reference states are at $D=\infty$ , $r=\infty$ [65].	43
Figure 29. Newton model for viscosity definition two parallel sheets (or planes) of area “A”, separated by a infinitesimal distance “dx”, moving in the same direction with different velocities “ $V_1$ ” and “ $V_2$ ”. The difference between the sheets is kept by the application of an external force “F” in one of the sheets.	48
Figure 30. Newtonian fluid behavior	49
Figure 31. Basic fluids behaviors	50
Figure 32. shear-thinning or pseudoplastic behavior	51
Figure 33. dilatant or shear thickening rheological behavior	52



Figure 34. Schematic diagram of a stress controlled (a) and a strain controlled (b) rheometer [93].	54
Figure 35. Possible shapes of hysteresis loops [90].	56
Figure 36. Imposed stress or deformation in red and deformation or stress response in blue.	57
Figure 37. Evolution of elastic moduli $G'$ and $G''$ of the viscous cement paste [102].	59
Figure 38. The storage modulus $G'$ and the loss modulus $G''$ as functions of the strain amplitude ( $\gamma_0$ ) for an aqueous solution (1.25 wt%) at $\omega = 10 \text{ rad} \cdot \text{s}^{-1}$ and the corresponding stress response in SAOS and LAOS [104].	60
Figure 39. Amplitude test – strain sweep [94].	61
Figure 40. Evolution for the storage modulus $G'$ (a) and loss modulus $G''$ (b) as a function of strain amplitude for different dosage rates of CE (grade MHEC-A20000). ( $\circ$ ) 0% CE; ( $\square$ ) 0.03% CE; ( $\blacklozenge$ ) 0.06% CE; ( $\Delta$ ) 0.09% CE; and ( $\nabla$ ) 0.12% CE [9].	62
Figure 41. Shear moduli vs. frequency sweep ( $w/c=0.5$ , $T=25^\circ\text{C}$ ) [119].	63
Figure 42. Geometries used for rotational rheometry: (a) Cup and Bob; (b) Cone and Plate; (c) Parallel Plates.	64
Figure 43. Haake viscometer SV geometries: vane with six-bladed (left), serrated cylinder (middle) and smooth cylinders (Right) [123].	65
Figure 44. Typical load vs. displacement curve of a displacement-controlled squeeze flow test, illustrating the three main stages of the material's behavior. Stage I: small strain — elastic deformation; Stage II: moderate strain — plastic deformation or viscous flow; and Stage III: large strain — strain hardening [138].	67
Figure 45. Scheme of initial and final test conditions of squeeze flow in a constant area configuration. $D$ = upper plate diameter; $h_0$ = sample initial height; $h$ = sample final height, which depends on the plate displacement [133].	68
Figure 46. Constant volume configuration. Example of flow lines for the interface slip conditions – no slip (infinite friction) and free slip (no friction) [133].	69
Figure 47. Failure modes on tack test: (a) Cohesive rupture and (b) Adhesive rupture	72
Figure 48. Cartoon illustrating schematically three different failure modes [147].	72
Figure 49. Analysis of the tack test results. (a) General shape of the tack force curves; (b) evolution of the force peak versus stretching velocity [127].	73
Figure 50 . Graphical representation of failure energy.	74
Figure 51. Granulometric distribution of sand used in this investigation obtained from the manufacturer.	75



Figure 52. Rotational and oscillatory rheometry vane geometry and cup system dimensions used in this investigation. ....	77
Figure 53. Illustration of adhesive mortar sample preparation: the metallic comb turns around axis to form the cylindric shape of the sample.....	78
Figure 54. Scheme of squeeze flow and tack test montage – the geometry press.....	79
Figure 55. Simplified normal force/load vs time curve of a squeeze test, relaxation and tack test .....	79
Figure 56. Storage modulus ( $G'$ ) and Loss modulus ( $G''$ ) of adhesive mortars with different CE content formulated with white cement (a) and gray cement (b).....	81
Figure 57. Storage modulus of adhesive mortar with different cellulose content formulated with gray cement. ....	82
Figure 58. Storage modulus ( $G'$ ) and Loss modulus ( $G''$ ) of adhesive mortars with different CE types formulated with white cement (a) and gray cement (b).....	83
Figure 59. Flow curve cycle of acceleration ( $\blacktriangleright$ ) and deceleration ( $\blacktriangleleft$ ) of adhesive mortars formulated with gray cement and different CE content and table with thixotropy values.....	84
Figure 60. Parameters obtained from the Herschel-Bulkley model application on deceleration of flow cycle of formulations with different CE content: (a) Yield Stress; (b) Consistency and; (c) Flow index .....	87
Figure 61. Squeeze flow graphs of adhesive mortars with different CE content (0.1%, 0.25% and 0.4%) at different open times: (a) 0 min; (b) 10 min; (c) 20 min; (d) 30 min; (e) 40 min; (f) 50 min; (g) 60 min.....	88
Figure 62. Final normal force of squeeze flow test of adhesive mortar with different open time .....	90
Figure 63. Peak force of tack test of g_0.1% CE-A adhesive mortar with different open time .....	91
Figure 64. Peak force of tack test of g_0.25% CE-A adhesive mortar with different open time .....	92
Figure 65. Peak force of tack test of g_0.4% CE-A adhesive mortar with different open time .....	92
Figure 66. Failure energy of the tack tests of the formulations with different CE content measured at different open times, calculated by the integral of normal force vs gap curve. ...	93
Figure 67. Peak force of tack test of adhesive mortar formulation with gray cement and different CE content at 0, 10, 20, 30, 40, 50 and 60 min of open time. ....	93





Figure 68. samples after squeeze and tack test of adhesive mortars with gray cement and different CE content .....	95
Figure 69. Scheme of Langmuir trough [159].....	99
Figure 70. Interfacial rheometry apparatus – Bicone and Nöuy Ring.....	99
Figure 71. Moisture profile of unsealed mortar samples a) 0 wt.% MHEC, b) 0.4 wt.% MHEC, c) 1.3 wt.% MHEC and d) 2.1 wt.% MHEC. All the profiles have been plotted every 24 min [165]. .....	102
Figure 72. MRI samples scheme: (a) 2D MRI – sample dimensions and section cut of signal visualization; (b) 1D MRI – sample dimensions and representation of signal distribution obtained .....	104
Figure 73. Scheme of the rheological measurements of the adhesive mortars using a vane geometry: (a) bulk measurements were done at 84.5 mm depth; (b) interfacial measurements were done at 3 mm depth with the mortar exposed to air at the interface.....	105
Figure 74. Scheme of interfacial rheology test in windy environmental condition. ....	105
Figure 75. 2D MRI Result - 1 <sup>st</sup> echo signal mitigation of water signal of an adhesive mortar sample (w_0.25% CE-A) exposed to air on the top: (a) water vanishing after 30 min; (b) water vanishing after 1 h; (c) water vanishing after 2 h.....	106
Figure 76. 1D MRI Result – 1 <sup>st</sup> echo map signal vs time of adhesive mortar samples exposed to air on the top: (a) W_0.1% CE-A; (b) W_0.25% CE-A; (c) W_0.4% CE-A.....	107
Figure 77. (a) Bulk measurements ( $G'_{bulk}$ ) and 3mm measurements ( $G'_{3mm}$ ) of adhesive mortars with different CE content formulated with white cement (b) $G'_{interface}$ calculated by the different of the $G'_{3mm}$ and $G'_{bulk}$ (c) $G'_{interface}$ vs water loss of adhesive mortars with different CE content formulated with white cement. ....	109
Figure 78. (a) $G'_{interface}$ of adhesive mortars with different CE content formulated with gray cement and curves of water loss over time of each formulation (b) $G'_{interface}$ vs water loss of adhesive mortars with different CE content formulated with gray cement.....	111
Figure 79. $G'_{interface}/$ Water loss vs CE content at $t = 2$ hours of formulations with grey and white cement. ....	112
Figure 80. $G'_{interface}$ of adhesive mortars with different CE types formulated with white cement (a) and gray cement (b). Each color represents a type; continuous and dashed lines are test repetitions. Water loss over time of the same formulations is represented by dotted curves. ....	113
Figure 81. Interfacial storage modulus of adhesive mortars with different CE content in windy conditions (continuous line) and the reference without wind (dashed lines).....	114



Figure 82. Illustration of the principle of a 3D acquisition by X-ray tomography from a series of 2D radiographs obtained by a sample in a fixed axis [Source: Phoenix X-ray].	118
Figure 83. Achievable resolution vs. measuring range [174,177].	119
Figure 84. A mortar sample reconstructed slice image (a), and a sectioned 3D rendering (b). In these images, the brightness is a function of X-ray absorption, with bright spots showing regions of high absorption, and dark spots showing regions of low absorption [178].	122
Figure 85. Tomographic sections of a reconstruction volume of an ETICS at different states of deformation; in the left, the XY sections; and in the right, the XZ sections at the fissuration [176].	123
Figure 86. Section of a mortar sample at different evolution times [172].	124
Figure 87. X-ray micro-tomographer available at ENS-Cahan (left); x-ray tube micro-oven of 225kV and detector of 3072x3888 pixels at high resolution (right). Adapted from [176].	125
Figure 88. Sample example: concrete substrate on bottom, mortar with ribs and ceramic tile on top.	126
Figure 89. Cross and longitudinal sections of a ceramic-mortar-tile sample	126
Figure 90. Cross and longitudinal sections of a tile-mortar-tile sample	126
Figure 91. Exemplification of the zones of the sample: (a) upper, (b) middle), and (c) bottom.	127
Figure 92. Graph of adhesive stress of mortar formulations with different CE content (a – adhesive; c – cohesive).	128
Figure 93. Longitudinal section of mortar-tile contact: (a) g_0.1% CE-A; (b) g_0.25% CE-A; and (c) g_0.4% CE-A.	129
Figure 94. Longitudinal section of mortar-tile contact for formulations with (a) 0% and (b) 5% Latex.	130
Figure 95. Longitudinal section of mortar-tile contact applied with a flat spatula and toothed comb (same scale)	130
Figure 96. Gray level distribution of formulations with different CE content	132
Figure 97. Gray level distribution of formulations with different Latex content	133
Figure 98. Sample of g_0.4% CE-A (rib) formulation mortar.	134
Figure 99. Mortar and tile interfaces of g_0.4% CE-A (rib) formulation: (a) Upper and (b) bottom.	134
Figure 100. Contact between upper tile and mortar g_0.4% CE-A with different application methods: (a) comb and (b) flat spatula	135
Figure 101. Velocity field for squeeze flows with no slip [128].	135



Figure 102. Experimental setup with two options for sample illumination. If the glass plate is illuminated directly from above (lamp “T” is on and lamp “S” is off), it can be observed how well the mortar ribs are deformed underneath the glass plate [180] .....	138
Figure 103. (a) Photograph of 10x10 cm glass plate embedded 30 min after the mortar (formulation F-ref in Table 1) was combed. Sample produced according to EN 1347. Mortar ribs are pressed to a degree of 96 area% (measured within the marked area). (b) Same sample illuminated from the side as described by Zurbriggen et al. [180]. Skin appears dark. Bright wetting area measures 33% (measured within the marked area). .....	138
Figure 104. Contact generated [59]. .....	139
Figure 105. no-slip squeeze of a isothermal material for different compression ratio (C.R.) of a material with power-law index equal 0.3 [181] .....	139
Figure 106. Digital microscope VHX (Right) and scheme of image obtained (Left).....	140
Figure 107. Sample mapping for image acquisition.....	141
Figure 108. Samples of adhesive mortars with different CE content for contact visualization with optical microscopy .....	142
Figure 109. Microscopy images of contact .....	143
Figure 110. g_0.1% CE-A contact visualization at different open times, at the rib and between ribs.....	145
Figure 111. g_0.25% CE-A contact visualization at different open times, at the rib and between ribs.....	146
Figure 112. g_0.4% CE-A contact visualization at different open times, at the rib and between ribs.....	147
Figure 113. Samples of microscopical visualization of adhesive mortar with different CE content at different open time.....	148
Figure 114. Contact evolution of adhesive mortar g_0.25% CE-A at rib and between ribs for different open times.....	150
Figure 115. Contact evolution of adhesive mortar g_0.25% CE-B at rib and between ribs for different open times.....	151
Figure 116. Contact evolution of adhesive mortar g_0.25% CE-C at rib and between ribs for different open times.....	152
Figure 117. Contact evolution of adhesive mortar g_0.25% CE-D at rib and between ribs for different open times.....	154
Figure 118. Failure modes of transfer tests .....	155



Figure 119. Transfer of g\_0.1% CE-A and g\_0.25% CE-A adhesive mortar formulations for different open time ..... 157

Figure 120. Transfer of g\_0.4% CE-A adhesive mortar formulation for different open time 158

Figure 121. Transfer of g\_0.25% CE-A and g\_0.25% CE-B adhesive mortar formulations for different open time ..... 160

Figure 122. Transfer of g\_0.25% CE-C and g\_0.25% CE-D adhesive mortar formulations for different open time ..... 161



## List of Tables

Table 1. Main families and characteristics .....	6
Table 2. Classification and designation of industrial adhesive mortar [4] .....	7
Table 3. Oxides abbreviations .....	10
Table 4. Compounds abbreviations .....	11
Table 5. Phase compositions, density and blaine fineness of the investigated cements .....	74
Table 6. Formulations of adhesive mortars with gray cement, with different cellulose ether content and types (wt%) .....	76
Table 7. Properties of the cellulose ethers used in this investigation, as provided by the manufacturer: Viscosity (mPa.s), molar substitution (MS) and degree .....	76
Table 8. Measured peak force at 0 min open time and calculated peak force and maximum delta pressure.....	94
Table 9. Formulations of adhesive mortars with white and gray cement, with different cellulose ether content and types (wt%) .....	103
Table 10. Formulations of adhesive mortars with different cellulose ether content and types (wt%).....	140





## Chapter 1 – Context and objective

### 1.1 Context and relevance

Cement is the most used industrial product in volume in the world. Modern life and cities are based on cementitious foundations. The reason why cement became such an important material is that it can be easily shaped when mixed with water, and through chemical reactions with water—called hydration—cement obtains outstanding mechanical properties and durability. From this important material, different sub-products are produced, such as: concrete; grouts; and mortars (adhesive mortar, finishing mortar, bricklaying mortar, etc.). These are then used to build a great majority of our construction: dams, highways, bridges, buildings, houses, etc. All these “major systems” are made of smaller sub-systems in civil engineering, such as: foundation; structure; electric, water and sewer systems; coatings; etc. Each of them takes advantage of cementitious materials according to their requirements.

Adhesive mortar is used to glue a variety of types of materials to different surfaces; thus, this type of mortar is used either for residential and non-residential construction, for fixation of different types of tiles. Adhesive mortar is used in facades, floors, walls, swimming pools, etc. The Tile Adhesive Market will cross USD 4.5 billion by 2022, according to Tile Adhesives Market Research Report. Thus, due to its importance in system and volume, the industry has been developing to create more reliable and durable systems. Less than 50 years ago, the use of industrial pre-mixed mortars was a turning point in construction material technology, since it enabled the production of highly technological powder mixes with the use of additives, with predictable mechanical properties and more reliable application and durability.

The additives considerably improved rheological properties, mechanical uses and the productivity of adhesive mortars, and they also corrected basic formulation issues. There are many different types of additives, such as: air-entraining admixture, thickening admixture, accelerators, retarders, plasticizers, etc. In adhesive mortars, two of the main additives that started being used are cellulose ether and redispersible polymer powder (latex in redispersible form). Both additives can improve some essential characteristics of the tile adhesives.

Cellulose ether (CE) is used for thickening and water retention. This is important to create the adhesive mortar “stick” property and maintain water for cement hydration by avoiding water loss to the substrates and air. Latex is used to improve adhesion and flexibility of mortars, which is often required due to flexion stresses in hardened state resulting from differential expansion of substrate and tiles. Cellulose ether, latex and all additives action over the properties may be



complex and generate undesired side effects. Thus, as the mortars technology advances, the demand for research to understand how different additives work and how to improve them is growing.

The use of additives can bring improvements to tile adhesive performance, but frequently, its use is based on final performance tests and applicator feeling, and when some complex problems occur, its understanding demands further comprehension of how the additives work inside the system and in a synergic with the other components of the formulation. Furthermore, obtaining optimal formulations, with lower cost and higher performance is only possible with a deep understanding of the additive's mechanisms and how they influence the complex system of cementitious materials.

In the adhesive mortar context, skin formation is often an issue in real application. Research has been done concerning its matter, but this problem has still many open questions [1]. The skin is a surface layer with different properties compared to the body underneath [2] and, in adhesive mortars, it is formed due to water drying from the surface layer; it is also related to film formation and carbonation [1,3]. This dry external layer (skin) at the mortar-air interface should be avoided because it may be difficult to be deformed during tile emplacement and it can hinder the mortar's capability to wet the tile surface properly [1,2]

Not many studies focus on the rheological properties of skin, despite its major control of contact generation and ability to allow fresh material inside the rib to wet the tile. Due to its importance, different studies have tried to characterize the skin, but they fail to separate the mortars skin and the bulk properties.

## 1.2 Objective

The objective of this thesis is to characterize rheological properties of skin formation and understand its influence on adhesive properties.

## 1.3 Thesis structure

This thesis is structured with 7 Chapters, including Chapter 1, in which the context, objective and motivations of this research are presented. Chapter 2 provides an overview of adhesive mortar's current state of art with standards and regulations; as well as an overview of additives used by industry, with deeper exploration on cellulose ether and latex redispersible polymer powder.





Results and discussions are organized in four chapters, with each exploring one aspect of adhesive mortar's skin formation and adhesive properties. Chapter 3 covers bulk properties of adhesive mortars, evaluated by different test methods: oscillatory rheometry, rotational rheometry, squeeze test, and tack test. This chapter offers relevant rheological properties, which help explain further chapters' results, specially contact generation on Chapter 6.

Chapter 4 introduces the concept of interfacial rheology applied to cementitious materials, describing the development of the method and evaluating the effect of CE content type on the interfacial properties of adhesive mortars. Additionally, MRI is used to assess water distribution at the interface and characterize the skin. This chapter offers the main contributions to the scientific community.

Chapter 5 covers a microstructure evaluation of adhesive mortars depending on the polymer content (CE and RPP) and application mode. Micro-tomography is used to generate 3D and 2D visualizations of the microstructure of mortars. The goal is to verify traces of the skin in the microstructure. The technique gives some indications of contact generation and the consequences of the rheological properties of the mortars.

Chapter 6 explores contact visualization and gives a transfer evaluation of different adhesive mortars formulations, observing the effect of CE content and type. It also illustrates the process of contact generation. The use of small depth of field for contact visualization is innovative and offers valuable insights on the impact of rheological properties of the bulk and interface on contact.

Finally, Chapter 7 provides overall conclusions and suggestion for the direction of future research.





## Chapter 2 – State of art review: Adhesive mortars, Cement hydration, mortar additives, skin formation and adhesion

### 2.1 Introduction

Adhesive mortar skin formation is the main focus of this research; thus, an overview of current “state of art” is presented in this chapter. First, adhesive mortars system, requirements and techniques are presented. This overview offers an understanding of the industrial adhesive mortar requirements for serviceability.

Second, adhesive mortars main raw materials are shown and details on their mechanisms are introduced. This includes additives such as latex and cellulose ethers admixture. In this research, MHEC is studied, and therefore, we provide an overview of cellulose ether, and details about the type of cellulose ether used will be given in this chapter.

After this overview, skin formation mechanisms, wetting, polymers impact and skin rheological properties will be introduced. This literature presentation is important when the results of this study are discussed, as it provides an understanding of the different properties.

Finally, we present an overview of concepts of adhesion, cohesion, and particle interactions. These interactions have a relevant impact on rheological behavior, which is one of the main properties evaluated in this thesis.

#### 2.1.1 Adhesive mortars

##### 2.1.1.1 Adhesive mortar system

Adhesive mortars are construction materials used to glue adhesive tiles to a substrate. The tiles and substrates can be of different types and can also be applied inside and outside of a building. Inside of a building, they can be used in bathrooms, offices, kitchen and many different types of rooms either in floor and walls. Outside of the building, they can be used in façades and in terraces. For each different environment, adhesive mortar should be adapted to have a better performance.





Figure 1. Examples of use of adhesive mortar system (left to right): bathroom, swimming pool, facade.

In the simplest system, the mortar is applied to a substrate where the tiles are put. They are applied with a toothed comb, so the tiles can be more easily placed.

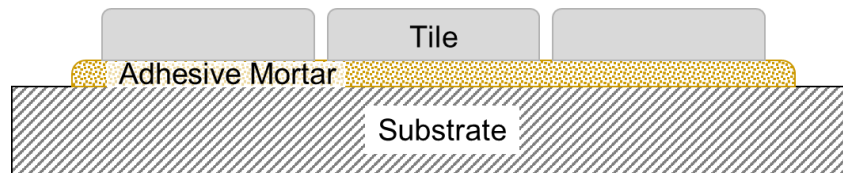


Figure 2. Simplest adhesive mortar system: Substrate-adhesive mortar-tile.

### 2.1.1.2 Dry-mix adhesive mortar types

In the past, most of the adhesive mortars were produced on site, resulting in a heterogeneous and performance-varied product. With the development of construction, the necessity of industrial products grew. In France, industrial mortars started to be used around 1979-86. This “ready-to-use” industrial product came to provide constraints of costs, quality and delays. And since then, industrial mortars have increased to a huge market that provide different types of mortars.

Organic adhesives, which are non-cement based, were also developed, due to being ready to use in practical application. Today, different types of dry-mix mortars are classified depending on their application as seen in Table 2. In the following, Table 1 summarizes the main families and characteristics of commercial adhesive mortars types.

Table 1. Main families and characteristics

Family	Binder		Characteristics
C1	Cement	Powder	Initial tensile adhesive stress $\geq 0,5 \text{ N/mm}^2$ Open time (after 20 min): tensile adhesive stress $\geq 0,5 \text{ N/mm}^2$



C2	Cement + resin	Powder (mono component) or (bi component)	Initial adhesive stress $\geq 1$ N/mm <sup>2</sup> Open time (after 20 min): tensile adhesive stress $\geq 0,5$ N/mm <sup>2</sup>
C2S1 or C2S2	Cement + resin	Powder (mono component) or powder+latex (bi component)	Initial adhesive stress $\geq 1$ N/mm <sup>2</sup> Open time (after 20 min): tensile adhesive stress $\geq 0,5$ N/mm <sup>2</sup> Deformability $\geq 2,5$ mm

Table 2. Classification and designation of industrial adhesive mortar [4]

SYMBOL		DESCRIPTION
TYPE	CLASS	
C	1	Normal setting cementitious adhesive
C	1 F	Fast setting cementitious adhesive
C	1 T	Normal setting cementitious adhesive with reduced slip
C	1 F T	Fast setting cementitious adhesive with reduced slip
C	2	Improved cementitious adhesive with additional characteristics
C	2 E	Improved cementitious adhesive with additional characteristic extended open time
C	2 F	Improved fast setting cementitious adhesive with additional characteristics
C	2 T	Improved cementitious adhesive with additional characteristics and reduced slip
C	2 T E	Improved cementitious adhesive with additional characteristics, reduced slip and extended open time
C	2 F T	Improved fast setting cementitious adhesive with additional characteristics and reduced slip
D	1	Normal dispersion adhesive
D	1 T	Normal dispersion adhesive with reduced slip
D	2	Improved dispersion adhesive with additional characteristics
D	2 T	Improved dispersion adhesive with additional characteristics and reduced slip
D	2 T E	Improved dispersion adhesive with additional characteristics, reduced slip and extended open time
R	1	Normal reaction resin adhesive
R	1 T	Normal reaction resin adhesive with reduced slip
R	2	Improved reaction resin adhesive with additional characteristics
R	2 T	Improved reaction resin adhesive with additional characteristics and reduced slip

### 2.1.1.3 Adhesive mortars serviceability requirements

With the introduction of industrial dry-mix mortars, new serviceability requirements were also introduced to ensure minimal conditions of durability, overall stability, cracking and safety. Depending on each application requirement, adapted performance is defined. Environments that demand flexibility, resistance to inclement weather and other conditions will influence these requirements. To predict the material's ability to attend its requirements, standard tests were introduced; though not perfect, they are able to ensure minimal quality of the products. DIN EN 12 004, which specifies the criteria for the C1 and C2 ratings (for cementitious adhesives), D1 and D2 ratings (for dispersion adhesives) and R1 and R2 (for reaction resin adhesives) along with extra optional parameters.



### 2.1.1.3.1 DIN EN 12 004 Performance Requirements for Adhesives:

#### **Cementitious mortars**

C1: Normal - Tensile bond strength of  $\geq 0.5 \text{ N/mm}^2$  when tested per ISO 13007 curing parameters, including water immersion, heat aging, and freeze-thaw cycling. Twenty-eight-day tensile adhesion bond strength  $\geq 0.5 \text{ N/mm}^2$  after 20 minutes open time.

C2: Improved - Tensile bond strength of  $1 \text{ N/mm}^2$  when tested per ISO 13007 curing parameters, including water immersion, heat aging, and freeze-thaw cycling. 28-day tensile adhesion bond strength  $\geq 0.5 \text{ N/mm}^2$  after 20 minutes open time.

#### **Dispersion Adhesives**

D1: Normal - Shear adhesion strength of  $\geq 1 \text{ N/mm}^2$  when tested per ISO 13007 curing parameters, including heat aging. Twenty-eight-day tensile adhesion bond strength  $\geq 0.5 \text{ N/mm}^2$  after 20 minutes open time.

D2: Improved - D1 performance plus additional shear adhesion strength of  $\geq 0.5 \text{ N/mm}^2$  after 21-day air cure and 7-day water immersion; also shear adhesion strength of  $\geq 1 \text{ N/mm}^2$  at elevated temperatures.

#### **Reaction Resin Adhesives (epoxy or polyurethane)**

R1: Normal - Shear adhesion strength of  $\geq 2 \text{ N/mm}^2$  when tested per ISO 13007 curing parameters, including water immersion. Twenty-eight-day tensile adhesion bond strength  $\geq 0.5 \text{ N/mm}^2$  after 20 minutes open time.

R2: Improved - R1 performance plus additional shear adhesion strength of  $\geq 2 \text{ N/mm}^2$  after thermal shock testing.

Other requirements are applied to optional characterizes for adhesives such as: Fast-Setting/Fast-Drying, Extended Open Time, Thixotropic, Deformability and Plywood Adhesion Bond Strength.

### 2.1.1.3.2 Wetting standard and open time standards

Two main standards related to skin formation are the EN 1347:2007 - Adhesives for tiles — Determination of wetting capability and the EN 1346:2007 - Adhesives for tiles - determination of open time.

The EN 1347 is the European standard for adhesive for tiles to determine the wetting capability of the mortar to a tile [5]. For this test, first the adhesive is applied a thin layer of adhesive



mortar on a concrete slab with a straight edge trowel. Then, a thicker layer is applied and combed with a notched trowel. The comb should be held at an angle of approximately 60° to the substrate at a right angle to one edge of the slab and drawn across the slab parallel to that edge (in a straight line). Glass plates (10 cm X 10 cm) should then be placed on the adhesive mortar immediately and, after 10 min, 20 min and 30 min, each plate is loaded with  $(50 \pm 0,5)$  N for 30 s. Care should be taken to align the adhesive ribs parallel with the edge of the glass plate, ensuring that the outer rib is flush with one edge of the glass plate. The contact surface between the combed adhesive layer and the glass plate are determined in terms of the percentage of the total area of the glass plate.

The EN 1346 is the European standard for determining the open time of adhesive mortar, evaluating the open time, by measuring the adhesive stress at 5, 20 and 30 minutes open time. For the measurements, the adhesive mortar is mixed according to EN-196-1, then it is applied with the help of a toothed comb at an angle of 45° at the standard substrate. After 5, 20 or 30 minutes of waiting time, the tiles of 5x5 cm<sup>2</sup> are then positioned on the top of the applied mortar, and 2kg of weight are put on top of each tile for 30 seconds. For each waiting time, 10 tiles should be applied. The sample is then kept for 28 days at 23°C and 50% RU. The days and the environmental conditions can be different depending on the specific type of test. After the 28 days, the traction test is done, and the pull-out force is measured for each tile, and from then that the pull-out strength is calculated.

## 2.2 Cement hydration

### 2.2.1 Portland cement

Cement is an inorganic or mineral binder, like lime and plaster. It is produced through the thermic transformation of its raw materials. For these materials, the binder properties are based on the chemical transformation of the chemical species present in the material, either by reaction with water or in the presence of water, obtaining consistency, originating products that have mechanical resistance. The reaction is favored by the high surface area, as they are provided as powders [6].

Cement is hydraulic binder, which means it reacts with water, and after hardening, it should resist even water action. The most common type, Portland cement, consists mainly of silicates and aluminates, and is obtained from Portland clinker grinding with the addition of calcium sulfate. Cement is produced from natural resources; therefore, its constituents are variable and





depend on the used raw material. The cement industrial production process is shown in Figure 3.

The calcium sulfate (gypsum or anhydrite) addition, as will be described on the clinker phases equations, is important to avoid the “flash set” phenomenon. It occurs when one of the phases of the clinker, tricalcium aluminate, in the absence of sulfate, starts to react rapidly and exothermically to form hydrogarnet. Therefore, about 5% of calcium sulfate is added to the cement to control the setting.

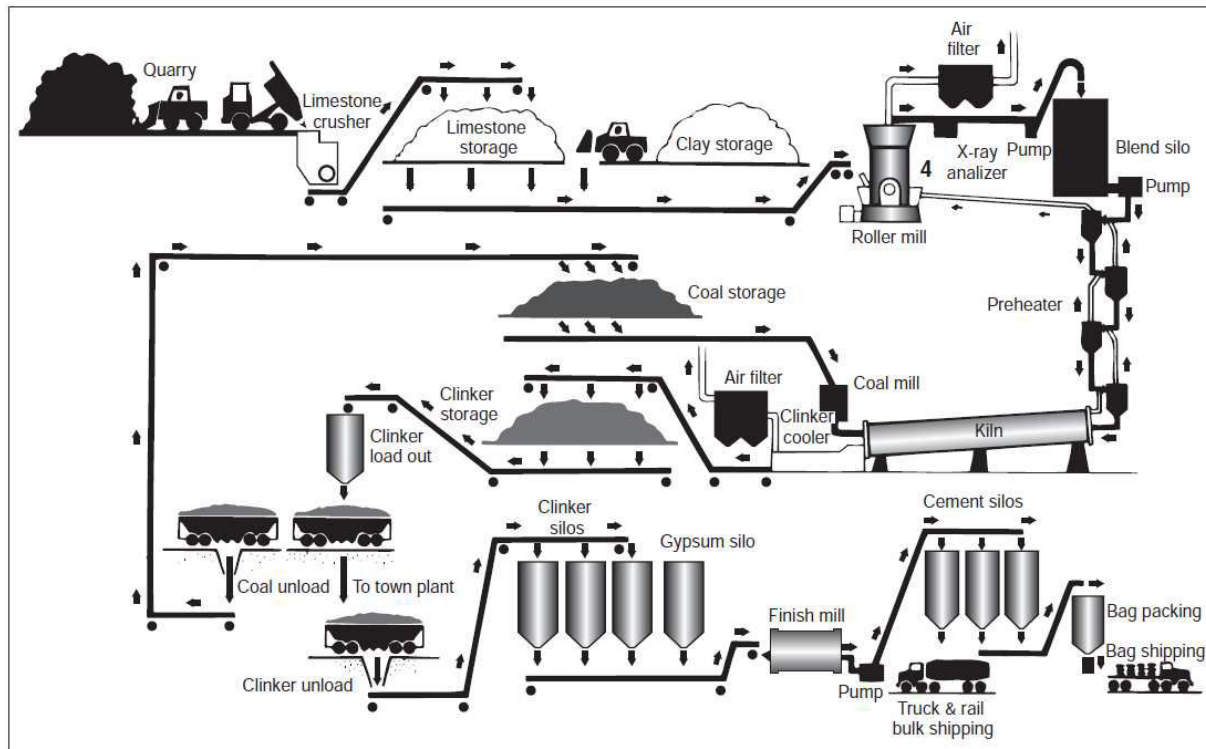


Figure 3. Flow diagram of the dry process for portland cement manufacture [7].

Portland cement phases are often expressed by their abbreviations, which consists of a formula of the abbreviations of the oxides present. In Table 3 the oxides abbreviations are shown.

Table 3. Oxides abbreviations

Oxide	Abbreviation	Oxide	Abbreviation
CaO	C	MgO	M
SiO <sub>2</sub>	S	SO <sub>3</sub>	S
Al <sub>2</sub> O <sub>3</sub>	A	H <sub>2</sub> O	H
Fe <sub>2</sub> O <sub>3</sub>	F		

From these oxide abbreviations, compound abbreviation used in construction materials domain is obtained, as shown on Table 4. The hydrate is a variable composition, so it is usually called calcium silicate hydrate (C-S-H), instead of C<sub>3</sub>S<sub>2</sub>H<sub>3</sub> or 3CaO·2SiO<sub>2</sub>·3H<sub>2</sub>O.



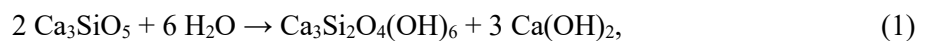


Table 4. Compounds abbreviations

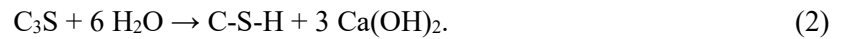
Compound	Abbreviation
$3\text{CaO}\cdot\text{SiO}_2$	$\text{C}_3\text{S}$
$2\text{CaO}\cdot\text{SiO}_2$	$\text{C}_2\text{S}$
$3\text{CaO}\cdot\text{Al}_2\text{O}_3$	$\text{C}_3\text{A}$
$4\text{CaO}\cdot\text{Al}_2\text{O}_3\cdot\text{Fe}_2\text{O}_3$	$\text{C}_4\text{AF}$
$4\text{CaO}\cdot 3\text{Al}_2\text{O}_3\cdot\text{SO}_3$	$\text{C}_4\text{A}_3\bar{\text{S}}$
$3\text{CaO}\cdot 2\text{SiO}_2\cdot 3\text{H}_2\text{O}$	$\text{C}_3\text{S}_2\text{H}_3$
$\text{CaSO}_4\cdot 2\text{H}_2\text{O}$	$\text{C}_3\bar{\text{S}}\text{H}_2$

The main portland cement clinker phases are: Alite ( $\text{C}_3\text{S}$ ), Belite ( $\text{C}_2\text{S}$ ), aluminate ( $\text{C}_3\text{A}$ ) and Alumino-Ferrite ( $\text{C}_4\text{AF}$ ). Since cement is based on natural resources, its chemical compound is a rough approximation of the actual mineral. The high temperatures prevalent during clinker formation causes the elements present in the system, including the impurities such as magnesium, sodium, potassium, and sulfur, to combine into solid solutions with each of the major compounds of the cement in the clinker. Very small amounts of impurities in solid solution may not significantly alter the crystal structure and reactivity of a compound, but larger amounts can do so [7].

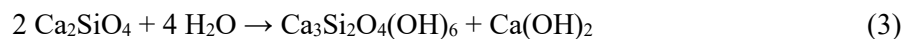
**Alite** is usually indicated as  $\text{Ca}_2\text{SiO}_4$  ( $\text{C}_3\text{S}$ ). It forms distinctly hexagonal crystals. The crystal unit cell of pure tricalcium silicate contains 27 calcium ions, 9 oxide ions and 9 orthosilicate ions. The oxide ions in its structure give its high reactivity, causing it to develop "early strength" (strength developed in mortar or concrete during the first seven days). Alite hydration is represented by the following equation:



or in its abbreviated form,

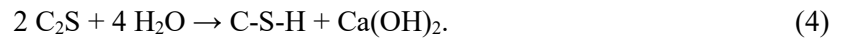


**Belite** is usually indicated as  $\text{Ca}_2\text{SiO}_4$  ( $\text{C}_2\text{S}$ ). The crystal unit cell contains 8 calcium ions and 4 orthosilicate ions. Belite's reaction with water much takes longer periods than alite, and after 28 days, only part of it is hydrated. The structure of belite in industrial cements is irregular, but the interstitial holes thus formed are much smaller, and this makes belite far less reactive than alite [7]. Belite hydration is represented by the following equation:



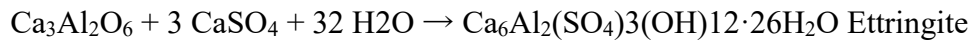
or in its abbreviated form,



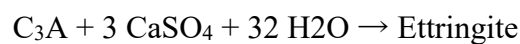


**Aluminate** or Tricalcium Aluminate, is usually indicated as  $\text{Ca}_3\text{Al}_2\text{O}_6$  ( $\text{C}_3\text{A}$ ). Aluminate has high reactivity, which decrease for high content of substitution of alkalis. It is an interstitial phase where crystals grow to fit into the available gaps between the silicate crystals.

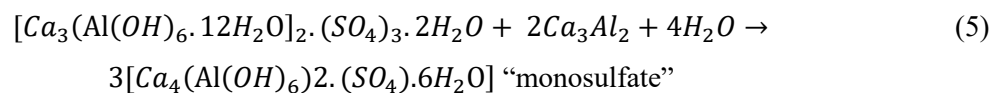
In the presence of calcium sulfate added to the cement, the Tricalcium Aluminate reacts to form ettringite:



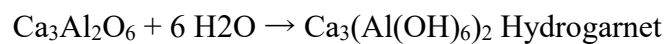
or in its abbreviated form,



The final reaction of the aluminate involves slow conversion of the ettringite into "monosulfate" (AFm):

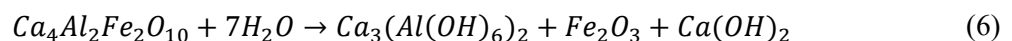


In the absence of sulfate (if calcium sulfate is not added to the clinker) the tricalcium aluminate would react rapidly and exothermically to form hydrogarnet:



Tetracalcium Alumino-Ferrite, is usually indicated as approximately  $\text{Ca}_4\text{Al}_2\text{Fe}_2\text{O}_{10}$  ( $\text{C}_4\text{Af}$ ). It is the most variable phase and can have high amounts of substitutes. Its reactivity increases as the Al/Fe is increased.

Tetracalcium Alumino-Ferrite, like tricalcium aluminate, hydrates to hydrogarnet:



As cement is produced from natural raw resources, a many other phases can be present, such as: free lime ( $\text{CaO}$ ), Periclase ( $\text{MgO}$ ), Arcanite ( $\text{K}_2\text{SO}_4$ ), Thenardite ( $\text{Na}_2\text{SO}_4$ ), Langbeinite ( $\text{K}_2\text{O} \cdot 2\text{CaO} \cdot 3\text{SO}_3$ ) and Apthitalite ( $3\text{K}_2\text{O} \cdot \text{Na}_2\text{O} \cdot \text{SO}_3$ ).

Different resources besides limestone can also be used to produce cement, such as slag furnace, fly ash, slag, etc. These other raw materials are used as cement additions to produce other types of cements (i.e. CP-II-F, CP-II-E, CP-III). In this research, the simplest type is used, CP-I, based on clinker and calcium sulfate (<5%). Two different CP-I's are used though, with different phases composition. The main reason for its different types of use is the iron content,



which affects some tests, such as MRI used in this research. Cements with higher iron content, however, are more common, which is why it is still used in this research.

## 2.3 Mortars additives

### 2.3.1 General types of additives

A variety of additives exist to improve mortars to obtain desirable properties. Depending on the application, where specific behavior is desirable, different additives, mineral or organic can be used. Some additives can have multiple functions, affecting different properties of materials.

**Air entraining:** this type of additive is also based on surfactants, but the orientation of the molecules determines if the effect is of plasticization or air entraining. At the air-water interface the polar groups are oriented toward the water phase lowering the surface tension, promoting bubble formation, and counteracting the tendency for the dispersed bubbles to coalesce. As illustrated on Figure 4, at the solid-water interface where directive forces exist in the cement surface, the polar groups become bound to the solid with the nonpolar groups oriented toward the water, making the cement surface hydrophobic so that air can displace water and remain attached to the solid particles as bubbles [7,8]. These effects are important when cellulose ether admixtures are discussed, since they also have an impact on bubble stabilization as associative polymers.

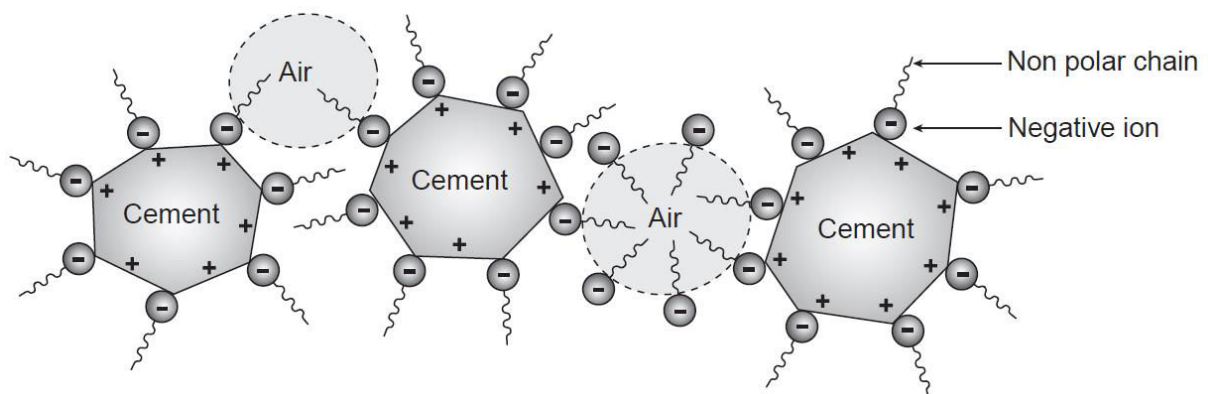


Figure 4. Mechanism of air entrainment when an anionic surfactant with a nonpolar hydrocarbon chain is added to the cement paste [7].

**Thickener:** Viscosity enhancers include mineral and polymeric additives. Mineral additives including, plaster, clay (as kaolin), etc. usually have high surface area and small particle size, which increase particle agglomerations and, consequently, viscosity. Polymeric additives include guar ether, starch ether and cellulose ethers.

This property is desirable for adhesive mortars, which requires high cohesiveness to hold tiles to the wall. Further details of cellulose ether mechanism and impact on cementitious materials are explored in the following sections.

**Superplasticizer:** This type of additive is used to avoid particle agglomeration and then flowability. It is usually based on surfactants molecules that adsorb on particle's surface, which generate either a physical, chemical or both types of barrier to the particles contact and interaction. This type of additive is widely known for enabling mix-design of self-compacting concretes. Also, high performance concretes, where particles packing need to be maximized, superplasticizers enable reducing entrained air, and by reducing grain friction, allow to obtain a concrete with lower liquid/solids ratio.

**Accelerating admixtures:** This group of accelerators consists of chemicals, which principally influence the rate of hydration of the alite phase of Portland cement, resulting in an increase in heat evolution and C-S-H gel formation at an early age. Calorimetry can be used to demonstrate the effect of accelerators on the general hydration of Portland cement. Most are soluble salts of alkali and alkaline earth metals in which both the anion and cation contribute to the overall effect of the admixture [8].

**Retarding admixtures:** Similar to accelerating admixtures, retarding admixtures are used to control cementitious materials setting. This type of admixture impedes the dissolution of the cement cations or anions, preferably that anion, which has the highest dissolving rate during the early hydration period (such as the aluminate) [7].

### 2.3.2 Cellulose ether (CE)

Cellulose ether has a close relation with skin formation and bibliographical review is important for comprehension of the present results in this thesis. An overview CE's chemical properties as well as the state of art of its studies on cementitious materials is presented. Also, a smaller introduction of guar ether and starch ether is presented.

#### 2.3.2.1 CE chemical structure

CEs are water-soluble polymers with high molecular weight derived from cellulose (consisting of a long chain of repeating anhydroglucose units) through replacement of a certain fraction of the hydroxyl groups by hydroxy-alkyl groups to form various CEs: HydroxyPropyl Cellulose



(HPC), HydroxyPropyl Methyl Cellulose (HPMC/MHPC), Hydroxyl Ethyl Methyl Cellulose (HEMC/MHEC), etc. Fundamentally, the substitution process allows for transforming the water-insoluble cellulose into a water-soluble polymer, which can then be easily dispersed in various industrial products that comprise an aqueous phase [9,10].

The number of substituent groups on the anhydroglucose units of cellulose can be designated by weight percent or by the average number of substituent groups attached to the ring, a concept known to cellulose chemists as "**degree of substitution**" (DS). The number of substituent groups on the ring determines the CE properties, such as water solubility. Too low DS may generate a CE with lower water solubility, leading to additives that are only soluble in caustic solutions. Too high DS may produce additives that are soluble only in organic solvents. The degree of substitution may vary up to 3.0 since there are three available positions on each anhydroglucose unit. The kind of substitution also has an effect on the physical properties of the cellulose material [11]. The **Molar substitution** (MS) reports the number of moles of hydroxypropyl groups per mole of anhydroglucose [12].

Another parameter that characterizes CE is the "**degree of polymerization**" (DP), which is the number of monomer units in a macromolecule, polymer or oligomer molecule [13]. This number will define the length of the polymer as well as the molecular weight of the polymer. This parameter is used also to adjust the desired viscosity when solubilized; the Mark-Houwink-Sakurada equation gives the relation between intrinsic viscosity ( $\eta$ ) and molecular weight (M) [14]:

$$[\eta] = K \cdot M^\alpha, \quad (7)$$

where  $\alpha$  and K are Mark–Houwink parameters depending on the solvent, polymer and the environmental conditions.

### 2.3.2.2 Synthesis of CE

The manufacturing process of Cellulose ether (CE) undergoes different steps, summarized in Figure 6 for MHEC. Cellulose is a polyvalent alcohol and is used as the raw material, the hydroxyl groups of cellulose, however, form inter- and intramolecular hydrogen bonds, which prevent direct etherification. Thus, the cellulose goes through a process of alkalization to dissolve the H-bridges, producing the "Alkali cellulose" [15]. In Figure 5, cellulose's chemical structure is shown.



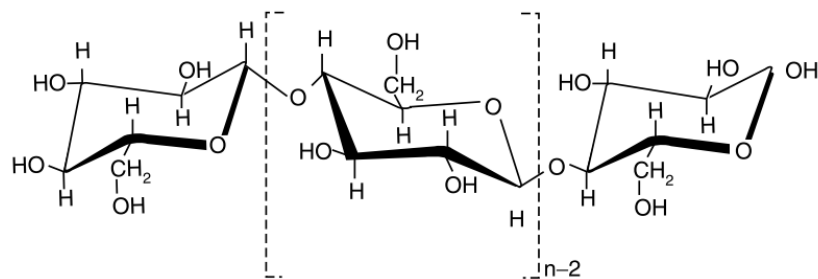


Figure 5. Cellulose [16].

In the preparation of the alkali cellulose, caustic soda (NaOH) is usually used, typically at 18-50% concentration to penetrate between the associated cellulose chains, then break the hydrogen bond between the adjacent OH groups, and thus loosen the rigid structure. This produces an expansion of the lattice structure of the cellulose [15]. Treating the cellulose with caustic alkaline solution disrupts hydrogen bonding between and within the polymeric strands, making the majority of the hydroxyl groups available for modification, with the C2 and C6 hydroxyl sites typically more reactive than a C3 site [17].

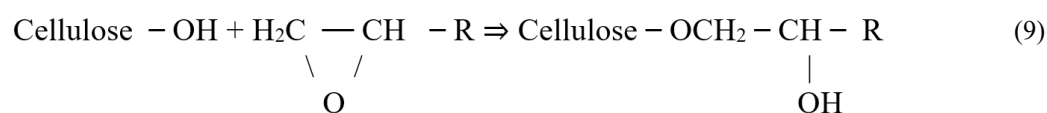
Depending if high viscosities are desired or if the pulp has low degree of polymerization, the Alkali Cellulose can be submitted to a maturation process. This process is a controlled alkaline oxidation.

The main industrial synthesis processes of CE are the Alkylation (Williamson ether synthesis) and base-catalysed oxyalkylation. In the Williamson ether synthesis, a nucleophilic alkoxide ion reacts with an alkyl halide to give an ether and a salt [16]. For the addition of epoxides to the OH groups of cellulose, the cellulose has to be 'opened' also with alkalis, through base-catalysed oxyalkylation process [15].

(a) Williamson ether synthesis:



(b) Base-catalysed oxyalkylation:



Depending on the type of cellulose ether, one or the other, or the combination of both are generally used. MHEC used in this research synthesis is carried out through a reaction with methyl chloride and then a reaction with ethylene oxide [18].

After the synthesis, the product is then purified, where undesired products that are formed during the process are removed. These substances can be alcohols, alcoholates, or alkoxides, or other ethers, depending on the type of ether process. This purification varied according to the type of ether and the manufactures, usually consisting in a type of wash. After cleaning, the still



moist products are dried and brought to the desired particle size, using appropriate methods (grinding, screening, sifting) [15,16].

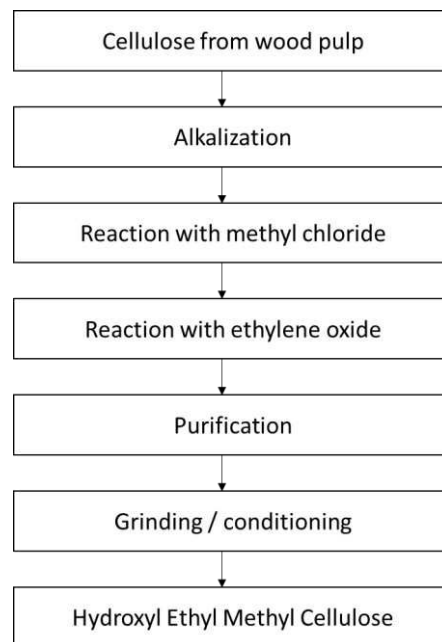


Figure 6. Production of MHEC [15].

### 2.3.2.3 Types of CE

The commercial relevance of additives in various industries led to the development different types of cellulose ethers polymers and multifunctional additives. Advances on this type of polymer are currently occurring, with introduction of new modified versions every year. The most commonly used cellulose ethers in cementitious materials today are: methyl cellulose (MC), HydroxyPropyl Methyl Cellulose (HPMC/MHPC), Methyl Hydroxyethyl Cellulose (HEMC/MHEC) and hydroxyethyl cellulose (HEC) [19]. Some of these type's chemical structure are illustrated on Figure 7. In this research, Methyl Hydroxyethyl Cellulose (MHEC) is used. For adhesive mortar use, it is considered an effective additive.



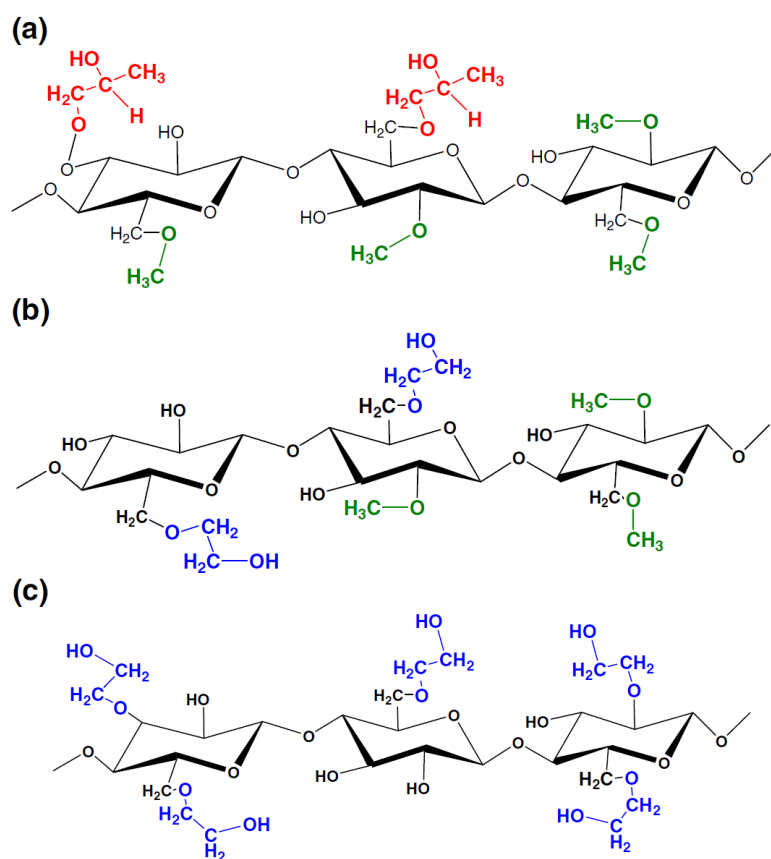


Figure 7. Structure of cellulose ethers: (a) HPMC, (b) MHEC, (c) HEC.[20].

### 2.3.2.4 CE in aqueous solution

#### 2.3.2.4.1 Associative polymer characteristics

Cellulose ether is part of this group called “Associative polymers”, which are water-soluble polymers with pendant hydrophobic substituents that associate in water to form extended structures [21]. This ability gives these polymers interesting rheological properties [22], which is why they are often used as rheology modifiers.

Figure 8 shows various architectures of polymers that have been employed as rheology modifiers and Figure 9 shows the backbone chemical structures of some of the more common HM- polymers. Both architecture and chemical structure are a way to classify these polymers [21]. These characters control the tendency for the different types of association [23].

In aqueous solution, the hydrophobic groups form locally phase-separated entities which resemble micelles. For individual polymer molecules to associate into networks, they must contain at least two hydrophobic substituents so that the polymer backbone can form bridges between micelles [21]. They have the tendency to associate with each other to minimize the surface of contact with water [23,24].





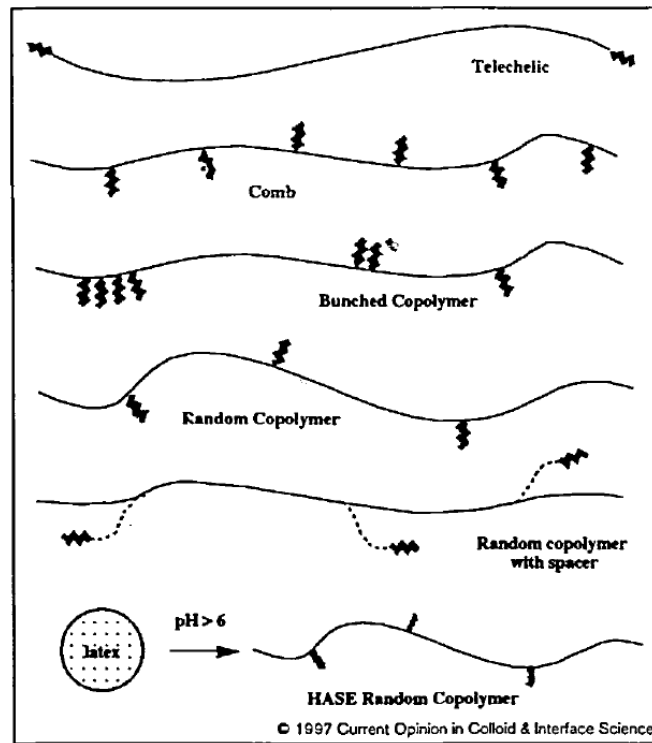


Figure 8. Representative architectures for polymers which undergo intermolecular association in aqueous solution [21].

The association model can be influenced not only by the polymer characteristics, but also by external factors, such as pH, ionic force, temperature, concentration, shear and other additives. In an association network, there may be weak interactions that may be broken depending on the test conditions, as temperature or shear rate for example [23].

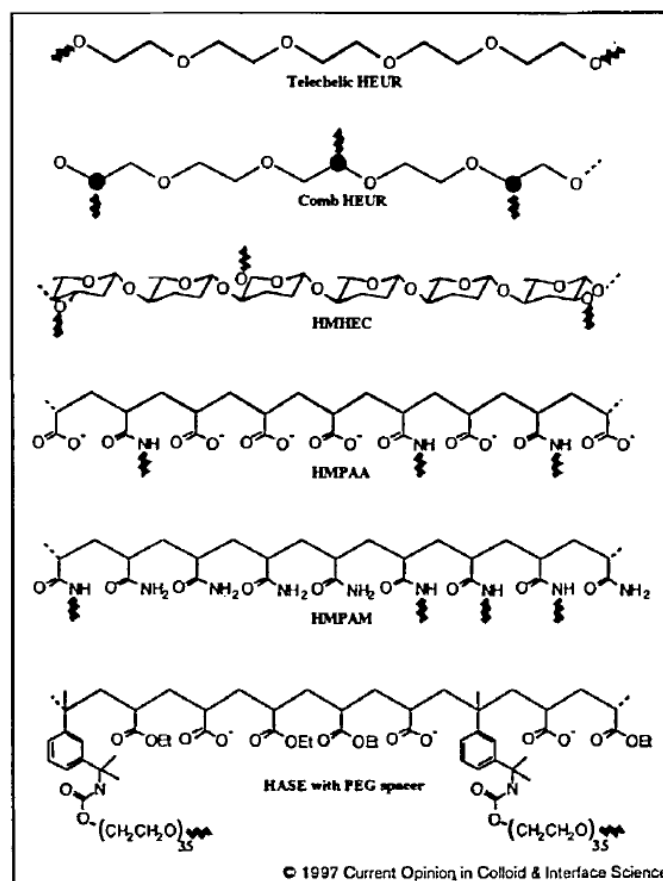


Figure 9. Representative chemical structures for polymers which undergo intermolecular association in aqueous solution. Note that for several of the structures (e.g. the polysaccharide) only part of the structure suggesting the attachment sites of the hydrophobes is indicated [21].

#### 2.3.2.4.2 Solubility

Etherification causes transfer of the water-insoluble cellulose into a swellable to completely water-soluble derivative. For the properties of the cellulose ethers – especially their solubility – the following factors are relevant [15,25]:

- Type and size of the substituents
- Uniformity of substitution: statistical distribution (uniform and even) or block-wise distribution (irregular and uneven). The more evenly distributed the substituents are, the lower the degree of substitution for which a specific solubility of the cellulose ether is achieved
- Degree of substitution (DS)
- Molar substitution (MS)
- Degree of polymerization (DP)
- Particle size distribution or granulometry: The finer the particles are, the faster hydration process of the polymer will be. Cold-water-soluble CE, however, tend to form lumps.

Besides the polymer characteristics, external factors also will influence solubility, as the temperature, pH, etc. Studies have demonstrated that increase of salinity generates a reduction of solubility, while surfactants have the opposite impact [26].

#### 2.3.2.4.3 Rheological behavior

MHEC are in the family of Methyl Cellulose (MC) family. The solution behavior of the nonionic MC is markedly different from that of the ionic types; the effect of pH is especially reduced, and the temperature-dependent rheology is much more complex. When dissolved in water these gums give clear, smooth-flowing solutions that are pseudoplastic and nonthixotropic [16,27]. Molecular weight, concentration, temperature and the presence of other solutes can also affect rheology of a CE aqueous solution.

Cellulose ethers, as many other associative polymers have a characteristic polymeric behavior with appearing to be Newtonian in the very low shear rates [12,23]. This behavior can be observed in Figure 10, with different nominal viscosities MHECs at 2% concentration. The pseudoplastic behavior of MC is a function of molecular weight, with MC of higher molecular weight exhibiting greater pseudoplasticity [16]. This pseudoplastic behavior is related to the reduction of the viscosity, consequence of the deconstruction of the associative network and an orientation of the polymeric chains in the direction of the shear [23].

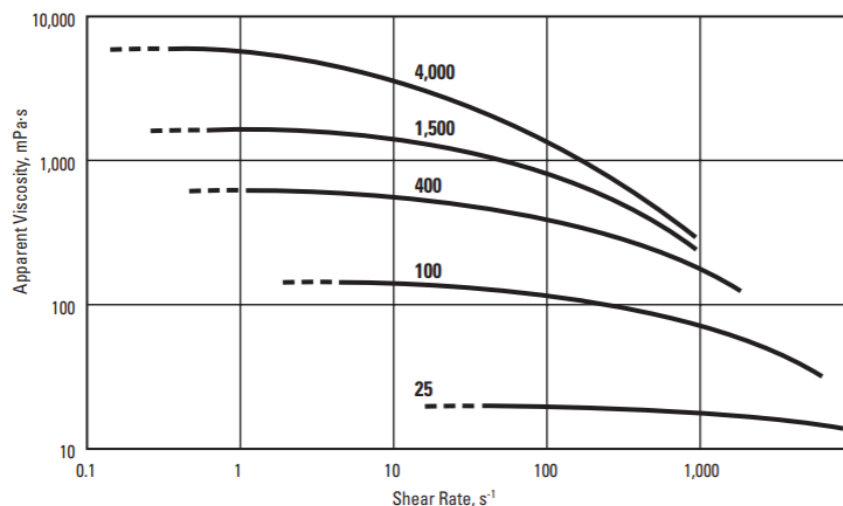


Figure 10. Apparent Viscosity vs. Shear Rate, 2% aqueous solutions of an MHEC of different nominal viscosities [12].

Another important parameter that affects rheological properties is the concentration; similar to the molecular weight effect, the higher the concentration, the higher the pseudoplasticity.



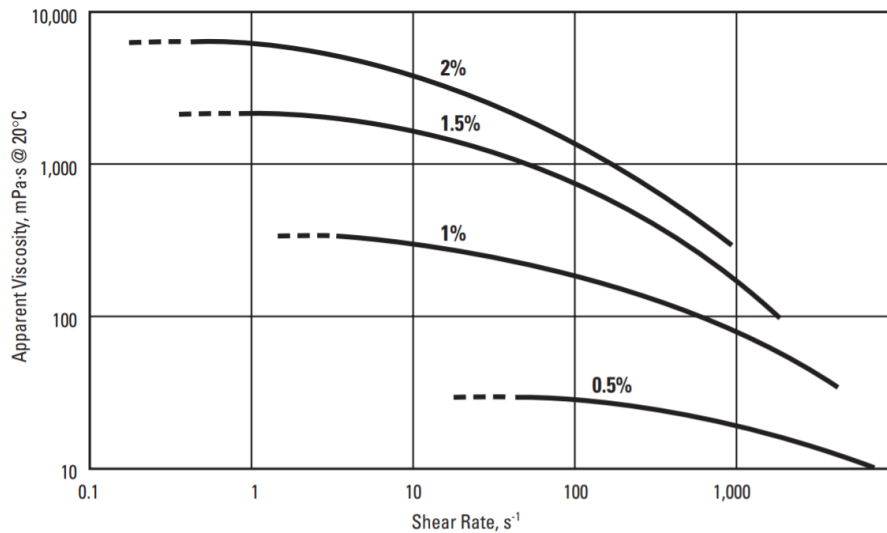


Figure 11. Apparent Viscosity vs. Shear Rate, for Aqueous Solutions of 4,000 mPa.s CE at different concentrations

#### 2.3.2.4.4 Gelation of CE

MC and HPMC behave inversely to the classic gel formers gelatine and  $\kappa$ -carrageenans. At room temperature, there is a viscous solution that gels ('floculates') upon heating and then, upon cooling, reverts 100% reversibly back into the viscous state. Figure 12 shows the behavior of methylated cellulose ethers during heating and cooling [15]. The mortars are at the stage 1 of the curve.

Bulk thermal gelation is primarily caused by a hydrophobic interaction between molecules containing methoxyl groups. In a solution state at lower temperatures, molecules are hydrated and there is little polymer-to-polymer interaction other than simple entanglement. As the temperature is increased, the polymers gradually lose their water of hydration, and viscosity decreases. When the gel point is reached, sufficient dehydration of the polymer occurs to cause polymer-to-polymer association, and the solution begins to gel. Gel strength continues to build as the temperature is held above the gel point. When the solution is cooled, the gel effect begins to reverse, and viscosity drops rapidly. Finally, the viscosity of the cooling solution merges with the original heating curve and increases as the temperature decreases. Once the solution has cooled, the viscosity is the same as it was originally. Thus, the thermal gelation process is reversible [12].

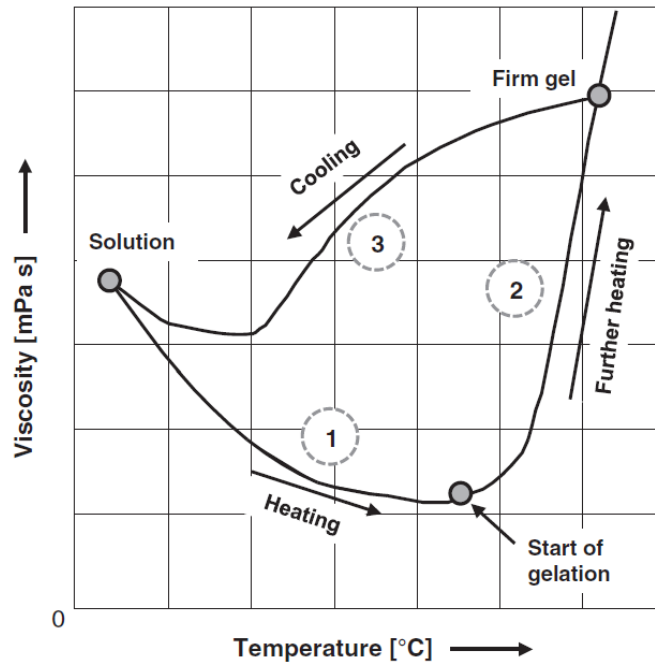


Figure 12. Temperature-dependent viscosity and gelation of methylcellulose [15].

The gelation temperature is controlled and influenced by the following factors: type and level of substitution; concentration of CE; total solid content in the system; type of solvent and presence of additives that influence gelation point [15].

### 2.3.2.5 CE in cementitious materials

In construction, CE is used in mortars as thickening and water retaining agents [28]. Due to its surfactant behavior, it also influences air entrainment and air-voids stabilization. The addition of CE in mortars is important in adhesive mortars, to improve workability, guarantee stickiness and extend open time. Air-entrainment and bubble stabilization can improve workability and efficiency. Its thickening effect improves tackiness and stickiness, so the tile and the substrate work well when attached during a fresh state [29]. The water retaining effect is important to maintain enough water for hydration and allow longer open times (time between the mortar spreading and tile application where good adhesive properties are obtained). In this section, the main impact of CE on cementitious materials will be presented.

#### 2.3.2.5.1 Rheological impact

Cellulose ether is as an associative polymer, and in solution, it has the ability to form a network and keep water physically connected, avoiding its mobility and, consequently, reducing its exudation, segregation and ionic transport [30]. This viscosity increases the effect of water mobility, which leads to a reduction in water evaporation, since associative polymers interact



with many different substances. Using them to their “full potential” requires resolution of many of the issues of general interest to the scientific community [21].

CEs mode of action can be classified in three categories [30]:

- (1) Adsorption: The long-chain polymer molecules adhesive to the periphery of water molecules, thus adsorbing and fixing part of the mix water and thereby expanding. This increases the viscosity of the mix water and that of the cement-based product.
- (2) Association: Molecules in adjacent polymer chains can develop attractive forces, thus further blocking the motion of water, causing a gel formation and an increase in viscosity.
- (3) Intertwining: At low rates of shear, and especially at high concentrations, the polymer chains can intertwine and entangle, resulting in an increase in the apparent viscosity. Such entanglement can disaggregate, and the polymer chains can align in the direction of the flow at high shear rates, hence resulting in shear thinning.

#### 2.3.2.5.2 Effect on water retention

Cementitious materials mechanical strength is mainly obtained by cement hydration. Losing water in the system may result in anhydrate cement that will not react, with a direct consequence on its mechanical properties. Water retention is a mortar property that prevents the rapid loss of water to the substrate by suction. This property avoids bleeding or “water loss” when the mortar is in contact with relatively permeable surfaces. They are also important to reduce segregation [20].

By solubilizing CE, interstitial solution’s viscosity increases, affecting its mobility to be absorbed by the substrate or migrate to the surface, influencing the water evaporation. Depending on the CE nature, MHEC and MHPC have stronger water retaining effect in comparison to HEC [20]. This can be related to the slower dissolution speed and associative mechanism smaller of HEC, therefore, smaller impact over the viscosity of the media [23]. Pourchez considered two hypotheses: (i) a rheological effect similar to those produced by other polysaccharides; (ii) an effect that could be inherent to cellulose ethers, such as a modification of the porous network in the fresh state, osmotic pressure, or the presence of a cellulose ether film playing the role of diffusion barrier [31]. Jenni et al. [1] observed film formation that may play an important role on water retention.

Patural et al [20] demonstrated that the molecular weight is crucial to control water retention and mortar consistency. Also, molecular weight improved water retention; on the contrary, the molar substitution seems to have a lower impact on the water retention of admixed mortars.



The particle's size has also a small impact over the water retention, and the smaller the particle's size, the more water retention increases. The reduction of particle size allows a faster dissolution of CE, and thus, for the same mixing, a higher concentration of polymer will be solubilized [32].

#### 2.3.2.5.3 Effect on hydration

One of the main disadvantages of CE is its impact on cement hydration. This is related to the adsorption ability of the polymer over the cement particles [23]. CE adsorption on the clinker phases inhibits the growth of portlandite [33]. CE strongly effects C-S-H precipitation, leading to a decrease in the amount of initial C-S-H nuclei, delaying the formation of a continuous C-S-H shell around the  $C_3S$  grain, and finally delaying the formation of a thicker and more permeable hydrated calcium silicate layer. When CE is added, a gradual reduction of  $C_3A$  dissolution rate is observed; this is also associated with ettringite and calcium hydroaluminate precipitation [19].

HEC induces a stronger adsorption on calcium hydroaluminates and a longer  $C_3A$  hydration delay than does HPMC [9]. The lower the content of methoxyl groups, the larger will be the retardation of cement setting time [19]. Thus, DS is a key parameter that governs the delay of precipitation of portlandite. The Degree of etherification has a higher impact on solubility and water absorption, while the molecular weight on the mechanical properties [34].

### 2.3.3 Other polysaccharides admixtures: guar ether and starch ether

In this section, other polysaccharides admixtures used in cementitious materials are introduced. Guar ether and starch ether, like cellulose ether, are natural resources used as thickeners. Commercially available admixtures are often a combination of different polymers and additions and can also have multiple functions. Some manufactures produce additives that can combine cellulose with starch, guar and other polysaccharides to obtain higher performing additives.

#### 2.3.3.1 Guar ether

Guar ether is a polymer admixture derived from guar gum. It is a thickener admixture commonly applied in food industry and others (cosmetics, paper manufacturing, cementitious materials, coatings) [23]. Guar gum is a high molecular weight, hydrophilic, non-ionic natural polysaccharide extracted from the endospermic seed of *Cyamopsis tetragonolobus*. Guar gum consists in a D-mannopyranose backbone with random branchpoints of galactose [35]. The ratio



of mannose to galactose units ranges from 1.6:1 to 1.8:1 apparently due to climate variation [36].

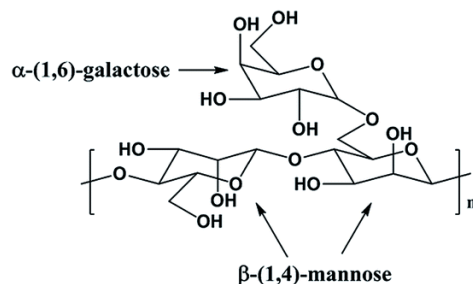


Figure 13. Molecular structure of Guar gum [37].

The most common guar derivate admixtures in constructions materials are the Hydroxypropyl guar (HPGs). They are obtained from the original guar gum via an irreversible nucleophilic substitution, using propylene oxide in the presence of an alkaline catalyst. Thanks to its branched-chain structure and the numerous hydroxyl groups, guar gum exhibits a high chemical reactivity and is soluble in cold water [35].

Depending on gum purity and method of isolation, guar gums may contain as much as 10-14% insoluble residue. This “residue” is not desirable for commercial applications. Additionally, its molecules have a tendency to aggregate mainly due to intermolecular hydrogen bonding [36]. For this matter some attempts to produce low-residue derivatives of guar gum have been developed. Treatment of guar with ethylene oxide, propylene oxide, and chloroacetic acid in an alkaline medium results in the formation of hydroxyethyl guar, hydroxypropyl guar, and carboxymethylguar, respectively [36].

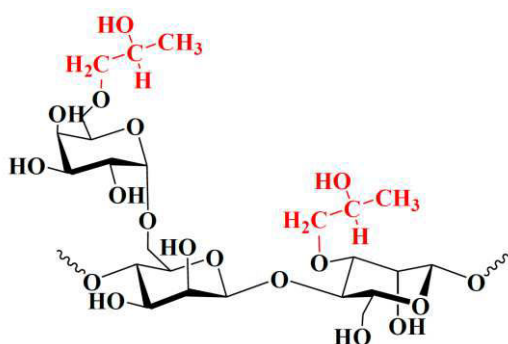


Figure 14. Molecular structure of HydroxyPropyl Guar [35].

The same parameters such as molar substitution (MS) and degree of substitution (DS) also apply to guar ethers. Cheng et al. studied the intermolecular interactions of hydropropyl guar solutions, evaluating the different MS levels on the solution properties. The study’s experiments demonstrated three regimes: the first regime ( $0 < \text{MS} < \sim 0.4$ ) shows a sharp decrease in





intermolecular interactions as a function of MS. In the second regime ( $\sim 0.4 < MS < \sim 1.0$ ), interactions are no longer a function of MS. In the third regime ( $MS > \sim 1.0$ ), inter- and intrahydrophobic effects can play a role at high temperatures ( $>40\text{ }^\circ\text{C}$ ).

### 2.3.3.2 Starch ether

Starch ether is also derived from a natural source, the starch. The use of starch and its derivatives are found in a diversity of domains. The total annual starch production worldwide is estimated to be about 45 million tons and the dominant raw materials used for the extraction of starch are maize, potato, tapioca and wheat [38]. In the form of the starch ether, it is used as a thickener. They are often part of the cellulose ether admixtures chemical structure to improve rheological properties. Also, its cost is much lower than cellulose ether, reducing the production costs [23].

Native starch occurs in the amyloplasts of seeds, roots and tubers, and in the plastids of green plant leaves as discrete, partially crystalline granules. The major constituent ( $\sim 99\%$ ) of the starch granule is  $\alpha$ -D-linked glucose, which occurs in two different polymeric forms; amylopectin and amylose, but there are also small amounts of phosphorus, lipids and proteins present in the granule. Furthermore, starch granules differ with regard to size, shape, morphology and constituent composition, mainly depending on their botanical origin, but also on the degree of maturity, weather, soil, etc. [26].

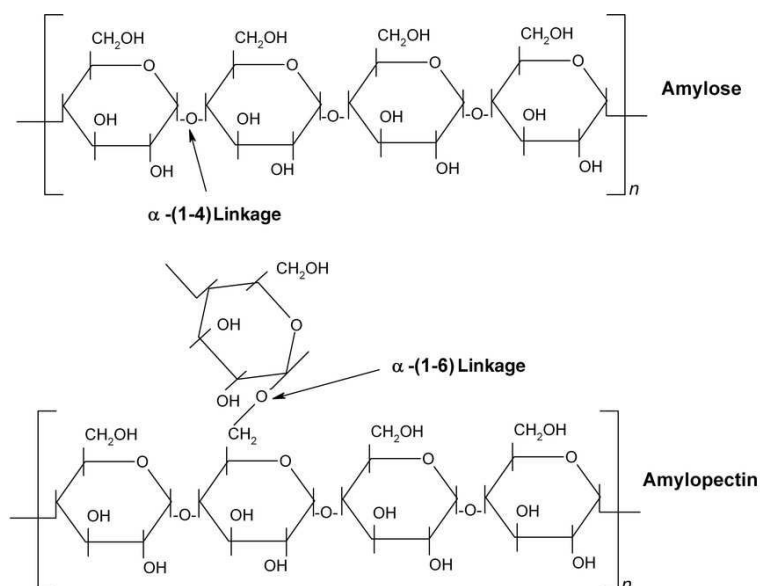


Figure 15. Amylose and amylopectin chemical structure [39].

Amylose is considered to be an essentially linear macromolecule consisting of several hundreds of  $(1\rightarrow4)$ - $\alpha$ -linked D-glucose residues [26]. But it is today well established that some molecules



are slightly branched by (1→6)- α -linkages [40]. The (1→4)-α-D-glucosidic linkages in amylose allow the molecule to rotate in such a way that the chains form left-handed helices with six glucose units in each full turn. The weight-average molecular weight (MW) of amylose has been estimated to be 105 to 106 Da [26,40,41]. The amylose content of most starches is generally about 20–30% [42], although there are starches that are comprised mainly of amylose [26,40].

Amylopectin is the major component of starch with a weight-average MW of 107 to 109 Da [26,40], making it one of the largest molecules in nature [40]. Common starches normally consist of 75–80% amylopectin, although there are natural mutants of, for example, maize, rice, sorghum and barley, which contain almost exclusively amylopectin (waxy starches) [26,40]. Furthermore, amylose-deficient potato amylopectin starch (PAP) has been produced by genetic modification [26,43]. Amylopectin, unlike amylose, is a highly branched molecule composed of (1→4)-α-glucosidic linked chains with an average chain length (CL) of 15–25 glucose residues, but with 4-6% (1→6)- α -d-glucosidic bonds at the branching points [42,43].

The native starch is water insoluble due to its semi-crystalline structure, which limits its application. Therefore, similarly to the cellulose ether, chemical modifications are done to obtain water soluble polymers with the desired properties, the starch ethers.

Compared to cellulose ether, starch ethers studies regarding its effect on cementitious materials properties are less found in literature. The starch derivatives are generally classified as a thickeners, but often they also present a dispersing effect [23].

Peschard et al [44] studied the effect of starch ether on cement hydration at early ages. The authors verified that low-molecular-weight starch showed enhanced retarding effect on the hydration of cement. C<sub>3</sub>A hydration is retarded by starch ether, probably related to an adsorption of the admixture on the first hydrates forming a less permeable coating. Starch Ether was efficient on delaying C-S-H formation.

#### 2.3.4 Latex

Latex has become widely used in construction materials because of its ability to improve properties such as mechanical strength, extensibility, adhesion, waterproofing, and durability. It is one of the main admixtures used in adhesive mortars in the form of redispersible polymer powder, which is why it is introduced here.



### 2.3.4.1 Latex film formation

Latex is a stable colloidal dispersion of polymeric particles. It can be obtained through natural resources and it is still intensively used for rubber production. Synthetic latexes can be obtained by polymerizing a monomer such as styrene.

Polymers can form a film, and this process are usually described in three steps [45–47]:

**Stage I** – Water evaporation and consequent increase of solid concentration. This is the slowest step and finish when the volumetric concentration is between 60-75% or when the superficial area of the latex’s air-liquid interface starts to decrease due to film formation.

**Stage II** – Particles’ packing and irreversible close-contact occurs, forming an arrangement with interstitial water. Conclusion of coalescence marks the end of the stage.

**Stage III** – Polymer diffusion occurs across the interparticle boundary to provide the entanglements that give strength to the film.

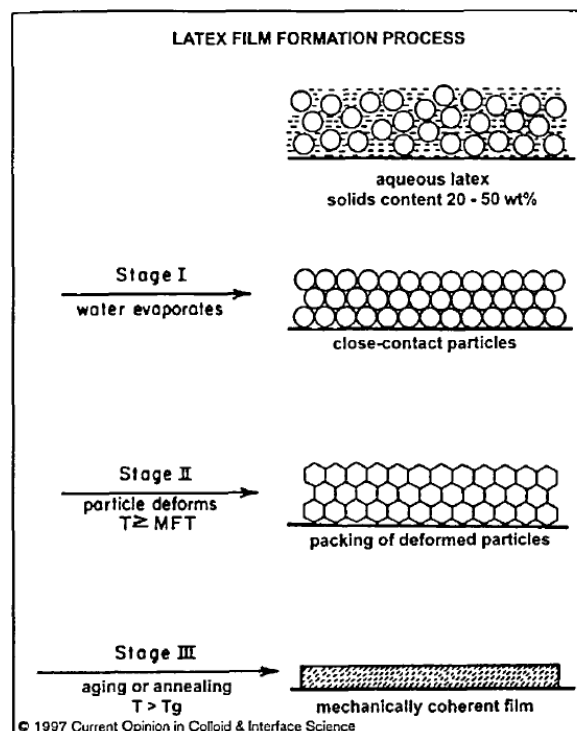


Figure 16. Representation of the successive stages in film formation as an aqueous dispersion of polymeric microspheres dries above the minimum film forming temperature (MFFT) [45].

Different factors can affect polymeric film formation: environmental conditions; and physical and chemical properties of the dispersion [48]. Regarding the chemical properties, minimum



film forming temperature (MFFT) and glass transition temperature ( $T_g$ ) are the relevant parameters.

#### 2.3.4.2 Redispersible polymer powder (RPP)

In construction materials, “latex” is often used to refer to another form of the polymer particles called redispersible polymer powder (RPP). This form of the polymer is a powder that has the ability of redisperse when water is added, and it can later coalesce when water is consumed or evaporated.

RPP was invented during the 1950s in Germany and allowed polymer modified dry-mix mortar. In a context of the industrial dry mixes and practical demands, RPP appeared as perfect match, since latex dispersion contains water, which cannot be involved with reactive materials such as cement in a pre-mix. With continuous innovation and progress in the production technique and subsequent products, in the 60s, the ethylene-vinyl acetate copolymer powder (EVA) was successfully produced as an RPP, significantly improving the flexibility of polymer powder.

EVA polymer powder of this kind can be used for the alkaline system of Portland cement [49–51]. This was the start of a huge market growth of RPP additives for construction materials, because they could be pre-mixed in the dry-powder, instead of added later during use as a liquid dispersion form. Now, for dry-mix adhesive mortars and other types of mortars, contain at least 2.5%-20% of weight percentage RPP, since it offers considerable improvement for the mortars. Thus, considering its high content and influence on its properties, its understanding became a necessity.

RPP cannot be regarded simply as a latex dispersion, it is a post-treated dispersion, and its changes during the process must be considered when understanding its behavior. In Figure 17, a simplified model of RPP production is shown, based on spray-drying process.

The main polymer types used are: Acrylic, Vinyl Acetate Ester (VAE), Vinyl Ester of Versatic Acid (Veova) and Styrene Butadiene (SB). Also, copolymers are available, such as VAC/E/VeoVA, VAc/E/VeoVa, VAC/A/VeoVa, EVA, etc. To avoid dispersion coalescence, a protective colloid Polyvinyl Alcohol (PVOH) and anti-caking agent is added in the spray drying process. The anti-caking agent can be Kaolin, Aluminum, Silicate, Talc, etc.



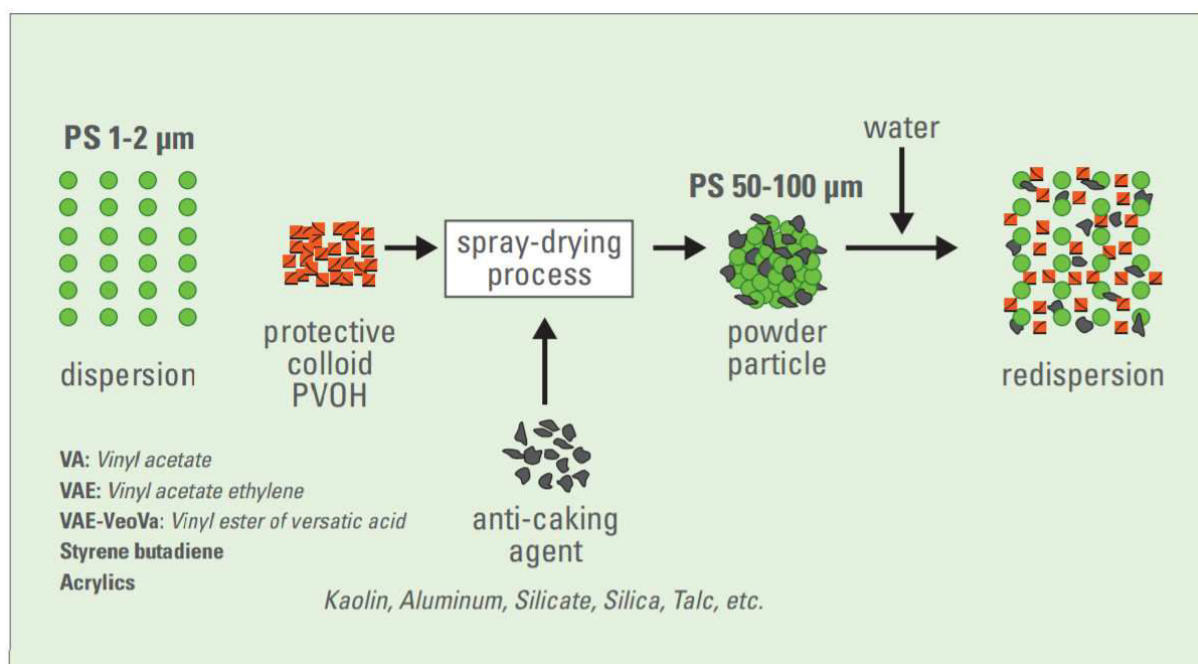


Figure 17. RPP production simplified model [52].

#### 2.3.4.3 Minimum Film Formation Temperature (MFFT) and Glass Transition Temperature (T<sub>g</sub>)

Film formation from latex particles is a process analogous to interface healing in bulk polymers or to polymer moulding in terms of interdiffusion requirements. It has been shown that full strength was achieved when the effective penetration depth of the chains by interdiffusion had reached a value comparable to the weight average radius of gyration of the critical entanglement weight in the case of high molecular weight (uncrosslinked) samples [53–55]. The time needed to reach this state of interpenetration depends on the degree of chain mobility or diffusion coefficient which in turn depends on the difference between the application temperature and the minimum film formation temperature (MFFT), closely related to the glass transition temperature (T<sub>g</sub>) [55].

Minimum film formation temperature (MFFT) and glass transition temperature (T<sub>g</sub>) are two important parameters of the polymers. The MFFT is the lowest temperature at which a polymer uniformly coalesces when laid on a substrate as a thin film. And, the T<sub>g</sub> describes the temperature at which a polymer turns from a hard, brittle film to an elastic flexible film. Because of its impact on film formation, these parameters are used for choosing the type of polymer used.

RPP admixtures are used to offer the mortars flexibility, therefore, it is important to have  $T_g$  values below the application temperature. And the MFFT should be lower than the room temperature when the polymer is drying to enable a uniform polymer film.

#### 2.3.4.4 Latex influence on cementitious materials

Polymer film formation is already complex and difficult topic by itself; thus, studying it in the cementitious complex systems is a challenge. The polymer-cement co-matrix is formed by both cement hydration and polymer film formation process [56]. The cement hydration process generally occurs before the polymer formation process [57]. Grosskurth proposed a model indicating the co-matrix formation as shown in Figure 18. The process consists of three steps [56]:

**Step 1:** After the cement mortar or concrete are mixed with polymer latexes, forming a uniformly dispersed mixture. Then, the cement gel starts to form by cement first hydrates and water phase saturates with  $\text{Ca(OH)}_2$  during hydration, on which the polymer particles start to deposit, forming a cement-gel-unhydrated cement particles mixture. This result in the formation of  $\text{Ca(OH)}_2$  crystals at the contact zone or interfacial zone between cement hydrates and aggregates.

**Step 2:** With the consumption of water with the development of cement gel structure, the polymer particles are gradually confined in the capillary pores. As water is consumed, the polymer particles flocculate to form a continuous close-packed layer of polymer particles on the surface of the cement-gel-unhydrated cement particle mixtures and simultaneously adhere to the mixtures and the silicate layer over the aggregate surfaces. In this case, the larger pores in the mixture are found to be filled by the adhesive and autohesive polymer particles.



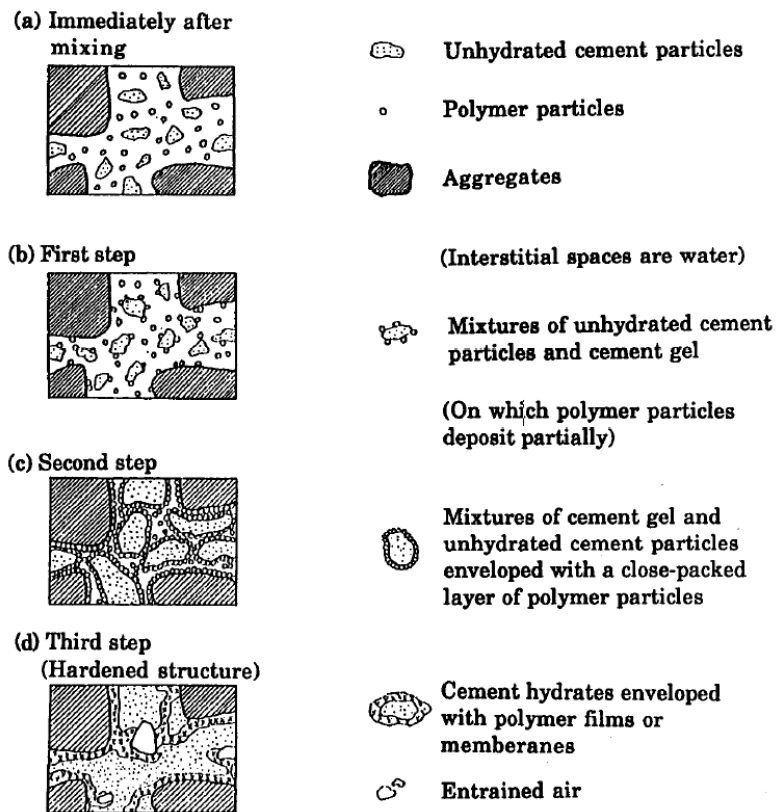


Figure 18. Simplified model of formation of Polymer-cement cc-matrix [56].

**Step 3:** With water withdrawal by cement hydration, the close-packed polymer particles on the cement hydrates coalesce into continuous films or membranes, and the films or membranes bind the cement hydrates together to form a monolithic network in which the polymer phase interpenetrates throughout the cement hydrate phase. This structure acts as a matrix phase, where the aggregates are bond by the matrix phase to the hardened mortar and concrete. In Figure 19, a simplified model of process of polymer film formation on cement hydrates is illustrated.

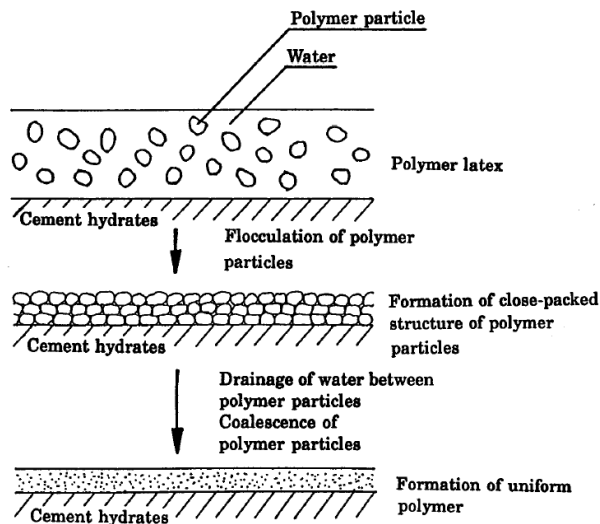


Figure 19. Simplified model of process of polymer film formation on cement hydrates [56].

In industrial pre-mixed powder, latex need to use in the form of RPP, which contains other constituents such as PVOH and anti-caking agent added for the spray drying process. These additions also need to be taken in account when studying RPP impact on mortar's properties. Baueregger et al [58] verified that Kaolin, one type of anti-caking agent, acts as accelerator for polymer film formation. Also, powders containing PVOH and kaolin, which both contain hydrophilic hydroxyl groups exhibit slower water evaporation.

## 2.4 Skin formation

A skin is a surface layer with different properties compared to the body underneath. A skin can be very thin, in the range of a micron or tens of microns, but as it coats the material it controls entirely the surface properties [2]. Water is one of the main ingredients of adhesive mortars; it not only has an essential role on hardened state by reacting with water, but also in fresh state, since it can be considered as a “glue”, due to its surface tension properties that allow the mortar to be cohesive and wetting the substrate and tile.

When the mortar is applied to the substrate, immediately the contact with the atmosphere generates the water evaporation of the material, taking away the water. In some cases, a skin can be formed at its surface, and when the applicator would attach the tile, the mortar skin does not enable a good contact and the tile easily detaches, either in fresh or at hardened state.

This problem can be related to different causes and have been studied by different authors, and in this section, part of this literature will be covered.





### 2.4.1 Skin formation mechanism

Many causes are believed to be related to skin formation such as polymer film formation, early hydration, carbonation, etc. Recent studies have been trying to chemically characterize the skin. Bühler et al. [2] studied the chemical composition, microstructure and physical properties change between the first 30 min. In this study, within the first 10 minutes of a freshly applied mortar: (i) the surface dries, (ii) organic and (ii) inorganic phases show up in the very thin surface layer depth that DRIFTS can obtain signal. The authors concluded that the generation of a skin can be explained by drying of the mortar surface and related mechanisms of formation of organic and inorganic films composed of cellulose ether, polymers, carbonates and minor hydrates. The skin is mainly influenced by parameters/mechanism [2]:

- (a) **Evaporation rate:** largely dependent on the climatic conditions, which are given by the specific environment on the construction site.
- (b) **Flow rate of mortar water:** It can be reduced by pre-treating the substrate or by adjusting the mortar formulation. Each raw material that affects the distribution and binding of water must be regarded. On one hand, the mortar water must be retained against capillary wicking of the substrate, but on the other hand, it should be able to flow towards the evaporation front in order to keep it as long as possible at the mortar surface in order to retard drying and related skinning.
- (c) **Passive transportation of dissolved ingredients with the flowing water:** the water flow towards the evaporation will transport the organics dissolved in the solution, but also cementitious ions which will enrich at the evaporation front causing locally early precipitation as hydrates and carbonates.
- (d) **Active enrichment of surface active ingredients (additives or chemical modifiers):** with an affinity to air-water interfaces will actively occupy the interface of entrained air and enrich at the mortar surface
- (e) **Rate of carbonation at the surface:** the carbonation is very influenced by the cement type, content and accelerators and retarders, since they influence the ionic strength that controls the hydration and carbonation reactions.

In Figure 20, a scheme of the skin formation mechanism is shown.



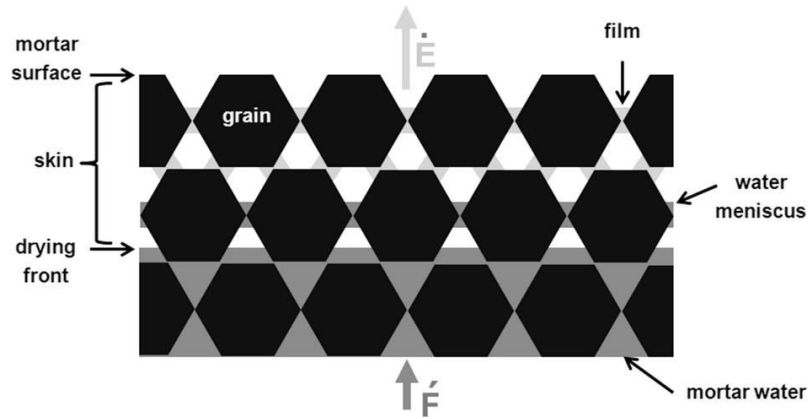


Figure 20. Scheme for illustrating skinning mechanism. Abbreviations:  $\dot{E}$  - evaporation rate;  $\dot{F}$  - flow rate of mortar water [2].

#### 2.4.2 Polymer migration in adhesive mortars

Jenni et al. [1] verified that as the mortar is applied, free water flows towards the porous substrate and towards the surface, which causes an enrichment of cellulose ether and polyvinyl alcohol (latex stabilizer redispersible powder component), water soluble mortar ingredients. The concentration variations of cellulose ether and polyvinyl alcohol are shown in Figure 22. This cellulose ether builds a flow barrier and provides water retention, since small sized porosity of the concrete substrate acts as a filter. The authors also evaluated the latex distribution patterns inside the mortar, and verified that it remains homogenous, as shown in Figure 21. In Figure 23, a summary of all physical and chemical properties evolution is shown.

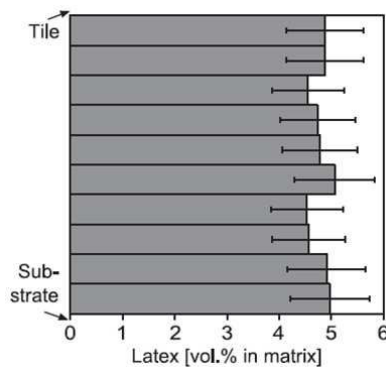


Figure 21. Concentration profile of VC latex in the cement-polymer matrix sampled across the mortar bed on an xy section [1].



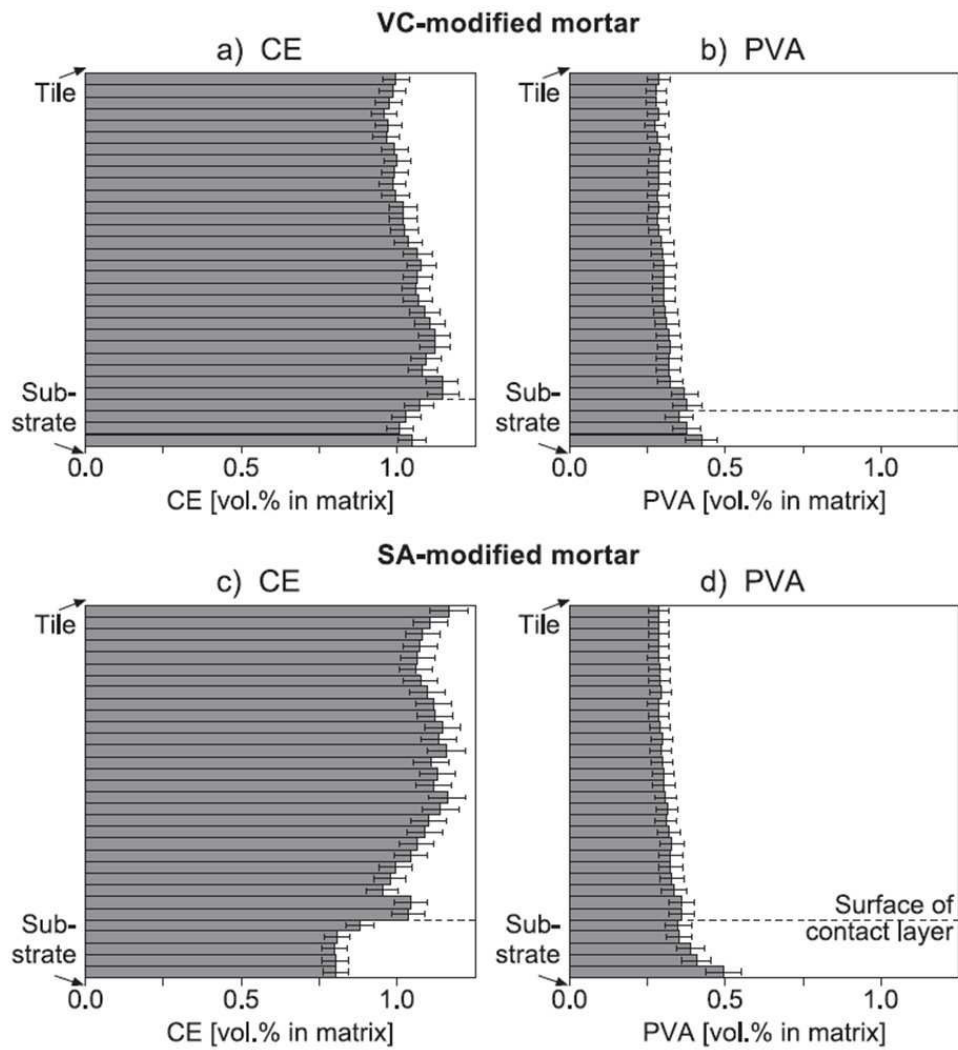


Figure 22. Concentration variations of CE and PVA in the cement–polymer matrix as a function of the distance from the substrate surface (along y axis in Fig. 2). (a, b) VC-modified mortar. (c, d) SA-modified mortar [1].

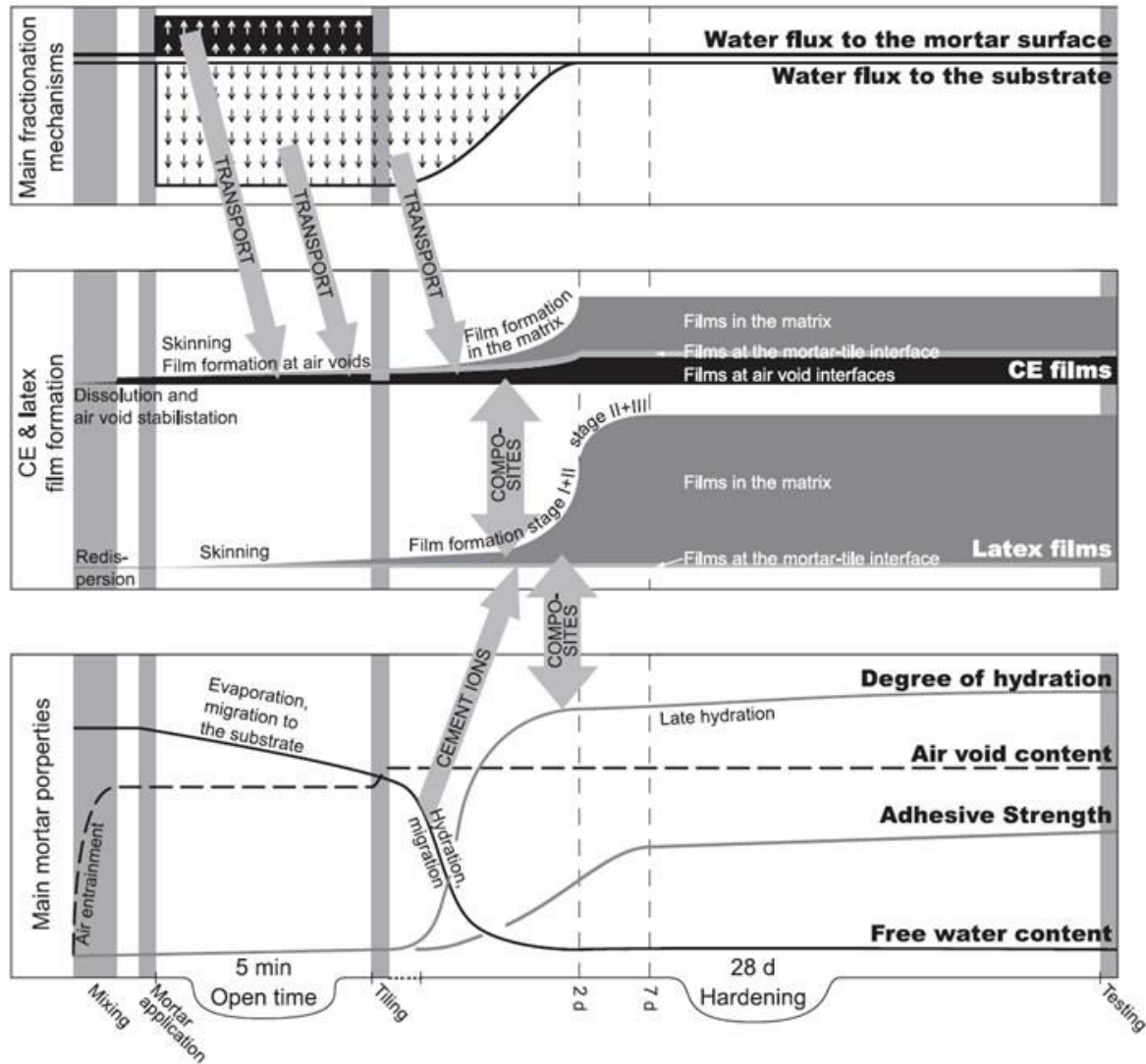


Figure 23. Schematic synthesis of the mortar evolution. The nonlinear horizontal time axis highlights the major stages of the mortar evolution [1].

### 2.4.3 Effect of skin formation on contact generation between mortar and tile

When a skin layer is formed at the surface of the mortar, it will impact the contact between the tile and the mortar. In Figure 24, mortar deformation during tiling application is illustrated. (a) With ongoing drying a skin evolves. The thickness, composition and property of the skin depend on temperature, humidity and the time of exposure until (b) the tile is laid. Thereby the ribs are deformed by the applied pressure (c). The skin on the top of the ribs is pressed downwards and only slightly sheared. Thus, the contact to the tile at these positions (x) is mainly build up by skin (former rib positions). On the other hand, the grooves are filled by the fresh mortar, which is pressed out of the sheared ribs (y). Therefore, the contact to the tile is mainly built up by the fresh mortar at these locations (former groove positions) [59–61].

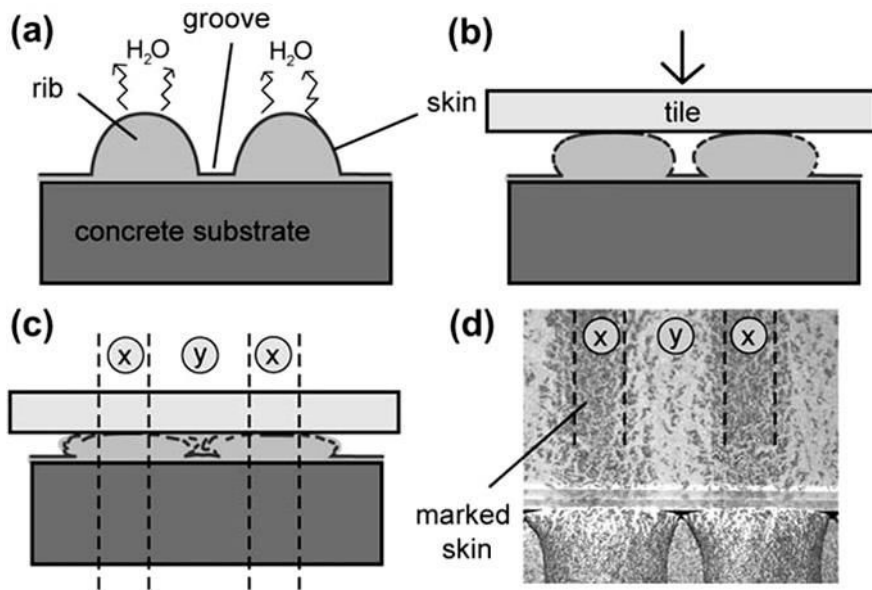


Figure 24. (a–c) Deformation of fresh mortar including skin at the surface during tile application. (d) Top-view of an applied glass plate; the skin of the mortar was marked by an ordinary spray paint [59].

#### 2.4.4 Skin rheological properties

The kinetics of skin formation is not yet fully understood. Despite its great importance, small attention has been given to the rheological properties of the skin, which is a key property that defines the ability of the mortar to generate good contact with the tile. Researchers at *Akzonobel* [61] developed a micro-rheology penetration test to evaluate its kinetics. The test is based on a 2 mm needle penetration at a constant velocity of 1.2 mm/min and the normal force variation is measured, illustrated in Figure 25. A micro-rheological intrusion-force diagram of an adhesive mortar is shown in Figure 26. It is possible to observe the force variation through the depth for each waiting time measured.

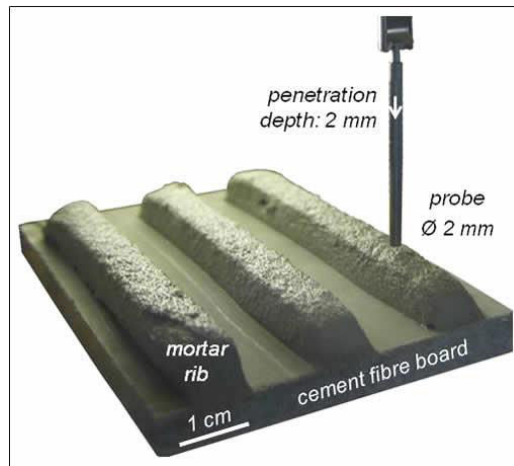


Figure 25. Dynamic in-situ micro-rheology with a Krüss tensiometer K-100 MK2 a cylindrical probe with a diameter of 2 mm is pushed with 1.2 mm/min from the mortar surface to a depth of 2.1 mm [2].

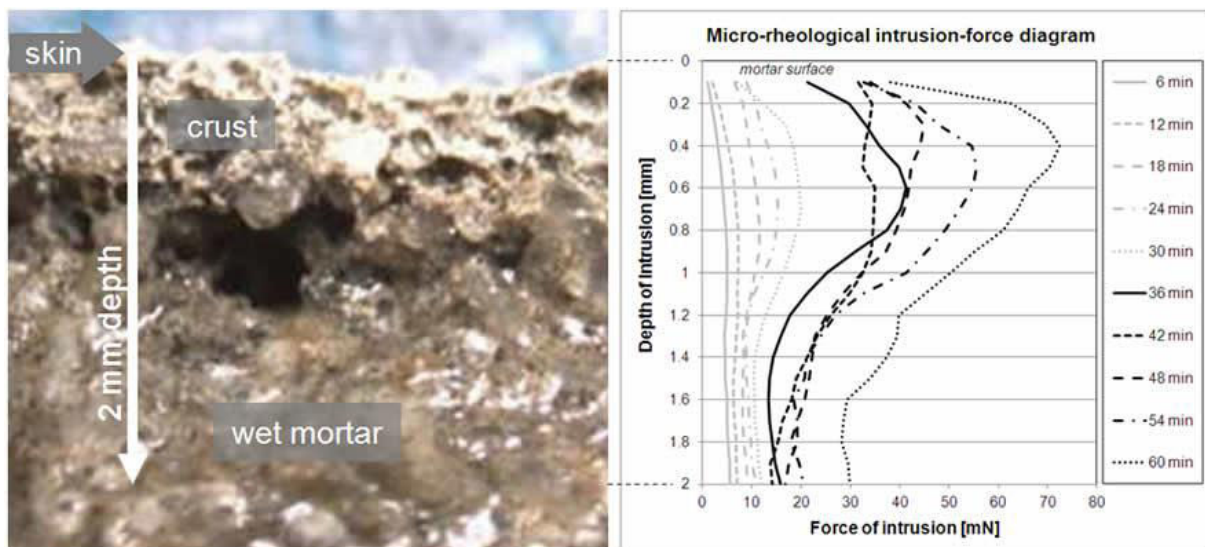


Figure 26. Micro-rheological intrusion-force diagram of an adhesive mortar for different waiting times (0-60 min) [61].

Petit et al. [62] adapted a food protocol for “solid” samples [63], making punctual shear measurement with a plan-plan geometry of a sample after 20 and 30 min resting, where a skin formed. The method was able to obtain a response on 30 min resting with two peaks in a shear measurement, but it was not able to affirm what concerns each peak.

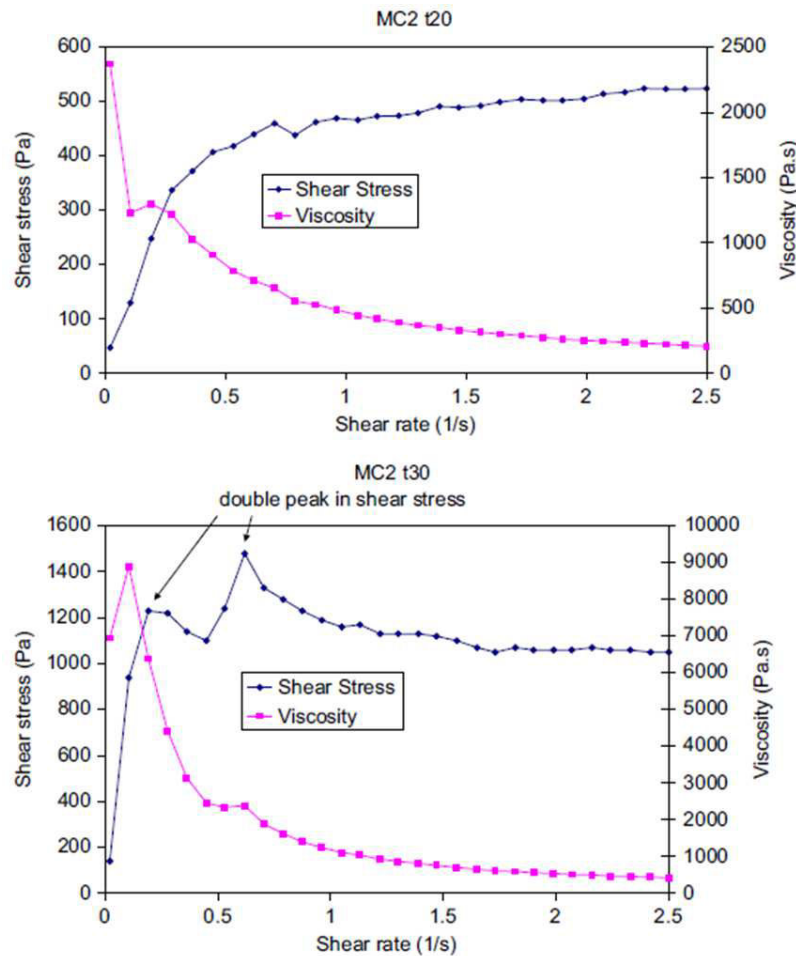


Figure 27. Plate/plate rheological response of a CE based mortar at 20min(a) and at 30min(b), Yield evaluation on shear stress response [19].

Both *Akzonobel* group [61] and Petit et al. [19] tried to evaluate the skin's rheological properties, which are essential since the skin can dominate the contact generation between the mortar and the tile. However, both methods have limitations regarding mixing bulk and the skin properties, since they are both measured during the process, which can affect the evaluation of material with different bulk properties. Also, despite the fact that some indicators can be obtained to give an idea of the skin property, no real rheological parameter was obtained.

## 2.5 Adhesion

The main role of adhesive mortar is to glue tiles to a substrate. Performing adhesive mortar is the one that generate good adhesion in fresh and hardened state, not leading to early detachment or failures. For any type of glue, a necessary requirement for adhesion is good contact. Without contact, most important physical or chemical bonds cannot act, since their acting range of distance is order of a nanometer.





Generating contact, when thinking in everyday life liquids like cooking oil seem to be simple, however, when it comes to multi-phasic materials as mortars it is not trivial. It is related to the ability of the material to deform itself to another one, that is rheological properties.

Non-performing adhesive mortar may lead to tiles detachment and failures, which can generate high costs of repairmen and in case of facades for example, risk of injury.

Mittal [64] defined practical adhesion as:

$$\text{Practical adhesion} = f(\text{fundamental adhesion} + \text{other factors})$$

For the adhesion mechanism comprehension, concepts of interaction that influence adhesion will be reviewed in this section.

### 2.5.1 Adhesion, cohesion and related forces

When discussing adhesives, concepts related to its properties need to be defined: adhesion, cohesion and work of adhesion and cohesion. Adhesion is related to the forces that connect two different medias ( $1 \neq 2$ ), being the work of adhesion  $W_{12}$  and having an interface that separates those medias. And cohesion is related to the same media, obtaining a work of cohesion  $W_{11}$ .





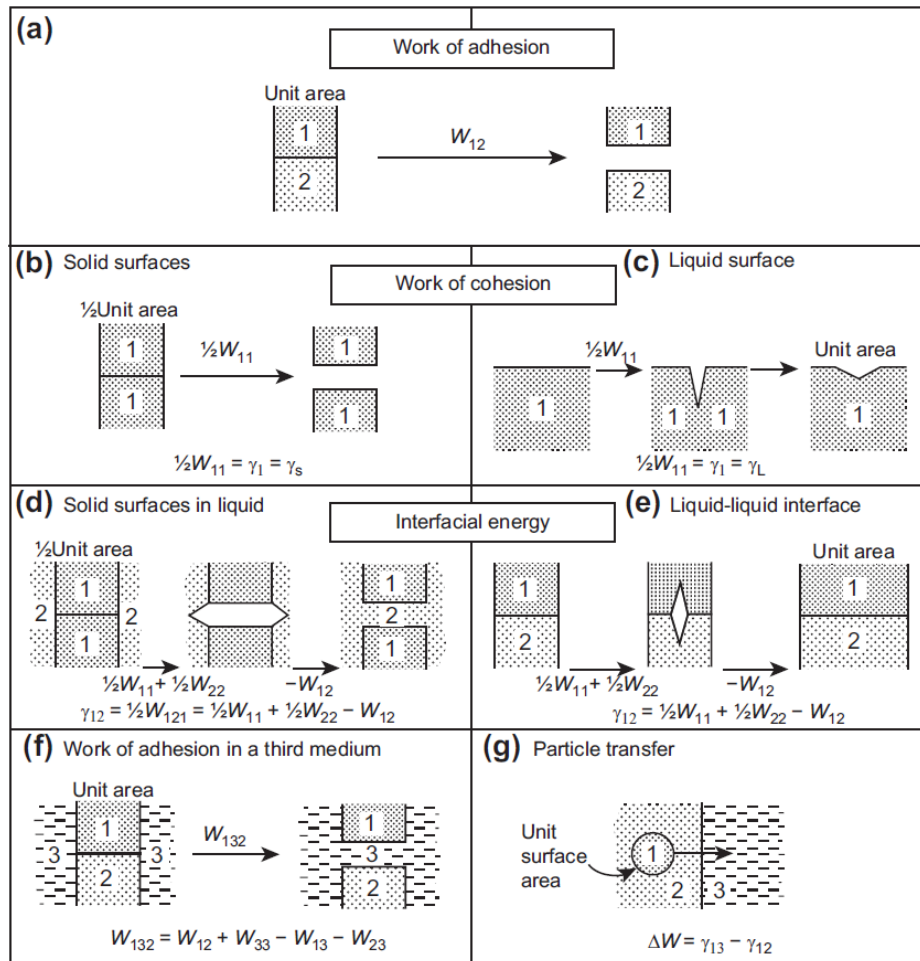


Figure 28. Definition of various energy terms associated with the adhesion of solid surfaces and the surface area changes of liquids. Note that  $W$  and  $g$  are idealized thermodynamic quantities, assuming reversibility and smooth surfaces. In practice, only with liquids can the area be changed gradually and reversibly, as in (c). For solids, their adhesion, cohesion, and debonding processes, as in (a) or (b), usually involve plastic deformations with the dissipation of irreversible energy as heat. Note the positive sign of  $W$  (i.e.,  $W > 0$ ) for the work of adhesion/cohesion where, by convention, the reference state (of zero energy) is the contact state ( $D=0$ ), compared to the negative values for  $W(D)$  and  $w(r)$  where, again by convention, the reference states are at  $D=\infty$ ,  $r=\infty$  [65].

The main forces that concern adhesion and cohesion are Van der Waals, electrostatic forces, capillary forces, surface tension, and friction between particles.

### 2.5.2 Capillary forces and surface tension

In granular materials, water is essential for the adhesion ability in fresh state. Surface energy of surface tension is the free energy change ( $\gamma$ ) when the surface area of a medium is increased by unit area. Usually expressed in  $\text{mJ m}^{-2}$  (or  $\text{erg/cm}^2$ ) for solids and  $\text{mN m}^{-1}$  (or  $\text{dyn/cm}$ ) for liquids.



$$\gamma_1 = \frac{1}{2}W_{11} \quad (1)$$

Interfacial energy ( $\gamma_{12}$  or  $\gamma_i$ ) is when two immiscible liquids, 1 and 2, are in contact the free energy change in expanding their “interfacial” area by unit area.

$$\gamma_{12} = \frac{1}{2}W_{11} + \frac{1}{2}W_{22} = \gamma_1 + \gamma_2 - W_{12} \quad (2)$$

### 2.5.3 Brownian motion

When there are very small particles in a liquid suspension, it is possible to observe that they move fast randomly due to the impact of the liquid molecules against its surface. This movement is known as Brownian motion. The theory of Brownian motion was independently explained by Albert Einstein in 1905 [66] and by Marian von Smoluchowski in 1906 [67].

The smaller the particle is, the bigger the Brownian motion effect, since it has higher probability of collision between the suspensions particles. Its effect can be greater or of equal magnitude to gravitational forces for particles of colloidal range size [68].

### 2.5.4 Van der Waals forces

Van der Waals forces is the attraction force between two atoms or molecules, and consequently, between particles. From the London concepts of Van der Waals interactions, Hamaker introduced the concept of interaction energy defining the Van der Waals force between two particles of radius R separated by a distance  $D \ll R$  [69]:

$$F_{vdw} = \frac{HR}{12D^2} \quad (3)$$

Where  $H$  is the Hamaker constant. The Hamaker constant ( $H$ ) is a function of the density of the particles and polarizability. It can be calculated by the equation below:

$$H = \pi^2 d_1 d_2 \lambda_{1,2} \quad (4)$$

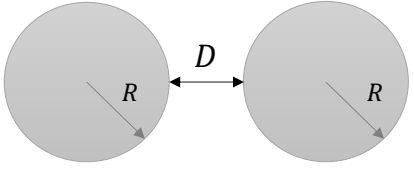
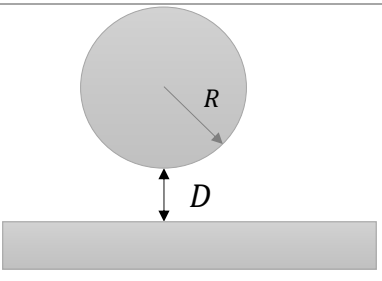
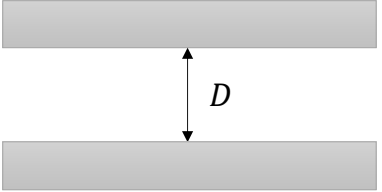
Where:

$d_1$  and  $d_2$  = density of the particles atoms ( $m^{-3}$ )

$\lambda_{1,2}$  = London constant ( $J.m^6 = N.m^7$ )

From the equation (3) it is possible to deduce different configurations of interactions [70]:



Configuration	Equation
	$F_{vdw} = \frac{HR}{12D^2}$ (Between two particles)
	$F_{vdw} = \frac{HR}{6D^2}$ (Between a particle and a flat surface)
	$P_{vdw} = \frac{H}{6\pi D^3}$ (between two flat surfaces)

From the equations, van der Waals interactions between two particles or planes are proportional to inverse of the square or cube of the distance, then as the distance increase its influence become smaller. Also, between particles, the force is proportional to the radius, so the dominance of this interaction is lower for smaller particles, where electrostatic interactions are dominant.

The van der Waals forces cause the tendency particles' agglomeration, and when the particles unify, it can form very stable agglomerate which need a high-energy technique for separation.

### 2.5.5 Particles agglomeration and surface charges

The agglomeration or formation of tridimensional particle structures occurs due to Van der Waals attraction forces between the suspended particles. Even though the interaction between two dipoles being weak, the sum of all attractive components of all electric dipoles of particles result in a relatively strong attraction force. Because of this, particles have a natural tendency to agglomerate [71].

In the surface of crystalline solid particles, the crystallographic atoms are normally exposed and there is a high number of incomplete atomic bonds at not only the surface, but also edges and vertexes. Due to this also know unsaturated bonds, oxide's particles that are put in contact with water are submitted to hydroxylation or superficial hydration. The charges at the surface



of the particles will be responsible for the electrostatic dispersion, because of the reaction of (-OH) at the particles surface and hydronium ( $H_3O^+$ ) and hydroxy ( $OH^-$ ). This process is highly dependable of the pH of the solution. For high pH, the interaction with ions hydroxy dominates and the total charge of the particle is negative. For acid pH, the situation inverts and the electric charges acquire a positive and tend to agglomerate [71].



## Chapter 3 – Bulk rheological properties of adhesive mortar with different cellulose ether contents

### 3.1 Introduction

Bulk rheological properties have an essential role on mortar application and consequent performance. In this chapter, the rheological properties of adhesive mortars and the influence of cellulose ether (CE) on them are reviewed. First, an overview of rheology fundamentals is detailed, followed by a more specific review of the measurement techniques used in this research to evaluate adhesive mortars. Rotational rheometry, oscillatory rheometry, squeeze flow and tack tests were introduced, and their results are shown and discussed in this chapter. Rotational rheometry is used to obtain rheological parameters of a mortar during flow. Oscillatory rheometry is then used to obtain storage modulus ( $G'$ ) and loss modulus ( $G''$ ) over time. Then, for a set of different waiting times condition, squeeze flow is used to evaluate mortar behavior in a geometric restrained condition and possible phase segregation. In the same set, tack test is used to evaluate adhesive properties and tackiness.

### 3.2 Literature review

#### 3.2.1 Rheology fundamentals, concepts of viscosity and yield stress

Rheology is the science of flow and deformation of materials when submitted to a shear or external mechanical stress. Its name radicals are *rhéō* (flow) and *-logos* (study of) [72]. Isaac Newton developed the first model that correlated flow deformation rates of a fluid to an external mechanical stress. To investigate the relation between tension ( $\tau$ ) and deformation rate ( $\dot{\gamma}$ ) of fluids, Newton suggested a model composed of two parallel sheets of area “A”, separated by an infinitesimal distance “dx”, and moving with different velocities “ $V_1$ ” and “ $V_2$ ”, as shown in Figure 29. In this model, ( $dv = V_2 - V_1$ ) is kept through a force “F” application at one of the sheets.



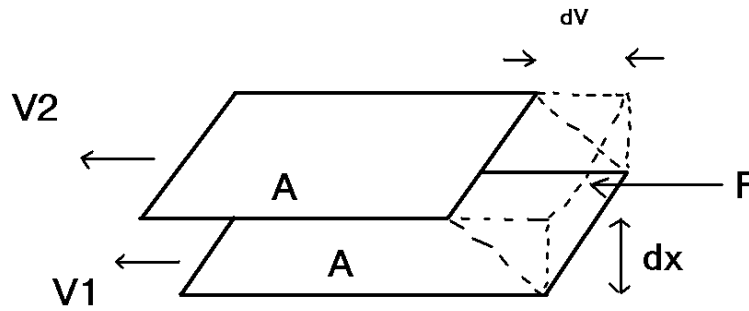


Figure 29. Newton model for viscosity definition two parallel sheets (or planes) of area “A”, separated by a infinitesimal distance “dx”, moving in the same direction with different velocities “ $V_1$ ” and “ $V_2$ ”. The difference between the sheets is kept by the application of an external force “F” in one of the sheets.

With this model, Newton verified the direct relation of proportion for a variety of fluids between the shear stress ( $\tau$ ) and shear rate ( $\dot{\gamma}$ ). The proportionality is known as the fluid viscosity ( $\eta$ ):

$$\tau = \frac{F}{A} = \eta \frac{dv}{dx} = \eta \dot{\gamma}, \quad (5)$$

where the shear stress is expressed by  $Pa = N/m^2$  and the shear rate by  $s^{-1}$  in the International System of Units (SI). It substitutes the Poise (1 Poise = 0,1 Pa.s), used in the past.

Viscosity is considered the main rheological property of a fluid because it indicates the ease of continuous flow with the action of an external shear stress. The lower the viscosity, the lower is the shear stress needed to put into a determined constant shear rate. Physically, it is related to the cohesion of the molecules that form the fluid sheets [73].

The fluids that obey the Newton equation (4) are denominated Newtonian fluids. This is the case for most pure fluid materials; however, most of the fluids used in technological processes have a different behavior.

Some fluids and suspensions demand the application of a minimum shear stress to generate flow, this minimum shear stress is the yield stress. When a stress smaller than the yield stress is applied, the fluid behaves as a rigid elastic solid. This may happen due to a rigid special structure throughout the suspension [74]. One of the main factors of yield stress is the attraction between the particles of the suspension. Therefore, all parameters that influence particles interactions can impact the yield stress—high surface area, surface electric charges and particles form.

Many mathematical equations were developed to describe fluid behavior. The simplest fluids with yield stress are considered “Bingham fluids” and obey the equation:

$$\tau = \tau_0 + \eta_{pl} \dot{\gamma}, \quad (6)$$



where,  $\tau_0$  is the yield stress and  $\eta_{pl}$  is the plastic viscosity of the suspension. Even though the plastic viscosity of this fluid is constant, the apparent viscosity reduces as a function of the flow rate [71].

Most industrial materials, however, are much more complex than Bingham fluids, and require other equations to describe rheological behaviors. Herschel and Bulkley proposed another equation to describe more complex fluids that present yield stress [75]:

$$\tau = \tau_y + K(\dot{\gamma})^n, \quad (7)$$

where,  $\tau_y$  is the Herschel-Bulkley yield stress,  $K$  is the consistency, and  $n$  is the flow index of obtained by experimental data  $\tau_y$  and  $\dot{\gamma}$ . For this equation, a Newtonian behavior is when  $n = 1$  and  $\tau_y = 0$ .

### 3.2.1.1 Rheological behavior of suspensions

In the case of suspensions with low volume fraction (<5%-volume) and low particle collisions, viscosity is constant depending on the deformation rate, and the suspension behaves as a Newtonian fluid. In this case, the concentration of solids, liquid characteristics and temperature are the main factors. However, in the case of cementitious materials, the solid concentration is very high (50-85% [76]) and the particles interact with each other, starting to diverge from the Newtonian model and becoming more complex with many other influential variables. Physical characteristics of particles include granulometric distribution, density, form, specific surface area, roughness, interaction of the particles and others [71].

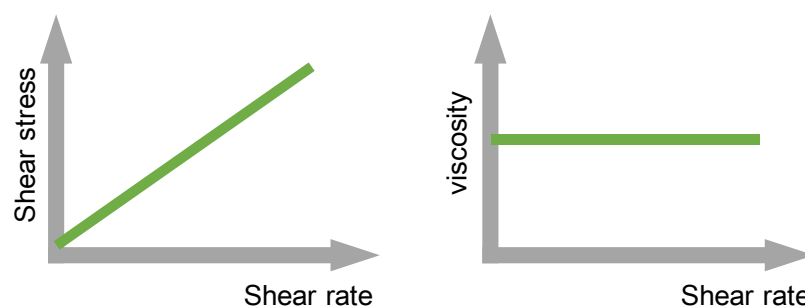


Figure 30. Newtonian fluid behavior

Rheological behavior becomes more sophisticated with the addition of polymeric additives to liquid media, which can adsorb to the particles and change media rheological behavior. Construction materials achieve an even deeper level of complexity since a great variety of



polymers are put in together and interact with each other inside a high particle volume fraction material.

Materials can have different rheological behaviors besides Newtonian fluids. The basic fluid behaviors that are independent of time are pseudoplasticity and dilatant. The time dependent behaviors are thixotropy and rheopexy.

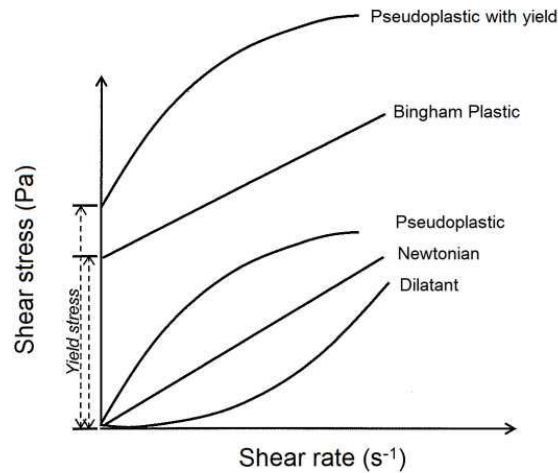


Figure 31. Basic fluids behaviors

#### 3.2.1.1.1 Pseudoplasticity or shear-thinning

Pseudoplasticity or shear thinning occurs when the apparent viscosity ( $\tau/\dot{\gamma}$ ) of the fluid reduces with the increase of the shear rate as shown in Figure 32. Many factors can induce shear-thinning behavior, such as: particles physical characteristics (specific surface area, form and dimensions); type of the particles interaction (attraction and repulsion); or polymeric additives in the liquid phase (concentration, molecular weight and conformation) [77]. In nature, bentonite clays are known for this behavior, and often used for drilling mud [78,79]. In coatings, shear thinning additives, like clay, acrylic, cellulosic based and others, are used to ease application [80].



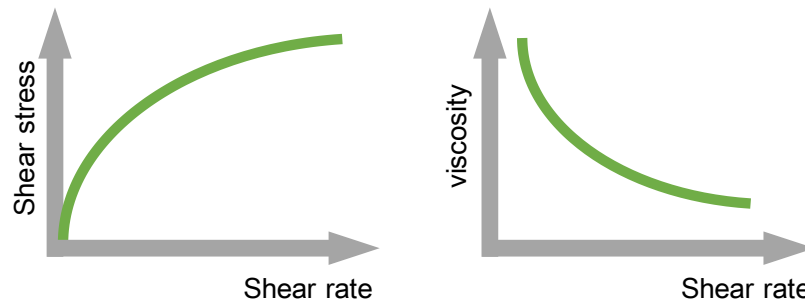


Figure 32. shear-thinning or pseudoplastic behavior

Pseudoplasticity can occur when Brownian motion is dominant at low shear rates and hydrodynamic forces occur at high shear, when particles interactions are negligible. Brownian motion random particles can also create a shear-thinning effect in a fluid [81,82]. Asymmetric particles can have a preferable orientation depending on the intensity of the shear. In low shear, they can oppose the applied flow, having a perpendicular orientation. However, with high shear, the hydrodynamic forces can be enough to align the particles parallel to the flow, resulting in the reduction of the viscosity [83].

Particle surface energy can also influence pseudoplasticity. High surface energy can cause particles agglomeration. These agglomerates, which are porous structures formed by the union of many particles that absorb the water used for particles separation and increasing the collisions in between, and consequently, its viscosity [84]. With the application of high shear rate, those agglomerates break, releasing water, increasing the particles distance, and reducing the viscosity. Agglomeration is usually related to van der Waals; however, additives can influence the particles interaction and consequently the suspension rheology.

The Herschel-Bulkley equation can also describe shear-thinning behavior; in this case, yield stress is 0, becoming Power-law equation:

$$\tau = k(\dot{\gamma})^n \quad (8)$$

Where  $k$  is a constant and  $n$  is a fluid behavior index smaller than 1 for shear-thinning suspensions. The same equation is used to describe dilatant behavior. In material with yield stress, the Herschel-Bulkley equation is used.

### 3.2.1.1.2 Dilatant

Shear-thickening behavior is characterized by the increase of apparent viscosity of the fluid as the shear rate increases, as seen in Figure 33.



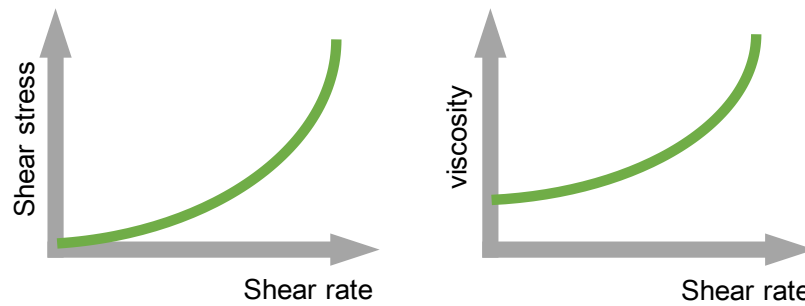


Figure 33. dilatant or shear thickening rheological behavior

In highly filled materials where particles are highly packed and close to each other, the flow can become more difficult in high shear rate conditions, even though it is easy in low shear conditions because it is necessary that the liquid media is able to flow between the particles. As the flow increase, the distance of separation of the particles reduces, and particles with high rugosity and/or asymmetric form may increase particle friction and collision [85,86].

The same equation ( 8 ) describes shear-thickening behavior, but in this case, the fluid behavior index,  $n$ , is bigger than 1.

#### 3.2.1.1.3 Thixotropy

The phenomenon of thixotropy consists of the reduction of the apparent viscosity in function of time in suspension when a shear rate or shear stress is applied, followed by a gradual recovery when shear is removed. [87,88]. This behavior should not be confused with shear thinning, where the viscosity decreases as the shear rate or stress increases, leading to a pseudoplastic (power law with index less than 1) flow curve which is independent of the time of shearing [88,89]. Thixotropy is observed in suspensions containing weak agglomerates as in pseudoplasticity. It occurs when the destruction of agglomerates is relatively slow, and therefore, it is dependent of the condition and time of the shear. Higher shear rates tend to favor agglomerate destruction and reduction of apparent viscosity. A particle's preferable orientation is also a time dependent process, then it can also generate thixotropic behavior [71]. Time dependent processes such as thixotropy are highly dependent on the history of the shear, which are the shear sequences that were applied before the measurement.

Cementitious materials are considered thixotropic materials during its fresh state, even though cement solidification is an irreversible process. This makes rheological measurements of cementitious materials challenging. The presence of particles and aggregates, the extreme shear thinning and the time effects all can introduce errors. Phenomena as wall slip, shear banding



or other shear heterogeneities, sedimentation, shear fracture and irreversible changes in the sample should be taken into account. A microstructure that varies with shear history also affects the mechanical behavior [90]. The use of additives, such as superplasticizers and cellulose ether, can also influence the thixotropic properties of a material.

#### 3.2.1.1.4 Rheopexy

The phenomenon of rheopexy consists of the increase of the apparent viscosity in function of time when a constant shear rate or shear stress is applied.

Rheopexy can also relate to weak agglomerates in the suspension; however, in this case, the history of the suspension is different. In this case, this phenomenon occurs when suspension is, first, intensely sheared for period of time, followed by a low shear for a small period of time. Differently from thixotropy, some of the particles in low shear start to form new agglomerates, which increase the apparent viscosity of the suspension.

Another example is suspensions containing particles that dissolve over time. The increase of ion concentration reduces the electrostatic repulsion between the particles, favoring mutual attraction and the suspension's agglomerations. This is the case for suspensions containing cement particles, in which ions  $Ca^{2+}$ ,  $Al^{3+}$  and  $Si^{4+}$  are responsible for the increase in viscosity over time [71,91].

### 3.2.2 Measurement techniques

Rheological properties can be measured by different methods, including simple flow methods such as observing a material to flow from a spatula or cup, feeling with the finger and laboratory methods: capillary rheometry, falling ball viscometer, squeeze flow, tack test, rotational rheometry, oscillatory rheometry and others.

In this section, some quantitative techniques that were used in this research and can describe material flow properties will be detailed. Rotational flow rheometry, oscillatory rheometry, squeeze flow and tack test are explained and an overview of the current state of the art of the method among the thesis topics will be described.

#### 3.2.2.1 Rotational and Oscillatory Rheometry

##### 3.2.2.1.1 Types of rheometers: stress-controlled, and strain controlled

Commercially available Rheometers are stress controlled, strain controlled or both. Their scheme is shown on Figure 34. Stress-controlled rheometers are the most common type of



rheometer. The mechanism is based on a stress-controlled motor that imposes a stress on the system. Due to improvements and advances on air bearing systems, drag cup discs and optical encoders allow stress-controlled rheometers to perform strain-controlled tests by precisely varying the stress to achieve a certain shear rate or strain [92]. Stress-controlled rheometers are popular due to their lower cost and for the range of stresses used on cementitious materials; with these rheometers, precise results can be obtained.

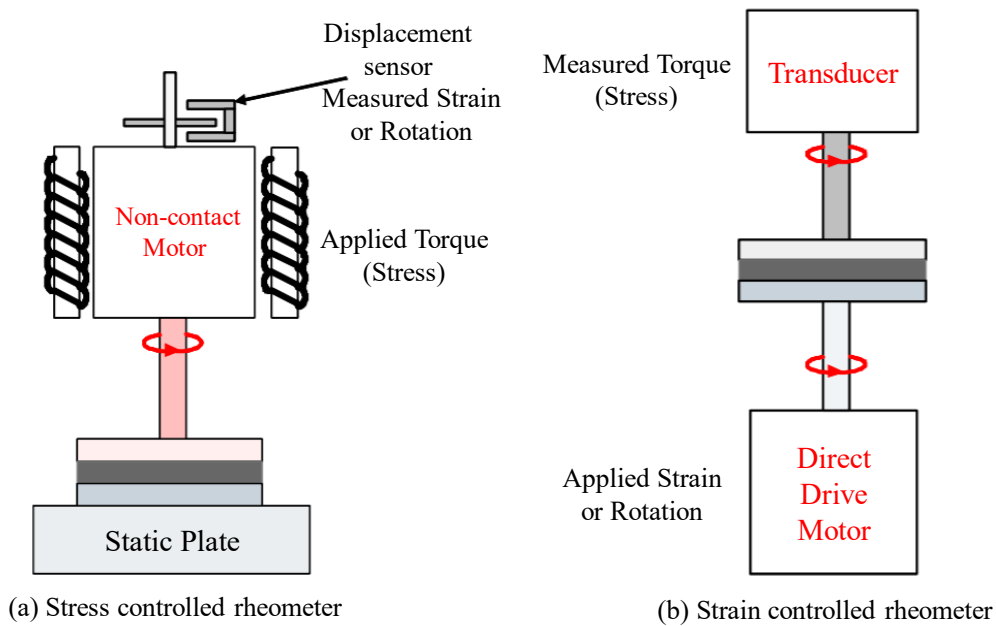


Figure 34. Schematic diagram of a stress controlled (a) and a strain controlled (b) rheometer [93].

Strain-controlled rheometers are based on a direct drive motor that applies the strain or rotation and measure the stress through a transducer. When performing oscillatory tests with low viscosity samples at high frequency or high inertia geometries, strain-controlled rheometers have better precision due to potential inertial effects of stress-controlled rheometers. In a rheometer, the torque output of the motor is composed of the torque required to overcome the instrument inertia and the torque deforming the sample. The torque contributions for inertia increase with the applied frequency to the power two and usually dominate the instrument response for low viscosity test samples. Rotational rheometers with a separate transducer are much less susceptible to inertia effects, since the sample torque is determined independently from the motor torque [93]. Then careful calibration of geometry inertia and mapping is necessary to correct the data. However, caution is necessary when interpreting data, since inertial effects may occur despite software corrections. Pastes and mortars have high viscosity, being out of the range of inertial effects, but pore solutions and other low viscosity materials may be subjected to it.



### 3.2.2.1.2 Rotational and Oscillatory Rheometry concepts

The rotation viscometer or rheometer is a device that measures the resistance of sample to flow when a torque or an external force that generates a specific flow is applied. From this torque, either a flow velocity is obtained or from an imposed velocity, the torque is obtained. With simple flow measurements, much information of the materials rheological properties can be obtained. As already discussed on the previous sections, many different flow behaviors can occur depending on the imposed shear. From the curves, it is possible to predict the material's behavior during application conditions, where a range stresses and shear will be applied. This can reduce possible costs, attend service requirements, and improve durability and safety.

To obtain a flow curve, the shear rate is defined while the shear stress is measured (or vice-versa). In the graphical representation of flow curve, the shear stress ( $\tau$ ) is usually plotted on the y-axis and the shear rate ( $\dot{\gamma}$ ) on the x-axis. In the viscosity curve, similarly, the viscosity ( $\eta$ ) is usually plotted on the y-axis and the shear rate ( $\dot{\gamma}$ ) on the x-axis. From the flow and viscosity curve, the flow rheological behavior of the material can be obtained as detailed in section 3.2.1 [94]. However, when a flow curve is obtained, the idea of the material's behavior is not enough for research and industry application, quantitative results are necessary. The majority of rheological software processes the result with a mathematical model [95]. There are many mathematical models available to predict cementitious materials rheological behavior: Bingham, Casson, Hershey Bulkley, and etc. By applying a fitting to a model, rheological parameters can be obtained. In the case of Hershey Bulkley model, which will be used in this chapter results analysis, the Hershel Bulkley yield stress ( $\tau_y$ ), consistency (K) and flow index (n) are obtained. Already introduced in this rheology fundamentals, Equation (7) is used to obtain these rheological parameters from shear stress ( $\tau$ ) and shear rate ( $\dot{\gamma}$ ) results.

$$\tau = \tau_y + K(\dot{\gamma})^n, \quad (7)$$

Another parameter that can be obtained from flow curves by using a hysteresis analysis is thixotropy. The hysteresis technique was introduced by Green and Weltmann [96]. It consists of systematically increasing and decreasing the shear rate between zero and a maximum value. The change can be a continuous ramp or a series of small steps. When the transient data are plotted as shear stress versus shear rate, a thixotropic sample will describe a hysteresis loop (Fig. 2a) because the stress will lag behind the shear rate. Performing the experiment slower will lead to less difference between the ascending and descending curves as the microstructure



has more time to come closed to the steady state one. The area enclosed by the loop has been used as a characteristic for thixotropy.

$$\text{Area of hysteresis} = \tau \times \gamma \text{ [Pa. 1/s]} = \text{N/m}^2 \times 1/\text{s} = \text{Nm/s} \times 1/\text{m}^3$$

$$A = \text{work/shear time} \times 1/\text{volume} = \text{energy/volume}$$

The area and the shape of the hysteresis loop can vary strongly according to the material [90].

In Figure 35, possible shapes of hysteresis loops are shown.

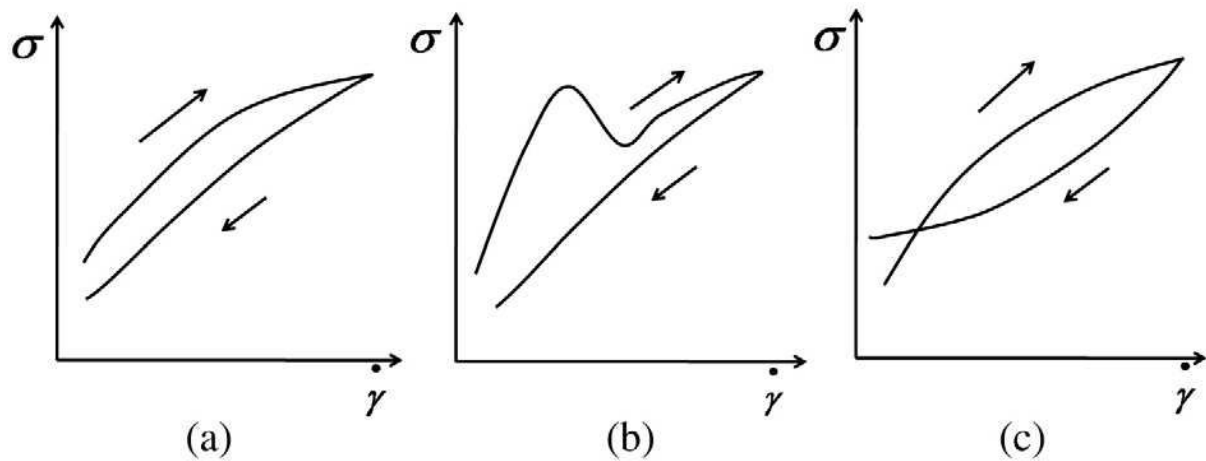


Figure 35. Possible shapes of hysteresis loops [90].

For a given material, however, the area enclosed will depend on test conditions such as the shear history prior to the start of the experiment, the maximum shear rate and the test conditions. The flow measurement mode has a considerable influence on results, it can be either a steady-state or a transient flow measurement. Depending on which mode is used, different results are generated, requiring different mathematical model application and analysis. It is accepted that cement viscosity depends on strain rate, and having different strain rate measurements and accelerations can influence results [96]. Steady-state flow measurements obtain each data point of the shear rate or shear stress (the imposed parameter) for a sufficient period to the material achieve an equilibrium, which means a response plateau. In the case of thixotropic materials, this is achieved when an equilibrium has been established between structure breakdown and rebuilding [97]. Transient flow measurements are obtained by acquiring the response of the material (shear stress or shear rate) during the variation of the imposed parameter (shear rate or shear stress) without waiting for an equilibrium. This type of can lead to the acquisition of a response that may vary according to the acceleration ramp, which means the rate that the imposed shear rate or shear stress increase to achieve the desired point. Models of transient flows are less numerous, however, relevant information can be obtained by transient flow measurements such as the deflocculating process [96].

Petit and Wirquin [19] perform a transient flow measurement with a linear ramp of shear rate from 0 to  $2.5 \text{ s}^{-1}$ , during 30 s, followed by a 30 s constant shear rate of  $2.5 \text{ s}^{-1}$  of an adhesive mortar after 5 and 20 min of evolution. The test obtains yield stress and rheological property parameters of adhesive mortars subjected to environmental conditions during different waiting times. The procedure was inspired by an applied procedure in food industry for ‘solid’ samples i.e. for non-Newtonian fluids and time dependent materials [98].

Flow curve measurements are one of the simplest rheological measurement techniques; however, their ability to provide analysis for cementitious materials is still controversial due to the material’s complexity. Multi-phasic, evolutive, thixotropic and viscoelastic behavior turns comprehension into a real challenge. On the top of it, new additives and additions are continuously being developed, increasing formation complexity and changing chemical and rheological properties. Therefore, research is necessary to keep up with the material’s development to provide a scientific explanation for its behavior.

**Oscillatory rheometry** measurements consist of applying a sinusoidal strain ( $\gamma$ ) to the mortar and if the amplitude is small enough, a sinusoidal stress ( $\sigma$ ) response is obtained with a phase lag ( $\delta$ ). Or inversely, applying a sinusoidal stress can be used to obtain a sinusoidal strain.

$$\gamma = \gamma_o \sin(\omega t) \rightarrow \sigma = \sigma_o \sin(\omega t + \delta),$$

where  $\gamma$  is the oscillatory strain,  $\gamma_o$  its amplitude,  $\sigma$  the oscillatory retrieved stress and  $\sigma_o$  its amplitude.

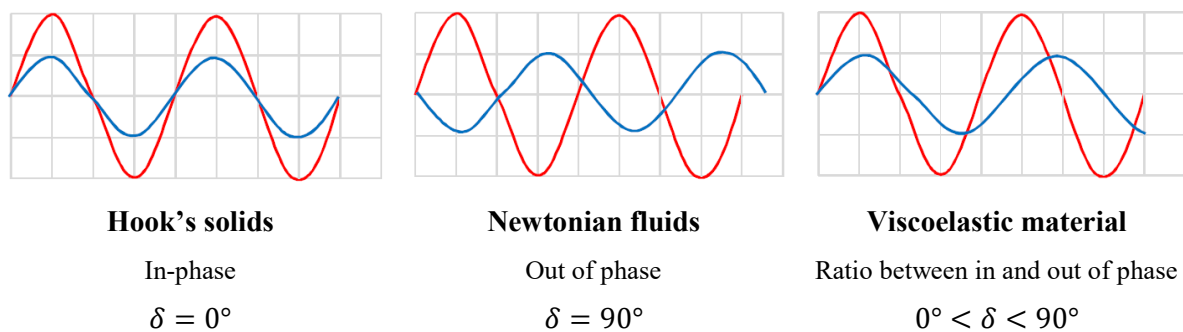


Figure 36. Imposed stress or deformation in red and deformation or stress response in blue.

Perfect elastic materials such as Hooke’s solids have an instantaneous response to a stress or deformation, then the offset angle is  $0^\circ$ . Newtonian fluids, such as water, have a different behavior, opposing the change of applied stress or deformation, viscous material. Viscoelastic materials, however, which are the cementitious materials in fresh states and most of the



materials found in nature are between these two behaviors, presenting both viscous and elastic properties.

From the measurements, the relevant oscillatory rheometry properties that can be obtained are:

$$\text{Shear modulus: } G^* = \sigma/\gamma = G' + i G''$$

$$\text{Storage modulus (in-phase component): } G' = G^* \cos \delta$$

$$\text{Loss modulus (out of phase component): } G'' = G^* \sin \delta$$

$$\text{Loss tangent (ratio between viscous and elastic effects): } \tan \delta = G''/G'$$

Shear modulus ( $G^*$ ) is defined as the ratio of shear stress to the shear strain, which means, the ratio of between the stress response of the material to the imposed strain, or vice versa. The shear modulus can be separated in two components, the “solid” response (storage modulus) and the “fluid” response (loss modulus).

The storage modulus ( $G'$ ) and loss modulus ( $G''$ ) provide an idea of the relative amounts of elastic energy and viscous dissipation in the material during flow; one can expect these parameters to evolve in a specific way at the transition from the solid to the liquid regimes [99]. The storage modulus reflects the strength and the density of the network of connected microstructures making up the material, which is directly related to the yield stress [9]. In a simplified explanation,  $G'$  indicates how much solid-like the material is, and  $G''$  indicates how much liquid-like the material is. Therefore, when  $G' > G''$ , the material is more solid-like and when  $G'' > G'$ , the material is more liquid like. Cement pastes in general have  $G' > G''$  since they are much more solid like.

Small amplitude oscillatory shear measurement (SAOS) is used to explore rates of structural rearrangement within a complex fluid, which does not significantly deform the fluid's microstructure. It is used to impose small-amplitude oscillatory shearing. Therefore, it is a technique commonly used to obtain soft material evolution at rest.

Oscillatory rheometry is powerful for cementitious material investigation, being intensively used to understand especially fresh state setting, first precipitations, early hydration and structure building [100–103]. Following the initial setting of a cementitious material with a time sweep test allows one to follow the evolution of the material from more viscous to more solid material during time, where many bonding and structuring processes occur. Because of this, oscillatory time sweeps are frequently used by researchers to verify the evolution of rheological parameters during the first hours.

Figure 37 shows the evolution of storage and loss modulus of a cement paste after 1 min of the end of mixing, where the material changes from a liquid character  $G'' > G'$  to a solid character





$G' > G''$  [102]. In literature, often this transition cannot be observed, either by the initial solid character of the material or by a late test start, where this transition has already occurred.

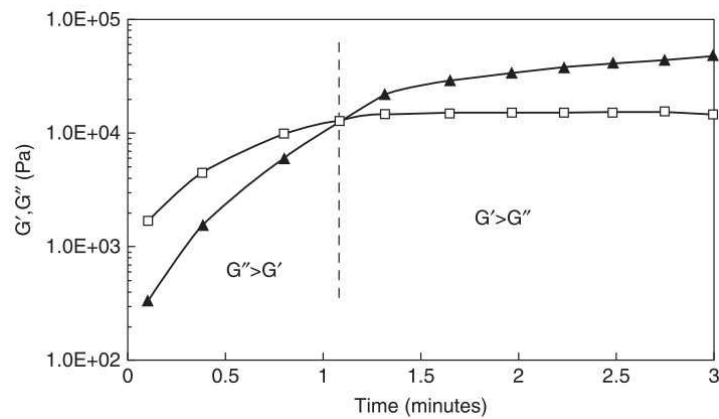


Figure 37. Evolution of elastic moduli  $G'$  and  $G''$  of the viscous cement paste [102].

Being able to follow rheological properties over time can be relevant when regarding tile adhesives. Betioli et al. [101] studied the influence of hydroxymethyl ethylcellulose HMEC (hydroxymethyl ethylcellulose) on cement pastes  $G'$  evolution and yield stress over time and correlated it with isothermal calorimetry. The authors observed that the polymer displayed a steric dispersant barrier effect during the first 2h of hydration associated to a cement retarding nature, consequently reducing the setting speed. However, despite this stabilization effect, the polymer increased the cohesion strength when comparing cement particles with the same hydration degree.

Beyond the linear regime, the non-linear regime is subjected to another range of measurements, called large amplitude oscillatory shear (LAOS). In Figure 38, SAOS and LAOS  $G'$  and  $G''$ , as well as its stress response are illustrated for an aqueous solution.

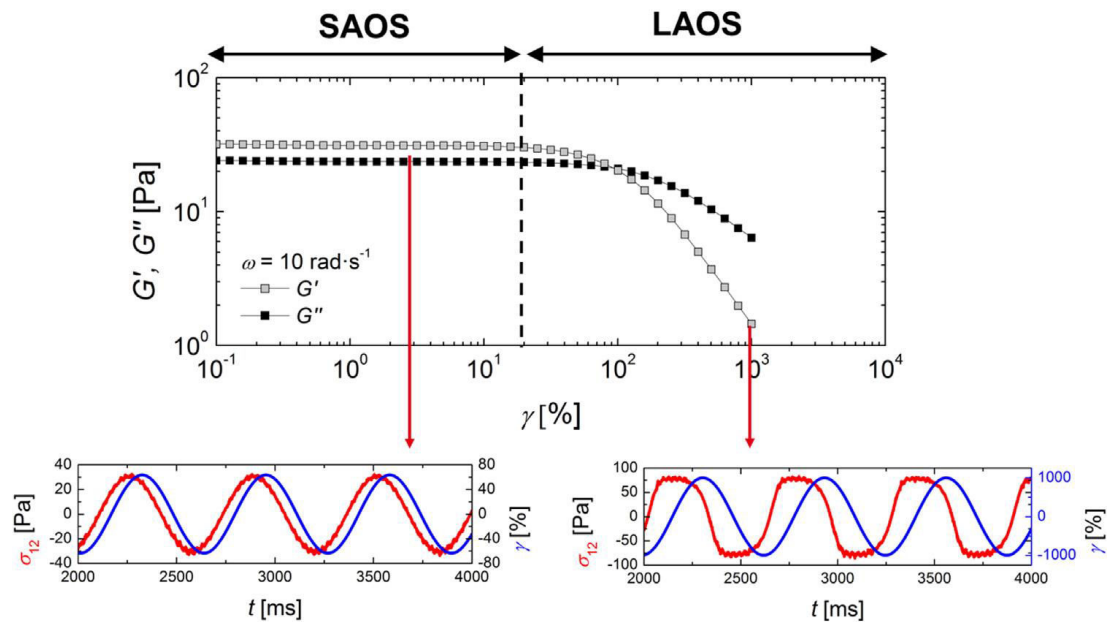


Figure 38. The storage modulus  $G'$  and the loss modulus  $G''$  as functions of the strain amplitude ( $\gamma_0$ ) for an aqueous solution (1.25 wt%) at  $\omega = 10 \text{ rad} \cdot \text{s}^{-1}$  and the corresponding stress response in SAOS and LAOS [104].

In this research, only SAOS will be performed. LAOS are more complex technique to be performed with time-dependent and evolutive materials as cement. Its application remains concentrated on polymers solutions and melts. Some recent studies have been exploring LAOS in a variety of materials [105–108]. Yet, for thixotropic materials, theoretical concepts are still in development and its analysis remains complex and requires further study to become a widespread technique [109–111]. Conte et al. [112] introduced the technique to cementitious materials, attempting to verify which rheological features can be inferred from the LAOS procedure.

In addition to the flow test and oscillatory tests described, a wide range of programs can be applied to obtain the rheological properties of the sample with a rotational rheometer. They can also give important information about which parameters should be used on another test's program, or they may even identify a material behavior that can disturb the data of other test programs. Common test programs are frequency sweep, strain sweep, creep and stress-relaxation.

**Amplitude sweep** is an oscillatory test performed to obtain the storage and loss modulus ( $G'$ ,  $G''$ ) at either a range of strains or a range of frequencies. It can be either a strain amplitude sweep or frequency amplitude sweep.

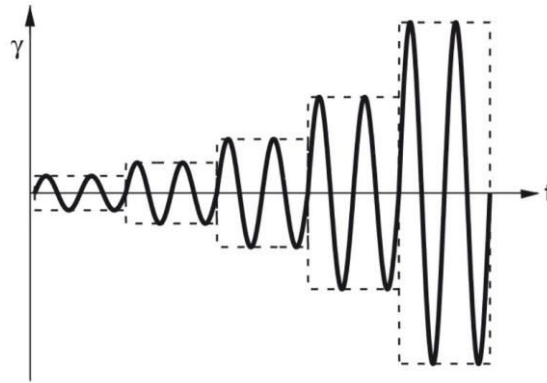


Figure 39. Amplitude test – strain sweep [94].

**Strain sweep** is performed as a preliminary test before oscillatory measurements. From strain sweep, yielding behavior and linear viscoelastic regime (LVER) should be obtained. The LVER is obtained by measuring the storage and loss modulus ( $G'$ ,  $G''$ ) for a range of strains at a specific frequency. The evolution of the oscillatory properties versus the strain generally consists of a plateau at small amplitudes followed by a decreasing branch. The LVER is the range of strain where the plateau is located, where the properties do not vary with the strain increase and make measurements of small amplitude oscillatory shear (SAOS). The strain that delimitates the LVER is the critical strain, which can provide information on the yield stress. Beyond the critical strain, the amplitude of the mechanical oscillation is so high that this will lead to an irreversible microstructure evolution of the sample, which corresponds to a macroscopic flow [9]. Therefore, analysis of beyond critical strain should be considered as a large amplitude oscillatory shear (LAOS) with different theoretical considerations.

In Figure 40, an example of strain sweep test of a rendering mortar with different CE content from Cappellari et al. [9] is shown. From the curve, one could assume that 0.01% and 0.1% stay at the linear regime, where small amplitude oscillatory tests could be performed.

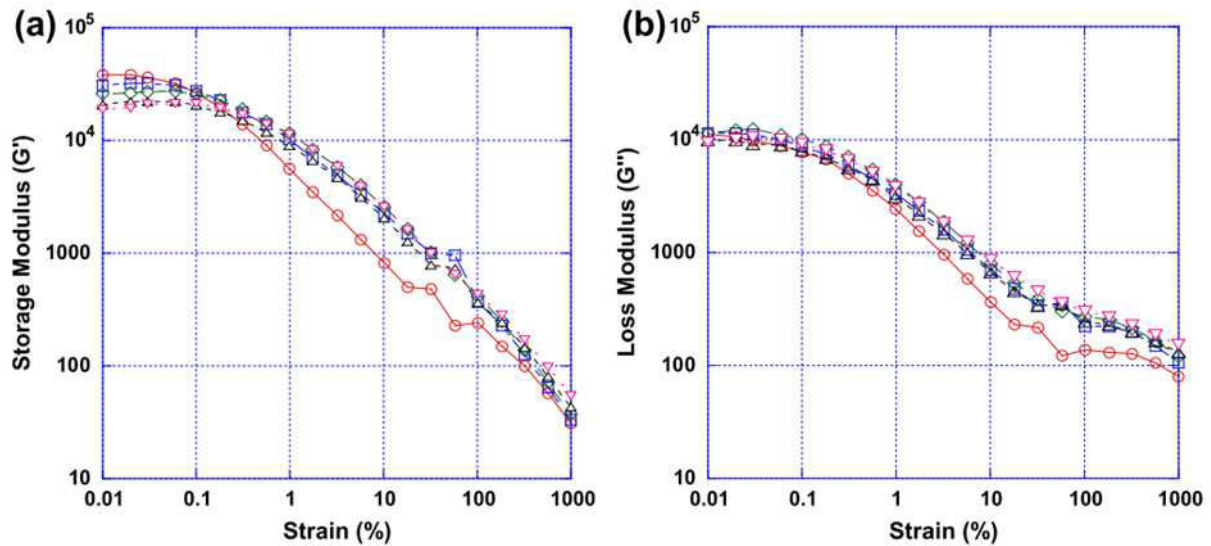


Figure 40. Evolution for the storage modulus  $G'$  (a) and loss modulus  $G''$  (b) as a function of strain amplitude for different dosage rates of CE (grade MHEC-A20000). (o) 0% CE; (□) 0.03% CE; (◆) 0.06% CE; (Δ) 0.09% CE; and (∇) 0.12% CE [9].

The strain range found in literature for mortars and cement pastes can vary depending on the composition and water content. Not all studies give information on the linear viscoelastic region, but for cement pastes, those that report provide a critical strain to be  $1 \times 10^{-4}$  [113,114],  $5 \times 10^{-5}$  to  $2 \times 10^{-4}$  [115] and  $3 \times 10^{-4}$  [116], values which are typically at, or just above, the lower limit of capacity of the instruments available [88]. Therefore, preliminary tests to verify the strain range are important to verify if the strain parameter for oscillatory tests is suitable.

The transition between the linear and non-linear regimes provides another way to determine the yield stress [117,118].

**Frequency sweep** is the application of an oscillatory strain at a range of frequencies. In other words, with a specific strain, measurements of the  $G'$  and  $G''$  are made at different oscillation frequencies. From frequency sweep, characteristic timescale, solid-like plateau and gel scaling can be obtained. The range of frequencies in LVER for cementitious materials is generally quite wide, differently from strain sweep tests. Many authors assume 1 Hz [9] for their measurements, which usually is in the LVER. Sun et al. [119] obtained the frequency LVER for a cement paste, obtaining a large range of frequencies in the LVER, with a critical frequency close to 10Hz. In other words, values for the lower frequency limit are given as 0.1 Hz [116] and 0.2 [113,114], with other work reported at fixed values of 0.69 [120] and 2.5 Hz [115].

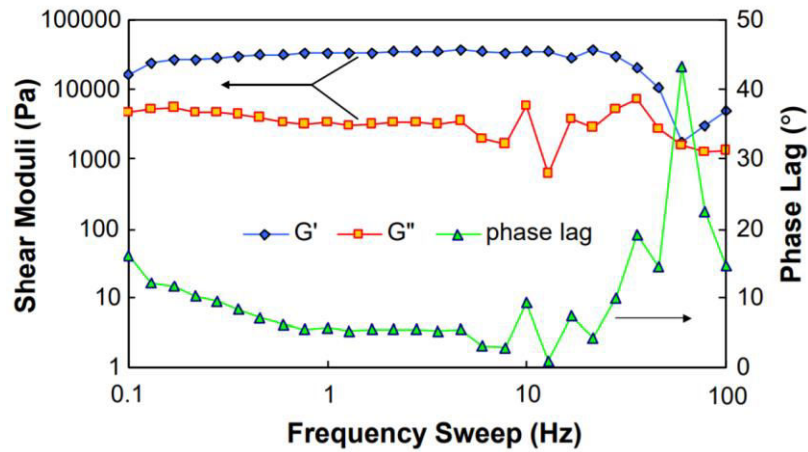


Figure 41. Shear moduli vs. frequency sweep ( $w/c=0.5$ ,  $T=25^{\circ}\text{C}$ ) [119].

**Creep** tests consist of a step or sudden application of a stress that results in a progressively increasing strain, which is measured over time. The compliance is the ratio of strain to stress, and can be fitted to a viscoelastic model [88]. In real application, adhesive mortars are subjected to a stress after a ceramic tile is put in the wall, and it should be able to hold the tile's weight without any creep/slip. Creep tests are already reported in literature to offer close results with yield stress estimated with flow curves by Hershel-Bulkley model [88,121]. Struble and Schultz [122] evaluated creep recovery of cement pastes and could observe a clear change in creep behavior above a critical stress level: at lower stress the behavior is characteristic of a viscoelastic solid with a retarded elastic strain while at higher stress the strain increases continuously and almost linearly with time, with no recovery when the stress is removed – behavior characteristic of a liquid. This transition also had strong relation with yield stress. Qian and Kawashima [121] found creep tests effective to measure static yield stress and structural rebuilding of fresh cement pastes.

**Stress relaxation** tests consist of applying a step strain deformation to generate an instantaneous strain and to monitor the stress decay as the sample is held over time in the same constrained state. It is similar to creep tests, but apply a constant stress and measures the strain variation, and stress relaxation apply a constant strain deformation step and measures the stress variation. The relaxation modulus is the ratio of the stress to the applied strain, and its variation can be fitted to a suitable viscoelastic model [88]. Either just the initial and equilibrium (long term) values are measured or the whole curve is fitted by computer to an exponential decay model with one or more relaxation times, estimated as a spectrum [98]. This is relevant for materials subjected to repetitive strain, to determine if the stress can be dissipated with the time scale of typical use. Overloading of stress in a material can cause damage and failure in later

use. In cementitious materials, this test can potentially provide information of the solid-like behavior; however, during the test, the sample is affected, which may affect the structure building of the paste.

### 3.2.2.1.3 Types of geometries

For rotational and oscillatory shear rheometry, different types of geometries are used, being the most usual: (a) Cup and Bob; (b) Cone and Plate; (c) Parallel Plates.

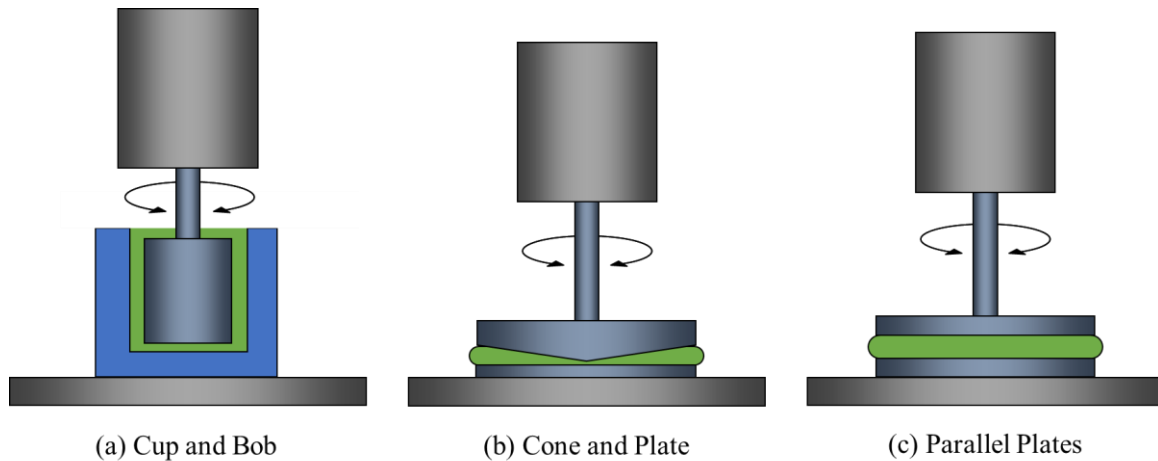


Figure 42. Geometries used for rotational rheometry: (a) Cup and Bob; (b) Cone and Plate; (c) Parallel Plates.

In addition to these examples, a variety of geometries can be used and designed depending on the type of material and measurements requirements, following the same physical principles. There are specific geometries that can measure rotational and oscillatory measurements of an interface (air-liquid or liquid-liquid), and these are going to be discussed on Chapter 4, where interfacial rheology concepts will be introduced.

There are different types of cup and bob types, some of them are illustrated on Figure 43.



Figure 43. Haake viscometer SV geometries: vane with six-bladed (left), serrated cylinder (middle) and smooth cylinders (Right) [123].

The concentric cylinder geometry is used for measuring the viscosity of liquids, it is an attribution to Maurice Couette in XVIII century [124]. Compared to the other examples shown in Figure 42, concentric cylinders have the advantage to be able to measure fluids that have the tendency to spread on the rheometer base. However, this geometry may have issues with wall-slip for measurements of cementitious materials, and to obtain reliable results, it is necessary to ensure the no-slip boundary condition. The vane geometry shown on Figure 43 (left) is a bob type, but it has fins to induce the flow, which can vary in quantity of fins. This geometry became popular in the past decades, since it eliminates serious wall-slip effects, besides the simplicity of fabrication and ease to clean [123].

In geological studies, vane shear strength is a standard test for evaluating the rheology of soils in situ [125]. Since most of cementitious materials raw materials have either an unprocessed or processed geological material, these similarities are undeniable, and scientific and technological exchange is frequent.

The cone and plate and parallel plates geometries are similar in its concepts. The cone and plate geometry has the advantage of demanding low amount of sample material, it is easy to clean and it also has a homogeneous strain field. On the other hand, cone and plate is not recommended for testing materials that contain particles, as cement pastes or mortars, because if the diameter of the particles is not about five to ten times smaller than the gap, there is a risk of “jamming” at the cone center, disturbing the data. The parallel plate geometry has the

advantage of having a homogeneous gap, then it is adapted to measure materials with particles such as cement pastes.

Geometry is often used to evaluate cement pastes properties. Ferraris studied effect of the gap on the use of rotation rheometry of cement pastes to predict concrete rheological properties with parallel plates [126]. Full comprehension of concrete and mortar rheological properties is limited when aggregates, and often, a further understanding is only possible by measuring the paste properties separately, where a precise measurement can be done with a rheometer. To avoid slip problems in this geometry, the geometry can either have a standard roughness such as cross hatch or sand blasted surface, or a sand paper can be attached to the geometry.

Parallel plates can also be used for squeeze flow and tack test (or pull out) as it will be discussed on sections 3.2.2.2 and 3.2.2.3, this can be an advantage when resources are limited and not many geometries options are available. Kaci et al. [127] studied the relationship between rheological and adhesive properties of fiber-reinforced joint mortars, using a vane geometry for rheological measurements and parallel plates for tack tests. From those results, yield stress and flow behavior predicted by vane geometry find to correlate to cohesive properties measured by tack test, though differences may occur due to extension-induced and shear-induced orientations of the fibers.

In the present research, cup and bob geometry was mostly used for rotation and oscillatory measurements, and as it will be discussed on Chapter 4, item 4.3.3.3, this geometry ability to measure at different depths of the sample and to enable superficial evaporation are going to be essential for interfacial measurements. Parallel plates, for example, despite being often used in the cementitious material field, do not allow researchers to consider water evaporation on rheological measurements, and varying the depth of the sample is not possible. Adhesive mortars considered in this work contain particles of a maximum of 600 microns, then the full system could be evaluated. This is an advantage considering the potential of the use of the techniques in industry where the final product is considerably more complex than laboratory formulations, then being able to evaluate the entire system is a requirement.

### 3.2.2.2 Squeeze flow

Squeeze flow is a measurement technique that consists on compressing a cylindrical sample with two parallel plates. The technique is widely used on other fields as cosmetics, ceramics, food and composites [88,128–132]. The large range of application is related to the absence of many problems found in rheological measurements, as loss of contact between the material and the shearing element, fibers entanglement, capillary clogging and restrictions due to torque





limitations [133]. Its use is becoming more frequent as an alternative/complementary method for cement-based pastes [134–136] and mortars [137–141], especially to simulate flow situations associated to geometric restrictions (extrusion, spreading, brick laying, flow through a nozzle during pumping or spraying) [142].

In the test, the sample is compressed at constant velocity and the normal force is measured, as illustrated in Figure 45. In Figure 44, a typical squeeze flow curve of a mortar shows three stages of behavior: Stage I: small strain — elastic deformation; Stage II: moderate strain — plastic deformation or viscous flow; and Stage III: large strain — strain hardening. Similar to the rotation rheometry, it is possible to either compress the sample at a constant velocity and measure the force or at a constant force and measure the displacement [128].

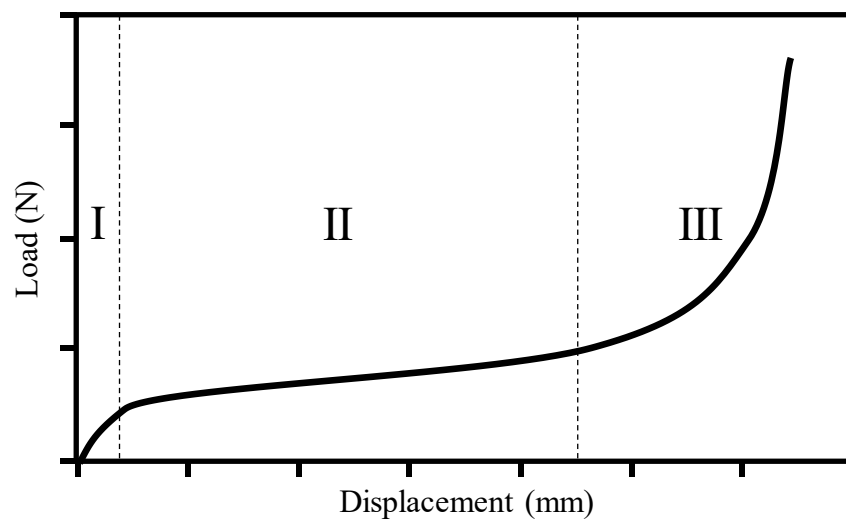


Figure 44. Typical load vs. displacement curve of a displacement-controlled squeeze flow test, illustrating the three main stages of the material's behavior. Stage I: small strain — elastic deformation; Stage II: moderate strain — plastic deformation or viscous flow; and Stage III: large strain — strain hardening [138].

The squeeze test can also be done with a constant volume, where the plates are much bigger than the sample, and the contact between the sample and the plates varies. This configuration can have two different test conditions: no slip and free slip. In the case with no slip, the sample flow is heterogeneous through the sample. In the case with slip, the dilatation is homogenous over the height of the sample. The slip configuration is useful to evaluate compaction and compressibility of mortars, especially with high degrees of entrained air. It can be more relevant with adhesive mortars since it can relate to the adhesive mortar squeeze during the application of the tile.

Toutou et al. [137] introduced the squeeze flow technique to evaluate cement-based material extrusion ability. The similarity of extrusion flow and induced squeezing test flow allows the

technique to work as an extrusion-ability-identifying tool. Mortar with low extrusion ability, when squeezed high compression speeds, show homogeneous and cohesive plastic behavior. However, at low compression speeds, the material shows a drained and frictional plastic behavior. This effect is related to extrusion, since the same percolation of the paste can also be induced during the flow. Collomb et al. [131] investigated theory behind this behavior, though the study of concentrated suspensions of spheres in both Newtonian and shear-thinning fluids is investigated experimentally. The authors verified that the transition between the two regimes is controlled by a Peclet number defined as the ratio of the characteristic time of the fluid filtration through the porous media made up by the particles to the characteristic time of the suspension flow.

Recently, Cardoso et al. [142] verified a phase segregation effect on cement pastes while being squeezed during rheometer's test preparation; the results show that it has an impact on rotational measurements in rheometers. This may extend to many materials where phase segregation may be an issue, so this technique has a great potential to predict rheological measurement issues due to phase segregation, as well as offering understanding for avoiding these issues.

Cardoso et al. [133,138,139] studied the use of squeeze flow for rendering mortars, finding good correlation with the applicator feeling while spreading and prediction of phase segregation, enabling optimization of formulations with the technique.

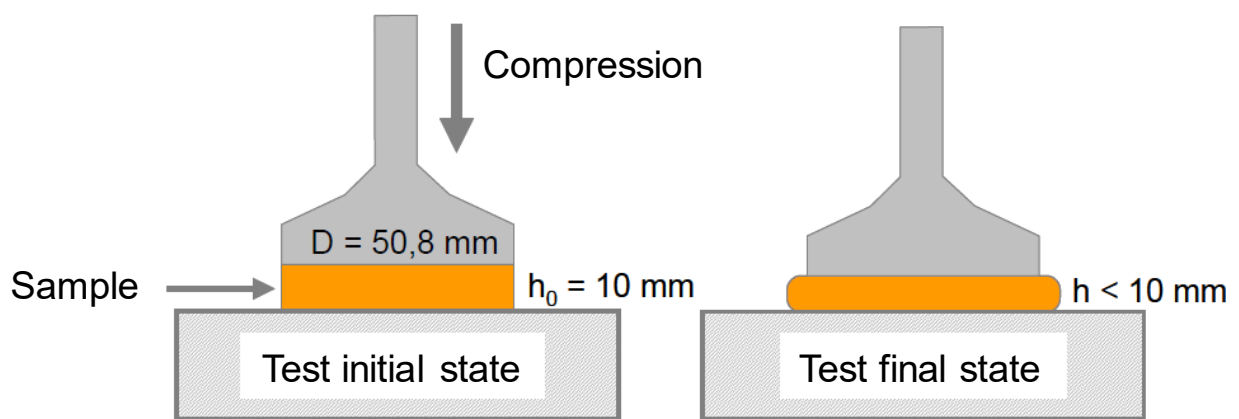


Figure 45. Scheme of initial and final test conditions of squeeze flow in a constant area configuration.  $D$  = upper plate diameter;  $h_0$  = sample initial height;  $h$  = sample final height, which depends on the plate displacement [133].



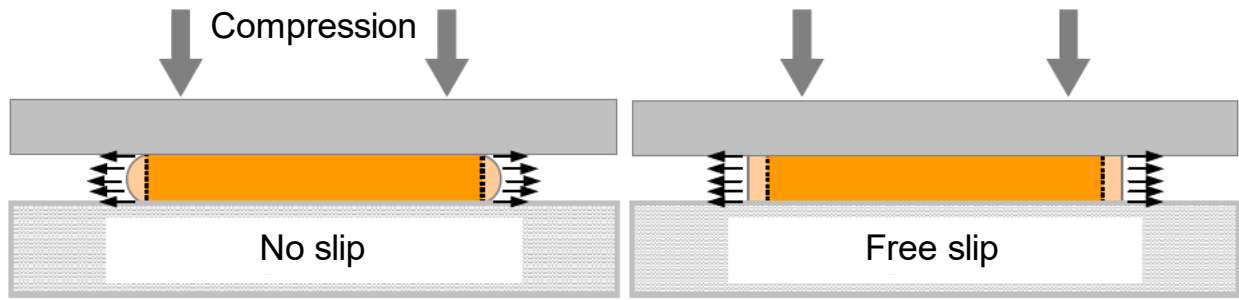


Figure 46. Constant volume configuration. Example of flow lines for the interface slip conditions – no slip (infinite friction) and free slip (no friction) [133].

Phase separation can also be a problem in Self-Compacting Concretes (SCC), since the paste requires very low viscosity necessary to “self compact” by itself. Phan & Chaouche [136] used squeeze flow to evaluate different cement pastes qualities, and verified an undergoing fluid-solid separation due to filtration of the fluid phase through the porous media made up by the grains.

Recently, the Brazilian association of technical standards published the NBR 15839:2010 - Rendering mortar for walls and ceiling – Rheological evaluation by squeeze flow. As a guide for industrials and researchers evaluate rheological properties of mortar through squeeze flow. In Figure 45, the test configuration described on the Brazilian standard is shown. The test however could have different configurations of initial height and sample form. Another common configuration is where the material volume is constant, and the contact of the material is variable.

The Brazilian standard, however, is applied for rendering mortars, and for tile adhesive, it has the limitation of depending on the ability to demold the sample, which is more complicated due to tile adhesive “stick” consistency. The test was also adapted for adhesive mortar, by the use of a circular material mold that can be used during the test [46,143].

This method is also useful to verify phase segregation of liquid and solid phases. This technique can predict phase segregation tendency that can be problematic during pumping by causing block of the flow. Chaouche et al. [130] studied squeeze flow of liquid phase in a granular system, and depending the squeezing conditions (fluid viscosity, grains size, squeeze velocity) phase segregation can be induced. It was found that smaller squeezing velocities intensifies phase segregation tendency.

Depending on the suspension, during the squeeze, the fluid phase can have a more intense flow to the outer part of the sample generating a dryer and highly concentrated material in the middle, which will cause an increase of squeezing forces. This problem is often neglected in rheological



measurements in which squeezing is part of the sample preparation. Cardoso et al. [142] showed that during the sample preparation of parallel plates rheometry, phase segregation can be induced, generating a more concentrated and inhomogeneous material, which can cause measurement errors.

For adhesive mortar in general, due to the high concentration of cellulose ether, this effect is usually less important due to the high cellulose ether content. Cellulose ether increases the viscosity of water, which in the cement pastes and mortars represent the interstitial liquid, and with a higher viscosity, the fluid phase will have more difficult to percolate through the solid phase. In other words, the increase of the fluid phase viscosity, will reduce the Darcy's law effect, which is the theory that describes the flow of fluid in a porous media.

The shear properties of the material can be obtained by squeeze flow data. Power law fluid properties can be obtained, for example, in the case of non-lubricated parallel plate squeeze flow, when the material adheres firmly to the plate. Other approaches can also evaluate Newtonian fluids and lubricated conditions, but in this investigation, mainly non-lubricated conditions were considered.

Nonlubricated squeezing flow produces a barreling effect due to shear flow caused by adhesion of the sample to the plates. The resulting complex flow is not purely viscometric or extensional, but some combination of each [144].

The nonlubricated squeezing flow of a power law fluid, in an experimental system using an immobile bottom plate with a full gap, is [145]:

$$F = \left(\frac{2n+1}{n}\right)^n \left(\frac{2\pi KR^{n+3}}{n+3}\right) \left(\frac{u_z^n}{h^{2n+1}}\right) \quad (9)$$

where  $h = f(t) = h_0 - u_z t$ . Winther et al. [145] suggest evaluating Equation ( 9 ) by multiplying both sides by h giving:

$$Fh = \left(\frac{2n+1}{n}\right)^n \left(\frac{2\pi KR^{n+3}}{n+3}\right) \left(\frac{u_z^n}{h^{2n}}\right) \quad (10)$$

then, taking the logarithm of each side of the equation, to get:

$$\ln(Fh) = \ln \left[ \left(\frac{2n+1}{n}\right)^n \left(\frac{2\pi KR^{n+3}}{n+3}\right) \right] + n \ln \left(\frac{u_z^n}{h^{2n}}\right) \quad (11)$$

Using Equation ( 11 ), n may be found from the slope of  $\ln(Fh)$  versus  $\ln(u_z/h^2)$ . The value of K is determined from the intercept. Since the inertia terms in the equations of motion are neglected in developing Equation ( 11 ), the earliest data points may not lie on the line and should be neglected [144]. The average shear rate for a power law fluid nonlubricated is [145]:



$$\dot{\gamma}_{average} = \left( \frac{2(2n + 1)}{3n} \right) \left( \frac{u_z R}{h^2} \right) \quad (12)$$

### 3.2.2.3 Tack test

The pull-out test or tack test is commonly used to evaluate adhesiveness, especially polymeric adhesives. In granular mineral or granular materials, however, it has been much less researched. Mohamed Abdelhaye et al. [146] evaluated the tackiness of smectite muds in diluted regime. Kaci et al. [127] studied the effect of fiber-reinforced mortars with different fiber content and at different velocities, where it was found that higher fiber content reduced adherence, but increased cohesion when it was over a certain minimum content.

In construction, applicators usually evaluate if the adhesive mortar is tacky with the thumb or after applying the tile to the mortar, verify if the material transfer to the tile, but this is rather subjective and not quantitative.

Tack testing can be described as the opposite test of squeeze flow, consisting of pulling out the material. However, differently from squeeze flow, it evaluates the “stickiness”. Evaluating tackiness of an adhesive is important to evaluate initial bonding, otherwise, after the tile is applied, it may result in detachment or unperfect attachment that can cause problems on the system serviceability. Also, the applicator feeling quality of an adhesive is also related to the tackiness, cohesive rupture, which means, a rupture that occurs at the adhesive, not at the interface between the substrate and the adhesive, is considered a “good adhesive”. Two main types of rupture mode can occur in this test in the case of adhesive mortars:

- **Cohesive rupture:** occurs at the material, can be either long and present stringiness or sudden brittle fracture;
- **Adhesive rupture:** occurs at the interface between the adhesive and the substrate or geometry.



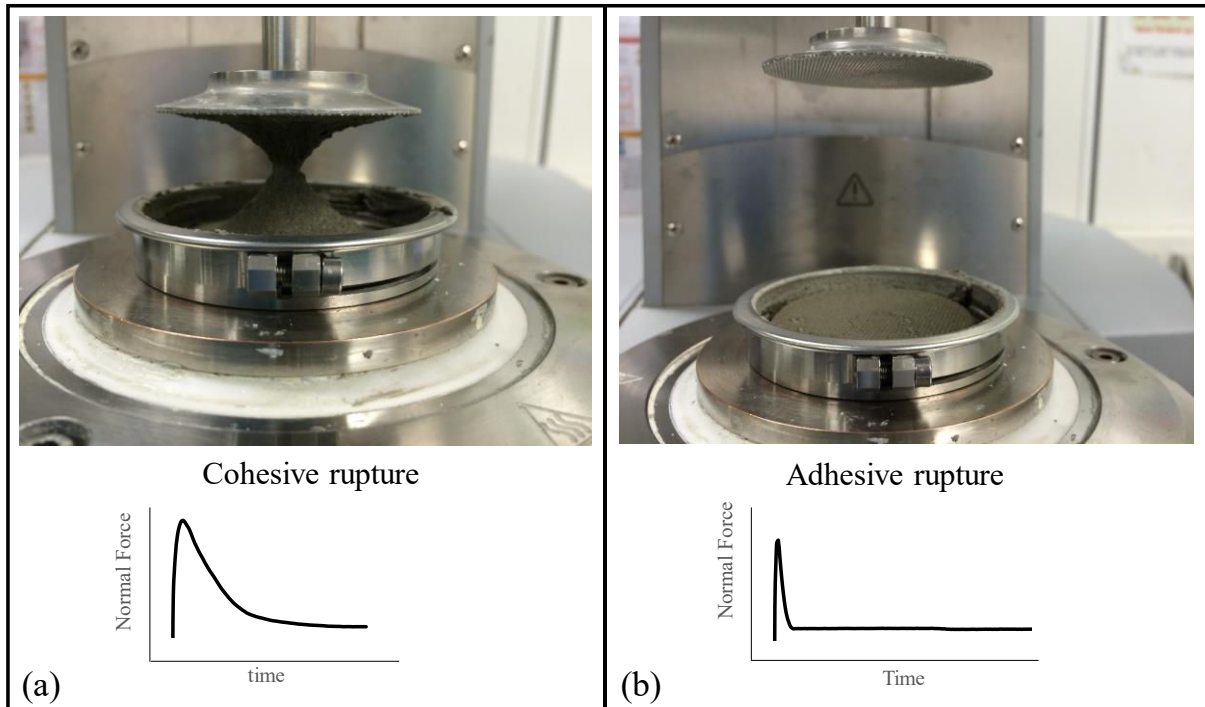


Figure 47. Failure modes on tack test: (a) Cohesive rupture and (b) Adhesive rupture

In the case where adhesion to the plates is not an issue, only cohesive ruptures are obtained. Into the detail of cohesive ruptures, different types of failures modes can occur. In Figure 48, three modes of failure are sketched: A, B and C. In mode A, the paste was flowing towards the center of the plates and the pattern just before debonding is a central and narrowing paste column. In mode B, several narrow columns are formed, much like with very soft PSAs, and a thin layer of paste is remaining on (almost) the total plate surfaces. Finally, in mode C, a thin and homogeneous but very rough and prickly layer of paste remains on each plate. Mode B and mode C are clearly akin to each other. [147].

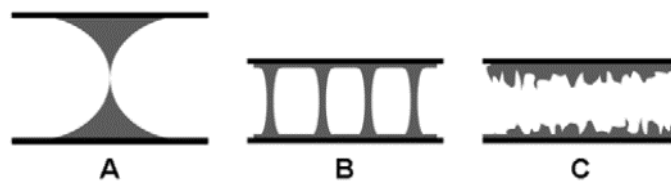


Figure 48. Cartoon illustrating schematically three different failure modes [147].

These failure modes will influence the tackiness, the displacement or normal force generated during a tack test. In this work, since the test was done at a constant velocity, the normal force variation was evaluated.

When evaluating a tack test result, different parameters can be evaluated. The peak force ( $F_{max}$ ) is the maximum normal force achieved during the pull out, it is related to viscous dissipation

(dynamic property) and cohesion strength (static property) whose origin includes intermolecular and capillary forces. A common cohesive rupture displays a curve similar to Figure 49, which can be divided in three zones [28,127]:

Zone 1: the force first increases until it achieves  $F_{max}$ . The mortar displays mainly elastic and then viscoelastic behavior. The force peak is related to the adhesive strength of the material

Zone 2: the decrease after  $F_{max}$ . The material has an irreversible rupture and inward flow of the material towards the plates center. Analysis of the force decay in this zone allows characterizing rupture dynamics of the mortar.

Zone 3: starts as soon as the rupture process is completed. The average value of the force plateau is related to the amount of material remained stuck onto the mobile plate. This gives the adherence strength of the mortar relative to the surface of this plate.

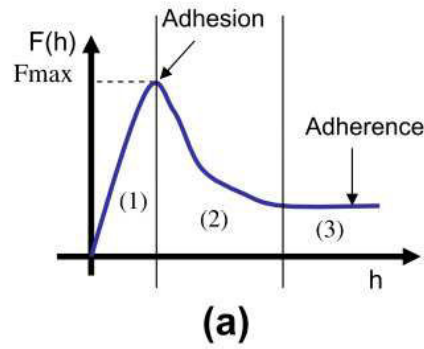


Figure 49. Analysis of the tack test results. (a) General shape of the tack force curves; (b) evolution of the force peak versus stretching velocity [127].

The peak force can be estimated with flow index ( $n$ ) and consistency ( $K$ )

$$F_{max,calc} = 2\pi K \frac{(2 + 1/n)^n u_z^n R^{3+n}}{(3 + n) h^{1+2n}} \quad (13)$$

Where  $F_{calc}$  is the estimated peak force, “ $h$ ” is the sample height, and  $u_z$  is the velocity of the pull out. With  $F_{max,calc}$  calculated with equation ( 13 ), the maximum pressure drop can be obtained by the following equation:

$$\Delta p_{max} = |\Delta p_{min}| - |\Delta p_{atm}| = \frac{(3 + \alpha) F_{max}}{(1 + \alpha) \pi R^2} \quad (14)$$

Abdelhaye et al. [147] studied the influence of the plate diameter, the gap, the pull out velocity and the type of the paste on tack test.



Another parameter that can be calculated from tack test curves is the energy of failure, which is proportional to the area under the tack test normal force vs displacement curve as illustrated on Figure 50.

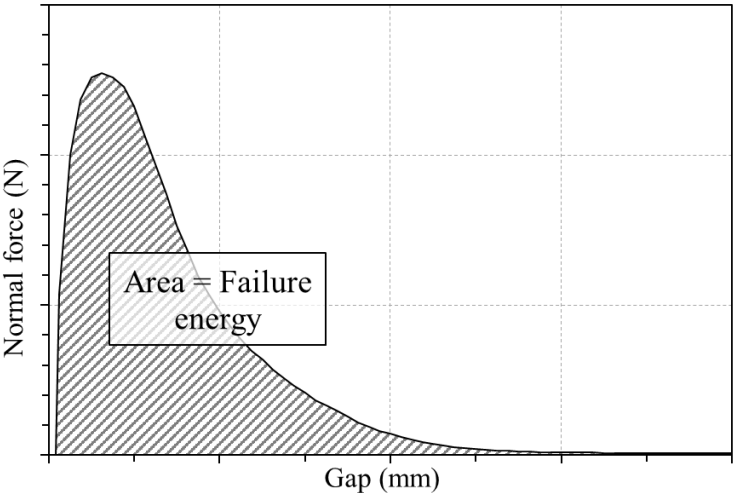


Figure 50 . Graphical representation of failure energy.

The adhesive failure energy ( $W$ ) can be calculated through the Equation ( 16 ), where  $F$  is the normal force and  $A$  the contact area, as it was defined by Andrews, Gent and Kinloch.

$$W = \frac{1}{A} \int F \cdot v \, dt \tag{15}$$

The same equation can be written in function of the gap with ( 16 ).

$$W = \frac{1}{A} \int F \, dh \tag{16}$$

### 3.3 Experiments

#### 3.3.1 Materials and formulations

This work used basic compositions of adhesive mortars with white and gray CEM I 52,5 N CE CP2 NF from Lafarge. Cement phases, density and blaine fineness obtained with the manufacturer are shown in Table 5. The gray cement color is attributed to a higher iron content and it is more abundant, consequently being more commonly used. White cement, however, is often used in adhesive mortars and other application mortars because of aesthetic requirements related to color.

Table 5. Phase compositions, density and blaine fineness of the investigated cements

Phase	white CEM I	gray CEM I
C <sub>3</sub> S (wt%)	58	61
C <sub>2</sub> S (wt%)	28	14.3





<b>C<sub>3</sub>A (wt%)</b>	6	12
<b>C<sub>4</sub>AF (wt%)</b>	1	7.9
<b>Gypsum (wt%)</b>	5	4.6
<b>Density (g/cm<sup>3</sup>)</b>	3.08	3.14
<b>Blaine fineness (cm<sup>2</sup>/g)</b>	4250	3519

The sand used in this study was a silica sand PE2LS from FULCHIRON. ASTM granulometric distribution from the manufacturer is shown on

Figure 51.

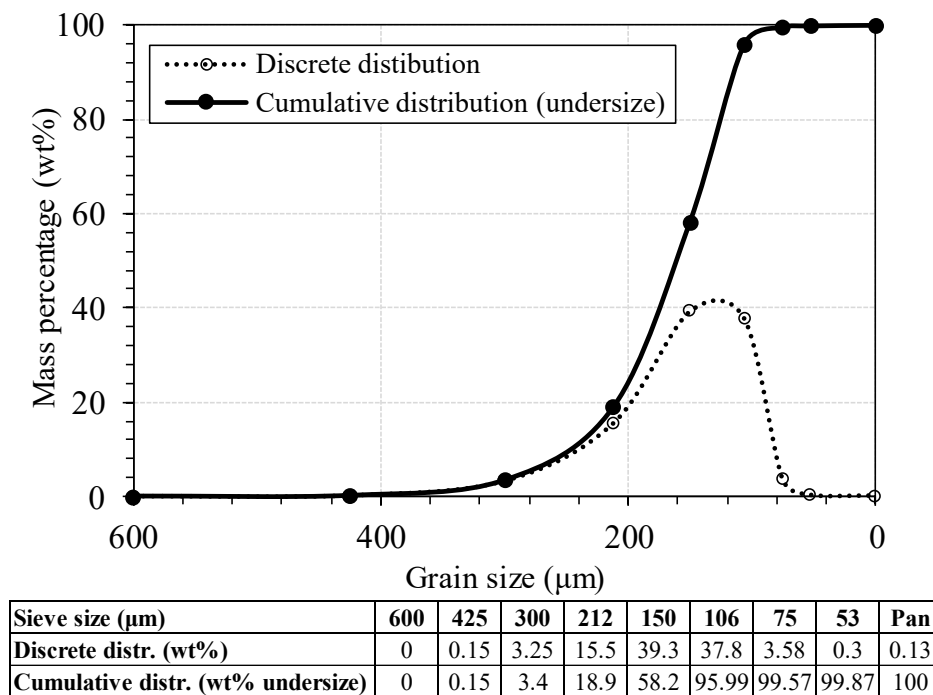


Figure 51. Granulometric distribution of sand used in this investigation obtained from the manufacturer

Common formulations of adhesive mortars were used (Table 6). Besides white or gray Portland cement and silica sand, two types of polymers were used: an organic binder in redispersible powder form (latex: vinyl acetate, vinyl versatate and a maleic ester copolymer resin) and an organic modifier (CE: hydroxyethyl methyl cellulose). The CE samples were provided by *Dow Chemical Company* and used as received. They varied in the following molecular parameters: viscosity, molar substitution ratio (MS) and degree of substitution (DS). These parameters were provided by the manufacturer and are shown in Table 7. The viscosity corresponds to that of a 2% by weight aqueous polymer solution, as measured with a Brookfield RV viscometer at 20 rpm. The value of the viscosity gives an indication of the average molecular weight of the polymer. Yet, the interstitial solution in the mortar matrix presents a different pH and ionic strength that may affect the polymer interactions and, as result, may affect the final viscosity



that would be obtained. The latex used was a commercial redispersible polymer powder form provided by *Momentive*.

Different contents of CE (CE-A) were used and three different cellulose ethers with varying degree of substitution and molecular weight were also employed (CE-A, CE-B, CE-C). No formulation with less than 0.1% of CE was used to avoid significant phase separation. The formulations names in Table 6 are defined to its content: “w” or “g” refers to white or gray cement; the percentage is the CE content and; “A”, “B” or “C” refers to the type of polymer. Entrained air was calculated from the density measurements done with a cup of known volume of 314 ml and the density could be calculated by the mass.

The amount of substituent groups on the anhydroglucose units of cellulose can be designated by weight percent or by the average number of substituent groups attached to the ring, a concept known to cellulose chemists as "degree of substitution" (DS). The number of substituent groups on the ring determine the CE properties, such as water solubility. Too low DS may generate CE with lower water solubility, leading to additives that are only soluble in caustic solutions. Too high DS may produce additives that are soluble only in organic solvents. The Molar substitution (MS) reports the number of moles of hydroxypropyl groups per mole of anhydroglucose [12]. The different CE used in this research have different chemical structures, but equal nominal viscosity. The viscosity can be controlled by the degree of polymerization.

Table 6. Formulations of adhesive mortars with gray cement, with different cellulose ether content and types (wt%)

Formulations	gray CEM I	white CEM I	sand	latex	CE-A	CE-B	CE-C	water/ powder	entrained air
w_0.1% CE-A	-	30%	67.40%	2.5%	0.1%	-	-		14%
w_0.25% CE-A	-	30%	67.25%	2.5%	0.25%	-	-		19%
w_0.4% CE-A	-	30%	67.10%	2.5%	0.4%	-	-		21%
w_0.25% CE-B	-	30%	67.25%	2.5%	-	0.25%	-		20%
w_0.25% CE-C	-	30%	67.25%	2.5%	-	-	0.25%		19%
g_0.1% CE-A	30%	-	67.40%	2.5%	0.1%	-	-		13%
g_0.2% CE-A	30%	-	67.30%	2.5%	0.2%	-	-	0.205	20%
g_0.25% CE-A	30%	-	67.25%	2.5%	0.25%	-	-		20%
g_0.3% CE-A	30%	-	67.20%	2.5%	0.3%	-	-		22%
g_0.4% CE-A	30%	-	67.10%	2.5%	0.4%	-	-		22%
g_0.5% CE-A	30%	-	67.00%	2.5%	0.5%	-	-		22%
g_0.25% CE-B	30%	-	67.25%	2.5%	-	0.25%	-		19%
g_0.25% CE-C	30%	-	67.25%	2.5%	-	-	0.25%		18%

Table 7. Properties of the cellulose ethers used in this investigation, as provided by the manufacturer: Viscosity (mPa.s), molar substitution (MS) and degree

Labels in text	Viscosity (mPa.s)	MS	DS
----------------	-------------------	----	----



<b>CE-A</b>	40000	0.2-0.25	1.62-1.65
<b>CE-B</b>	40000	0.1-0.2	1.8-1.9
<b>CE-C</b>	40000	0.2	1.4

### 3.3.2 Methods

#### 3.3.2.1 Flow rheometry

Flow measurements were done in a rheometer MCR 301 from *anton paar* with a vane geometry. Vane is a commonly used geometry and one of its advantage is that wall slip is minimized, in comparison to other types of other types of geometry such as cylindrical [123]. The system vane geometry and cup as illustrated on Figure 52. The measurements consisted in one cycle of acceleration and deceleration from  $0 \text{ s}^{-1}$  to  $50 \text{ s}^{-1}$ , and  $50 \text{ s}^{-1}$  to  $0 \text{ s}^{-1}$ , and the shear stress was obtained. This allowed to evaluate the mortar behavior in different levels of shear. Each formulation was mixed in a planetary mix, according to EN-196-1, put in the rheometer cup, the excess material removed with the help of a common spatula and the cup was inserted in the rheometer for the test.

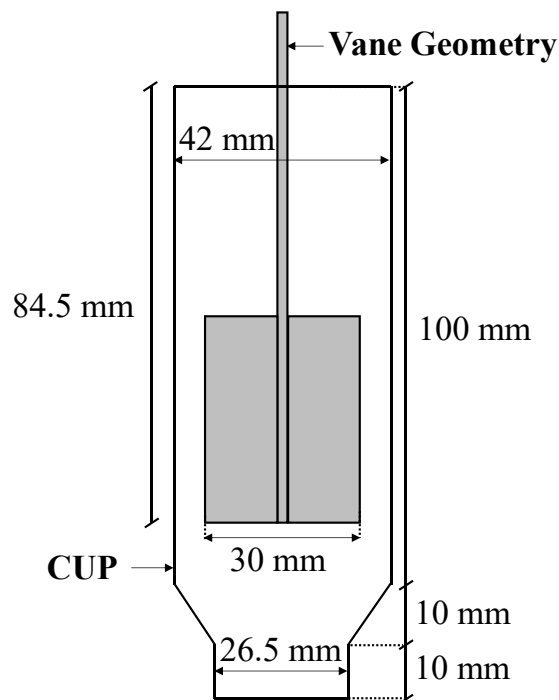


Figure 52. Rotational and oscillatory rheometry vane geometry and cup system dimensions used in this investigation.

#### 3.3.2.2 Oscillatory rheometry

Oscillatory measurements were done in a rheometer MCR 301 from *anton paar* with vane geometry as for flow measurements. The amplitude strain was defined as 0.05%, at the linear



viscoelastic region in strain sweep tests. The vane geometry and cup system are the same used for rotational rheometry of this section as illustrated in Figure 52. Each adhesive mortar formulation was mixed in a planetary mix according to EN-196-1, put in the rheometer cup, the excess material removed with the help of a common spatula and the cup was inserted in the rheometer for the test that last 2h. The environmental conditions were kept at  $23^{\circ}\pm 1^{\circ}\text{C}$  and 50% RU.

### 3.3.2.3 Squeeze and tack test

Squeeze flow and tack test measurements were done in a rheometer MCR 301 from *Anton paar* with a cross hatched geometry with a diameter of 50 mm and an aluminium cup of 52 mm. Each adhesive mortar formulation was mixed in a planetary mix according to EN-196-1.

The mortar samples were applied with the help of an aluminum tool in a cylindrical shape of 6 mm height and 40 mm diameter. Adhesive mortars consistency tends to be “stick” and hard to mold, thus, usual rendering mortars molding techniques are not efficient and causes deformed samples. Some adaptation to squeeze flow have been used by some authors. Costa et al. [143] used a cylindrical tube as mold that are many pieces assembled, during the test the pieces are able to slide with the mortar. Kudo et al. [148] used a cylindrical plastic mold that is fixed during the entire test, the puncture touches the sample and pull out the material with the wall, similar to a surface tension measurement of a liquid. The molding technique developed in this investigation prepares a uniform shape of the samples, allowing free squeeze without any constraints. The technique is based on a metallic comb that turns to form the cylindrical sample as illustrated on Figure 53.

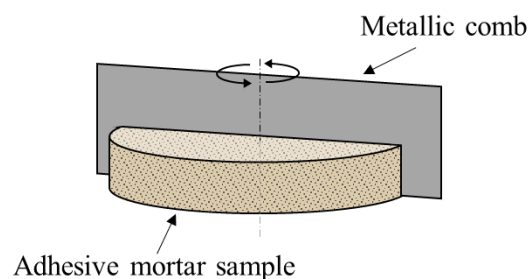


Figure 53. Illustration of adhesive mortar sample preparation: the metallic comb turns around axis to form the cylindric shape of the sample

The samples were put to rest for different waiting time, simulating mortars of different waiting times: 0, 10, 20, 30, 40, 50 and 60. After this time, the sample was put in the rheometer for the squeeze test, where it was compressed at an imposed velocity of 1 mm/s for 3 mm. The test is



then paused for 30 seconds for relaxation, and re-started with pull-out at an imposed velocity of 1 mm/s for tack test until the end of the test, resulting in a cohesive or adhesive rupture. The test set up is illustrated on Figure 54.

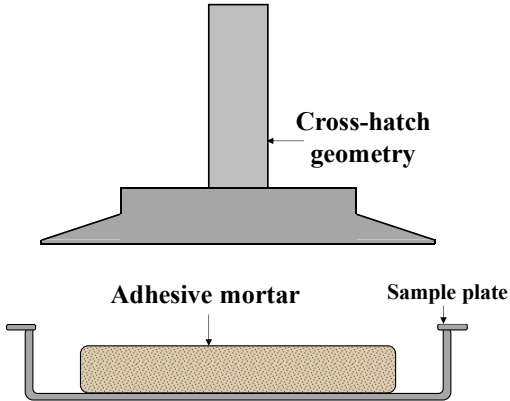


Figure 54. Scheme of squeeze flow and tack test montage – the geometry press

In this investigation, the different waiting times mortars were compressed for squeeze test until the same gap of 3 mm, thus the initial gap of the tack test was the same for all samples. The test objective was to evaluate the mortar squeezing ability and tackiness with after different waiting time.

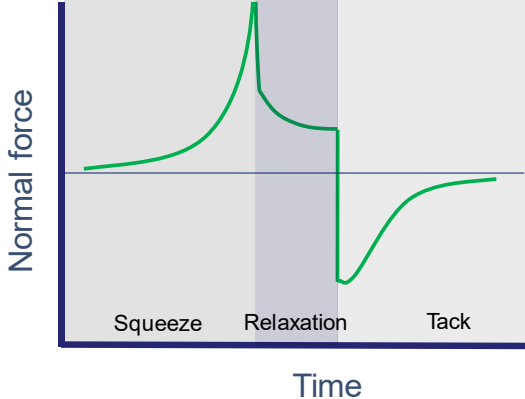


Figure 55. Simplified normal force/load vs time curve of a squeeze test, relaxation and tack test

### 3.4 Results and discussion of Chapter 3

#### 3.4.1 Bulk oscillatory properties

In this section, results of bulk rheological properties are shown and analyzed. The impact of different CE content on bulk rheological properties of mortar with gray and white cement is discussed. Then, the results of mortars with different degree of substitution’s CE are shown and discussed.



#### 3.4.1.1 Effect of CE content

In Figure 56,  $G'$  and  $G''$  evolution over time for white cement (a) and gray cement (b) mortars with different CE-A content are shown. In the graph, equal color and shape curves represent a repetition. The Loss modulus values have an inversed tendency compared to storage modulus, since w\_0.4% CE-A has higher values than w\_0.25% CE-A and w\_0.1% CE-A. These results' order of magnitude is much lower than the storage modulus since the elastic behavior is dominant. Thus, in the next sections, the  $G'$  will be mainly explored.

In the first minutes, for both types of cement,  $G'$  of the different CE content formulations are similar, with 0.25% CE-A being the lowest, then 0.4% CE-A in the middle, and 0.1% CE-A the highest. The reduction of the initial  $G'$  values of 0.1% and 0.25% CE-A is related to the air entraining effect of CE. From 0.1% CE to 0.25% entrained air increases from 14% to 19% for white cement and 13% to 20% for gray cement (Table 7). For 0.4% CE-A, however, air entrainment seems to have almost saturated, and the entrained air obtained is 21% for white cement and 22% for gray cement. The air entrainment effect is diminished at higher concentrations, the polymer thickening effect starts to influence, and  $G'$  becomes higher for higher CE-A content.

After around 8-10 minutes, an inversion of  $G'$  values occur. The formulation with higher CE content, 0.4% CE-A, became lower than 0.25% CE-A, and maintained lower values during the 2 hours of the test. This low value is probably related to the CE's ability to delay structuring of cement particles [28]. Weyer et al. [21] showed that the adsorption of the polymers onto the cement clinker phases inhibits the formation of  $\text{Ca}(\text{OH})_2$ . This is related to CE's strong influence on C-S-H precipitation, leading to a decrease in the amount of initial C-S-H nuclei, delaying the formation of a continuous C-S-H shell around the  $\text{C}_3\text{S}$  grain, and delaying the formation of a thicker and more permeable C-S-H layer.

When CE is added to a cementitious matrix, a gradual reduction of  $\text{C}_3\text{A}$  dissolution rate is observed; this is also associated with AFt and hydroxy-AFm precipitation [21,28]. Often the increase of viscosity generated by CE is associated with hydration retardation, however, Pourchez et al. [114] results have shown that the assumption of a diffusion barrier induced by the high viscous solution of cellulose ethers is not relevant.



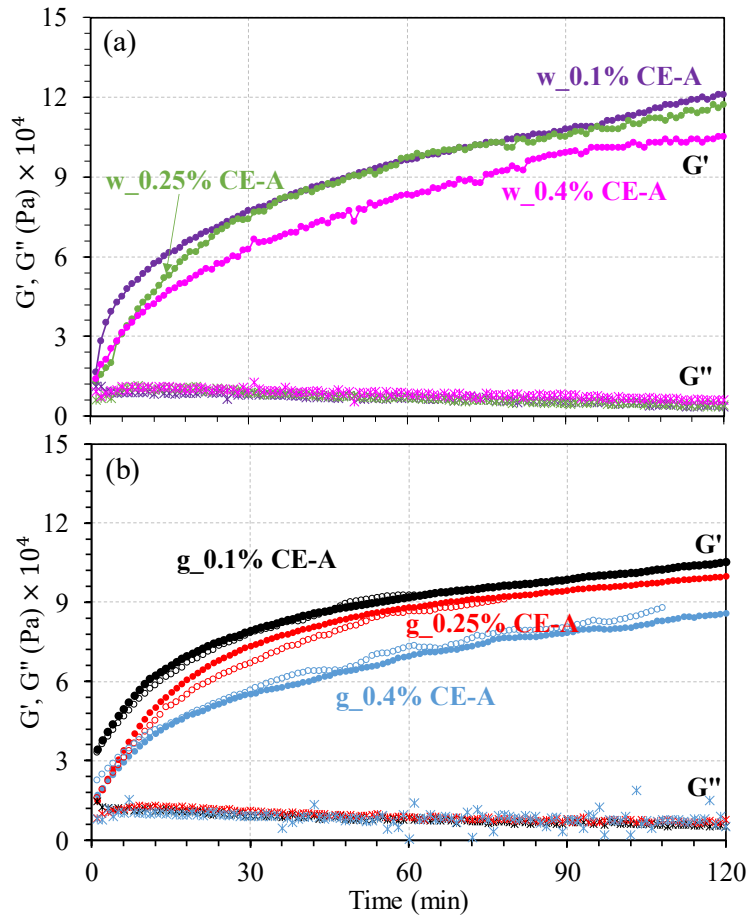


Figure 56. Storage modulus ( $G'$ ) and Loss modulus ( $G''$ ) of adhesive mortars with different CE content formulated with white cement (a) and gray cement (b).

To ensure the effect of the polymer concentration observed in the initial minutes, a series of tests with a wider range of dosages (0.1%, 0.2%, 0.25%, 0.3%, 0.4%, 0.5%) of CE were performed for gray cement and shown in Figure 57. From the initial start ( $t = 1$  minute), from 0.1% to 0.25%, the  $G'$  values decrease as dosage increases; it is related to the increase of air content, due to CE's air entraining ability. From 0.25% to 0.5%, however, the air content achieves saturation and remains stable; and as dosage increases,  $G'$  values increase, which is explained by CE's thickening effect. These results confirm the behavior observed earlier in Figure 56 with white and gray cement.

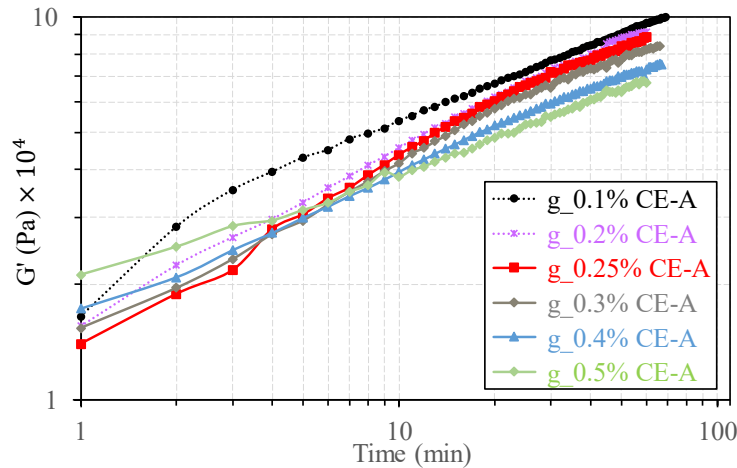


Figure 57. Storage modulus of adhesive mortar with different cellulose content formulated with gray cement.

### 3.4.2 Effect of CE types

CE is already known to delay cement hydration [30,101], and the degree of substitution is related to this effect [19]. In this section, the influence of CE type on bulk oscillatory properties of adhesive mortar with white and gray cement is evaluated.

In both types of cement, similar results can be observed in Figure 58 regarding the influence of DS on  $G'$  evolution. For both cements, the initial point of the three curves starts at the same place. This is expected since the three polymers have similar nominal viscosity and similar air entrained values. The first points represent the material just after mixing, and similar behavior is observed regardless of the DS. After the initial point, the formulation with CE-B delayed  $G'$  evolution for both cements. CE-C in both cases had a low impact on  $G'$  evolution, and in both cement types, higher  $G'$  values are observed. CE-A, however, had a slightly different effect depending on cement type. CE-A seems to have an intermediate impact in comparison to the other CE types, but for white cement, it was closer to CE-C and for gray cement, it was closer to CE-B.

The obtained results regarding the DS outcome indicate that polymer with higher DS has a stronger delay on  $G'$  evolution. As shown in Table 7, CE-B has the highest DS, around 1.8-1.9, followed by 1.62-1.65 for CE-A and 1.4 for CE-C. This result, however, is not compatible with what is found in literature. Weyer et al. [33] concluded that the lower the DS of the polymer, the stronger the retardation of  $C_2S/C_3S$ -hydration. The latter disagrees with results obtained in this investigation, where lower DS resulted in lower retardation of structuring.

The disagreement between literature and this investigation can be related to other characteristics that were not provided by the manufacturers such as molecular weight, degree of polymerization, and positioning of the free hydroxyl groups. Manufacturers of commercially





available CEs generally do not provide some of the information for confidentiality reasons [19]. Thus, even though the degrees of polymerization of the CEs in this research were not provided, it may have an influence on rheological property evolution. Pourchez et al. [149] verified that hydroxyethyl cellulose (HEC) with different molecular weights and similar degrees of substitution have negligible effects on cement hydration. The same parameter's impacts are also applied to hydroxyethyl methyl cellulose (HEMC), so perhaps molecular weight may not be the dominant parameter. The positioning of the free hydroxyl groups in cellulose ether molecules could influence the structuring process; however, other factors could also have an influence. Thus, verification is necessary.

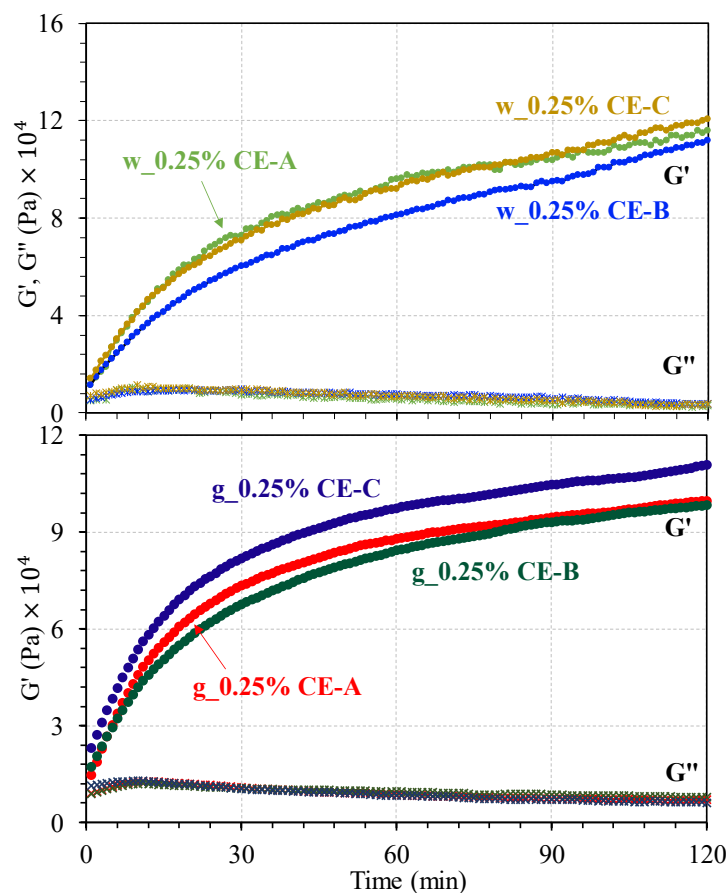


Figure 58. Storage modulus ( $G'$ ) and Loss modulus ( $G''$ ) of adhesive mortars with different CE types formulated with white cement (a) and gray cement (b).

As shown in Figure 58, the CE-A had a different impact on  $G'$  structuring depending on the cement type. This is probably related to the differences of the phases of each cement. From Table 7, while both cements have similar  $C_3S$  content (white cement – 58%; gray cement – 61%),  $C_2S$  is about 2 times higher for white cement (white cement – 28%; gray cement – 14.3%). Since CE affects  $C_3S$  and  $C_2S$  hydration, it is expected that the polymers have a

different effect on hydration and, consequently, influence the structure building of the mortar. Previous research demonstrated that CE adsorption is phase-specific and HEMC polymers also have impacts on the  $C_3A$  phase, even though HEMC's influence is lower than HEC polymers [150]. Since gray cement  $C_3A$  content is 2 times higher than white cement (white cement – 6%; gray cement – 12%), this is probably another source of variation on the effect. The impact of the DS is not fully understood, and further studies would be necessary to explain the behavior showed in this investigation. Molecular length measurements would be a possible approach to further understand the results.

### 3.4.3 Flow rheological properties of mortars with different CE content

Cellulose ether (CE) has a great effect on adhesive mortars flow properties as it can be observed on flow curves of adhesive mortar formulated with gray cement and different CE content in Figure 59. From the acceleration and deceleration cycle, the CE thickening effect is clearly observed on mortar viscosity, as the shear stresses are higher for higher CE content. The formulations with higher CE content, g\_0.25% CE-A and g\_0.4% CE-A show less hysteresis if compared with g\_0.1% CE-A.

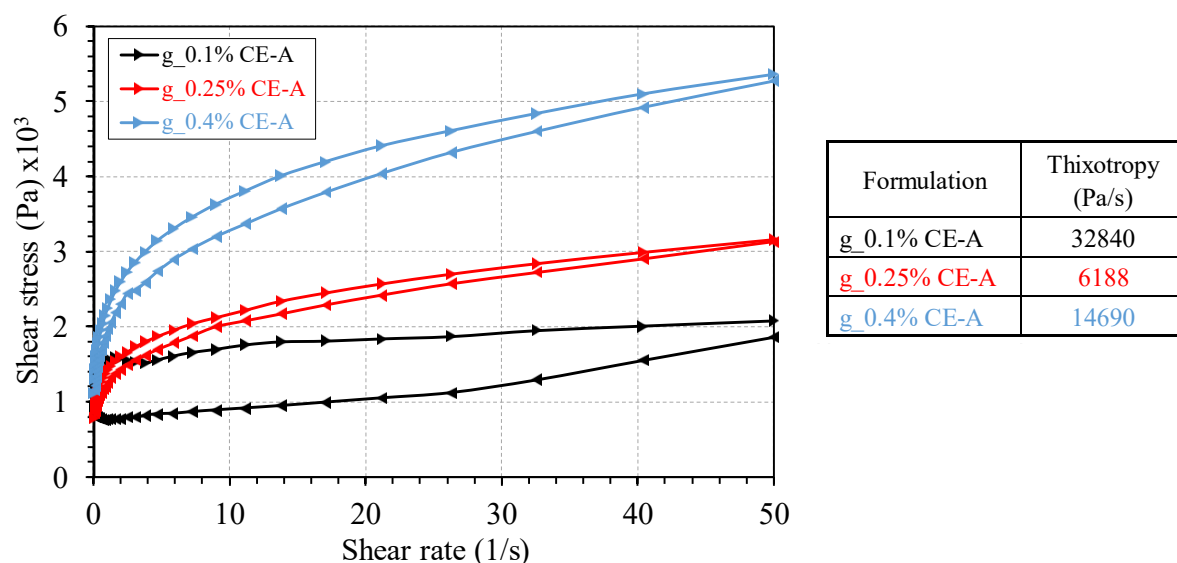


Figure 59. Flow curve cycle of acceleration (►) and deceleration (◄) of adhesive mortars formulated with gray cement and different CE content and table with thixotropy values.

The flow curves and the thixotropic values obtained are shown in Figure 59. The thixotropy values were obtained through hysteresis loop area. The values of thixotropy for the formulation with lower CE content, g\_0.1% CE-A, is 32840 Pa/s, when CE content increases to 0.25% CE-A is reduces to 6288 Pa/s and then increases to 14690 Pa/s. The thixotropy of the the



formulation g\_0.1% CE-A is considerably higher, which may be an indication of phase segregation effect, even though minimal value of CE content intended to avoid considerable bleeding [139]. Phase segregation generate high hysteresis areas because during the acceleration, the solid phase may tend to concentrate out of the shearing zone and the shear may concentrate in a material with higher water/solids ratio, which will cause a deceleration with lower stresses to generate flow are reduced since particles friction are reduced. Viscosity-enhancing admixtures (VEAs) such as CE are used to improve highly flowable cement-based materials to maintain homogenous suspension in the plastic stage [151]. Khayat et al. [151] verified that low dosages of liquid based CE not efficient in eliminating static and forced bleeding. The dosage of g\_0.1% CE-A may have not been enough to avoid phase segregation effect and generated a greater hysteresis area. With higher dosages of CE, g\_0.25% CE-A and g\_0.4% CE-A, however, the content of CE was sufficient increase of liquid phase viscosity and generate a stabilized mortar. The g\_0.4% CE-A formulation hysteresis area is about 2 times higher than g\_0.25% CE-A; this may be associated to the higher content of CE, which will generate a solution with more associative polymer disentanglements during acceleration, and consequently a deceleration with lower shear stresses [87].

The Herschel-Bulkley model was used to describe the behavior of adhesive mortar, which CE content are usually around 0.25% for this type of CE – higher than 0.1%. It has been largely used in literature for cementitious material behavior, but when applying any mathematical model, caution is needed. Figure shows Herschel-Bulkley model applied to g\_0.25% CE-A and g\_0.4% CE-A. The fitting with this model is fairly well, presenting a low standard error.

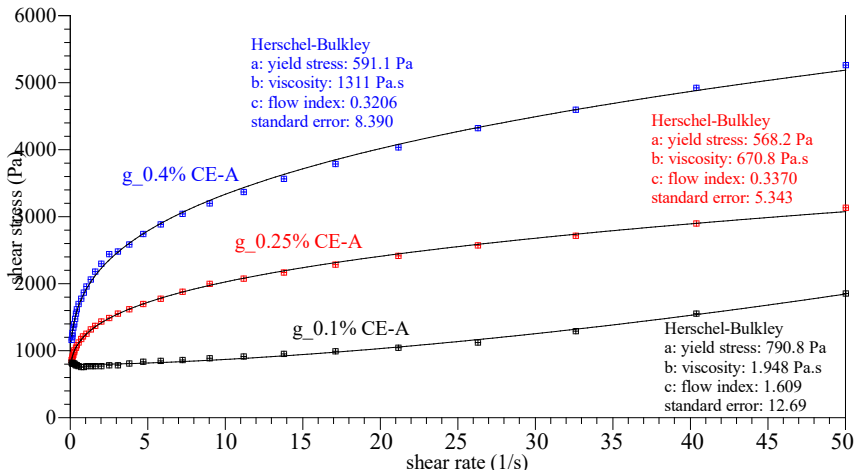


Figure. Flow curve deceleration of g\_0.1% CE-A, g\_0.25% CE-A and g\_0.4% CE-A with Herschel-Bulkley fitting and parameters



In Figure 60, parameters of the formulations with different CE content obtained by the application of Herschel-Bulkley model are plotted: (a) Yield Stress; (b) Consistency -  $K$ ; and (c) Flow index -  $n$ .

The increase of CE reduces the value of the yield stress as shown in Figure 60a. From g\_0.1% CE-A has the highest yield stress value, 790.8 Pa, and then g\_0.25% CE-A with 568.2 Pa and 591.1 Pa.

From 0.1% to 0.25%, the yield stress drop can be related to the air entrainment generated by the cellulose ether content increase. The entrained air is shown in Table 6, with 13% for g\_0.1% CE-A, 20% for g\_0.25% CE-A and 22% for 0.4% CE-A. Cappellari [23] verified the effect of yield stress for renders mortars and verified a reduction on yield stress with a content between 0.03% and 0.18%, explaining that this could be related to air entrainment and dispersant effect of CE. 0.1% to 0.25% of CE, air entrainment can explain the yield stress reduction or the dispersant effect, however from 0.25% to 0.4% of CE, the air entrainment difference is smaller, and a reduction could be expected, therefore a dispersant effect cannot explain it. From 0.25% to 0.4%, the increase of yield stress can be related a network formed by the bridging of cement grains by adsorbed ether molecules [152]. The increase could also be related to the ability of network formation of associative polymers. For dynamic networks (non-permanent), hydrophobic junctions which make up the network are constantly forming, breaking, and reforming by Brownian motion, can present properties similar to those of permanent networks when the lifetime of an association junction is nearly as long as the hydrodynamic relaxation time of the association unit [153].

The consistency ( $k$ ) can be translated to viscosity, and as the polymer content increases, consistency also increases. Considering the cellulose ether (CE) air entrainment effect that increase air content, and for g\_0.1% CE-A, there is 13% air, and for g\_0.25% CE-A, 20% and for g\_0.4% CE-A, 22%, a decrease could be expected. However, CE thickening seem to be dominant, and increases the mortar viscosity as CE content is increased.

Flow index measures the degree to which the fluid is shear-thinning or shear-thickening. If the flow index, “ $n$ ”, is smaller than 1, this material is shear-thinning and  $n > 1$ , it is shear-thickening. From the flow index results in Figure 60c, for the lower CE content formulation, the flow index showed a value higher than 1,  $n = 1.609$ , indicating a shear-thickening behavior. For the other formulations,  $n$  was smaller than 1, indicating a shear-thinning behavior. g\_0.25% CE-A with a  $n = 0.337$  and g\_0.4% CE-A with a  $n = 0.3206$ . The reduction of the flow index can be related to the shear-shinning effect of the cellulose ether to the aqueous phase, a common effect for associative polymer solutions. It is the result of disassociation of the hydrophobic bonds,



disentanglement and alignment of polymeric chains under shear. The interaction of the polymeric chains with the mineral particles could also contribute to a possible defloculation and consequently contribute to the shear-thinning behavior [9]. Therefore, results show that with higher CE content, the flow index was smaller, which agrees with Cappellari [23] results, who observed flow indexes reduction as CE content increased for dosages between 0.03% and 0.24%.

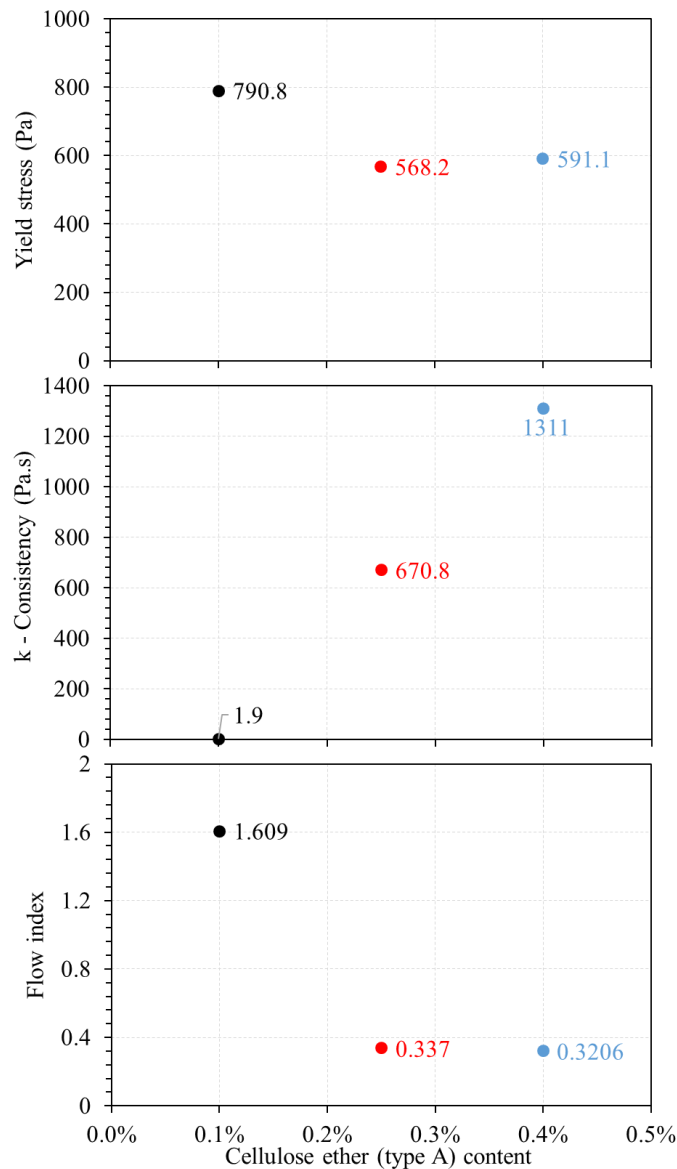


Figure 60. Parameters obtained from the Herschel-Bulkley model application on deceleration of flow cycle of formulations with different CE content: (a) Yield Stress; (b) Consistency and; (c) Flow index

### 3.4.4 Squeeze flow of adhesive mortar with different cellulose ether (CE) content

The squeeze flow curves of adhesive mortar with different cellulose ether (CE) content are shown in Figure 61. Each graph represents a specific waiting times, time between the mortar application and the test start: 0, 10, 20, 30, 40, 50 and 60 min.



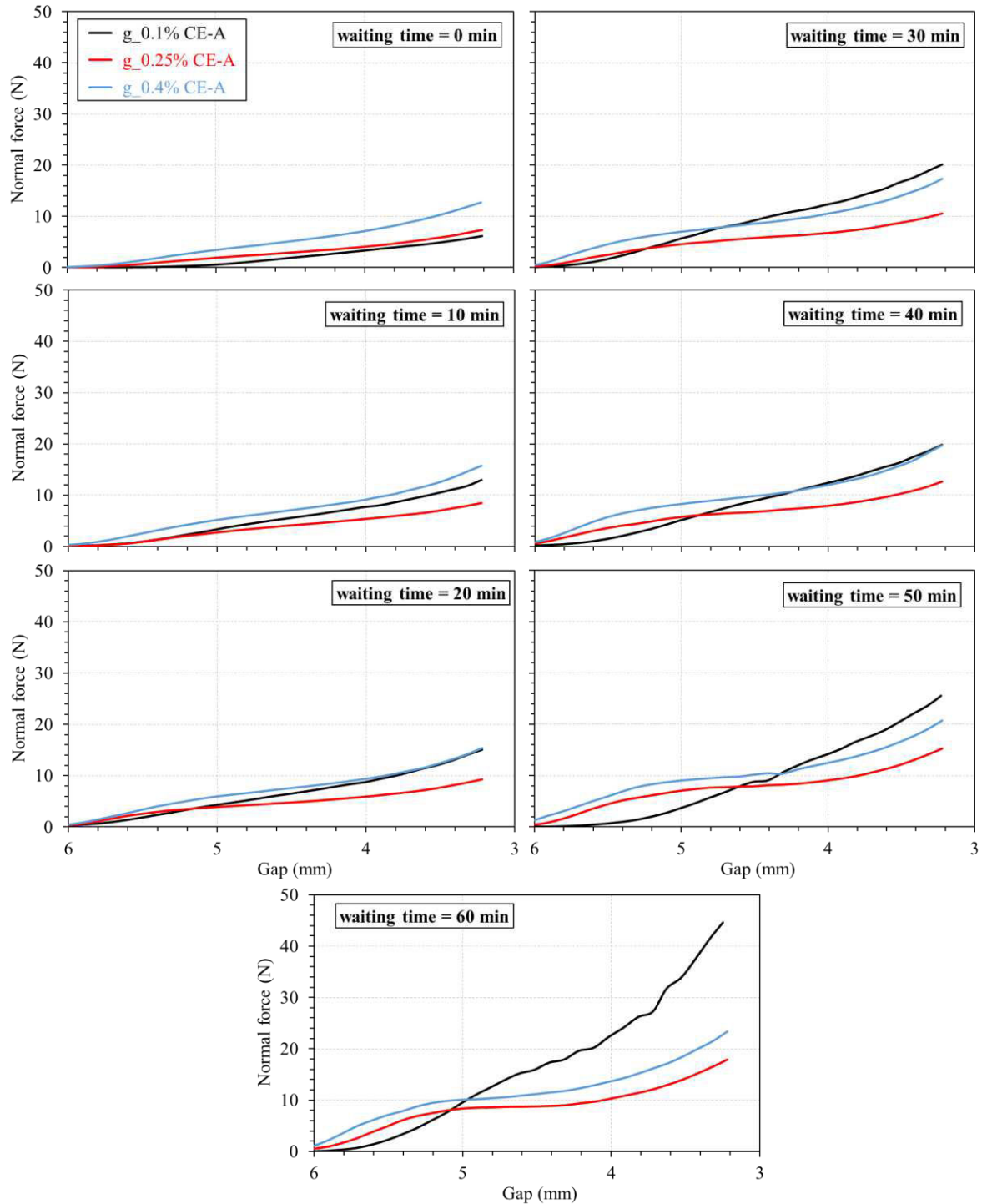


Figure 61. Squeeze flow graphs of adhesive mortars with different CE content (0.1%, 0.25% and 0.4%) at different waiting times: (a) 0 min; (b) 10 min; (c) 20 min; (d) 30 min; (e) 40 min; (f) 50 min; (g) 60 min.

Most of the curves present a similar behavior to typical squeeze flow curve represented on Figure 44, some curves only achieve the first – elastic deformation – and second stage – plastic deformation or viscous flow – without the strain hardening stage. With a waiting time of 0 min, the curves present a tendency of higher CE content, higher normal forces achieved. This result,

agree with the thickening effect of CE, which is a result of adsorption, association and intertwining. In section 3.4.3, flow measurements show the viscosity increase of the adhesive mortars with different CE.

At an waiting time of 10 min, however, the formulation g\_0.1% CE-A, which contains the smallest CE content, present higher normal force at the end of the test than g\_0.25% CE-A. Thus, g\_0.1% CE-A consolidation seems to be evolving at a higher rate than the other samples. When the waiting time was at 20 min, 30 min and 40 min, g\_0.1% CE-A curve gradually evolve, still producing lower normal at the beginning of the test, but with greater increase rate during the squeeze. At a waiting time of 50 and 60 min, the final normal forces of g\_0.1% CE-A achieve even higher values, of 25 and 45 N, while the other formulations show a slower increase with time. These results can be related to water evaporation and segregation, since the sample with lower CE content, tend to have lower water retention, consequently decreasing water/powder ratio and paste/aggregates ratio, which represents a reduced paste amount between the aggregates and therefore, higher particles friction when squeeze flow is induced. Due to the lower CE content, phase segregation may also have intensified particle friction, because the paste migrates to the outer part of the sample, leaving a drier material in the middle of the sample. The consequence is a strain hardening behavior, similar to stage III of a typical load on Figure 44, since the drier material requires a higher energy to surpass the particles friction generate a flow. Higher CE content increases the paste viscosity and reduces the impact of this effect. The other formulation's curves (g\_0.25% CE-A and g\_0.4% CE-A) have a shape more similar to typical load curves as shown in Figure 44, with Stage I: small strain — elastic deformation; Stage II: moderate strain — plastic deformation or viscous flow; and Stage III: large strain — strain hardening.

Also, the formulations with higher CE content have a layer of fresh mortar inside that is able to flow, even though higher dosages of CE cause the formation dryer layer at the interface as will be shown on section 6.4.1. g\_0.1% CE-A has a homogeneous distribution of dryer material, increasing grains friction and consequent high squeezing normal force.

Another factor that may influence squeeze flow results is the structuring building process of cement particles, this process has been observed on section 3.4.1 of oscillatory measurements, increase of CE generated a delay on structuring process in the first 2h. Therefore, delayed structure building may be a positive impact by delaying the rapid increase of squeeze flow stresses.

Additionally, as shown in Chapter 5, where micro-tomography was used to have a 3D view of bubble distribution inside the samples, the formulation g\_0.1% CE-A with lower CE content





presents greater size bubbles, which may be less stable, thus, influencing workability of the sample. This may explain the low entrained air of the formulation.

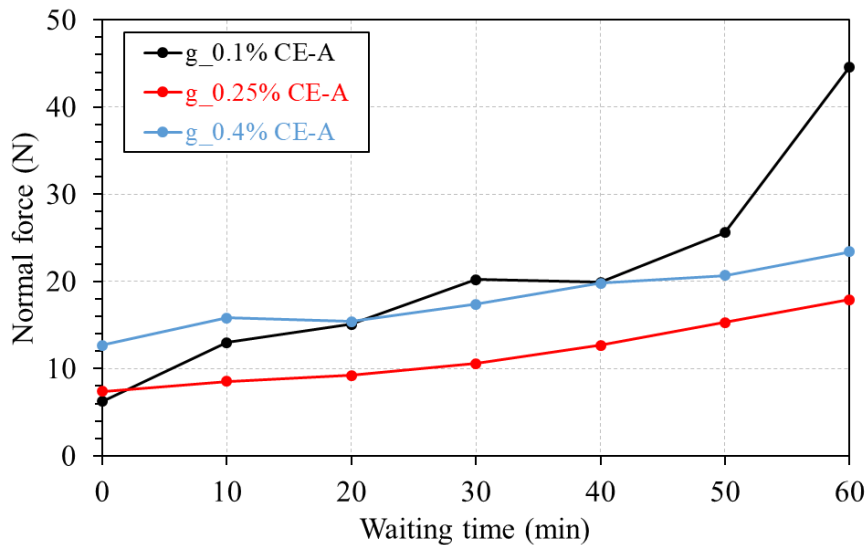


Figure 62. Final normal force of squeeze flow test of adhesive mortar with different waiting time

The graph with the final normal force evolution of squeeze flow test of adhesive mortar with different waiting times is shown in Figure 62. In this graph, it is clear how the evolution of the final normal force on squeeze is different for the formulation g\_0.1% CE-A and the others. With 0.1% CE-A, this formulation shows a faster increase as the waiting time is increased, from 6.2 to 44.6 N from 0 to 60 min (38.4 N variation). While the rate of normal force for the samples g\_0.25% CE-A and g\_0.4% CE-A is respectively 7.39 to 17.9 N (10.51 N difference) and 12.7 to 23.4 N (10.7 N difference). Despite the effect of CE on thickening, and different squeeze force at 0 min waiting time, from 0.25% to 0.4%, polymer content increase does not significantly influence the final normal force achieved after 3 mm displacement.

The increase of squeeze forces for low CE content is probably related to water loss that causes particles friction during squeeze. This behavior is not observed in mortars with higher CE content, since CE increases water retention. In Chapter 5, visualization of tomographic samples of traction tests at 28 days will show clear consequences of squeeze properties on test results.

### 3.4.5 Tack test

The tack test curves of adhesive mortar with different cellulose ether (CE) content are shown in Figure 63 (g\_0.1% CE-A), Figure 64 (g\_0.25% CE-A) and Figure 65 (g\_0.4% CE-A). Each graph represents the tack test after a specific waiting time (time between the mortar application and the test or tile positioning): 0, 10, 20, 30, 40\*, 50\* and 60 min (\*only shown on analysis).





Continuous line represents cohesive rupture and dashed lines, adhesive rupture. Each sample was pre-squeezed for about 3 mm before the tack test (squeeze results on section 3.4.4). The formulation g\_0.1% CE-A with lower cellulose ether content presents a less intense peak force at 0 min waiting time, achieving -3.0 N. After the initial waiting time, the peak force became more intense and for all samples from 10 to 60 min and stayed stable varying between -5.1 and -6.1 as it is clearly observed on Figure 63. The rupture for all samples were cohesive and are shown in Figure 68a.

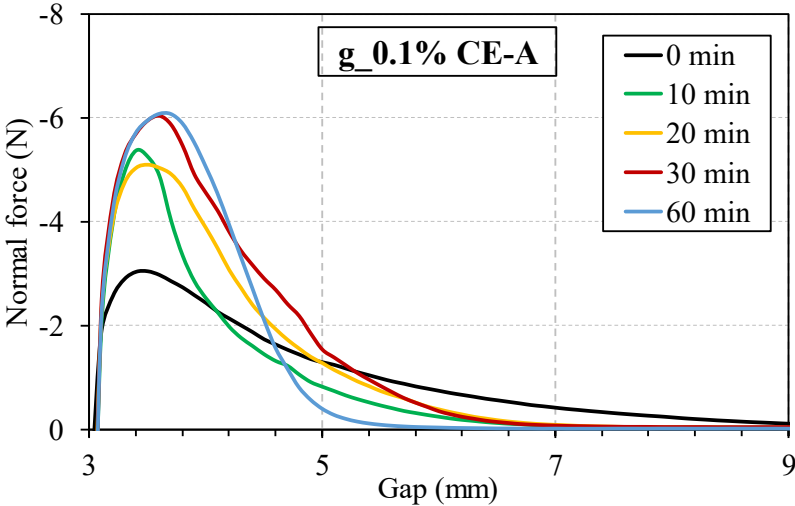


Figure 63. Peak force of tack test of g\_0.1% CE-A adhesive mortar with different waiting time

The tack test curves of sample g\_0.25% CE-A are shown in Figure 64. The peak force of the initial waiting time at 0 min in this case was more intense, achieving -4.6 N. For the following waiting times, the normal force has decreased considerably. As it is possible to observe on the graph of Figure 67, the peak force goes to -2.8 for 10 min waiting time and -0.9 for 20 min waiting time and then keeps at even lower peak forces for all other waiting times.

The cohesive rupture occurred only in the first sample and slightly in the middle of the 10 minutes one, and all the other samples had an adhesive rupture. The main cause is the skin formation that produces a layer at the interface that do not allow good contact between the mortar and the geometry. In Figure 68b, pictures of the sample g\_0.25% CE-A after the test can be observed, and the adhesive rupture can be observed for 20-60 min waiting time samples.



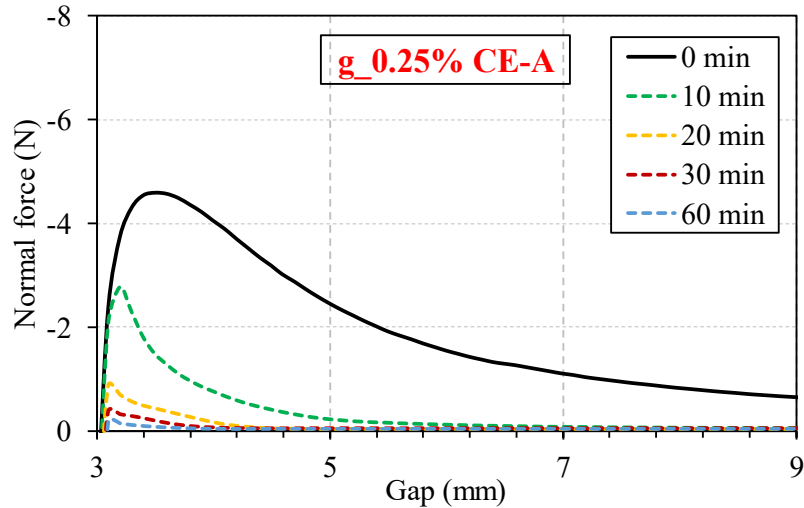


Figure 64. Peak force of tack test of g\_0.25% CE-A adhesive mortar with different waiting time

Figure 65 shows the tack test curves of the formulation g\_0.4% CE-A at different waiting time. Like g\_0.25% CE-A, the peak force had higher values for 0 and 10 min, and for bigger waiting times, low values. In this formulation, in comparison to g\_0.25% CE-A, g\_0.4% CE-A had higher values of peak force, 7.5 N for 0 min waiting time and 5.3 N for 10 min, than 1.0 N to 0.3 N from 20 min to 30 min. The loss of tack at 20 min is also probably related to skin formation, which did not enable a good contact generation between the mortar and the geometry.

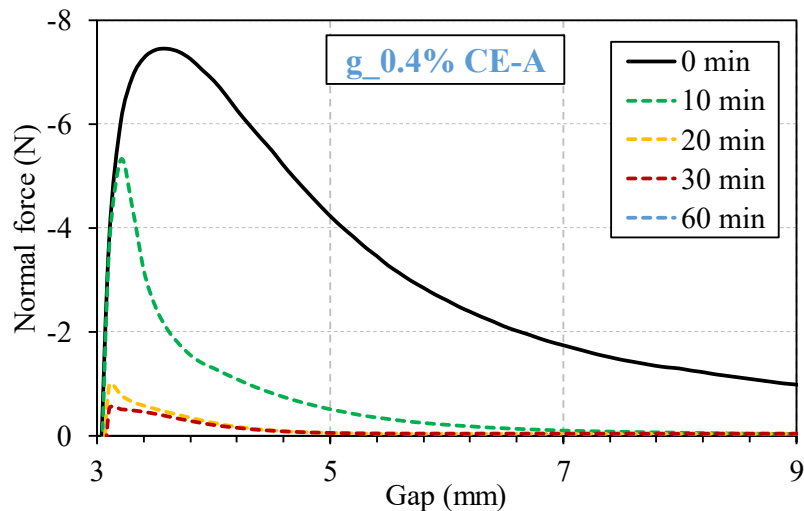


Figure 65. Peak force of tack test of g\_0.4% CE-A adhesive mortar with different waiting time

The failure energy of tack curves, which is the area under the curve, was measured for each waiting time of the formulations and is shown on Figure 66. From the results, it seems clear how g\_0.1% CE-A failure energy continues constant for all waiting times, and g\_0.25% CE-A and g\_0.4% CE-A have a considerable decrease from 0 min to 10 min waiting time. This loss



is mainly due to skin formation that inhibits the probe to obtain good contact and consequently obtaining low adhesion. Thus, the energy failure can relate to the failure mode.

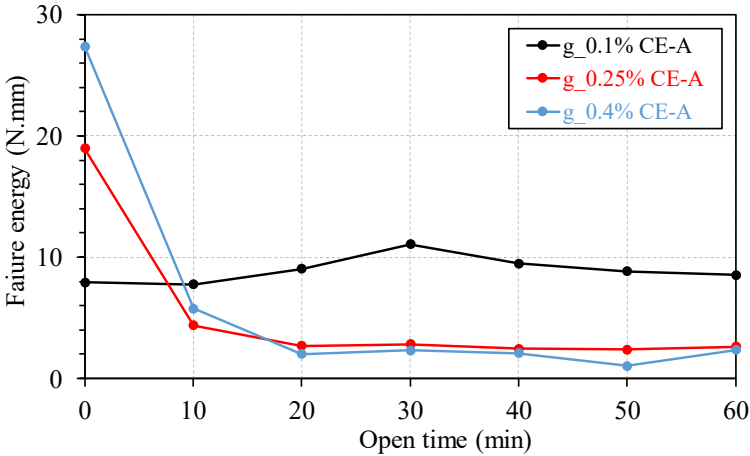


Figure 66. Failure energy of the tack tests of the formulations with different CE content measured at different waiting times, calculated by the integral of normal force vs gap curve.

The peak force, as discussed in literature review of this chapter, is a result of adhesive and cohesive properties of the mortar. From g\_0.25% CE-A to g\_0.4% CE-A, an increase of peak force was observed. The higher values of g\_0.4% CE-A in comparison to g\_0.25% CE-A, 7.5 N to 4.6 N for 0 min and 5.3 N to 2.8 N for 10 min are related to higher cohesion of mortar with higher CE content, as it has a thickening effect. For both samples, cohesive rupture occurred at 0 and 10 min.

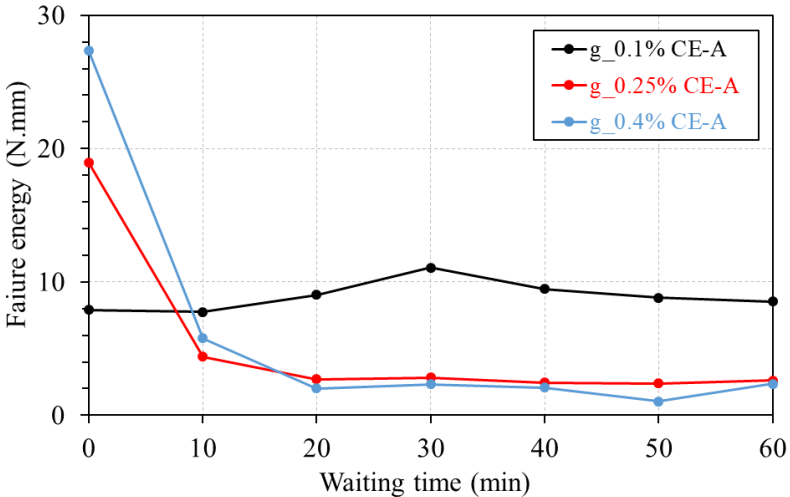


Figure 67. Peak force of tack test of adhesive mortar formulation with gray cement and different CE content at 0, 10, 20, 30, 40, 50 and 60 min of waiting time.

Meeten's [79] has shown that the pulling force,  $F$ , is related to the rheological parameters of the paste,  $K$  and  $\alpha$ , to the plate radius  $R = D/2$  and to the plate separation rate  $\dot{h}$  by the equation



( 13 ) described on section 3.2.2.3, tack test literature review of this chapter. For the g\_0.1% CE-A the calculated peak force and delta pressure of the bubbles do not predict what is obtained in real measurements. This discrepancy can be explained by high values “n” and “k” in flow measurements that result from aggregates friction.

Mohamed et al. [147] already questioned Meeten’s approach, since the author make use of a lubrication theory in shear flow is a priori a questionable assumption. Indeed, the flow of a fluid between two plates moved away from each other differs from a simple shear. Depending on the boundary conditions, either a lubricational or an elongational regime can be obtained. When the layer is thin compared to the plate radius (highly confined conditions), the first regime should be obtained while if the layer is thick or with perfect slip on the walls the second regime should be obtained. For g\_0.25% CE-A and g\_0.4% CE-A, the approach seems to better predict the peak force.

Table 8. Measured peak force at 0 min waiting time and calculated peak force and maximum delta pressure

	Measured Peak force (N)	Calculate Peak force (N)	$\Delta p_{max}$
g_0.1% CE-A	3.04	55.7	78305.6
g_0.25% CE-A	4.6	7.0	13930.4
g_0.4% CE-A	7.46	13.5	26918.9

From the sample pictures on Figure 68, it is clear how the formulation with low CE g\_0.1% CE-A present a rupture with a very rough and prickly layer of paste that remains on each plate for all waiting times measured. And, in the case of the samples with higher CE content, g\_0.25% CE-A and g\_0.4% CE-A have for 0 min waiting time, a cohesive rupture mortars flow towards the center of the plates and the pattern just before debonding is a central and narrowing paste column. For 10 min, the flow also occurs, but with a very small narrowing paste column in the middle. For higher waiting times, all ruptures are adhesive, with a clear upper plate. The results in this section will have further connections with the results of contact visualization discussed in Chapter 5.



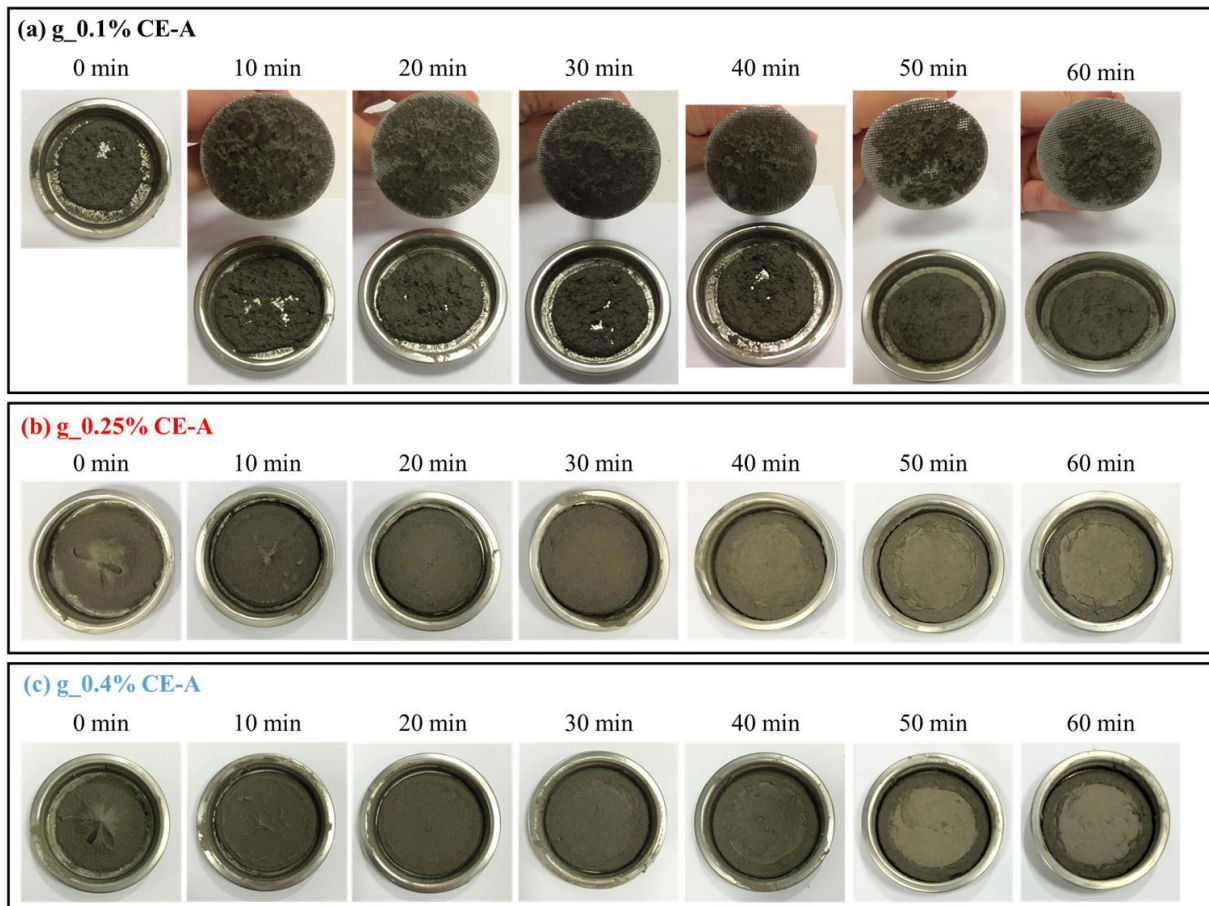


Figure 68. samples after squeeze and tack test of adhesive mortars with gray cement and different CE content

### 3.5 Chapter conclusions

In this chapter, the bulk rheological properties of adhesive mortar formulations with different cement, cellulose ether (CE) content and CE type were evaluated. The mortars were evaluated by small amplitude oscillatory rheometry, flow rheometry, squeeze flow and tack test.

Firstly, oscillatory rheometry was used to evaluate the impact of CE content on bulk properties of adhesive mortars with gray and white cement. It was observed that as CE content is increased, the mortars entrained air increase until a saturation point, where it stabilizes. This effect leads to a reduction of initial  $G'$  for dosages under the saturation point, but after the saturation point, as CE content is increased, a  $G'$  increase occurs due to the polymer's thickening effect. Over time, higher polymer content generates a delay on structure building for both cement types.

Mortars with different CE types were also evaluated, as were polymers with the same nominal viscosity but different degrees of substitution and molecular weight. Results showed the effect of degree of substitution (DS) on structuring of cement particles—the higher DS, the higher the delay generated. This behavior was found in both cements, but disagrees with what is found in literature and further investigation would be necessary to explain the phenomenon.

Molecular length measurements would be possible approaches to further understand the results. Found differences on the intensity of CE-A and CE-C impact on the different types of cements are probably related by the difference phases present in each cement.

Flow properties of mortars with different CE contents were evaluated and their respective Hershel-Bulkley model parameters calculated. Flow results indicated possible phase separation for formulations with lower CE, g\_0.1% CE-A, since considerably high hysteresis area is shown. In higher CE concentrations where phase separation is not an issue, increasing CE content generated increases in polymer disentanglements during acceleration and consequently lowered stresses during deceleration and higher thixotropy. The yield stress, consistency and flow index parameters could be obtained by the model. Results indicated that yield stress is considerably higher for smaller CE content due to air entrainment, but after air saturation point, as the polymer dosage was increased, network formation induced slight increase on yield stress. The consistency indexes have shown a similar behavior as yield stress. Flow index indicated a shear-thickening behavior for g\_0.1% CE and shear-thinning behavior for g\_0.25% CE and g\_0.4% CE. Disassociation of hydrophobic bonds, disentanglement and alignment of polymeric chains under shear are probably related to the reduction of flow index.

Squeeze flow was used to evaluate the different CE content on adhesive mortars formulations with gray cement after different waiting times (0, 10, 20, 30, 40, 50, 60 min). Initially, at 0 min, squeeze flow results indicated a thickening effect of CE. However, as the waiting time increased, g\_0.1% CE gradually evolved to a shape that indicates a strain-hardening behavior. The high normal forces indicate that phase separation and intensified water evaporation caused the increase of particle friction, and consequently stresses increased as the waiting time increased. Formulations g\_0.25% CE and g\_0.4% CE, with higher CE content, presented similar increase of final normal forces, with g\_0.4% CE higher, due to polymer thickening effect.

After each squeeze test, tack test was also conducted in the same samples, after the same 3 mm displacement. Results showed that the formulation g\_0.1% CE-A, does not lose tackiness for all waiting times, and had cohesive ruptures. However, higher forces were necessary to generate contact with the geometry. The mortars with higher CE content, however, due to skin formation, lost tackiness after 20 min waiting time with adhesive ruptures.



## Chapter 4 – Skin formation evaluation

### 4.1 Introduction

The science of interfacial rheology impacts systems in which interfaces are present. The study is mostly applied to two immiscible fluids, which enable a mobile and deformable interface. Nature and humankind have been taking advantage of surface and interfacial properties for a long time already. Sailors would use oil to calm sea waves many centuries ago, even though its understanding was achieved only last century by Lord Rayleigh [154]. Today its use is even more explored, offering us the most diverse uses in human's simplest situations to complex applications, from mayonnaise to water repellent glass.

Interfacial and surface rheology concerns most of the natural and industrial sciences, but its use is still limited and unknown to some fields. This is probably because there is no technique that is adaptable to granular material, and therefore, interfacial rheology is limited to suspensions, liquids and foams. Granular materials require a technique that reduces bulk effects (high boussinesq number – surface viscosity divided by the product of bulk viscosity and length scale [155]), and is able to measure materials with high viscosity and containing millimetric range particles. In cementitious materials, no studies are reported in literature regarding interfacial rheology, even though it can be a great source of problems such as: mortar coatings, adhesive mortar, structural concrete surface, etc.

Adhesive mortar skin formation is considered a problem since it can potentially disturb the adhesion between the mortar and tiles. Interfacial rheology was then considered in this investigation to be adapted and used to measure rheological properties of adhesive mortar's skin.

Firstly, Nuclear Magnetic Resonance Imaging was used to assess water distribution within the specimen during the first hours and to determine skin layer depth as well. With the skin characterization, it was observed that mortars with higher CE content form a dryer layer, which is probably the main area where the skin is located. With these results, it was possible to better implement the interfacial rheology technique, by measuring mainly the area where the skin is formed, reducing bulk effects.

Then, based on classic interfacial rheology, a technique for adhesive mortar's interface was successfully introduced. It was used to measure adhesive mortar's formulation with different CE content and CE types, since CE is reported to be one of the causes of skin formation. Different environmental conditions were also employed to evaluate the effect of wind. The new method was able to quantitatively measure skin rigidity.





In this chapter, with the results of MRI and interfacial rheology, it is verified that in formulations with higher CE content, water evaporation dominates the rheological properties at first and then polymer properties start to dominate. As the CE content is increased, the dominance change occurs earlier.

This chapter content is key to better understanding skin formation of adhesive mortar; and it includes valuable contributions on measuring techniques that enable assessing adhesive mortar interfacial properties and physical characteristics.

## 4.2 Literature Review

### 4.2.1 Interfacial rheology

Interfacial rheology is based on classical rheology introduced on Chapter 3, but applied to interfaces. In this field, other forces reign such as surface tension and interfacial interactions. A diversity of industries makes use of interfacial rheology, some examples are exemplified next.

In oil companies, water-in-oil and oil-in-water emulsion's characterization is important to reduce costs and improve productivity when extracting petroleum, for example by enabling companies to reduce water entrainment [156,157]. Interfacial properties are commonly used to verify stability of an emulsion. The oscillation drop method is often applied in this field, but also bicone and double wall ring are used for shear properties.

In the food industry, people's favorite products demand a lot of research regarding interfacial properties. Low-fat products in general can lose emulsion stabilization and desirable texture during their process; studies are necessary then to find additives and substitutes to make necessary compensations to keep the desirable texture and consistency.

In paintings and coatings, not only are surface tension and suspension stability concerns, but so is skin formation as in adhesive mortars. While the material dries on the wall, if a thin skin is quickly formed and brushed, marks that cannot be healed may be produced. Thus, the use of interfacial rheology is common for interfacial property's measurements and skinning formation identification.

Many techniques for measuring interfacial properties are used and have been developed over the years. Plateau was the first to suggest surface viscosity and suggested its measurement based on the motion of a needle under a known stress [158]. The same concept is still used today; a commercial instrument based on the detection of small deformations of a magnetic needle (strains down to  $10^{-7}$ ) allows the equipment to have modulus, viscosity and visualization of





eventual textural changes induced by the deformation [157]. Another early method is the channel viscometer shown in Figure 69. Applicable for only insoluble monolayers, the instrument is a *Langmuir troughs* with a fixed barrier.

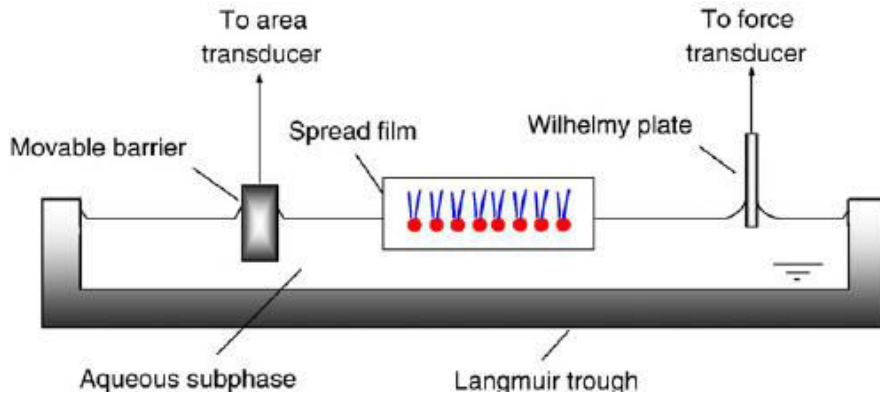


Figure 69. Scheme of Langmuir trough [159]

There are more recent approaches and devices such as bicone, double wall ring, du noüy ring and etc. The bicone geometry on Figure 70a, for example, is based on a measurement between the two interfaces, and the properties are evaluated by measuring the interface with the influence of the bulk of the fluids and then removing it by calibrations done by measuring the fluid A or fluid B separately. The Interfacial linear viscoelastic properties are then calculated by equations (1) and (2) [160].

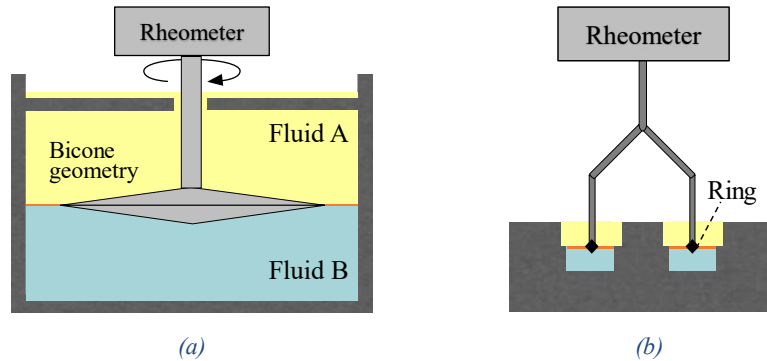


Figure 70. Interfacial rheometry apparatus – Bicone and Nöuy Ring

$$G'_{interfacial}(\omega) = G'_{total}(\omega) - [G'_{ACalibration}(\omega) + G'_{ACalibration}(\omega)]/2 \quad (10)$$

$$G''_{interfacial}(\omega) = G''_{total}(\omega) - [G''_{ACalibration}(\omega) + G''_{ACalibration}(\omega)]/2 \quad (11)$$

This requires that the bulk properties are not significantly higher in comparison to the interfacial effects. The ratio between the two effects is defined by the Boussinesq number.

$$Bo = \frac{\eta_s}{\eta_{subph} G_l} \quad (12)$$

Where  $Bo$  is the dimensionless Boussinesq number,  $\eta_s$  the surface viscosity (Pa.s.m),  $\eta_{subph}$  the viscosity of the subphase, and  $G_l$  a characteristic length scale of the measuring probe. If



$Bo \gg 1$ , the interfacial influence over the drag experienced by the measuring probe dominates. When the  $Bo$  is  $O(1)$  or smaller, the properties of the surroundings are dominant. In other systems like nøy ring device on Figure 70b, the effect is minimized by reducing the subphase contact surface [68].

#### 4.2.2 Magnetic Resonance Imaging (MRI)

Magnetic Resonance Imaging (MRI) was a key technique in this study, since it is able to quantitatively and spatially measure the moisture content inside cementitious materials, by measuring hydrogen. This is especially important in this thesis, since water distribution and evaporation is an important factor in rheological properties and skin formation.

##### 4.2.2.1 MRI Fundamentals

Magnetic Resonance Imaging (MRI) and Nuclear magnetic resonance (NMR) are based on the same concept of magnetic properties of certain atomic nuclei. Both are based on similar concepts, but MRI uses it to provide images of a sample, by obtaining NMR signal and spatially plotting the areas with higher signal density for each echo of an emitted signal.

MRI is based upon the interaction between a magnetic field and nuclei that possess a spin angular momentum. Every periodic table element, except argon and cerium, has at least one isotope that possesses this angular momentum. A nucleus containing an odd number of protons or neutrons has a characteristic motion or precession. Nuclei are charged particles, so their precession produces a small magnetic moment that can interact with an external magnetic field.  $^1\text{H}$  is one of the most abundant isotopes for hydrogen and its response to an applied magnetic field is one of the largest found in nature [161]. Thus, hydrogen is a natural choice for MRI measurements. When a sample is placed in a large magnetic field, many of the free hydrogen nuclei align themselves with the direction of the magnetic field. The nuclei precess about the magnetic field direction, which is known as Larmor precession behavior. The frequency of Larmor precession is proportional to the applied magnetic field strength, as defined by Larmor frequency,  $\omega_0$ :

$$\omega_0 = \gamma B_0 \quad (13)$$

The technique is based on the gyromagnetic ratio and  $\gamma$  is the strength of the applied magnetic field. The gyromagnetic ratio is a nuclei specific constant. For hydrogen,  $\gamma = 42.58 \text{ MHz} \cdot \text{T}^{-1}$ . To obtain an MRI image of an object, the object is placed in a uniform magnetic field,  $B_0$ . As a result, the object's hydrogen nuclei align with the magnetic field and create a net magnetic moment,  $M$ , parallel to  $B_0$ . Then, a radio-frequency (RF) pulse,  $B$ , is applied perpendicular to



$B_0$ . This pulse, with a frequency equal to the Larmor frequency, causes  $M$  to tilt away from a proton spin excitation followed by signal acquisition of the spin-spin relaxation. Once the RF signal is removed, the nuclei realign themselves such that their net magnetic moment,  $M$ , is again parallel with  $B_0$ . This return to equilibrium is referred to as relaxation. During relaxation, the nucleus lose energy by emitting their own RF signal. This signal is referred to as the free-induction decay (FID) response signal. The FID response signal is measured by a conductive field coil placed around the object being imaged. This measurement is processed or reconstructed to obtain MRI images [161,162].

#### 4.2.2.2 MRI studies on cementitious materials

Due to MRI's ability to identify water content and form inside a sample, it is a powerful technique for cementitious materials where water has a main role regarding hydration, agglomeration and rheology. Fourmentin et al. [163] evaluates the liquid transfer between a cement paste and a porous media with Nuclear magnetic resonance (NMR). Jarny et al. [164] combines rheological measurements and MRI technique simultaneously, following cement pastes liquid to solid transition.

Faiyas et al. [165] studied moisture distribution and hydration characteristics of adhesive mortars with MRI. In their work, the influence of methyl hydroxyethyl cellulose (MHEC) on unsealed mortars. Through MRI, it was possible to observe that MHEC reduce considerably the evaporation, leaving more water in the mortar for hydration to occur. However, MHEC lead to an inhomogeneous distribution of water, leaving a lower water concentration in the unsealed top and higher concentration in the bottom. Hydration is affected by water evaporation, consequently the measured degree of hydration was lower when the mortar was affected by evaporation. In Figure 71, the moisture distribution of unsealed mortars with different CE content are shown.



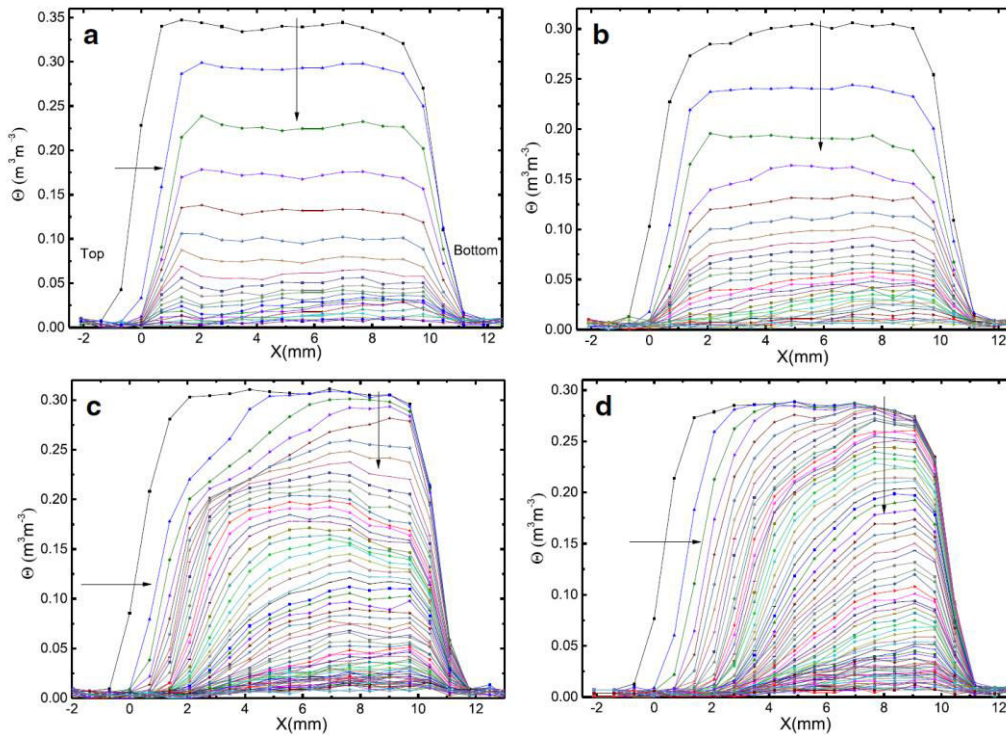


Figure 71. Moisture profile of unsealed mortar samples a) 0 wt.% MHEC, b) 0.4 wt.% MHEC, c) 1.3 wt.% MHEC and d) 2.1 wt.% MHEC. All the profiles have been plotted every 24 min [165].

In the context of this thesis, MRI could offer valuable information regarding water transportation and location, which are relevant factors in skin formation process. Skin thickness, dynamic of water transportation as well as water distribution over time.

## 4.3 Experimental

### 4.3.1 Materials

In this work was used basic compositions of adhesive mortars with gray CEM I 52,5 N CE CP2 NF from Lafarge. Cement phases, density and blaine fineness obtained with the manufacturer are shown in Table 5 of section 3.3.1. The sand used in this study was a silica sand PE2LS from FULCHIRON. ASTM granulometric distribution from the manufacturer is shown on Figure 51 of section 3.3.1.

### 4.3.2 Formulations

Common formulations of adhesive mortars were used (Table 6). They contained white or gray Portland cement, silica sand, an organic binder in redispersible powder form (latex: vinyl acetate, vinyl versatate and a maleic ester copolymer resin) and an organic modifier (CE: hydroxyethyl methyl cellulose). Different contents of CE (CE-A) were used and three different cellulose ethers with varying degree of substitution were also employed (CE-A, CE-B, CE-C). No formulation with less than 0.1% of CE was used to avoid significant phase separation.

The formulations names in Table 6 are defined to its content: “w” or “g” refers to white or gray cement; the percentage is the CE content and; “A”, “B” or “C” refers to the type of polymer. Entrained air was calculated from the density measurements done with a cup of known volume of 314 ml and the density could be calculated by the mass.

Table 9. Formulations of adhesive mortars with white and gray cement, with different cellulose ether content and types (wt%)

Formulations	gray CEM I	white CEM I	sand	latex	CE-A	CE-B	CE-C	water/ powder	entrained air
w_0.1% CE-A	-	30%	67.40%	2.5%	0.1%	-	-		14%
w_0.25% CE-A	-	30%	67.25%	2.5%	0.25%	-	-		19%
w_0.4% CE-A	-	30%	67.10%	2.5%	0.4%	-	-		21%
w_0.25% CE-B	-	30%	67.25%	2.5%	-	0.25%	-		20%
w_0.25% CE-C	-	30%	67.25%	2.5%	-	-	0.25%		19%
g_0.1% CE-A	30%	-	67.40%	2.5%	0.1%	-	-		13%
g_0.2% CE-A	30%	-	67.30%	2.5%	0.2%	-	-	0.205	20%
g_0.25% CE-A	30%	-	67.25%	2.5%	0.25%	-	-		20%
g_0.3% CE-A	30%	-	67.20%	2.5%	0.3%	-	-		22%
g_0.4% CE-A	30%	-	67.10%	2.5%	0.4%	-	-		22%
g_0.5% CE-A	30%	-	67.00%	2.5%	0.5%	-	-		22%
g_0.25% CE-B	30%	-	67.25%	2.5%	-	0.25%	-		19%
g_0.25% CE-C	30%	-	67.25%	2.5%	-	-	0.25%		18%

### 4.3.3 Methods

#### 4.3.3.1 2D MRI

Aiming to determine the layer thickness at the air-mortar interface affected by drying, the distribution of free water inside the sample was measured through magnetic resonance imaging (MRI). With spatially resolved T2 methods, a 2D distribution of free water was obtained from a section of the sample as illustrated on Figure 72a. The equipment was a 750WB UltraStrabilized from *Bruker*. The mortar was put in a cylindrical Teflon holder of 21 mm diameter and 7 mm height just after mix, flatten with the help of a spatula and put in the spectrometer immediately. Then, an acquisition of T2 echo was done every 5 minutes for 2 hours. The room temperature was kept at 23±1°C and 30% RU.

#### 4.3.3.2 1D MRI

The equipment was an Ascend 400 WB from *Bruker* with a static magnetic field of 9.4T. For the 1D distribution, the mortar was put in a glass cylindrical holder of 8 mm diameter and 4 mm height as illustrated on Figure 72b. The signal obtained was from a horizontal cut through all the sample depth. Data acquisition was done every 5 minutes for 2 hours. For 1D and 2D distribution, room temperature was kept at 23±1°C and 30% RU.



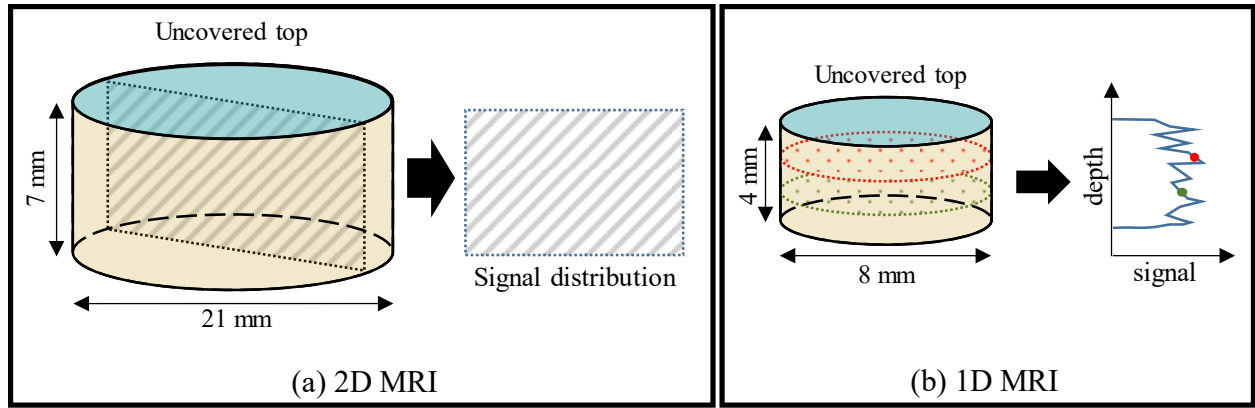


Figure 72. MRI samples scheme: (a) 2D MRI – sample dimensions and section cut of signal visualization; (b) 1D MRI – sample dimensions and representation of signal distribution obtained

#### 4.3.3.3 Interfacial measurements

The interfacial measurements are based on Gibbs definition of interface, the “excess property” [7]. The evolution of interfacial viscoelastic properties was obtained through two measurements: one in which the vane geometry is partially immersed (3mm) including the interface and another fully immersed that is the bulk properties. The excess property ( $G'$ ,  $G''_{interface}$ ) is obtained by the difference between the measurement at 3mm and at the bulk. In this investigation, small amplitude storage modulus and loss modulus were evaluated, thus, it was defined as:

$$G'_{interface} = G'_{3mm} - G'_{bulk} \quad (14)$$

$$G''_{interface} = G''_{3mm} - G''_{bulk} \quad (15)$$

The bulk and interfacial configuration are according to Figure 73. The 3mm depth was based on MRI measurements which will be explained on session 3.1 of MRI results. This depth was chosen to ensure encompassing the entire interface during the 2h measurement, but also, to minimize the bulk effects. The thicker the measurement including the interface, the larger the Boussinesq number, thus less precise is the measurement. Each formulation was then tested for 2h with a vane geometry at bulk ( $G'_{bulk}$ ) and at the interface ( $G'_{3mm}$ ) to calculate  $G'_{interface}$ . The test preparations and measurements conditions were the same as for the bulk rheological measurements. The vane geometry advantage for this measurement was the possibility of using different depths, differently from other geometries as parallel plate, cone-plate, bicone, where evaluating different depths or allowing evaporation to occur are not possible in a time sweep.

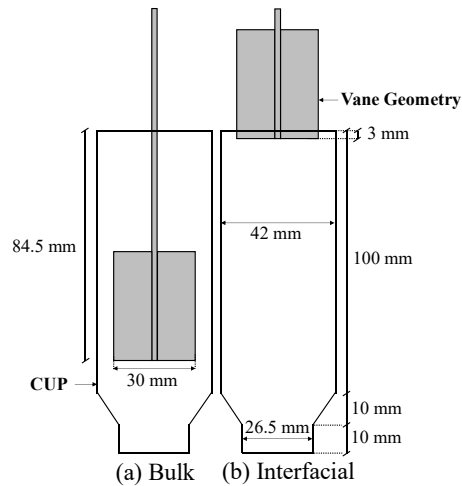


Figure 73. Scheme of the rheological measurements of the adhesive mortars using a vane geometry: (a) bulk measurements were done at 84.5 mm depth; (b) interfacial measurements were done at 3 mm depth with the mortar exposed to air at the interface.

To perform the interfacial measurements with variations on the environmental conditions, an electric fan was introduced to produce wind and increase drying rate, as illustrated on Figure 74. The fan was positioned 2 meters away from the rheometer at velocity level 1.

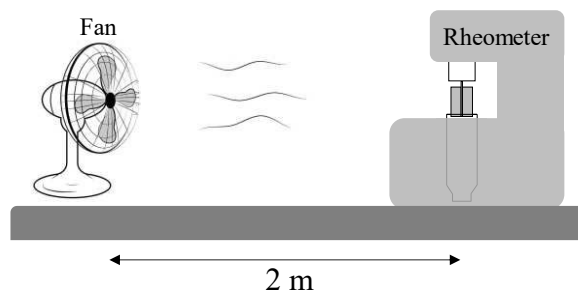


Figure 74. Scheme of interfacial rheology test in windy environmental condition.

#### 4.3.3.4 Water evaporation

Water evaporation was assessed in mortar samples (cylinder of 6 mm height and 100 mm diameter) with the top uncovered. The mass loss was measured for 2 hours by an OHAUS precision scale with 0.01 g readability and registered by a data logger every 10 seconds. The test simulated the water loss at the interface, by limiting the volume to two times the thickness of the considered 3mm-top layer.

## 4.4 Results

### 4.4.1 MRI

#### 4.4.1.1 2D MRI characterization of moisture spatial distribution

In Figure 75, the signal mitigation of moisture content inside a w<sub>0.25%</sub> CE-A sample can be observed. Each image represents the signal intensity difference between the initial time (0





minute) and a specific moment (30 minutes, 1 hour and 2 hours). On the image, white areas represent zones where there is no difference in comparison to the reference and dark areas represent the zones where the signal had mitigation in relation to the reference, where free water is disappearing from water evaporating. MRI could evaluate the spatial distribution of moisture inside the sample through the depth and horizontal direction. With this result, it is possible to observe that during the first 2h the moisture vanishing grew from the surface to the inner layers of the material until 3 mm.

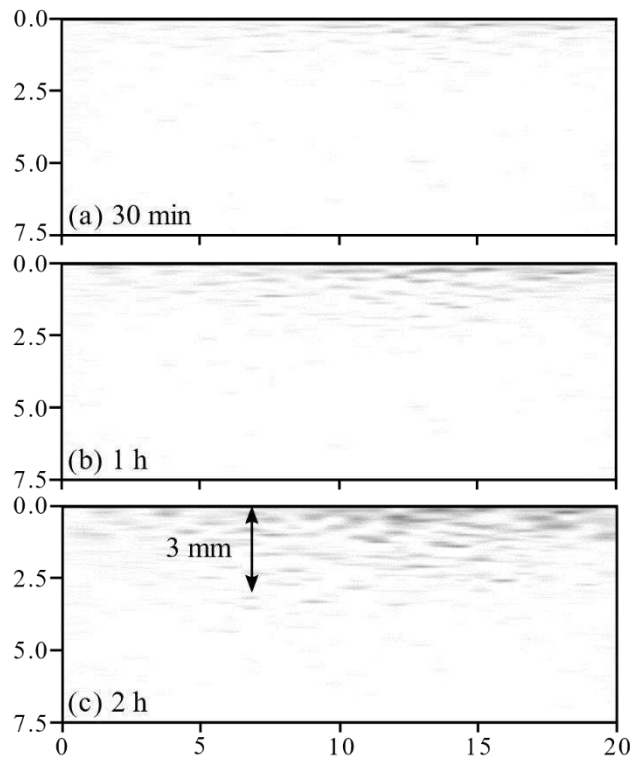


Figure 75. 2D MRI Result - 1<sup>st</sup> echo signal mitigation of water signal of an adhesive mortar sample (w\_0.25% CE-A) exposed to air on the top: (a) water vanishing after 30 min; (b) water vanishing after 1 h; (c) water vanishing after 2 h.

The relative humidity during MRI measurements was lower than the value during other types of tests (rheology and water evaporation), at 30% instead of 50% of RU, which could not be changed. This condition could have an influence on intensifying water evaporation during MRI; however, this result can offer an approximation of water distribution during skin formation.

The MRI technique provides detailed information of water distribution in a section cut, showing the water concentration diminishing along the vertical axis due to drying, but it does not take in account the entire sample as the measurements focus only on the central plane. For the skin formation matter, having quantitative information of the entire sample would provide more complete information.



#### 4.4.1.2 1D MRI characterization of moisture distribution along the depth

Figure 76 shows the formulation with lower CE content, w\_0.1% CE-A, where the moisture distribution through the depth is fairly homogeneous. In comparison to other samples, the signal intensity along the whole sample reduces considerably during the first 2h. This indicates that the mortar loses water from the surface by evaporation, but the moisture inside is able to move and re-homogenize.

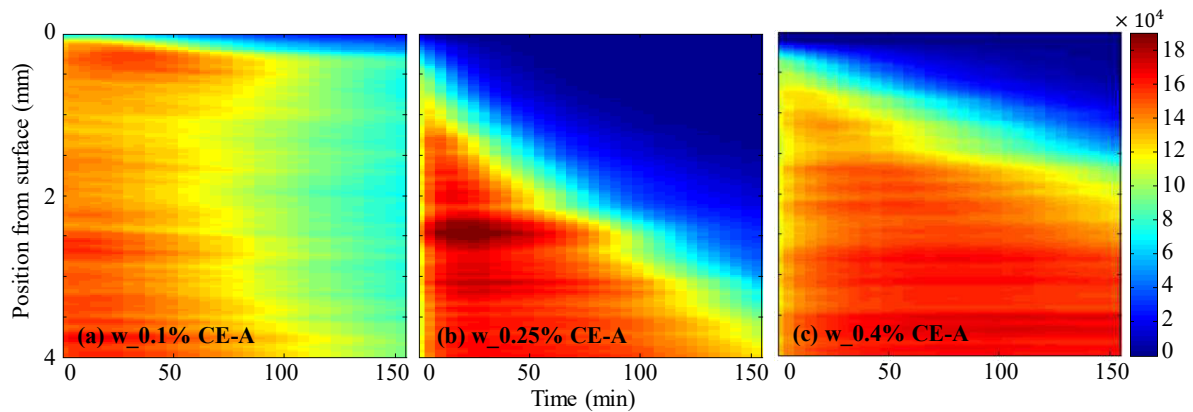


Figure 76. 1D MRI Result – 1<sup>st</sup> echo map signal vs time of adhesive mortar samples exposed to air on the top:  
(a) W\_0.1% CE-A; (b) W\_0.25% CE-A; (c) W\_0.4% CE-A

The result of the w\_0.25% CE-A formulation is shown in Figure 76b. A low signal layer linearly grows toward the inner part of the sample as a function of elapsed time and the dark blue area indicates a dry layer. The material that is located below this dryer zone has a more intense signal, showing that underneath the mortar keeps its moisture content. This result is different from w\_0.1% CE-A, where the material does not form these two zones of dry and moisturized mortar, staying homogeneous from the top to the bottom of the sample with higher mitigation of the water signal measured on the bottom of the sample for longer times. The nature of CE explains these results, as it forms an aqueous phase with higher viscosity that reduces water mobility [30,166], consequently inhibiting water flow towards the mortars surface. This means that as the mortar with higher CE content started to lose water from the surface, a layer of dryer material formed; this drying layer grew down the surface, but the material below this layer retained its moisture.

For w\_0.1% CE-A, on the other hand, as water evaporates, free water freely migrates in the direction of the surface, remoisturizing the top layers, obtaining a dryer, but homogeneous sample. At 2h, similarly to the 2D MRI in section 4.4.1.1, the w\_0.25% CE-A layer had approximately 3 mm of dryness; thus, the results obtained from both methods (2D and 1D MRI) were consistent.

The w<sub>0.4%</sub> CE-A formulation, with even higher CE content, also presented the linear formation of the dry layer material evolving with time toward the inner layers of the sample, similarly to w<sub>0.25%</sub> CE-A. However, the growing rate was less than the other sample and after 2h the dry layer was only 1.5 mm thick, which is smaller than the 3 mm seen for w<sub>0.25%</sub> CE-A. The slower growing rate and final thickness of the dry zone may be related to the higher CE content (0.4%), which intensifies polymer film formation that creates a barrier to water evaporation. This result reinforces CE's water retention ability, and by its increase, less water is lost from the mortars.

Bülischen et al. [3] studied methyl hydroxyethyl cellulose (MHEC) water retaining ability and identified two effects: the water sorption and the formation of a hydrocolloidal associated 3D polymer network, which may be the barrier that is reducing the rate of skin formation. Results from Jenni et al. [1], Bühler et al. [2] and Faiyas et al. [165] also indicated the formation of a polymer film at the granular structure. Jenni et al. [1] observed polymer enrichment at mortar's surface due to water flow towards the surface with evaporation and skin formation, while Bühler et al. [167] concluded that the flow of water towards the evaporation front did not only transport organics, but also cementitious ions which did enrich the evaporation front and locally caused early precipitation of hydrates and carbonates. In the present work, while the redispersible polymer powder is constant, the CE concentration is different for each formulation, and higher concentration could lead to earlier formation of polymer film barrier that prevents water evaporation. Thus, the present results cannot confirm or deny the hypothesis of organic transportation.

For adhesive mortars, the higher the CE content, the higher the skin rigidity. However, MRI results indicate that for 0.4% of CE, the dry layer formed is thinner than that of the composition with 0.25%; thus, the rheological properties of the skin are not only related to its thickness. Early precipitation, polymer enrichment, film formation and carbonation at the interface could influence rheological properties of the dry layer.

#### 4.4.2 Interfacial Rheology of skin

In this section, the results of the introduced technique, interfacial rheology for adhesive mortars, are discussed. Three parameters are evaluated that influence the interfacial properties of mortars with white cement and gray: CE content, DS of CE, and environmental conditions.



#### 4.4.2.1 Effect of CE content

In Figure 77a, the obtained results are shown with the vane fully immersed, at the bulk ( $G'_{bulk}$ ), and the vane partially immersed at 3 mm ( $G'_{3mm}$ ) of the interface for formulations with white cement and different CE content. It is clear from the graph that the measurements difference is about one order of magnitude, indicating that the properties of the interface increase faster. The number of boussinesq in this case is,  $B_0 \cong 10 \gg 1$ ; the properties of the interface are dominant in the measurements. From equation 2,  $G'_{interface}$  was obtained from the difference of  $G'_{3mm}$  and  $G'_{bulk}$  and shown in Figure 77b. Water loss was also plotted in Figure 77b.

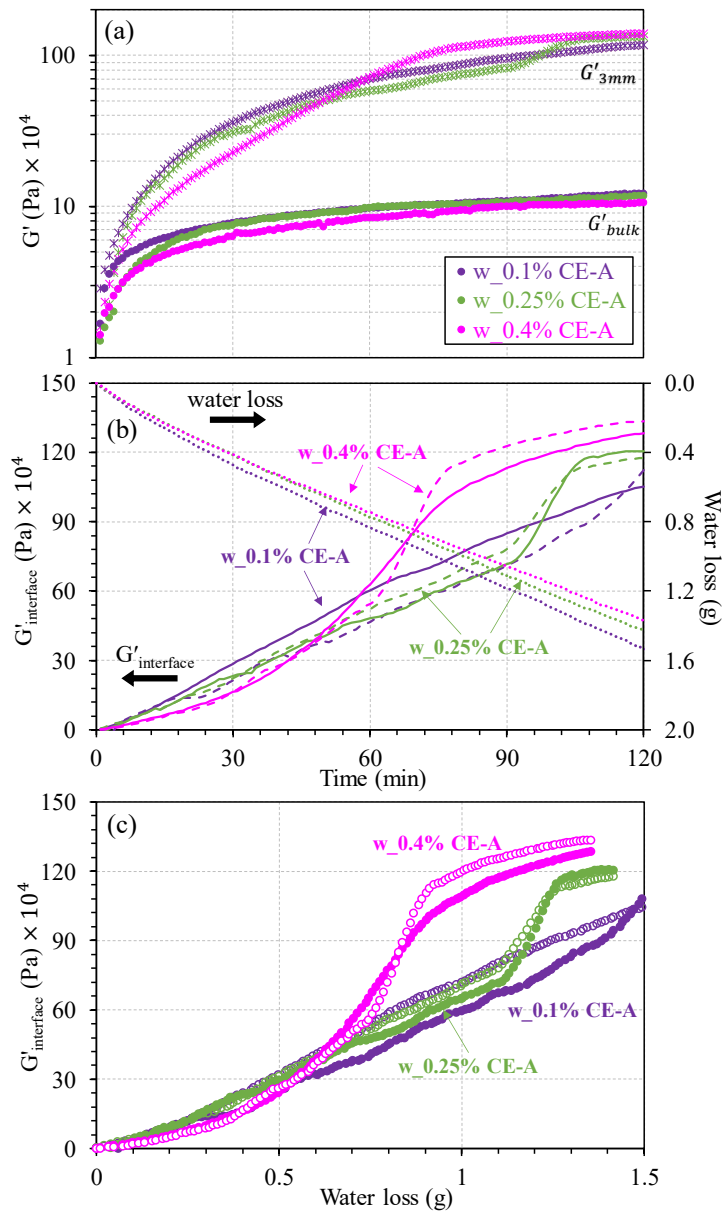


Figure 77. (a) Bulk measurements ( $G'_{bulk}$ ) and 3mm measurements ( $G'_{3mm}$ ) of adhesive mortars with different CE content formulated with white cement (b)  $G'_{interface}$  calculated by the different of the  $G'_{3mm}$  and  $G'_{bulk}$  (c)  $G'_{interface}$  vs water loss of adhesive mortars with different CE content formulated with white cement.

In the first 30 minutes, the  $G'_{\text{interface}}$  of all formulations has a linear increase, and the higher the CE content, the smaller the rate. The formulation with lower CE, w\_0.1% CE-A remains linear during the entire test. Around 90 minutes, w\_0.25% CE-A has an inflection and its values also increase at a higher rate, but stay between w\_0.1% CE-A and w\_0.4% CE-A. Between 30 and 60 minutes, the w\_0.4% CE-A curve has an inflection and its values achieve higher values than the other formulations.

Similar results regarding the influence of CE on the interfacial properties on  $G'_{\text{interface}}$  can be observed for gray cement in Figure 78a. g\_0.1% CE-A presented a linear increase during the entire test. In the other formulations, g\_0.25% CE-A and g\_0.4% CE-A, a period of linear evolution occurs in the beginning. In this first linear period, the higher CE content, the lower  $G'_{\text{interface}}$  increase slope. After a linear period, the formulations with higher CE content, g\_0.25% CE-A and g\_0.4% CE-A, show an inflection and change their increase rate. For g\_0.25% CE-A, the inflection occurs around 75 minutes, while for g\_0.4% CE-A, around 60 minutes. At the end of the test, at 2h, the formulation with higher CE content, g\_0.4% CE-A, achieves the highest values, followed by g\_0.25% CE-A and g\_0.1% CE-A.

Results indicate that higher CE content in the formulation initially generates a reduction on rheological property evolution of the interface, but it induces a higher final value. This is explained by CE's water retaining effect, which delays water/powder concentration decrease of the mortars with higher concentration of CE, and consequently delaying  $G'_{\text{interface}}$  evolution. In Figure 78b, the same  $G'_{\text{interface}}$  results correlated with the water loss for each cement type formulation are shown. This correlation reinforces that during a first moment, the interface evolution is related to water loss and increases linearly, but for the formulations with higher CE content, an inflection occurs. This inflection is related to a polymer property's dominance. The higher the concentration, the earlier this inflection occurs; therefore, the effect is seemingly related to the polymer concentration.



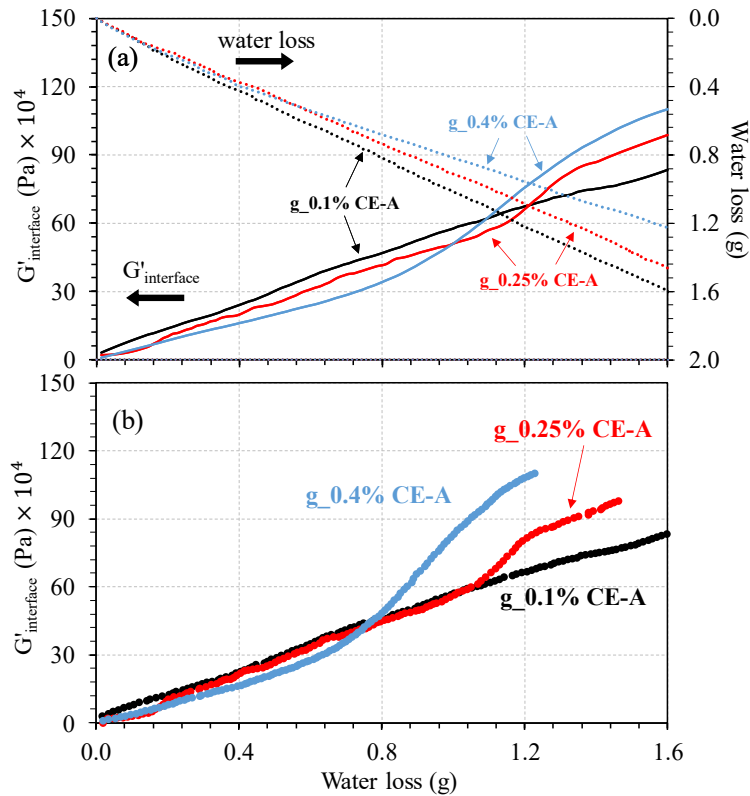


Figure 78. (a)  $G'_{\text{interface}}$  of adhesive mortars with different CE content formulated with gray cement and curves of water loss over time of each formulation (b)  $G'_{\text{interface}}$  vs water loss of adhesive mortars with different CE content formulated with gray cement

MRI results in Figure 76 reinforce that the change in behavior is related to the polymer dominance. One can observe that compared to w\_0.25% CE-A, w\_0.4% CE-A has smaller dryer layers; however, the interfacial properties show that during this period, the higher CE content got a much higher storage modulus ( $G'$ ). This indicates that in the first 30 minutes, the interfacial properties are related to water/powder concentration and evaporation, but then the polymer film, other early hydrates or carbonation start to influence rheological properties.

The results of  $G'_{\text{interface}}$  divided by water loss at the end of the test for both series with gray and white cement are shown in Figure 79 as a function of CE content. The increasing tendency of the  $G'_{\text{interface}}/\text{water loss}$  shows that  $G'_{\text{interface}}$  increase is not only related to water loss, but also to the effect of CE content on the skin composition.

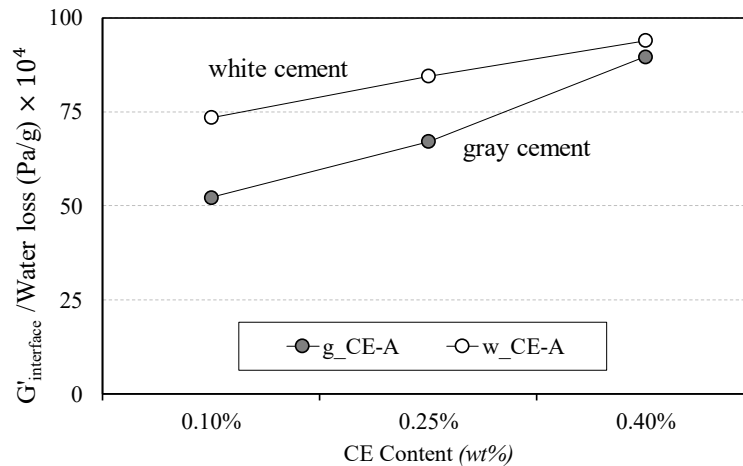


Figure 79.  $G'_{\text{interface}}/\text{Water loss}$  vs CE content at  $t = 2$  hours of formulations with grey and white cement.

Finally, the introduced method was able to extract a clear difference between the various formulations and enabled quantification of the rheological properties of the skin. Thus, it was possible to verify the level of influence that CE content has on skin properties.

#### 4.4.3 Effect of CE type

In Figure 80a,  $G'_{\text{interface}}$  of white cement formulations with different CE types and water loss over time are shown. The water loss is represented with dotted lines; from the curves, it appears that the type of CE did not have a considerable effect on water evaporation. Their nominal viscosities are equal, but have a different DS and MS. It did not affect the water loss considerably; however, the interfacial property's evolution presents some small differences.

In Figure 80b,  $G'_{\text{interface}}$  of gray cement formulations with different CE types and water loss over time are shown. Compared to white cement, the water loss results do not show a considerable change between the different CEs. For the gray cement, however, the differences on skin rheological properties are clearly noted. For  $g_{0.25\%}$  CE-B, an inflection occurred around 60 minutes, earlier than  $g_{0.25\%}$  CE-A and  $g_{0.25\%}$  CE-C at 90 minutes. This result may reinforce that the polymer properties start to be dominant and then an inflection occurs. These results indicate that the type of CE can have a different influence on skin formation depending on the cement type. The technique could also enable studies for comparing different polymers and predict non-performant raw materials.



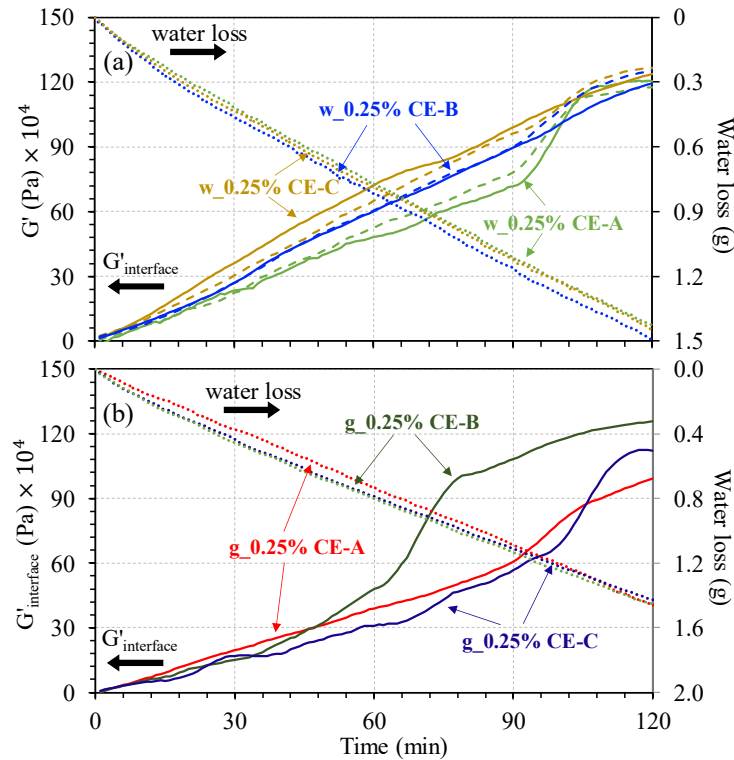


Figure 80.  $G'_{\text{interface}}$  of adhesive mortars with different CE types formulated with white cement (a) and gray cement (b). Each color represents a type; continuous and dashed lines are test repetitions. Water loss over time of the same formulations is represented by dotted curves.

#### 4.4.4 Wind effect for gray cement

In Figure 81,  $G'_{\text{interface}}$  of white cement formulations with different CE content at two different environmental conditions (with and without wind) are shown. The samples in windy conditions are represented with continuous lines and normal conditions with dashed lines. The graph shows that at windy conditions,  $g_{0.1\%}$  CE-A has a linear increase until 45 min when it starts to get into a plateau, in non-windy conditions, it linearly increases during the whole experiment. In the case of  $g_{0.25\%}$  CE-A in windy conditions, until 20 minutes it has a linear increase and then as inflection occurs with a high increase of  $G'$  until 60 min when it gets into a plateau. At non-windy conditions, this occurs at 90 min and have a faster increasing rate until the end of the test.

For  $g_{0.4\%}$  CE-A, in windy conditions it has a similar behavior to  $g_{0.25\%}$  CE-A. The formulation with 0.4% CE has a smaller increase rate in the first 20 minutes, but after the inflection, it has a strong acceleration and at 40 min overcome  $g_{0.25\%}$  CE-A (Wind) go then start a plateau. In non-windy conditions, the smaller rate in the beginning also happens until the inflection point where it accelerates and overcome the other CE content formulations.



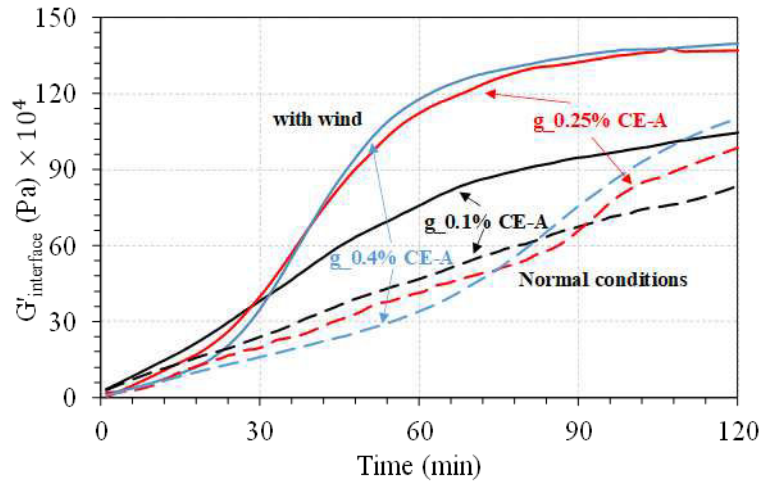


Figure 81. Interfacial storage modulus of adhesive mortars with different CE content in windy conditions (continuous line) and the reference without wind (dashed lines)

It seems that comparing with wind and non-wind conditions, all formulations have a similar behavior with a linear evolution rate until it have an inversion of behavior where the highest CE properties overcome the others. However, in windy conditions, all this process seems to have accelerated, since it accelerates water evaporation process.

#### 4.5 Chapter conclusions

In this chapter, an investigation regarding the formation of skin layer on fresh adhesive mortar is presented. The association of MRI, evaporation measurements and rheology techniques allowed to evaluate of the influence of cellulose ether (CE) content, different CE types and environmental conditions on the formation dynamics of the skin and the evolution of its rheological behavior. MRI was employed to assess the water distribution within the mortar specimens including the air-mortar interface. It was possible to observe that for low content, as low as 0.1% CE, despite the higher evaporation rate, a dryer layer did not form until 1 hour, and after 2 hours it was very thin or related to retraction, around 0.2 mm. For higher CE contents however, a dryer layer formed linearly, around 3 mm for w\_0.25% CE-A and 1.5 mm for w\_0.4% CE-A after 2 hours.

The rheological evaluation of bulk properties indicated that in the very beginning air entrainment predominantly influenced the mortar when smaller dosages of CE were used, from 0.1% to 0.25%. For 0.40% of CE, the air entrainment saturation was reached and the polymer effects increased  $G'$  initial value. However, CE also delays the structuring process of cement particles, which generates an inversion for the content above 0.25%. Finally, after about 3 minutes the tendency is that the higher the CE content, the lower  $G'$ . Regarding the cellulose





ethers with different DS, the delay of  $G'$  evolution was stronger for mortars with CE of higher DS. Further investigation is necessary since this measured effect contradicts the published literature.

An interfacial rheology technique for mortars was introduced in this work, aiming to evaluate the skin rheological behavior during the first two hours. The technique was able to quantitatively compare different formulations and conditions. For different CE contents, it was observed a transition from a dominant water evaporation effect to a dominance of the polymer effect on the rheological properties of the skin in mortars with two different cements. Higher CE contents induce less water evaporation, which dominates the skin behavior in a first moment, resulting in smaller  $G'$  values. Then, in a second moment, the polymer properties start to dominate, and higher contents induce higher  $G'$  values.

When CE with different degrees of substitution was evaluated, different inflection times were observed despite the similar viscosity of the polymers and water evaporation rate. Under different environmental conditions, similar behaviors of the mortars were verified, but with accelerated evolution when windy conditions were applied.

This new interfacial rheological method for suspensions can be useful to evaluate the influence of different conditions and mix designs, to better understand skin formation, and to improve adhesive mortar's performance.





## Chapter 5 – Microstructural evaluation with micro-tomography and adhesive stress

### 5.1 Chapter Introduction

Tomography is a known technique in scientific and non-scientific domains. It has been extensively used in other fields, such as the medical and biological field [168–170]. In construction material domain, the micro-tomography technique has gained attention in recent years. One of the reasons is its ability to obtain the mortar's microstructure 3D spatial visualization with a high degree of detail in a non-destructive way [171,172].

Microstructure has an important role on mortar's final performance; therefore, the technique was considered in this thesis to verify the mortar's microstructure in different conditions of application, additives formulation, and skin formation. The influence of polymers can be complex since the additives influence not only the rheological properties, but also the air entrainment, thus, the pores structure and size.

The influence of cellulose ether (CE) and redispersible polymer powder (Latex) on mortar's microstructure was evaluated by micro-tomography. The objective was to verify if skin traces can be observed in the microstructure depending on the formulation.

The mortar application method was also suspected to have an influence on the mortar's microstructure. Different application methods (with a flat spatula or toothed comb) were evaluated for different formulations. Possible changes in porosity due to air entrapping were considered, as well as if skin formation could have an impact on mortar's microstructure depending on the polymer content.

Through the images, defects on the generated contact is visualized in one of the samples, however, micro-tomography is not precise enough to observe interfaces, since it can be smaller than the pixel size. The contact is a critical factor for adhesion; however, Chapter 6 introduces a technique for contact visualization.

In addition to micro-tomographic measurements, waiting time evaluation, which consists of adhesive pull out tests for different waiting times, was also performed on adhesive mortars with different CE content. This allow us to verify the impact of CE content on adhesive properties in the hardened state.



## 5.2 Literature review

### 5.2.1 Fundamentals of tomography

Tomography is an imaging technique, focused on sections, that is based on computation reconstruction (CT) of X-ray images. The name Tomography derives from the greek *tomos*, "slice, section" and *graphō*, "to write". X-ray was discovered by a German physicist Wilhelm Conrad Röntgen in 1895, who earned the Nobel Prize in Physics in 1901. But, the implementation of the first X-ray computed tomography was only feasible with the development of modern computers. Thus, it was only made in 1972 by Godfrey Newbold Hounsfield (Nobel prize winner in 1979 for Physiology and Medicine), who constructed the prototype of the first medical CT scanner and is considered the father of computed tomography. After this, CT was immediately welcomed by the medical community and has often been referred to as the most important invention in radiological diagnosis, since the discovery of X-rays [173,174].

Computational tomography imaging systems usually consist of an X-ray source, motorized table, X-ray detector and a computation unit for data processing. The CT technique is based on the emission of a beam of photons by the X-ray source that is projected on the X-ray detector, creating cross section images of the objects for different defined angle positions of the complete revolution.

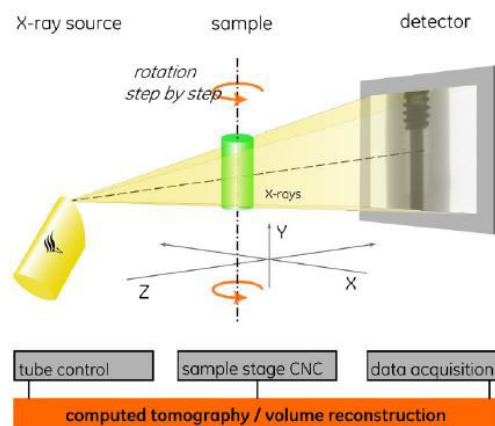


Figure 82. Illustration of the principle of a 3D acquisition by X-ray tomography from a series of 2D radiographs obtained by a sample in a fixed axis [Source: Phoenix|X-ray].

When a homogeneous sample of thickness,  $e$  for example, is exposed to an X-ray beam, the beam's intensity is reduced from  $I_0$  to  $I$ . Beer-Lambert came with the general empirical relationship of these two intensities, valid for all types of attenuation [175,176]:

$$I_0 = I \cdot \exp(-\mu e), \quad (16)$$



where  $\mu$  is the material's absorption coefficient. When the photons are emitted to the sample by the X-ray source, the photons can be absorbed, scattered or transmitted. The X-ray intensity reduction due to absorption and scattering is called attenuation; this signal does not reach the detector and only the transmitted photons that reach the detector are collected; and with this data, reconstruction of the scanned object is done.

In this investigation, micro-tomography is used. The classification of CT systems is based on their achievable resolution, measuring range and spot size as shown in Figure 83. Achievable resolution vs. measuring range [174,177]. Macro CT systems are used for large and micro CT systems for small objects. Micro CT can be achieved using X-ray tubes with small focal spot sizes (being in the range 1 - 50  $\mu\text{m}$ ) and by positioning the object close to the focus. In this way a higher geometrical magnification is achieved. The resolution of micro CT is limited by the size of the focal spot [174].

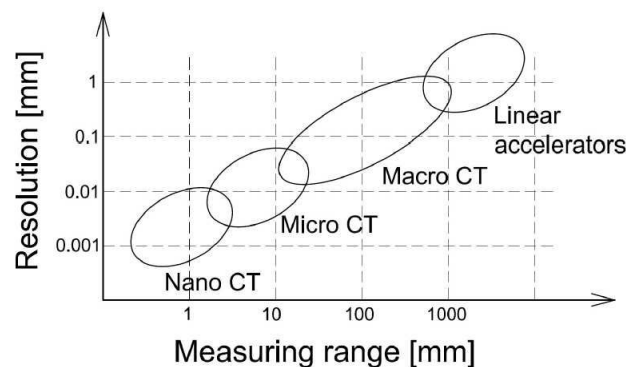


Figure 83. Achievable resolution vs. measuring range [174,177].

## 5.2.2 Influence factors of micro-tomography

One of the main limitations of micro-tomography is the large range of influence factors that affect the measurements. These parameters are important regarding the limitations of the technique when applied to our materials. Micro-tomography can give detailed information about a sample, but depending on its material or size, this level of detail can be considerably reduced. Therefore, in this section, the relevant aspects of the main parameters will be introduced.

### 5.2.2.1 X-ray source

X-rays are electromagnetic waves produced when an accelerated beam of electrons are emitted toward a metal. The interaction between the accelerated electrons and the metal's electrons generate a characteristic radiation and bremsstrahlung (braking) radiation, as a result, a spectrum of X-ray energy is produced within the X-ray beam. This spectrum can be



manipulated by changing the X-ray tube current or voltage settings, or by adding filters to select out low energy X-rays. Thus, different spectra of X-ray beams can be applied.

The source of X-rays can be: X-ray tubes, linear accelerators and isotopes. Each of them has the advantages and disadvantages. X-rays with higher energy penetrate more effectively than lower energy ones, so, linear accelerators offer better resolution and precision since its energy is higher. However, laboratories micro-tomographers have the advantage of being cheaper, therefore, easier to have access to experiments.

The X-ray source used in this research is an X-ray tube that has lower intensity if compared to a line accelerator's tomographer. This limits the ability to visualize some details of the materials, but it still offers enough resolution to many applications with lower resources application.

#### 5.2.2.2 Sample's size and material

The sample size and material have a considerable impact on the tomographic images resolution. According to the Beer-Lambert's equation, shown in section 5.2.1, the attenuation is proportional to the absorption coefficient ( $\mu$ ) and material thickness ( $e$ ). Materials with a greater thickness or higher absorption coefficient attenuate the signal that achieves the detector, which compromise the precision of the images.

In this research, tomographic images were used to identify possible traces on the mortars microstructure. Smaller samples would offer better resolution; however, in the case of adhesive mortars too small samples would not enable the representability of the system. Therefore, the samples need to be small enough to obtain precise images but should not be too small where the parameters evaluated cannot be implemented.

#### 5.2.2.3 Detector

An X-ray detector is used to measure the transmission of the X-rays through the object along the different ray paths. The purpose of the detector is to convert the incident X-ray flux into an electrical signal, which can then be handled by conventional electronic processing techniques. The detector also plays a role on the resolution obtained in tomographic image. The detector's quantum efficiency, number of pixels, read out speed (frame rate) and dynamic range affects quality of the image [174].

#### 5.2.2.4 Number of projections

The number of acquisitions represents the number of positions from a sample, hence the number of angles that the sample stops at until it reaches a complete turn of 360 degrees. The larger the



number of projections, the better the quality of the 3D image; however, the time of acquisition increases during this process.

#### 5.2.2.5 Exposition time

The exposition time corresponds the time which the receptor is detecting the image. It allows a better quality of the image, since higher density of signal can be obtained, but it is necessary that the material is perfectly still and not changing. It is similar to photographic camera's shutter speed, where movement during a photo shoot generates a blur. Thus, for in-situ tests or evolutive material's acquisition, the exposition time needs to be smaller than the characteristic time microstructure evolution [176]. Other parameters can compensate if the exposition time is limited, such as when using a higher intensity X-ray source.

#### 5.2.2.6 Limitations

Tomography in the recent years has represented a great tool for construction materials and other fields. However, some limitations still impact the use of this technique. One of the main limitations of tomography is the difficult-to-compare results and defining a standard, since there are a number of parameters that considerably affect the results. Therefore, there is no accepted procedure yet.

The scan time can dramatically change depending on many of the parameters. This can be a limitation considering limited time of equipment use availability. Also, cementitious materials are time dependent materials, and depending on the application such as fresh state evaluation, large scan times are not possible if the materials microstructure is changing over time.

### 5.2.3 Micro-tomography applied in cementitious materials

Landis et al. [178] describes X-ray microtomography applied to material characterization, such as mortars. This work focuses on synchrotron-based systems, which are a source of x-ray beam of high intensity. In the example shown in Figure 84, a 3D reconstruction of a mortar sample shows different levels of absorption, which represents the different phases of the mortar. This characterization can offer precious information of the microstructure in a non-destructive method.



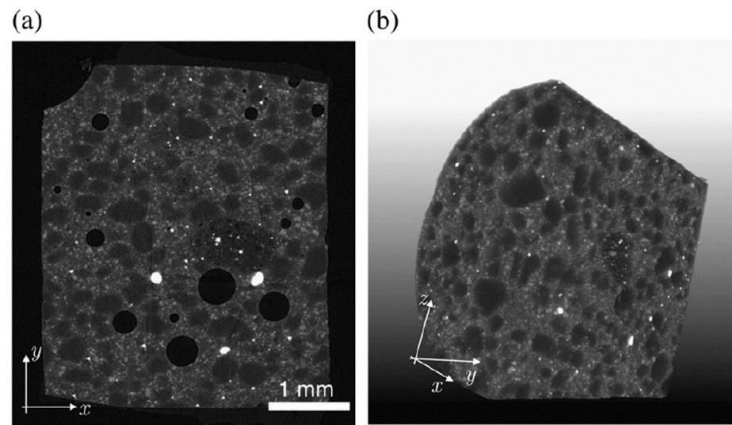


Figure 84. A mortar sample reconstructed slice image (a), and a sectioned 3D rendering (b). In these images, the brightness is a function of X-ray absorption, with bright spots showing regions of high absorption, and dark spots showing regions of low absorption [178].

Tamayo [176] used tomography to evaluate External Thermal Insulation Composite Systems (ETICS). Tamayo used 3D tomography for an in-situ characterization of an ETICS system during a mechanical flexion test. It is possible to observe the crack growing during the test, which offers valuable information concerning the mechanical properties. This is especially useful for materials that have some flexibility; brittle materials such as adhesive mortars and concretes are harder to obtain in-situ tests details, since does not present plastic deformation.



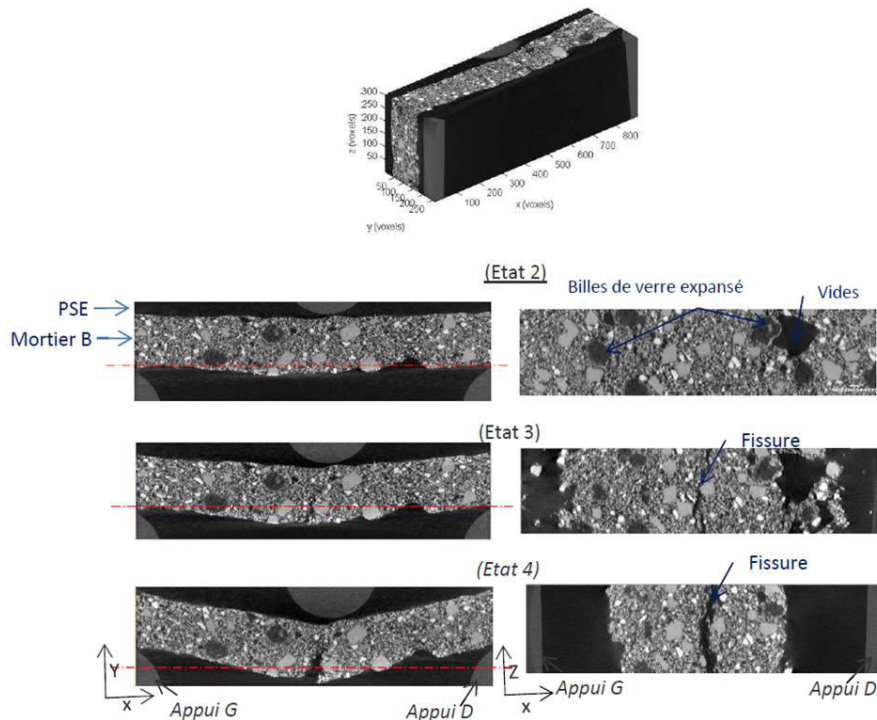


Figure 85. Tomographic sections of a reconstruction volume of an ETICS at different states of deformation; in the left, the XY sections; and in the right, the XZ sections at the fissuration [176].

Bentz et al. [172] studied the air-void instability and growth during drying of tile adhesive mortars. In this study, X-ray tomography was used to follow the evolution of air void during the fresh state of mortars. The technique was able to evaluate the stability of air voids, allowing to compare formulations with different polymer contents. In Figure 86, it is possible to observe a reference adhesive mortar voids changing over time, which the collapsing of air bubbles. Results show that air voids instability in adhesive mortars formulations; however, the information concerning the quantitative comparison of the formulations is limited. This type of analysis demands equipment that can acquire high quality images in a considerably fast acquisition time.

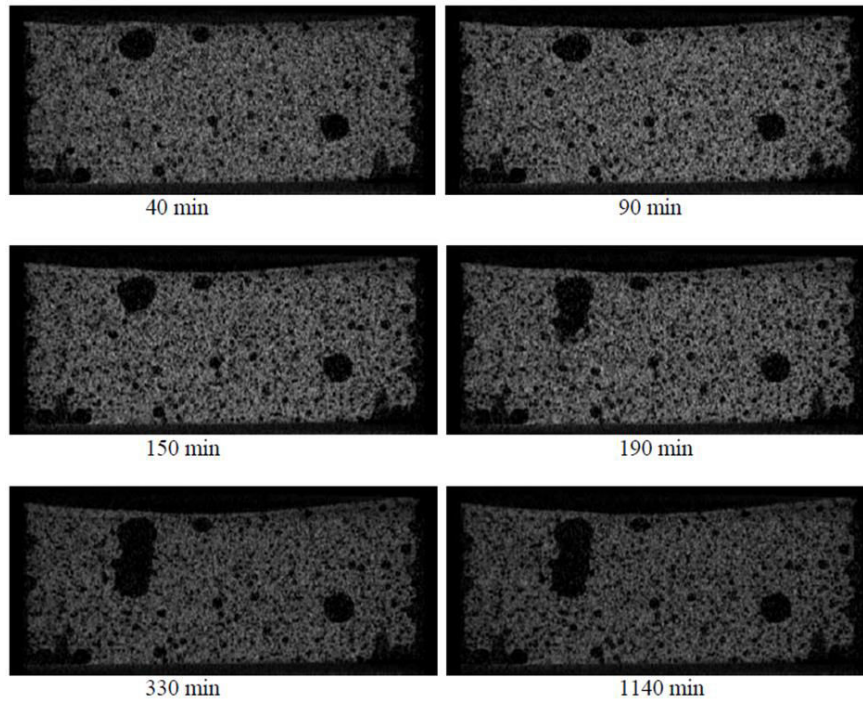


Figure 86. Section of a mortar sample at different evolution times [172].

Studies using tomography can offer useful information regarding the microstructure characterization either during a mechanical test or a fresh state evolution. since it is a recent technique; however, it is often limited by equipment or the analysis process, which is still being developed.

## 5.3 Experimental

### 5.3.1 Materials

Formulations	gray CEM I	white CEM I	sand	latex	CE-A	CE-B	CE-C	water/ powder	entrained air
<b>g_0.1% CE-A</b>	30%	-	67.40%	2.5%	0.1%	-	-		13%
<b>g_0.25% CE-A</b>	30%	-	67.25%	2.5%	0.25%	-	-		20%
<b>g_0.4% CE-A</b>	30%	-	67.10%	2.5%	0.4%	-	-		22%
<b>g_0.5% CE-A</b>	30%	-	67.00%	2.5%	0.5%	-	-		22%
<b>g_0.25% CE-B</b>	30%	-	67.25%	2.5%	-	0.25%	-		19%
<b>g_0.25% CE-C</b>	30%	-	67.25%	2.5%	-	-	0.25%		18%
<b>g_0% Latex</b>									

### 5.3.2 Methods

#### 5.3.2.1 Adhesive stress

The adhesive stress measurements were in accordance with the standard test EN 1346: Adhesives for tiles — determination of open time [179]. The summarized test procedure is:

- Application of a thin layer of mortar with a spatula on the standard concrete;
- spread of a line of adhesive mortar with a toothed comb at an angle of 45°;

- wait the specific minutes of the waiting time (5, 20 or 30 minutes);
- the tiles are then put in the position and put 2 kg weight on each tile, leave for 30 seconds and then remove the weight;
- After 28 days, the pull-out test is performed and the adhesive stress is calculated.

The ceramic tiles used were in accordance with the standard test EN 12004-2: Adhesives for ceramic tiles — Part 2: Test methods [180], which requires that the tiles used shall be enameled porous tiles, in accordance with EN 14411, group BIII, with a water absorption of  $(15 \pm 3)\%$  by mass, having a thickness of between 7 mm and 10 mm and reliefs with a thickness of less than 0.25 mm on the rear face, cut to obtain a beautiful face of dimensions  $(50 \pm 1) \text{ mm} \times (50 \pm 1) \text{ mm}$ .

### 5.3.2.2 Micro-tomography

The X-ray micro-tomographer used in this investigation was an X50 Computational Tomographer from *North Star* available at ENS-Cachan. The x-ray tube was a copper 225kV.



Figure 87. X-ray micro-tomographer available at ENS-Cahan (left); x-ray tube micro-oven of 225kV and detector of 3072x3888 pixels at high resolution (right). Adapted from [176].

#### 5.3.2.2.1 Sample preparation of microstructure evaluation of mortar applied with and without ribs (toothed comb and flat comb) and a ceramic tile applied with a fixed force

To evaluate the effect of the application of ribs on the microstructure of the mortar, samples with combed mortar and flat mortar with different CE content and Latex content were evaluated. A normalized substrate was cut to approximately 5 mm, since the normalized thickness of substrate would generate a sample 3-4 times bigger, which would reduce the quality of the 3D tomographic image. The mortar thickness (gap) varied according to the mortar's rheological properties.

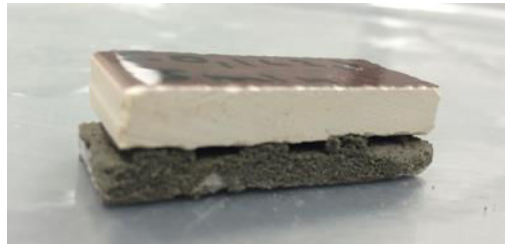
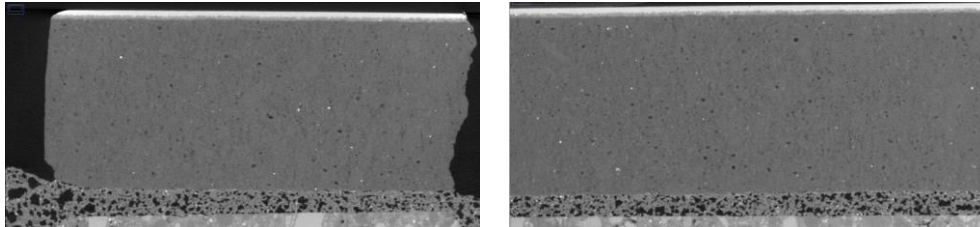


Figure 88. Sample example: concrete substrate on bottom, mortar with ribs and ceramic tile on top.



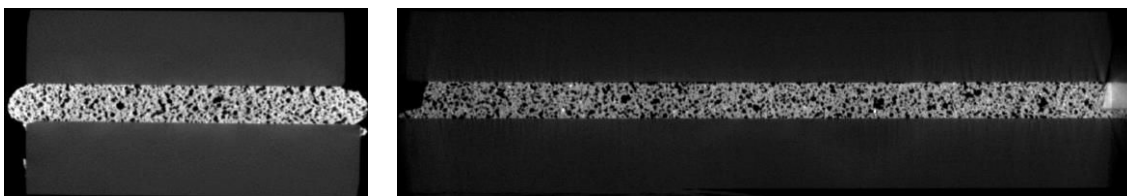
Cross section

Longitudinal section

Figure 89. Cross and longitudinal sections of a ceramic-mortar-tile sample

#### 5.3.2.2.2 Sample preparation of microstructure evaluation of mortar applied with and without ribs (toothed comb and flat comb) and the gap fixed to 2 mm

To evaluate the effect of the application of ribs on the microstructure of the mortar, samples with combed mortar and flat mortar with different CE and Latex content were evaluated. Plexiglass tiles of  $20 \times 50 \times 5 \text{ mm}^3$  were put together with the mortar, one with a toothed comb and another with a spatula to generate the flat surface. After 5 min waiting time, another tile was put in top of the samples with a 2 mm spacer to ensure the gap size and squeezed with a 1 kg weight, in the case where the gap was not achieved; it was manually squeezed until it achieved the 2 mm gap. In this case, the mortar's thickness was kept constant around 2 mm. In this case, plexiglass tiles were used instead of normal tiles and substrates, since it would guarantee a perfect gap to compare the different formulations, and also the main goal of this series of tests was to verify if the use of toothed comb would have a relevant effect on air entrapping and consequently affecting the microstructure.



Cross section

Longitudinal section

Figure 90. Cross and longitudinal sections of a tile-mortar-tile sample

For the analysis of the samples, *Fiji* software was used to analyze gray distribution and porosity. Each formulation's porosity was calculated using the gray distribution from the sum of a considerable part of the 3D volume. The peaks were divided by the lowest region between the two peaks. Each formulation was applied with a toothed comb and a flat spatula and the porosity

was compared. The samples' mortar zones were divided in three regions: upper, middle, and bottom and the gray distribution was also evaluated.

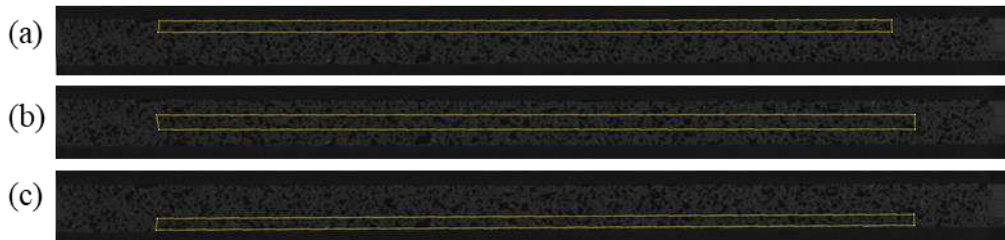


Figure 91. Exemplification of the zones of the sample: (a) upper, (b) middle), and (c) bottom.

## 5.4 Results

### 5.4.1 CE content effect on adhesive stress

In Figure 92, the adhesive stress results of formulations with different CE content for 5, 20 and 30 minutes waiting time are shown. The formulations used in this research are model adhesive mortars, thus they may not adhere to adhesive stress performance requirements for commercial use.

For the initial waiting time, the higher the CE content, the higher the adhesive stress. This result is probably related to CE's effect on water retention, since it maintains the moisture in the mortar, allowing a higher degree of cement hydration, generating higher mechanical properties at 28 days. This is highlighted by the linear increase of the adhesive stress values as the CE content is higher. During the first 10 minutes, according to the results in Chapter 3 section 3.4.4 about squeeze flow, squeeze properties of the different formulations do not present considerable change yet, which means squeeze did not affect adhesive stress values.

For 20 and 30 minutes waiting time, g<sub>0.1%</sub> CE-A has low values, which means that for low CE content as 0.1%, the waiting time is lower than 20 minutes. This can be related to the fast structuring and high squeeze forces of the mortar, which was observed in bulk oscillatory properties in Figure 56 in Chapter 3 section 3.4.1.1 (pg. 80). Fast structuring and high squeeze forces influence the contact generated between the tile and mortar, resulting in low adhesive stress.

The type of rupture of the adhesive stresses also indicates the fragility of the interface, since it mostly occurred at the interface of the tile and mortar. The absorption of concrete substrate also accelerates the water loss, reducing the water/powder of the formulation and consequently hardening the squeeze of the sample. The air-entraining effect also improves squeezing properties of mortars; however, despite considerable differences in entrained air between the samples (0.1% CE-A – 13%; 0.25% CE-A – 20%; 0.4% CE-A – 22%), the adhesive stresses at



28 days do not show the same tendency, which indicates that this property was not dominant at the initial waiting time.

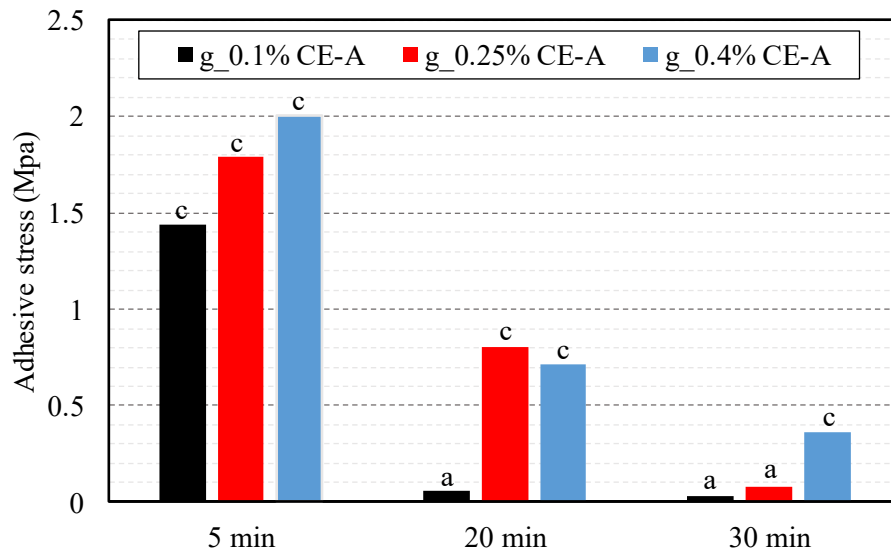


Figure 92. Graph of adhesive stress of mortar formulations with different CE content (a – adhesive; c – cohesive).

For the higher concentrations of CE, g\_0.25% CE-A and g\_0.4% CE-A, a similar performance was obtained for 20 minutes waiting time, but for 30 minutes, adhesive stress is lost for g\_0.25% CE-A. These results show that higher CE content and skin formation did not generate low adhesive stress as would be expected by higher skin formation observed on tack test results; alternatively, better adhesive stress performance was obtained. This better performance can be better explained by the better contact generated between mortar and tiles with higher CE content, which will be discussed on Chapter 6 section 6.4.1. The delay of structuring of the bulk rheological properties associated with the water retention maintains a fresh material inside the skin formed, and when squeezed, the ribs can be smoothly compressed, and fresh material can generate a good contact between the mortar and the tile.

#### 5.4.2 Concrete substrate-mortar-tile system micro-tomographic characterization

In this section, results of the samples of substrate-mortar-tile prepared as described in section 5.3.2.2.1 on micro-tomography are shown and discussed according to the CE effect, RPP latex effect, and application method.

##### 5.4.2.1 CE effect

In Figure 93, micro-tomographic images of adhesive mortar application with different CE content are shown. The images show a longitudinal cut of the sample, which is perpendicular to the direction of the ribs application. These samples were applied with a toothed comb and the waiting time is 5 minutes.





The mortars with lower CE content in Figure 93a show significant differences compared to the other formulations. Despite being applied in the same conditions of other formulations with 1 kg weight for 30 seconds, the squeeze and contact obtained is poor and there is space between the ribs. These results relate to the adhesive stress shown in previous sections and squeeze flow results in Chapter 3 section 3.4.1.1 (pg. 80). It illustrates how the mortar squeeze forces necessary to form a good contact are higher for this formulation, which is why poor contact and space between ribs is obtained. In the micro-tomographic image, it is already possible to observe failures between the mortar and tile contact, and in Chapter 6, the poor contact generated by formulation g\_0.1% CE-A will be further understood and observed.

The contact generated by the formulation with higher CE content, on the other hand, obtained a much better contact and no traces of the ribs can be observed, showing that the ribs merged when squeezed. The current results illustrate previous rheological evaluation, which indicate that the use of CE lowers squeeze forces, enabling a homogenous layer of adhesive mortar between the tile and substrate.

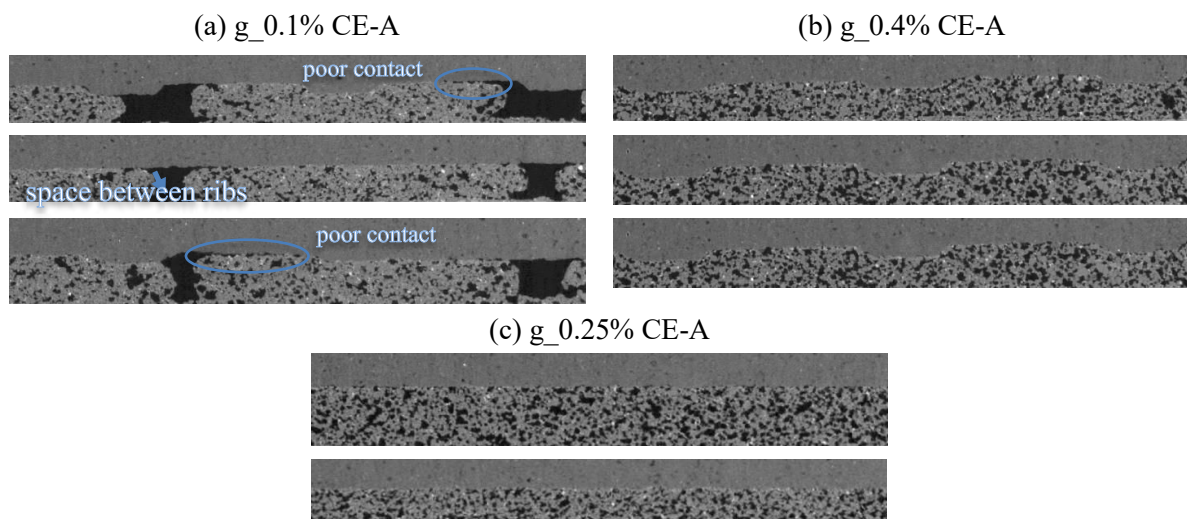


Figure 93. Longitudinal section of mortar-tile contact: (a) g\_0.1% CE-A; (b) g\_0.25% CE-A; and (c) g\_0.4% CE-A.

#### 5.4.2.2 Latex effect on constant force conditions

Latex has a considerable impact on the rheological properties of mortars. The addition of Latex to mortars causes a reduction of viscosity for the same water content. In Figure 94, it is clear that the contact generated for the formulations with 0% and 5% latex is considerably different. The ceramic tile was squeezed at an imposed force to the mortar, which responds accordingly to its rheological properties. The mortar formulation with 0% latex, has shown a much lower deformation, which can be clearly seen by the space between ribs in Figure 94a. The



formulation with 5% latex, on the other hand, had a complete deformation and a perfect contact generation.

Formulations with higher redispersible powder latex content have lower viscosity due to the “ball bearing” action of the polymer particles, the air entraining effect and a dispersing effect of surfactants [56]. The images illustrate higher pore concentration for the formulations with higher latex content, which eases the squeezing and, therefore, the contact between the mortar and the tile.

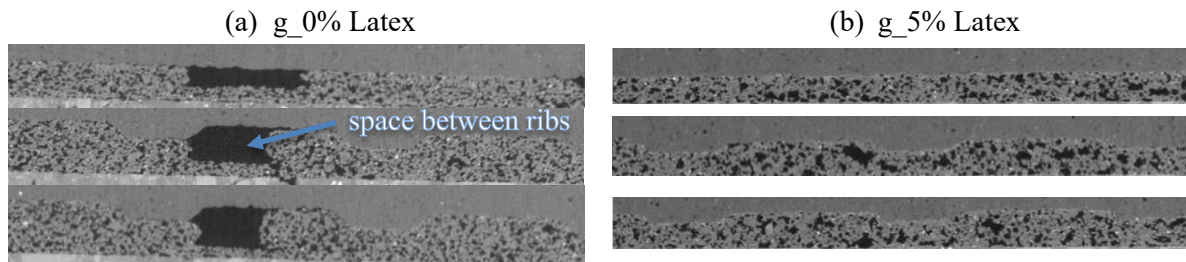


Figure 94. Longitudinal section of mortar-tile contact for formulations with (a) 0% and (b) 5% Latex

#### 5.4.3 Ribs and flat application effect on a tile-mortar-substrate system at constant force

In this section, formulation g\_0.25 CE-A was evaluated in two different conditions of application: by a flat spatula and by a toothed comb. In Figure 95, a cross section of each type of application is shown. In Figure 95a, one can observe that the use a flat spatula generated a failure between the mortar and the tile. This can be explained by the higher force necessary to squeeze the mortar; since it is a flat continuous layer, it requires a higher load to generate the contact and consequently, may not create a good contact.

Skin formation can also generate poor contact between mortar and tile, as it does not allow fresh material from the inside to get in contact with the tile, thus wetting the tile. Contact generation will be further discussed in Chapter 6 using a contact visualization technique.

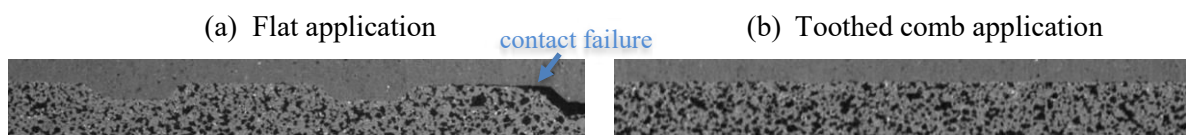


Figure 95. Longitudinal section of mortar-tile contact applied with a flat spatula and toothed comb (same scale)

#### 5.4.4 Pores distribution of mortar on a tile-mortar-tile system at constant gap

In this section, pore distribution is evaluated through micro-tomography. Polymer content (CE and RPP latex) and application methods impact on porosity and pore distribution through the depth are discussed.





#### 5.4.4.1 CE content and application method effect

Concerning the zones of the formulations, one of the hypotheses was that the mortar could have different pores distribution along the depth, and possibly a concentrated porosity in the middle zone. If this middle zone had a more concentrated zone of pores, this could induce cracking in this area.

In Figure 96, the gray level distributions of the formulations with different CE content with their respective application method are shown: on the left, histograms of the mortars applied with a toothed comb (rib) and on the right, the mortars applied with a flat spatula (flat).

From the results, little difference can be observed from the curves, also the porosity measures for each formulation were similar, leading to the conclusion that application method has no considerable effect on pore distribution or concentrated pores in the middle of the sample.

Due to difficulties on maintaining similar conditions and other factors, porosity calculation using micro-tomography is not yet established technique; however, consistent results in comparison to the results obtained during the fresh state indicate that the technique is reliable. Therefore, the hypothesis that the application method induces higher porosity in the middle of the sample was not confirmed through the technique. The porosity in the middle was not increased, and thus, there is no tendency of cracking in the middle of the sample.

This conclusion reinforces that the influence of the contact generation and good adhesion between the mortar and the tile are the most sensitive part of the system. Good contact and adhesive properties at this interface is crucial for good adhesive properties at the hardened state.



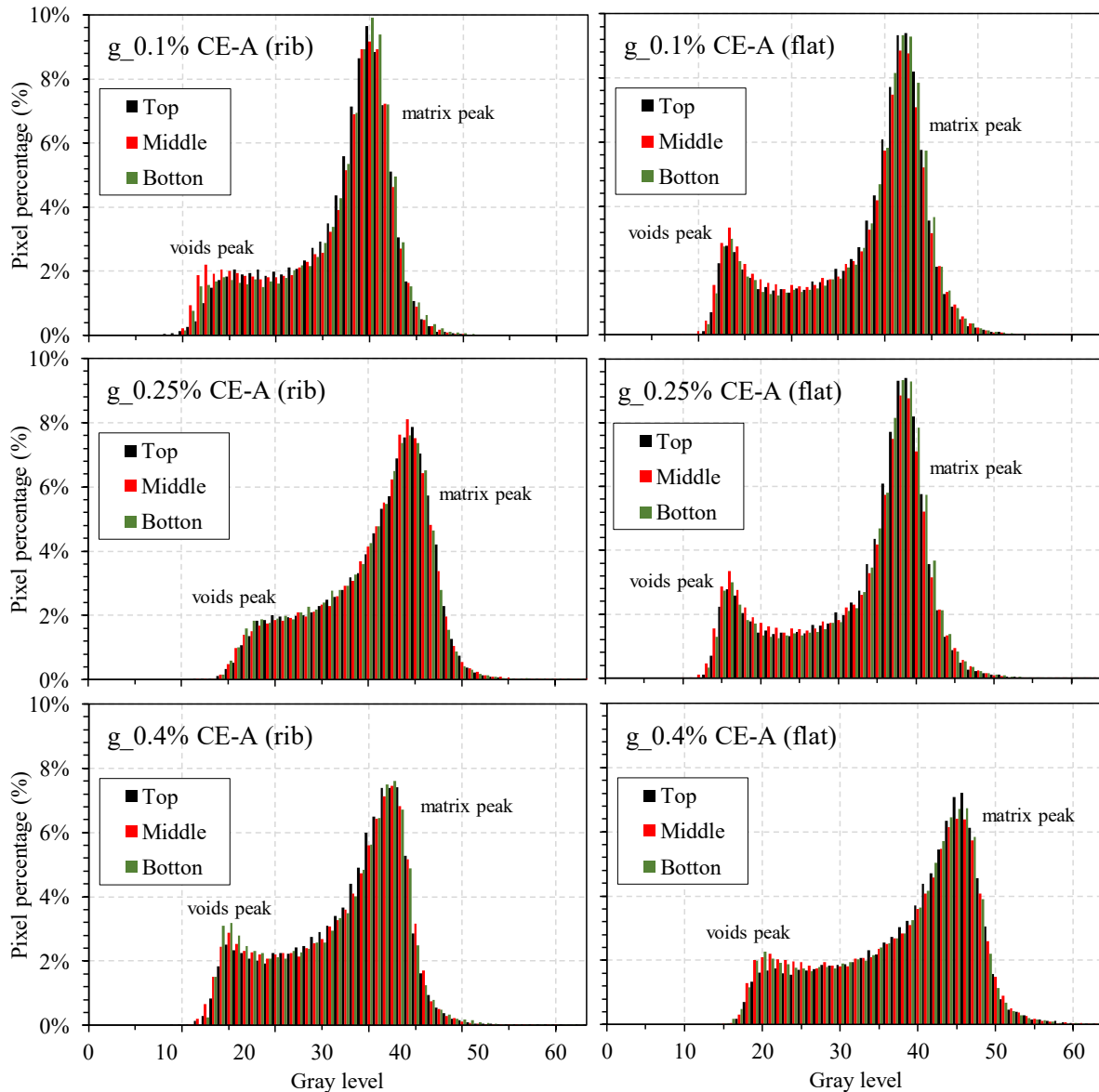


Figure 96. Gray level distribution of formulations with different CE content

#### 5.4.4.2 Latex content and application method effect

In this section, similar results to the previous section are shown, but the influence of RPP latex is regarded for the toothed comb and the flat spatula application. In Figure 97, a histogram of the formulations with 0% and 5% of latex with constant CE of 0.25% is shown. On the left side, the mortars applied with a toothed comb and on the right side, the mortars applied with a flat spatula are shown.

Similar results to the previous section are observed, with little difference in the gray distribution of top, middle and bottom of the samples. Therefore, it seems that the air incorporation in the middle of the sample is probably not due to the use-toothed comb.



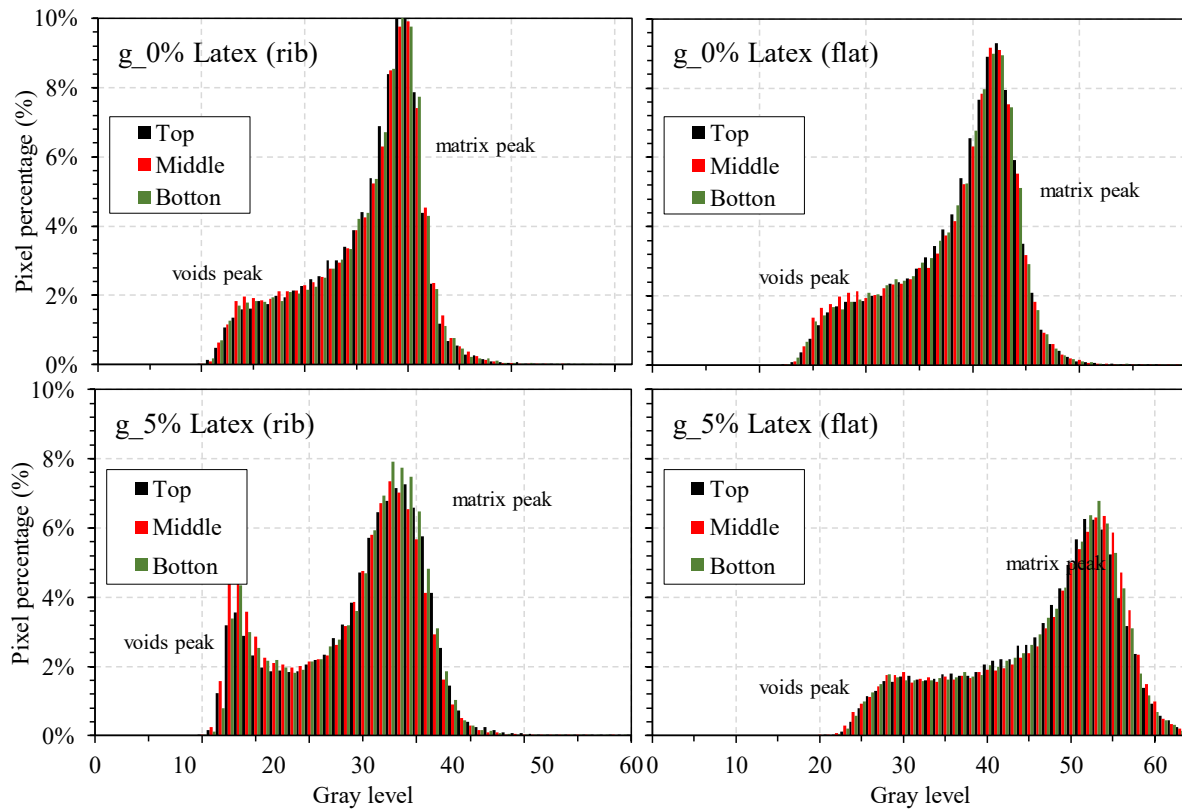


Figure 97. Gray level distribution of formulations with different Latex content

#### 5.4.4.3 Contact of adhesive mortar and tile

In Figure 99a, a micro-tomographic slice of  $g_{0.4\%}$  CE-A (rib) sample at the region between mortar and the tile is shown. In the image, one can clearly observe different zones of the squeezed ribs of mortars, the middle of the ribs where voids are observed, the zone between the ribs where smaller voids are observed and a line between the ribs, where air is entrapped at the interface, can be seen.

The upper tile was applied after 5 minutes of waiting time, which allows the mortar's interface to evolve, influencing the contact generation. The slice of the interface shows that voids can represent failures at the interface; thus, poor contact was generated in this region. These zones cannot be observed at the interface between the mortar and the bottom tile, shown in Figure 99b where the mortar was applied prior to the upper tile application, where the contact is expected to have a perfect contact, since the mortar is freshly applied at the bottom.



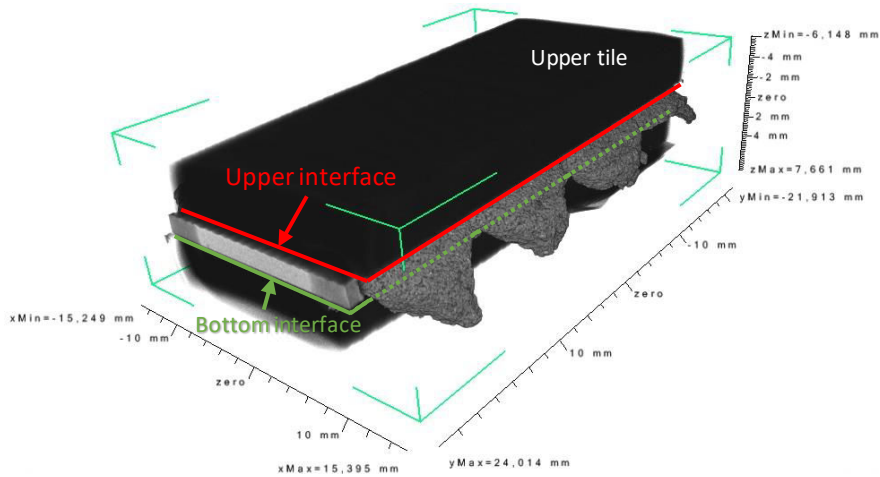


Figure 98. Sample of g\_0.4% CE-A (rib) formulation mortar.

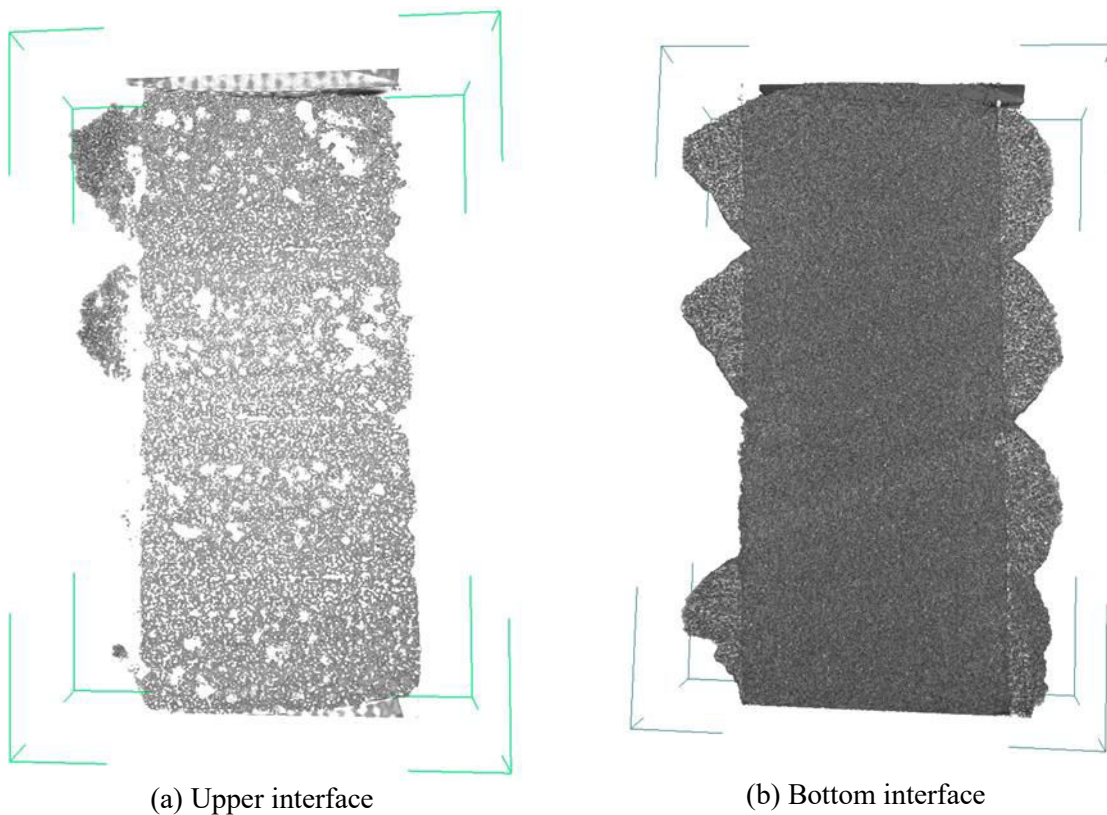


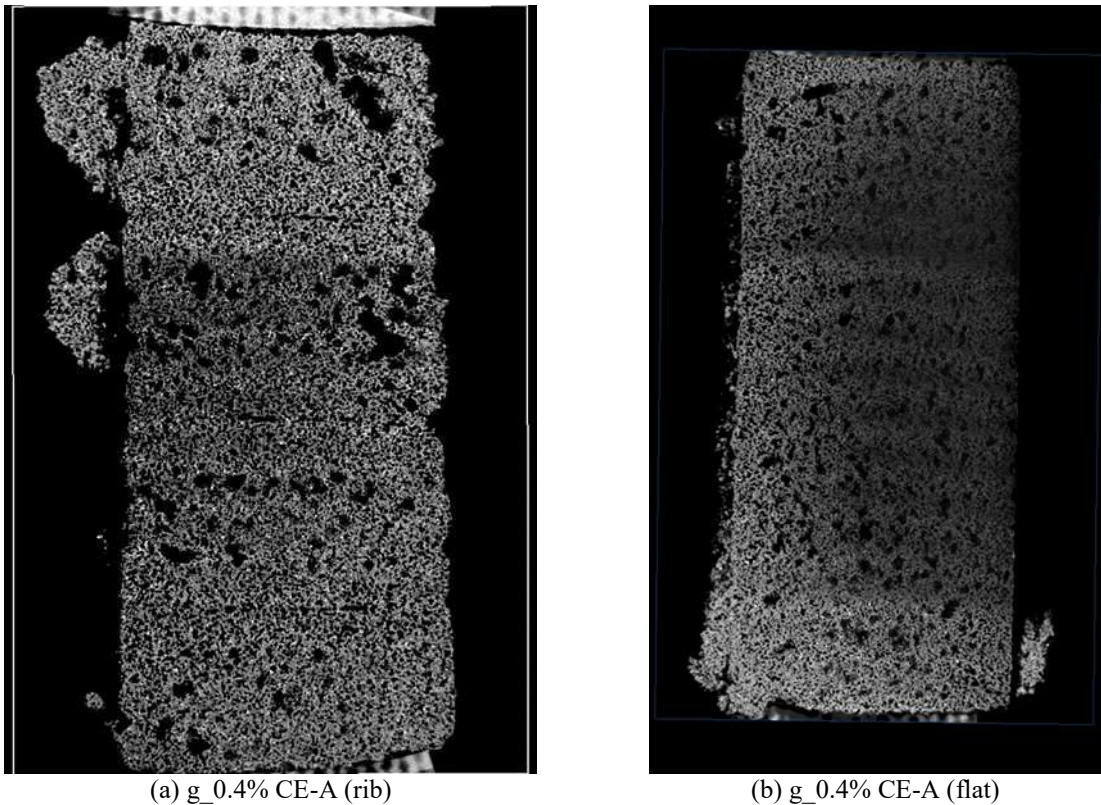
Figure 99. Mortar and tile interfaces of g\_0.4% CE-A (rib) formulation: (a) Upper and (b) bottom.

When toothed comb and flat spatula applications are compared in Figure 100, the region at the interface of the mortar and the tile shown are different. While the toothed comb, as already discussed, show regions at the middle of the ribs of larger voids and regions of small voids between them, the flat application shows a continuous zone of larger voids, which indicates that the generated contact was more imperfect.

This worse contact for the flat application can be explained by the squeeze properties in no slip conditions, where the material at the center of the squeeze flows outwards and little or no flow occurs at the plates in the outwards direction. The flat application can be compared to a rib



of a dimension of the tile; since there is no space for the inner material that flows outwards to make contact with the tile, there is no fresh material contact, which would generate a perfect contact. In this case, the skin that forms at the interface makes contact with the tile, as evaluated in the previous chapters, it has higher rigidity and less moisture content, interfering in the wetting of the tile.



(a) g\_0.4% CE-A (rib) (b) g\_0.4% CE-A (flat)  
 Figure 100. Contact between upper tile and mortar g\_0.4% CE-A with different application methods: (a) comb and (b) flat spatula

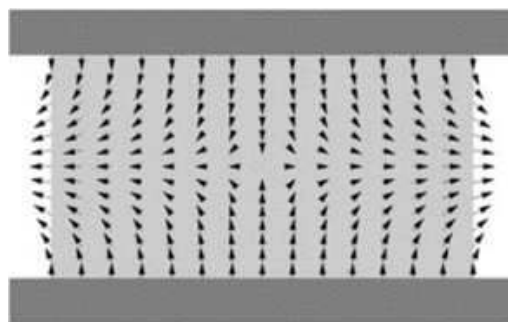


Figure 101. Velocity field for squeeze flows with no slip [128].

## 5.5 Chapter conclusions

The main goal of this chapter is to characterize the microstructure of adhesive mortar with micro-tomography. Different approaches to evaluate a variety of factors that may influence the

mortar's microstructure were used, such as: the pore distribution through the depth of an applied adhesive mortar; polymer's impact on the microstructure; and the application method on the mortar-tile interface.

The initial waiting time adhesive stress measurements, in addition to the micro-tomography, illustrated the impact of CE in the hardened state. Results show that CE improves adhesive properties in the initial waiting time and extended waiting time. This can be explained by the improvements on squeeze flow properties of the mortars when CE is added, which allows for better contact generation. Micro-tomographic images of the system show that the mortar with lower CE does not flow properly, leaving spaces between the ribs zones of contact failure between the mortar and the tile. The RPP latex impact was similar, and higher latex content resulted in better contact.

From the image of formulations with higher CE content, where skin is formed, it was expected that traces of the skin inside the microstructure could be observed, but for the level of details obtained from the micro-tomography, no traces of skin were observed, which indicates that the skin is probably able to re-homogenize when the tile is applied.

When the pore distribution was evaluated, results indicated that for the studied formulations, toothed comb use did not induce increased porosity in the different regions of the adhesive mortars. The gray levels distributions show a fairly homogenous distribution for all formulations, either with different CE content and Latex content.

The micro-tomography also allowed a visualization at the region of the interface between mortar and tile. The images show that the use of toothed comb improves contact generation between the mortar and tile, due to the squeeze behavior, which induces the inner fresh material to flow outwards and fill the gaps between the ribs, generating good contact zones.

Finally, the micro-tomography technique was able to verify some of the hypothesis of this thesis and illustrate clearly adhesive mortar's behavior discussed in the previous chapters.





## Chapter 6 – Evaluation of mortar-substrate contact generation with optical microscopy

### 6.1 Introduction

Contact is necessary for adhesion forces to act, which is why wetting capability, or contact generation, is an important concern when using adhesive mortars. In this chapter, a new visualization technique for interfaces will be introduced and used to describe different adhesive mortars and plexiglass contact generated during squeeze.

The technique is based on another available technique in literature, where a shallow light shows contrast between the areas of contact and non-contact in applied mortar in a hardened state [181]. Here, the technique is based on small depth of field microscopy, so precise and detailed analysis are possible in contact generated during the fresh state. Formulations with different CE content and CE types were evaluated using this technique and by transfer measurements.

The present chapter has key results to further comprehend the influence of skin properties on adhesion, also helping also to understand previous results.

### 6.2 State of art

#### 6.2.1 Contact visualization

##### 6.2.1.1 EN 1347 standard modification proposal

The mortar is applied in the form of ribs to allow fresh material to get in contact with the glass, as illustrated in Figure 103a. However, depending on the mortar's interface evolution, this skin can get rigid enough and not break during the squeezing of the tile. The wetting standard 1347 described on section 2.1.1.3.2 verifies the mortar's ability to wet the tile, however, it does not accurately predict the problem. Zurbriggen et al. [181] proposed a modification to the standard, using a light at an angle of  $90^\circ$  — setup illustrated in Figure 102 — which enables the



visualization of the interface between the glass and the mortar as shown in Figure 103. It is a clear illustration that the mortar skin can generate poor contact between the mortar and the tile.

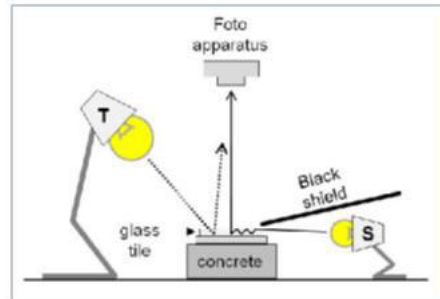


Figure 102. Experimental setup with two options for sample illumination. If the glass plate is illuminated directly from above (lamp “T” is on and lamp “S” is off), it can be observed how well the mortar ribs are deformed underneath the glass plate [181]

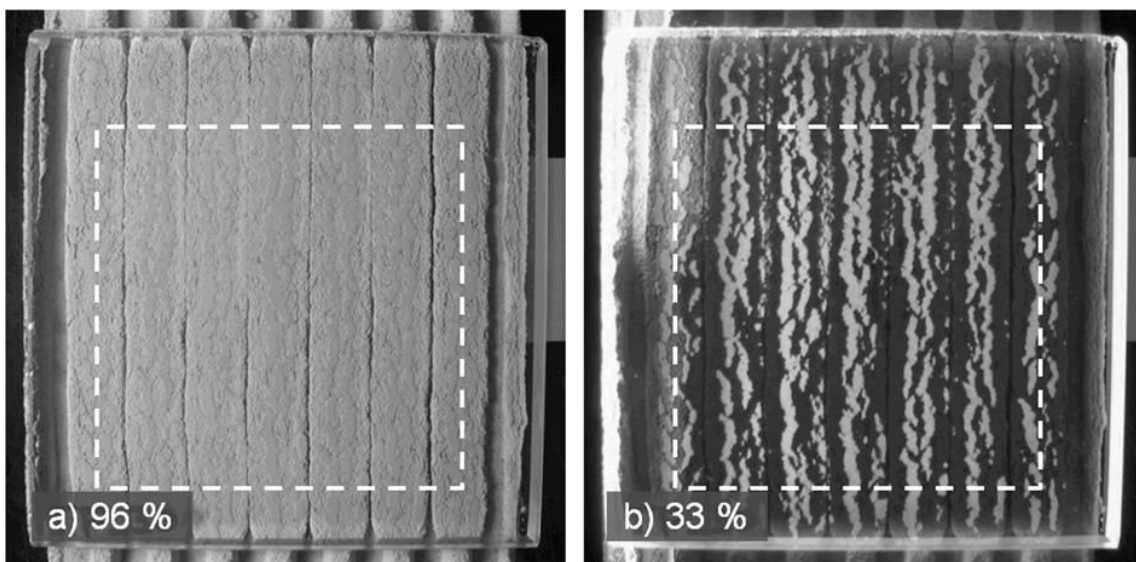


Figure 103. (a) Photograph of 10x10 cm glass plate embedded 30 min after the mortar (formulation F-ref in Table 1) was combed. Sample produced according to EN 1347. Mortar ribs are pressed to a degree of 96 area% (measured within the marked area). (b) Same sample illuminated from the side as described by Zurbriggen et al. [181]. Skin appears dark. Bright wetting area measures 33% (measured within the marked area).

### 6.2.1.2 Contact visualization of glass tile and mortar sprayed with red lacquer

In Figure 104, contact was generated by an adhesive mortar sprayed with red lacquer to mimic a skin and a glass plate tile. This technique was used to illustrate the areas where the fresh mortar was able to wet the glass tile and where the red skin stayed between the mortar and the tile. This agrees with squeeze flow no-slip behavior discussed in section 3.2.2.2. In Figure 105, a no-slip squeeze of an isothermal material is shown for a material of power-law index equal





to 0.3. It shows how the material from the middle of the cake flows toward the outer part, while the material where the skin would be located, at the surface, maintains at the same area. Even though the red lacquer used shows interesting results and illustration, it is avoided in this investigation due to concerns regarding if the red lacquer would affect the contact generation.

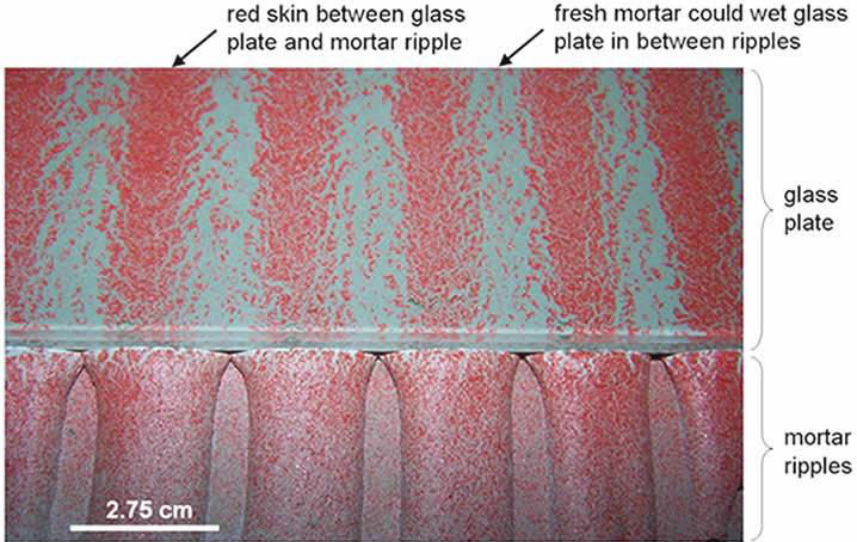


Figure 104. Contact generated [61].



Figure 105. no-slip squeeze of a isothermal material for different compression ratio (C.R.) of a material with power-law index equal 0.3 [182]

### 6.3 Experimental

#### 6.3.1 Materials and formulations

This work used basic compositions of adhesive mortars with gray CEM I 52,5 N CE CP2 NF from Lafarge. Cement phases, density and blaine fineness obtained with the manufacturer are



shown in Table 5 of section 3.3.1. The sand used in this study was a silica sand PE2LS from FULCHIRON. ASTM granulometric distribution from the manufacturer is shown on Figure 51 of section 3.3.1.

Table 10. Formulations of adhesive mortars with different cellulose ether content and types (wt%)

Formulations	gray CEM I	white CEM I	sand	latex	CE-A	CE-B	CE-C	CE-D	water/powder	entrained air
g_0.1% CE-A	30%	-	67.40%	2.5%	0.1%	-	-	-		13%
g_0.25% CE-A	30%	-	67.25%	2.5%	0.25%	-	-	-		20%
g_0.4% CE-A	30%	-	67.10%	2.5%	0.4%	-	-	-	0.34	22%
g_0.25% CE-B	30%	-	67.25%	2.5%	-	0.25%	-	-		19%
g_0.25% CE-C	30%	-	67.25%	2.5%	-	-	0.25%	-		18%
g_0.25% CE-D	30%	-	67.25%	2.5%	-	-	-	0.25%		-

### 6.3.2 Microscopical visualization method

To visualize the contact between the tile and the mortar with a high definition, we developed a microscopical technique. It is based on a simple concept of lens focusing. Using a microscopical set-up with a small depth of field, it is possible to visualize only a specific focus distance where the interface is placed.

In this work, a Digital Microscope Keyence VHX with VH-Z100R lens was used; the set-up is shown in Figure 106. The adhesive mortars were applied with a toothed comb on 5 cm x 5 cm x 5 mm prexiglass tiles and after 0, 5, 10, 20, and 30 minutes of waiting time, another tile was put with a 2 kg weight on the top for 30 seconds. The 2 Kg weight after different waiting time, as defined by the EN 1346 – Determination of open time [179].

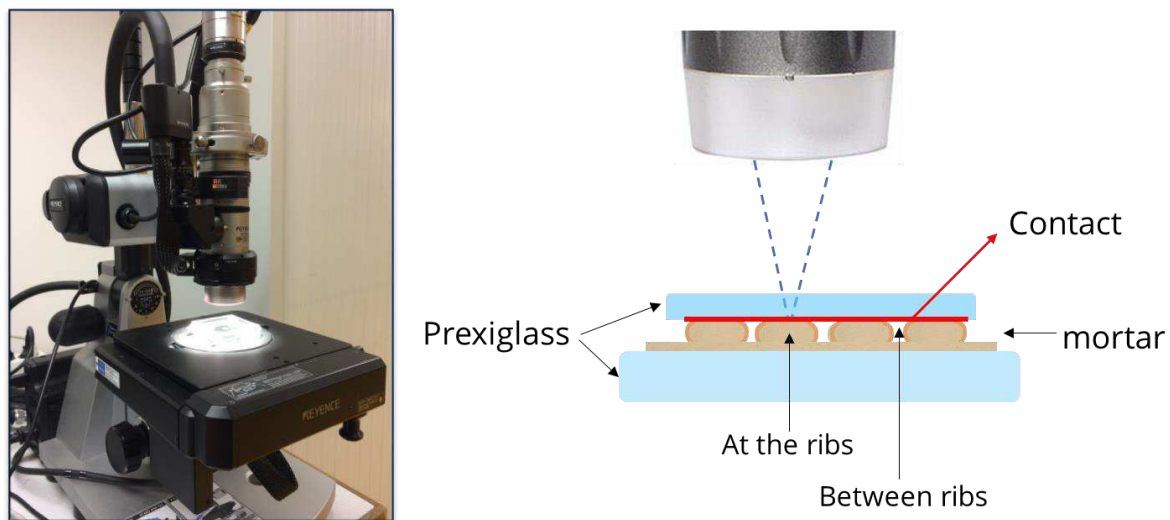


Figure 106. Digital microscope VHX (Left) and scheme of image obtained (Right)

After application, the samples were divided in different zones for the sample analysis, and also divided by the areas where the contact was generated by the compression from the top of the ribs (rib) or the material that squeezed between the ribs (between ribs).



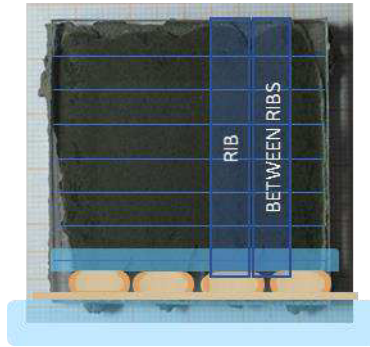


Figure 107. Sample mapping for image acquisition

The environmental conditions were kept at  $23^{\circ}\pm 1^{\circ}\text{C}$  and 40-50% RU. This test was carried for two studies; the first studied the influence of CE content, and the second studied the influence of CE type. To improve reliability, each study sample preparation was done on the same day and one after another. This ensured that the environmental conditions of the room between the formulations of the same study were similar, but discrepancies could occur between the two studies samples.

### 6.3.3 Determination of wetting capability/transfer

In this work, an adapted version of the European standard EN 1347 [5] was used to determine the wetting of the formulations studied. Since the study regarded the air-mortar interface and the skin formation, the effect of water loss on the substrate was eliminated using a non-absorbing substrate, a standard glass tile. The mortar was applied with a toothed comb, and glass tiles (5 cm X 5 cm) were placed on the adhesive mortar immediately for 10 min, 20 min, 30 min, 40 min, and 50 min, and loaded for 30 s. The glass tiles were then removed, and the transferred material was then visualized.

## 6.4 Results and discussion of Optical microscopy

### 6.4.1 CE content effect on adhesive mortars contact generation

The samples prepared for optical microscope visualization are shown in Figure 108. From the photos, it is possible to notice squeezing deformation differences between the different adhesive mortars formulations with different CE content. For the sample with lower CE content (g\_0.1% CE-A) after 10 minutes, it is noticeable that the ribs are not completely squeezed with the 30 sec of 2 kg weight, and with 20 min and 30 min waiting time, the squeezing was even less. For the sample with 0.25% CE-A, the squeeze was more squeezed and with 0.4% CE-A, it was even more. The higher the CE content, the more the sample squeezed.

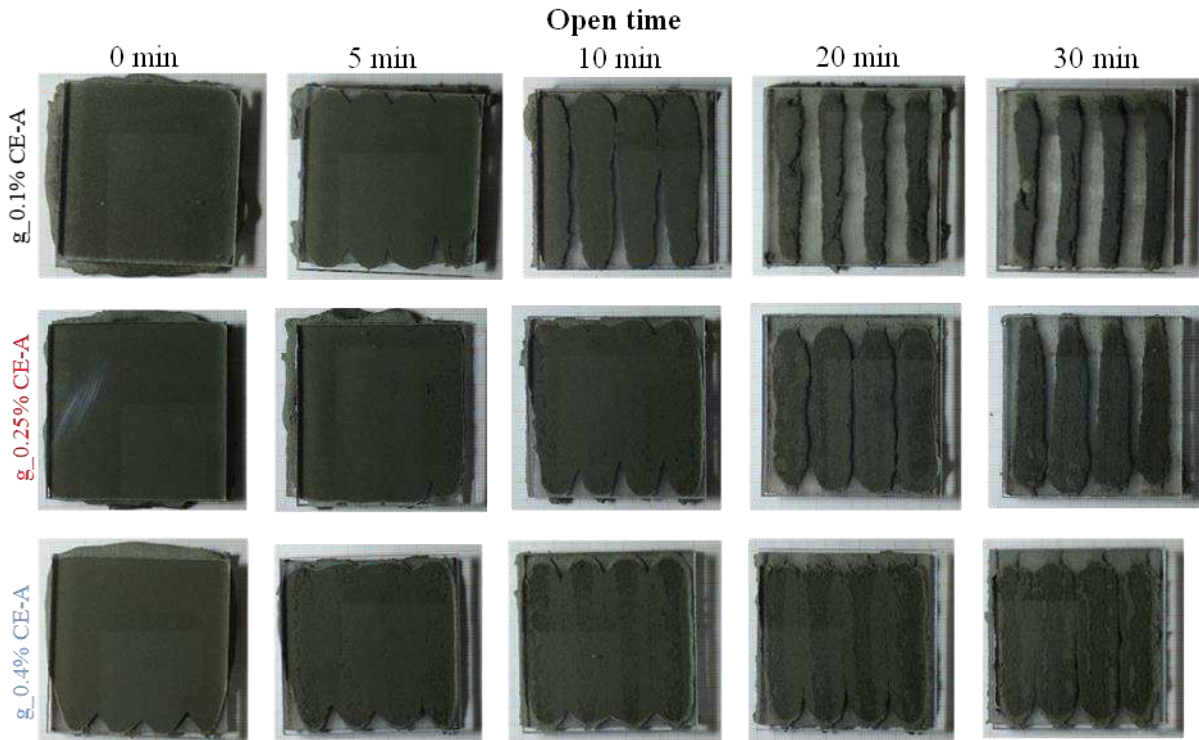


Figure 108. Samples of adhesive mortars with different CE content for contact visualization with optical microscopy

These results can be compared with squeeze flow results in section 3.3.2.3, of squeeze test results and also oscillatory tests. In the case of lower CE content mortar, as the waiting time increased, the normal force demanded for squeezing increased. Consequently, in this case, where the force is the same (2kg during 30 s), the displacement achieved is smaller.

When observing the samples of 5 min waiting time, it is not possible to observe the difference between the contact generated by the different formulations and at the ribs and between the ribs clearly. However, when these samples are observed by optical microscope, as in Figure 109, the differences become very clear. For the sample g\_0.1% CE-A, the contact seemed homogeneous, with many small spots of non-contact, and both the areas between and at the ribs had the same contact pattern. The sample g\_0.25% CE-A, on the other hand, had a perfect contact between the ribs, and at the ribs had some spots of non-contact. The same was found on g\_0.4% CE-A, but there were more non-contact spots.

These results can be explained by the skin formation of the adhesive mortar with higher CE content. After the mortar is applied, the skin started to form in mortar with higher CE, and as a result, when the tile was placed, the mortar's rib were squeezed, but the rigid material of the skin could not deform and generate good contact with the tile. The fresh material inside the rib, in the other hand, was able generate good contact with the tile. The mortar ribs behave as

described by the squeeze flow theory of non-slip condition squeeze flow. The material at the interior of the sample flow towards the out direction.

The sample g\_0.1% CE-A with lower CE content had an equal contact generated because there was no skin formed and the material lost moisture evenly, generating similar contact at the ribs and between them.

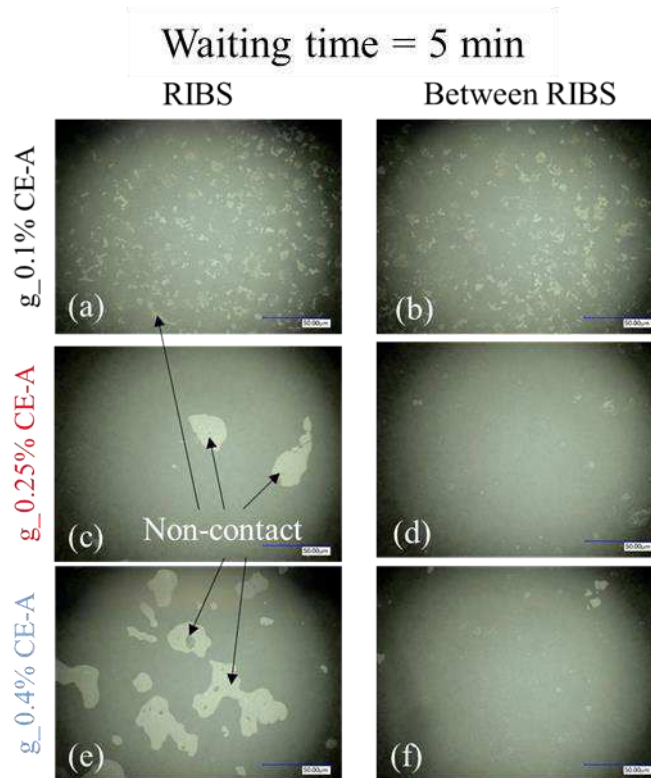


Figure 109. Microscopy images of contact

In Figure 110, the contact generated by g\_0.1% CE-A is shown for 5, 10 and 20 min waiting time. For 0 min, the sample was damaged and images were not able to be completed. At 10 and for 20 min, the sample squeezing ability was not enough to enable an area between the ribs where the materials merge. For 30 min, due to tile instantaneous detachment, it was not possible to visualize the contact generated. Finally, the contact generated by the squeezing of the ribs in this formulation, generated homogenous contact; however, the material demanded high forces to be squeezed and, in this case, it generated poor squeeze displacement, not enabling the material ribs to merge, and causing poor contact after 20 min.

When the evolution of the contact at the ribs is observed over the waiting time increase in Figure 111 for g\_0.25% CE, it is clear how the skin formation affects the contact generation at the area where it is squeezed; however, the area between the ribs had better contact for a longer waiting time. In the case of g\_0.1% CE-A, there were no ribs merging at 10 min, but for g\_0.25%, there was good contact generated at 10 min waiting time.





For the formulation with higher CE content, g\_0.4% CE-A, the effects of skin formation seem to have intensified. The contact became poor much faster at the ribs, indicating that the skin formed much faster. For 5 min, 10 min, and 20 min, the area of non-contact is larger for g\_0.4% CE-A in comparison to g\_0.25% CE-A. On the other hand, the rib squeezing ability, seems to have extended the contact by generating the between ribs contact for a longer waiting time. It means that despite the contact loss due to skin formation, the contact is extended due to the adjacent zones.

As discussed in Chapter 4, the higher CE content, the higher the rigidity of the skin formed. This would lead us to the conclusion that this skin would be generate a dryer and worse contact. However, the present contact visualization show that the opposite occurs, and the higher CE content, the better the contact for longer waiting times. This can be explained by the rheological properties discussed in Chapter 3 and interfacial characterization in Chapter 4. These results showed a slower evolution as CE is increased, either in oscillatory measurements, such as squeeze flow measurements, and MRI results showed a moisturized zone under the skin with higher CE content. This fresh material inside the skin is released when the ribs are squeezed and creates a good contact with the tile.



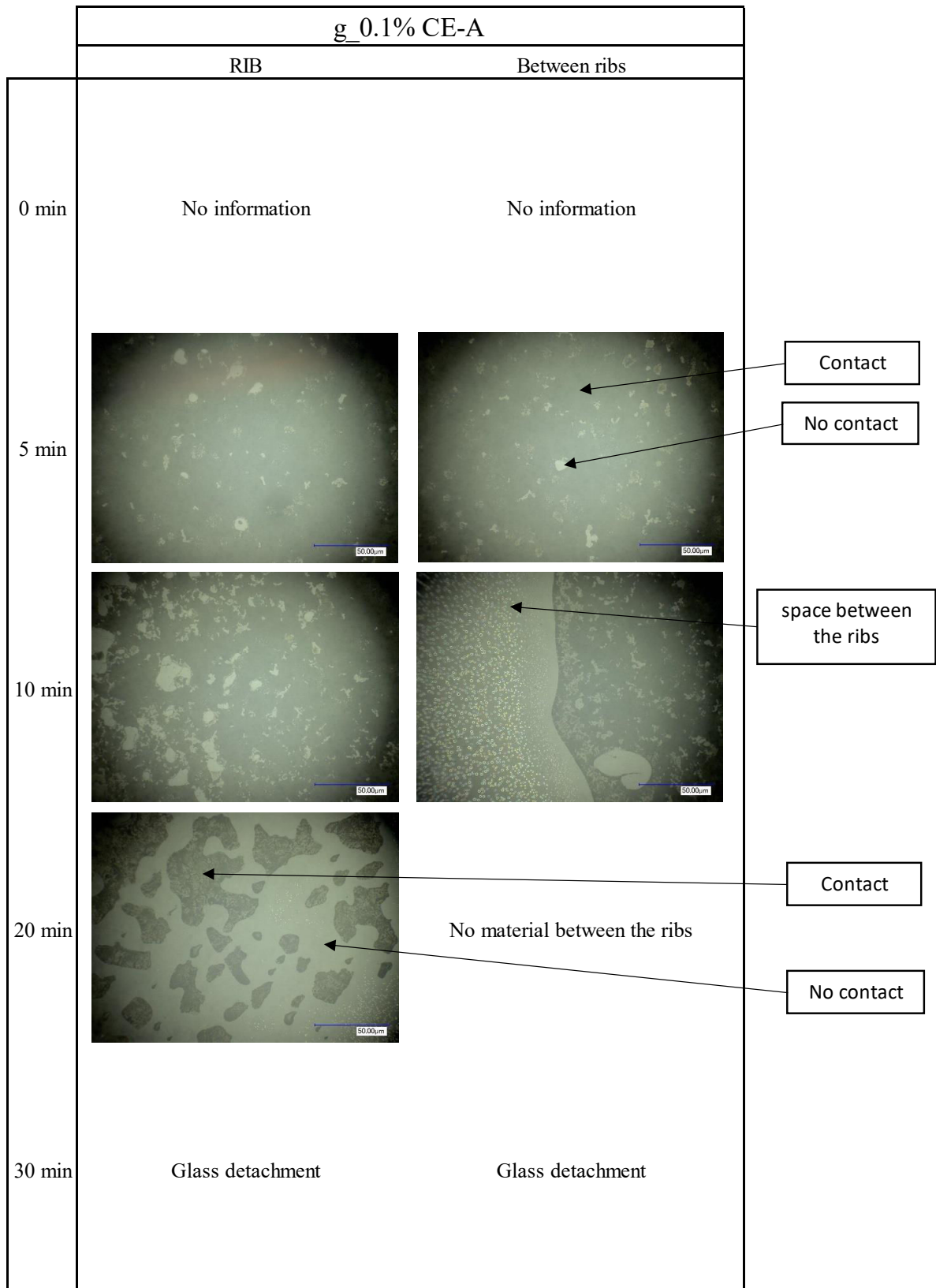


Figure 110. g\_0.1% CE-A contact visualization at different waiting times, at the rib and between ribs

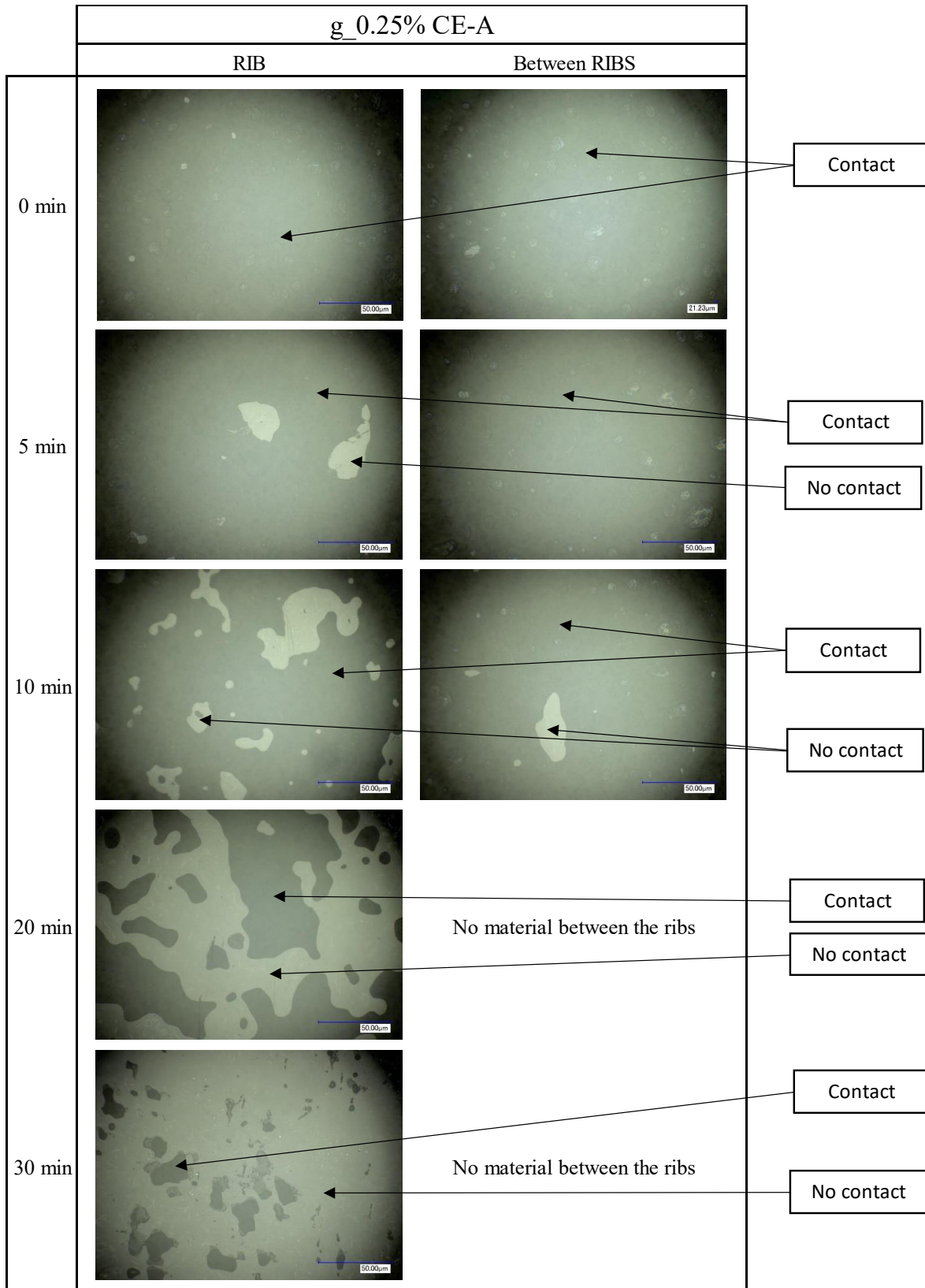


Figure 111. g\_0.25% CE-A contact visualization at different waiting times, at the rib and between ribs



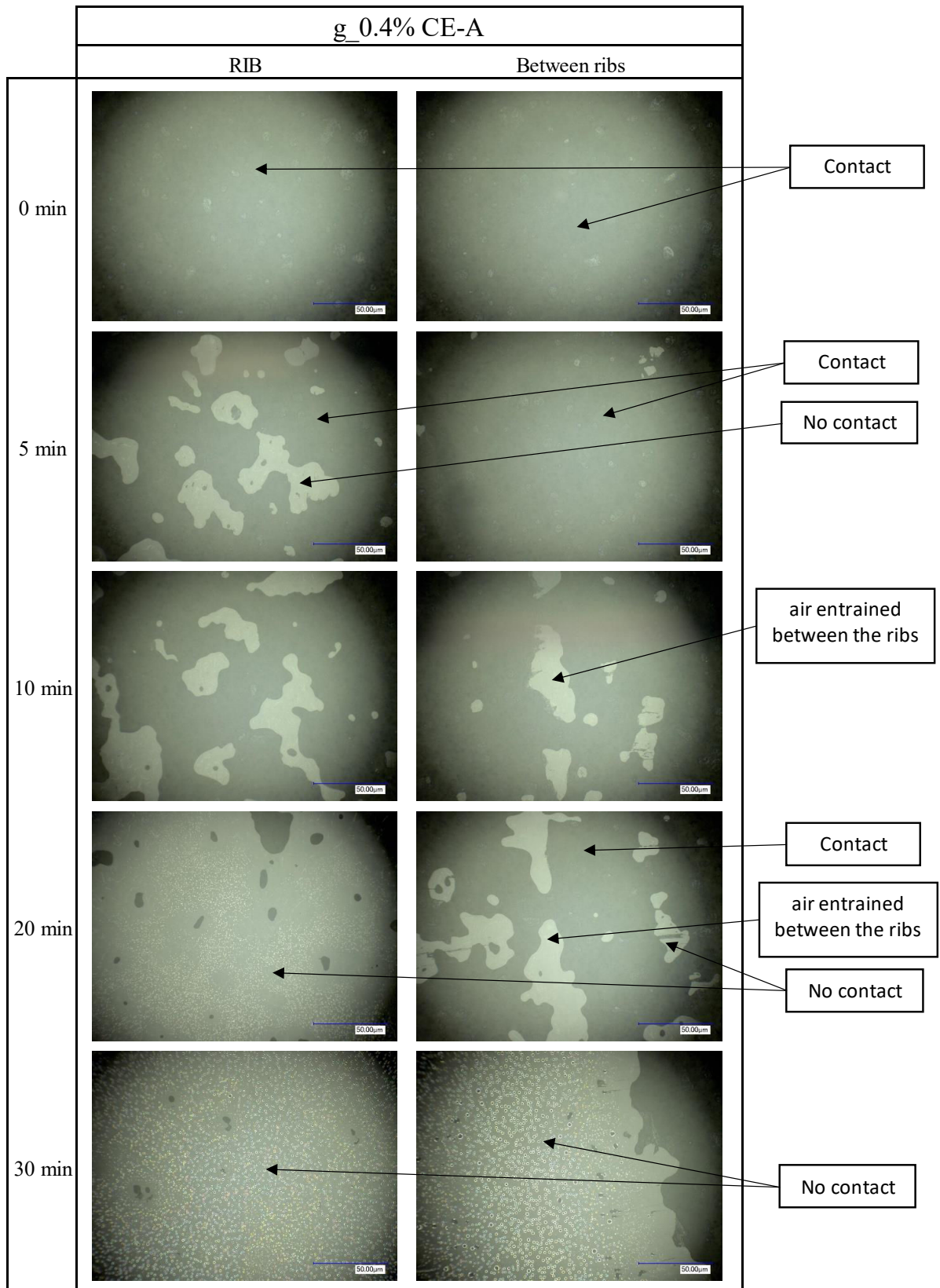


Figure 112. g\_0.4% CE-A contact visualization at different waiting times, at the rib and between ribs

#### 6.4.2 Impact of CE degree of substitution on contact generation

In Figure 113, the samples of adhesive mortar with different CE content and waiting time are shown. Four different CEs were used—CE-A, CE-B, CE-C and CE-D—each with a different degree of substitution (DS) and molecular weight (MW), but the same nominal viscosity. Observing the samples pictures, the different CEs do not seem to considerably affect the squeezing and contact generation from this overall observation.

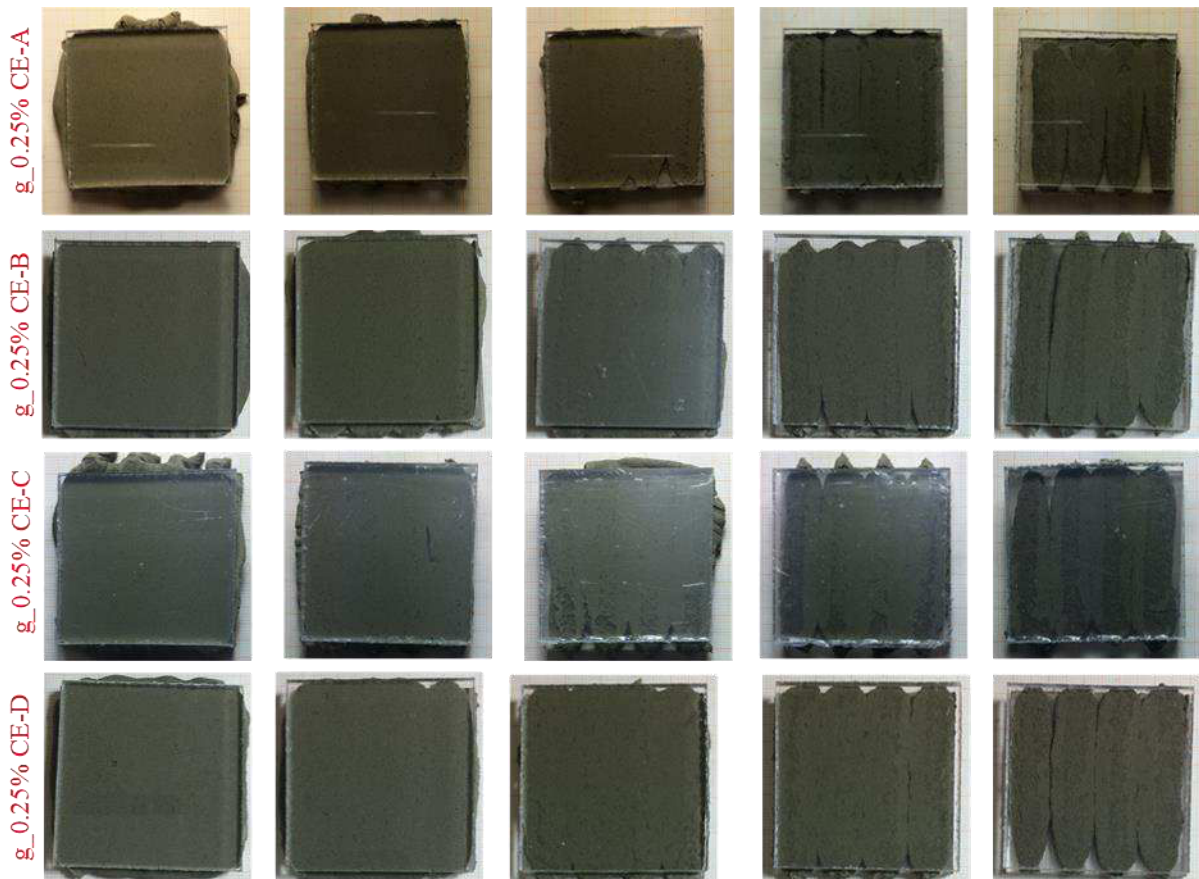


Figure 113. Samples of microscopical visualization of adhesive mortar with different CE content at different waiting time

In Figure 114, the contact of g\_0.25% CE-A formulations at the rib and between ribs was observed for different waiting times. Good contact was obtained at the ribs and between the ribs until 5 min waiting time. After 10 min, the contact start presenting increasingly no-contact spots, and between ribs, the contact was good, but it was possible to observe that the ribs didn't merge completely after 20 min waiting time.

In Figure 115, the contact of g\_0.25% CE-B formulations at the rib and between ribs was observed for different waiting times. The results were similar to g\_0.25% CE-A formulation, but at 5 min, at the ribs, it was possible to observe spots with no contact. Also, at 20 minutes and 30 minutes, the ribs merged and entrapped air could be seen. Since the rib application was manually done with the use of a toothed comb, the difference of material when applied could

influence the merging of the samples; since the difference is not considerable, it could be either related to a difference in the material properties or part of an error during application.

In Figure 116, the contact of g\_0.25% CE-C formulations at the rib and between ribs was observed for different waiting times. The results are similar to g\_0.25% CE-B formulations, where from 5 min waiting time, at the ribs, no contact spots started to appear until 30 min, where the no contact area was dominant. Between ribs, the contact was almost 100% perfect, at 20 min some entrapped air appeared and at 30 min, the air entrapped area between the ribs was larger.

In Figure 117, the contact of g\_0.25% CE-D formulations at the rib and between ribs was observed for different waiting times. The results were similar to g\_0.25% CE-A, with no-contact areas starting to appear at the ribs at 10 min waiting time, and at 20 min and 30 min waiting time, entrapped air started to appear between the ribs.

Therefore, no considerable difference could be observed regarding the different degree of substitution. The bulk rheological properties and the water loss results discussed in other chapters are similar too, which contribute to validate these results.



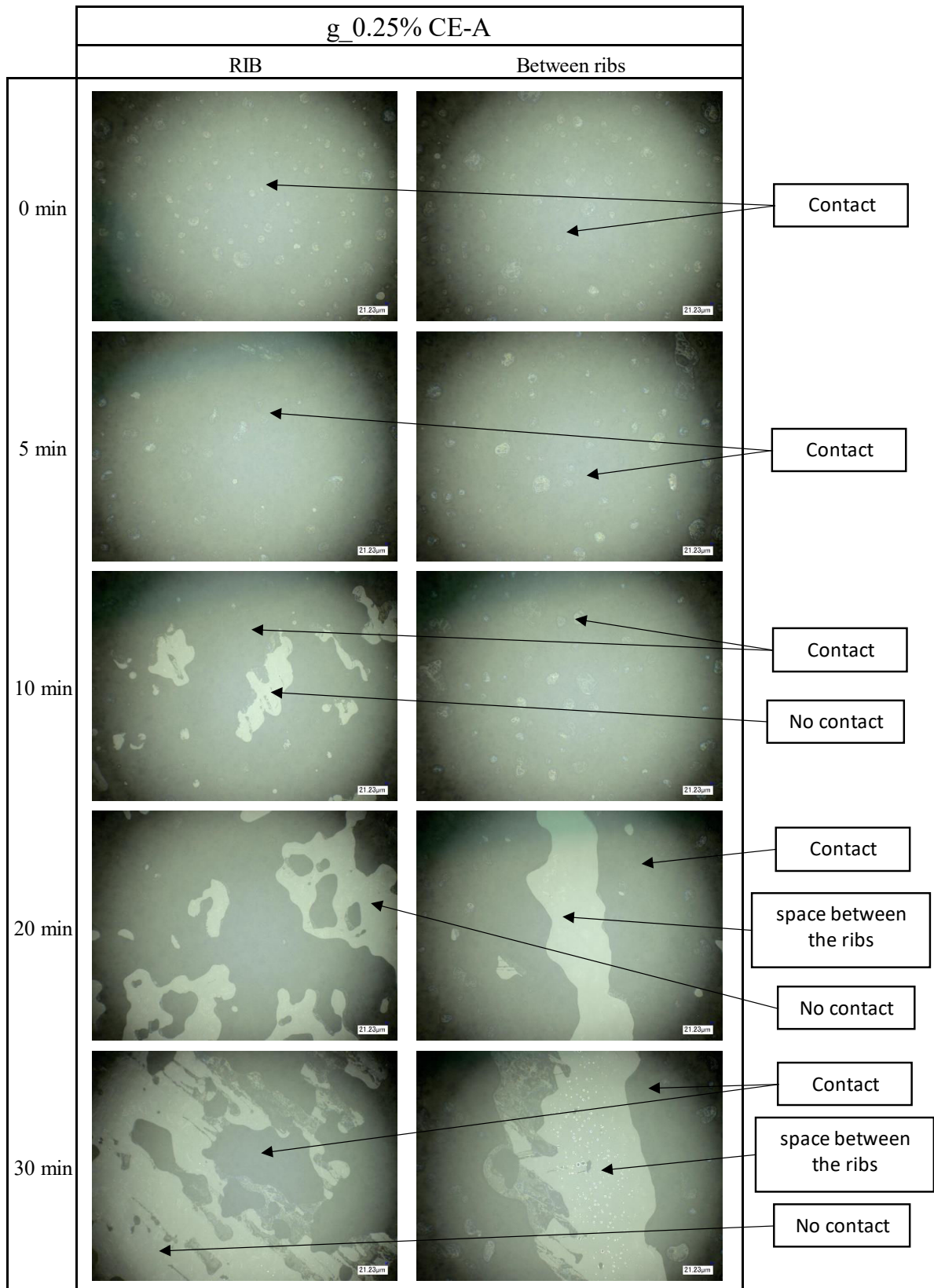


Figure 114. Contact evolution of adhesive mortar g\_0.25% CE-A at rib and between ribs for different waiting times



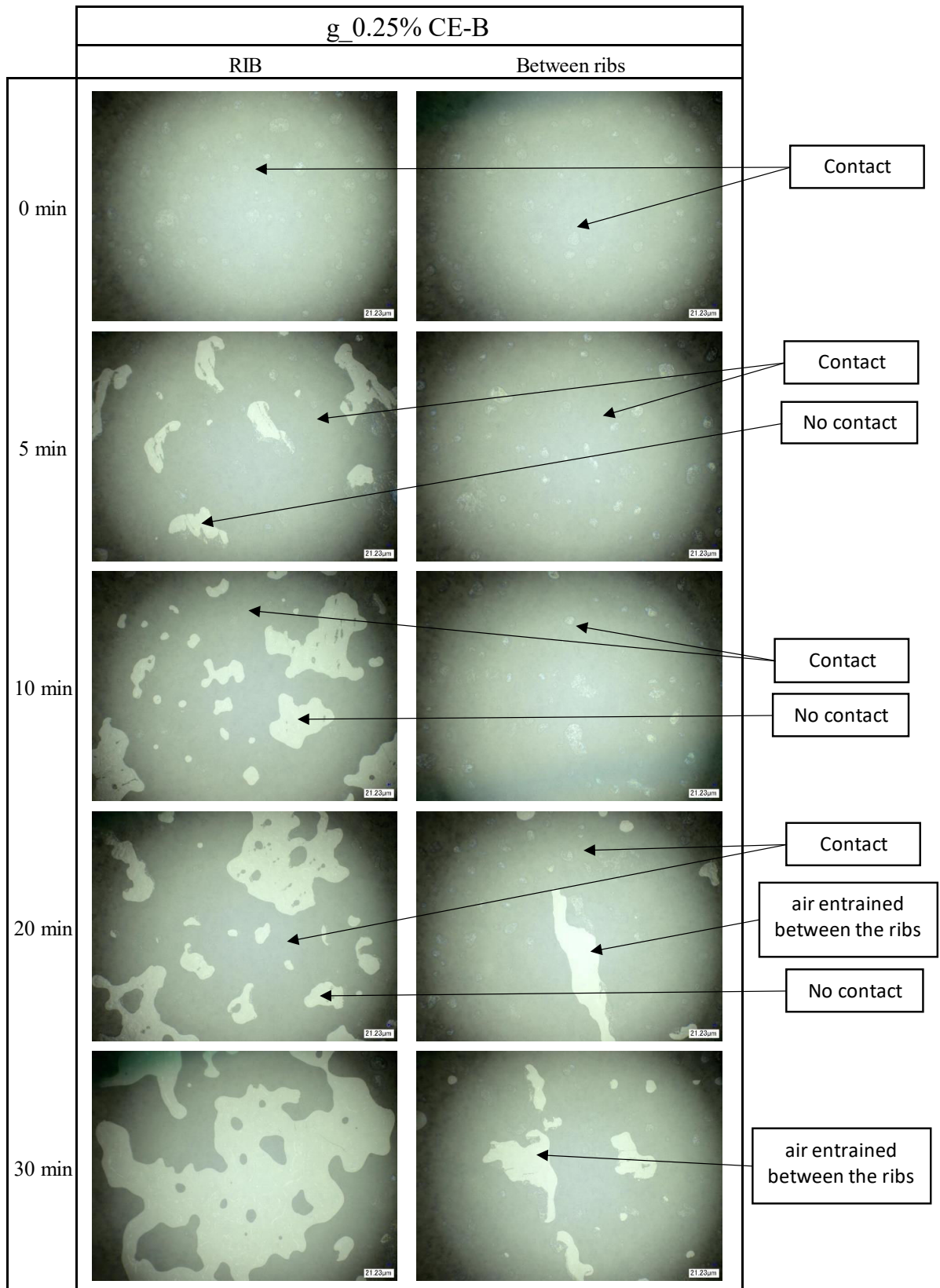


Figure 115. Contact evolution of adhesive mortar g\_0.25% CE-B at rib and between ribs for different waiting times

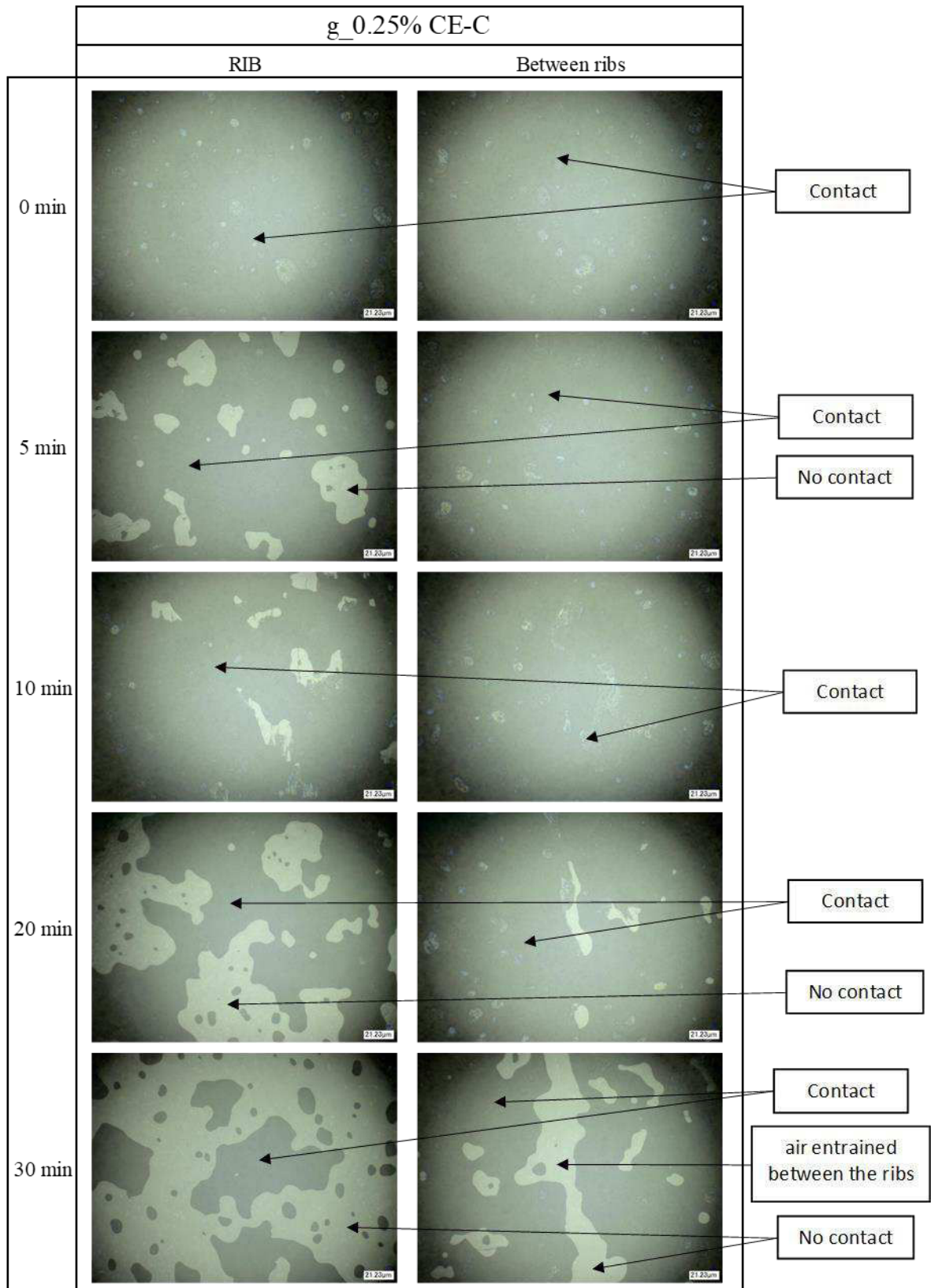


Figure 116. Contact evolution of adhesive mortar g\_0.25% CE-C at rib and between ribs for different waiting times



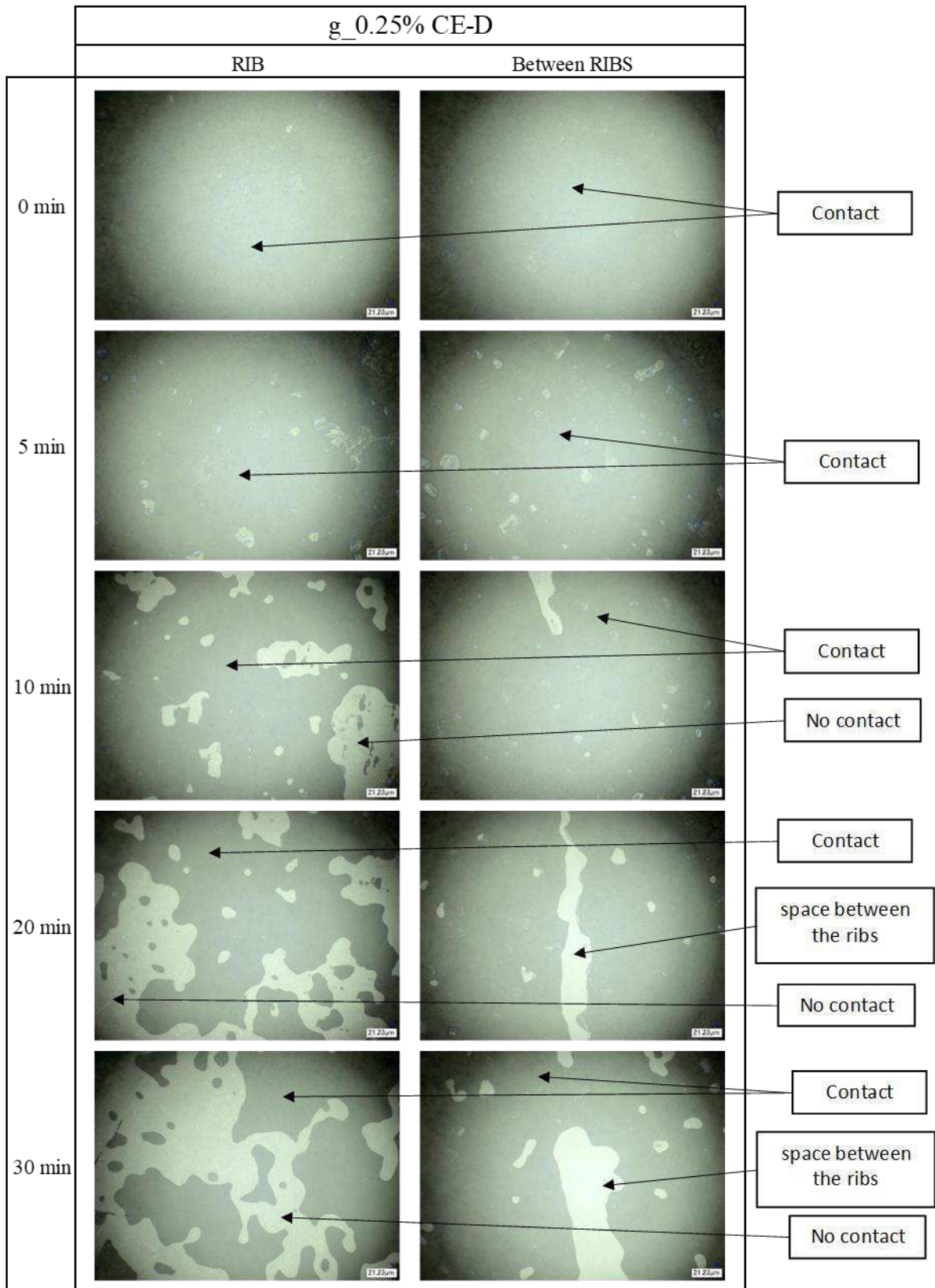


Figure 117. Contact evolution of adhesive mortar g\_0.25% CE-D at rib and between ribs for different waiting times



### 6.4.3 Transfer – effect of CE content

In this section, the effect of CE content on transfer results are discussed. In Figure 119 and Figure 120, wetting/transfer results of different CE-A content with different waiting times (0, 10, 20, 30, 40 and 50 minutes) are shown.

For all formulations, the transfer at 0 minutes of waiting time, the transfer is equal, since the material is fresh. After that, the formulation g\_0.1% CE-A evolves differently from the other formulations, and for 10 minutes, it does not seem generate a fresh transfer, and from 10 to 30 minutes waiting time, the ribs are not fully squeezed, and the transfer generated the block of material, lowering the amount as the waiting time increased. For 40 and 50 minutes, no material transferred to the tile.

The increase of CE seems to have extended waiting time, as with higher CE content, the longer it took the material to transfer to the tile. At 40 and 50 minutes, the g\_0.4% CE-A shows slightly more transferred material than g\_0.25% CE-A.

The results can relate to the contact visualization results discussed in Section 6.4.1, which show, for the formulations with higher CE content, a region of dry contact and wet contact. In Figure 118, the failures modes (A and B) are illustrated, showing how rib squeezing and contact generation affect the transfer tests. The fresh material that is released from the rib through the borders generates a good contact, while the dry contact zone generates a contact with dry zones that were observed in the previous sections. For smaller waiting times, this zone has lower dry spots, and therefore the transfer is more like A failure mode. For longer waiting times, the dryer spots areas are larger, and the failures tend to become more like B.

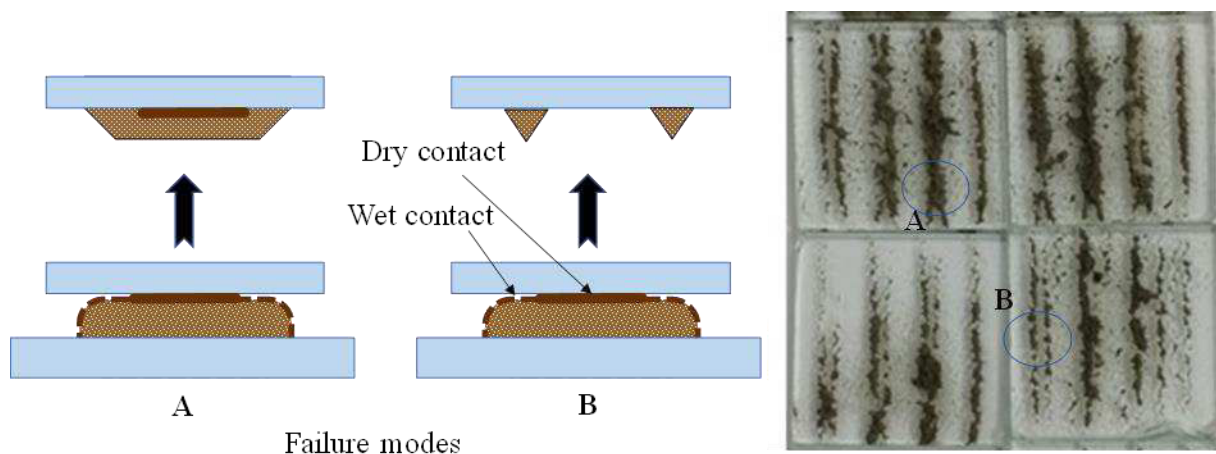


Figure 118. Failure modes of transfer tests

The g\_0.1% CE-A, on the other hand, showed an equally distributed contact generation in the previous section, with micro spots of dry areas equally distributed through the center and adjacent zones. This type of contact associated with a more homogenous, fast evolutive material



as shown in Chapter 3 and Chapter 4, resulted in a transfer of the entire rib or none, as the generated contact become weaker.

Squeeze deformation considerably affected transfer and contact generation. In the case of g\_0.1% CE-A, squeeze and tack test results in section 3.3.2.3 indicated that if enough deformation is done, contact and tack are outstanding; however, squeeze forces necessary to generate the defined deformation, as the waiting time is increased, achieve high values. For the constant force, however, contact and tack are quickly lost with waiting time increase.

For formulations with higher CE content, the rate of evolution of squeeze forces is lower due to the fresh material, which maintains inside the ribs, and when the rib is squeezed, it can have contact with the tile, allowing good adherence.



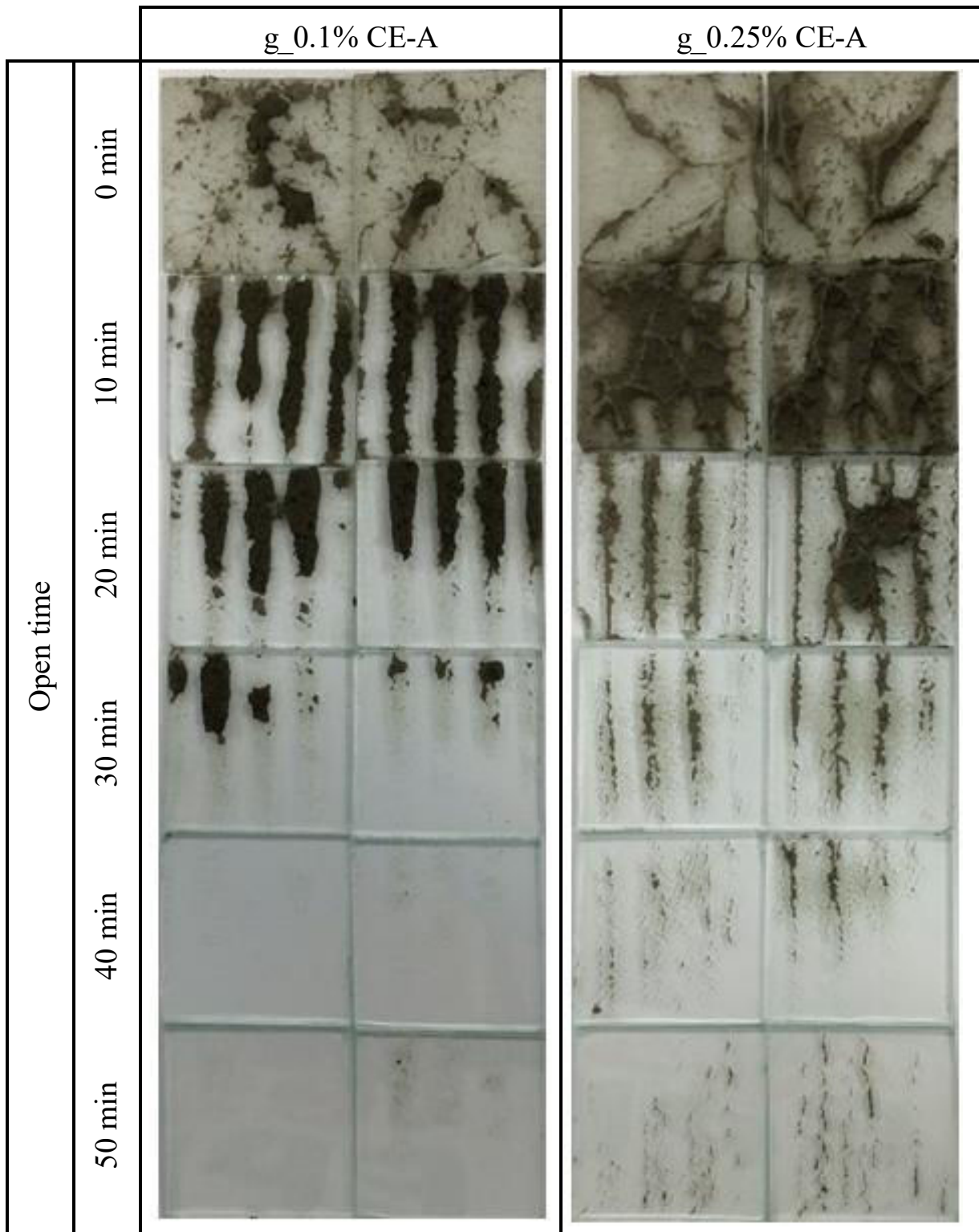


Figure 119. Transfer of g\_0.1% CE-A and g\_0.25% CE-A adhesive mortar formulations for different waiting time

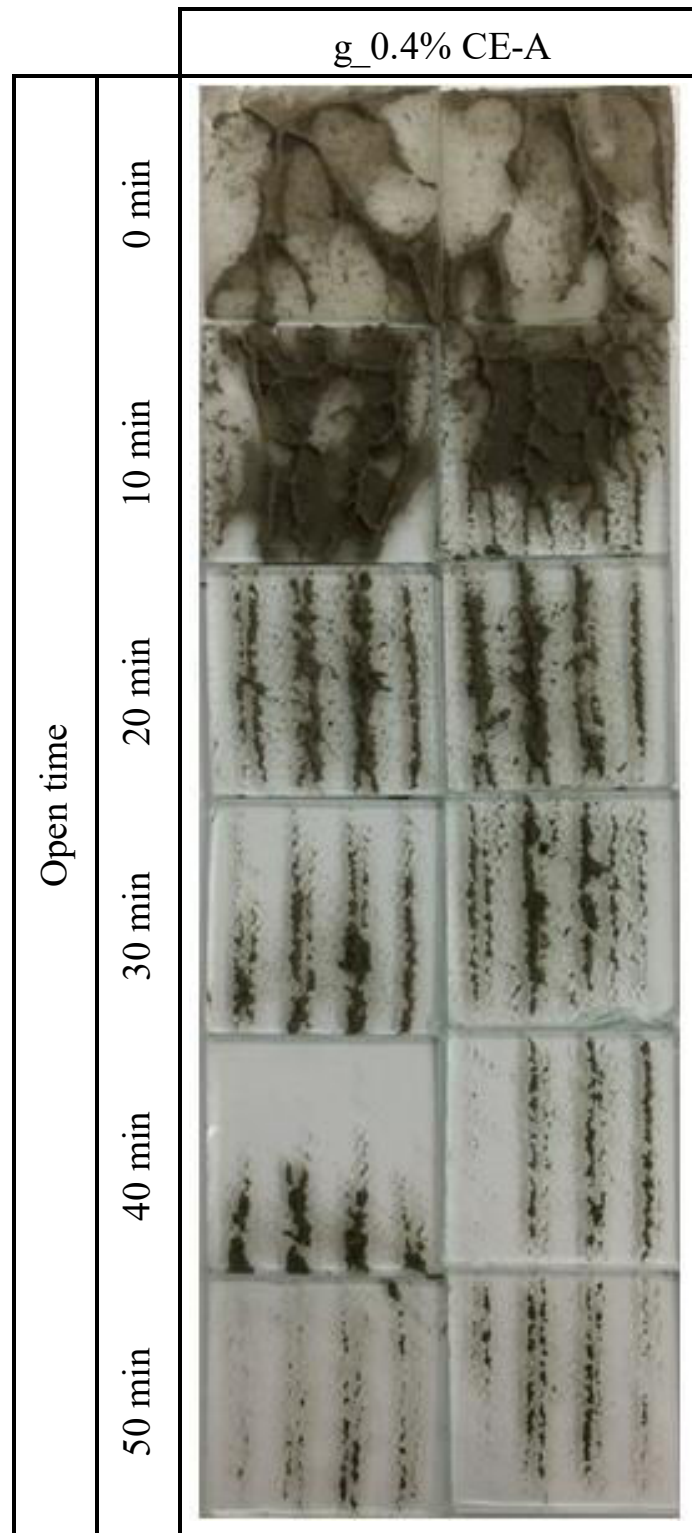


Figure 120. Transfer of g\_0.4% CE-A adhesive mortar formulation for different waiting time

#### 6.4.4 Transfer – effect of CE DS

The transfer results regarding the cellulose ether with different DS is shown in Figure 121 and Figure 122. The DS does not seem to show a noticeable impact on the transfer results. This

indicate that the other types of CE would be an equivalent substitute for CE-A, with also similar contact generation as seen in the previous sections.

As observed in the previous section, for all the CE types in this section, the adhesive mortar initially generates a perfect contact of the mortar with the tile at the 0 and 10 minutes waiting times. Gradually, as skin is formed, it starts to generate transfer with the failures modes A and B, illustrated on Figure 118.





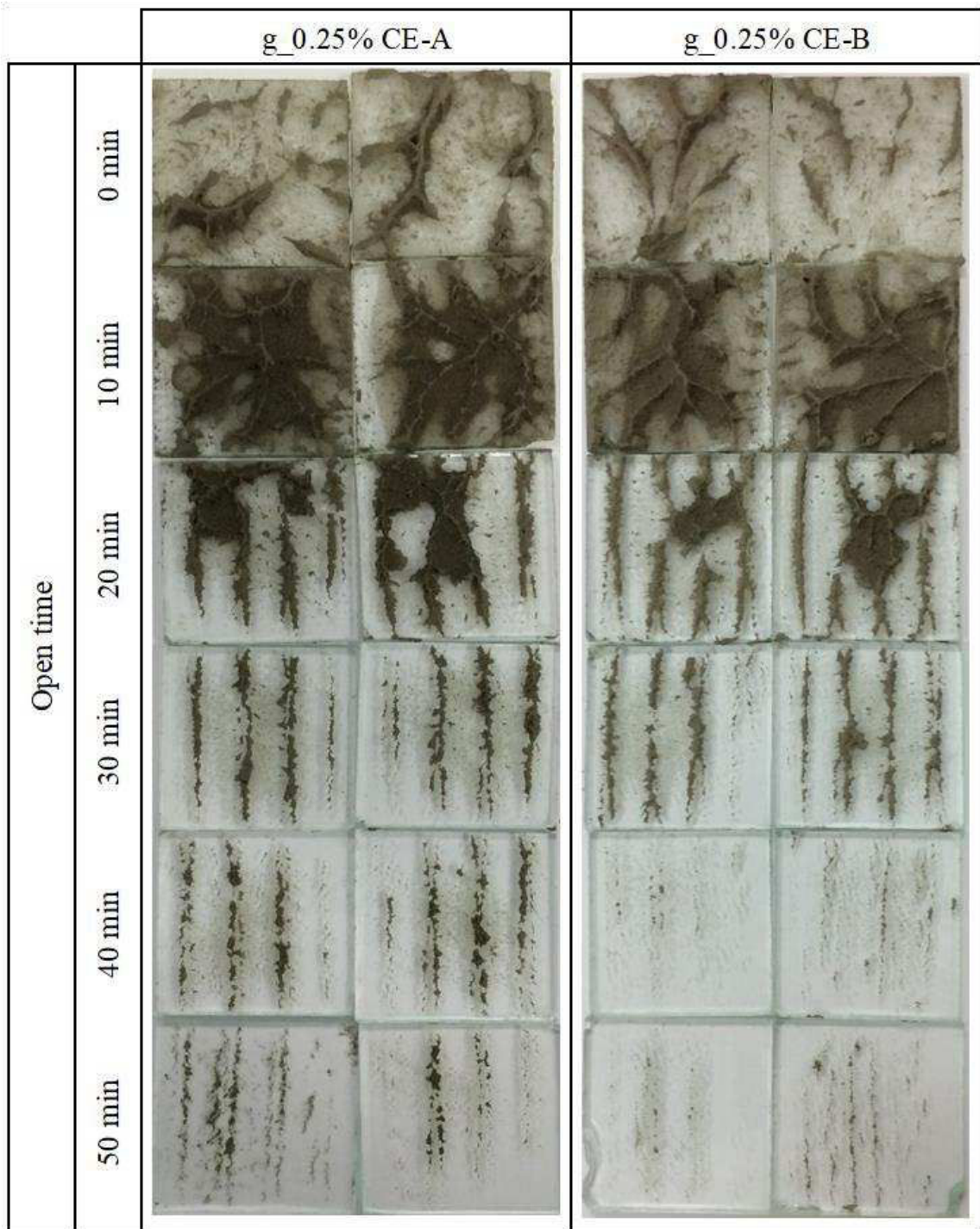


Figure 121. Transfer of g\_0.25% CE-A and g\_0.25% CE-B adhesive mortar formulations for different waiting time

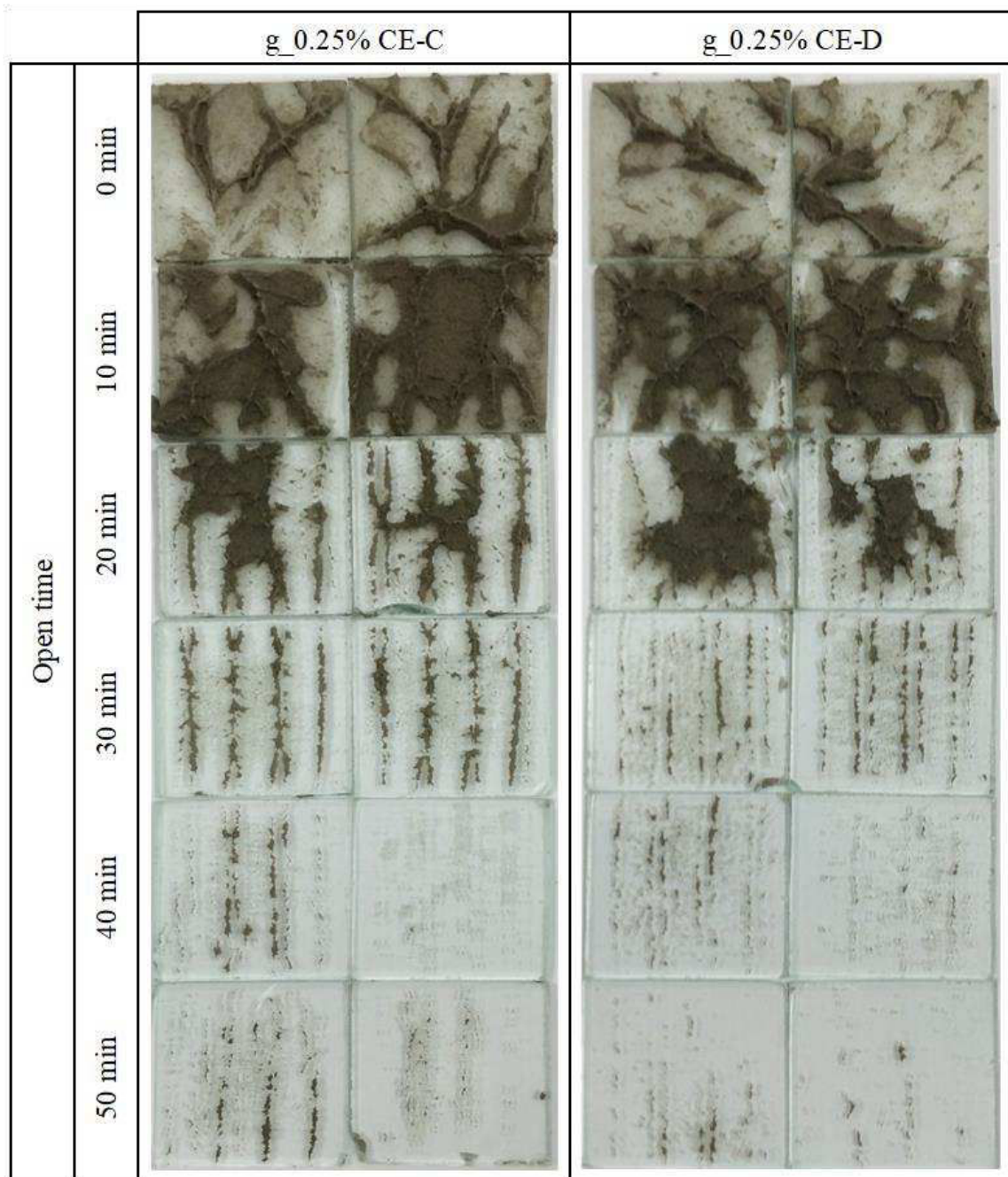


Figure 122. Transfer of g\_0.25% CE-C and g\_0.25% CE-D adhesive mortar formulations for different waiting time

## 6.5 Chapter conclusions

The present chapter focused on understanding the contact generation of adhesive mortar application. Optical microscopy and transfer results are used to evaluate CE content and degree

of substitution (DS). These methods are complementary to bulk rheological properties and the interface, and are helpful to further understand the skin formation of adhesive mortars.

The small depth of field used to observe the wetting and contact of adhesive mortar is innovative. Similar techniques using light as an improvement to wetting standard was introduced by Zurbriggen et al. [181], but with it offers a smaller degree of details. With the use of the present technique, the skin formation and rheological property's influence on contact generation could be better understood.

The increase of CE content generates a dry skin at the air-mortar interface; however, the waiting time of the contact generation is actually improved, since the higher CE content maintains the moisture in inner volumes and delays structuring, and this fresh material allows proper squeeze, and which finally releases from the skin and makes contact with the tile. When a skin is formed, as in the case of 0.25% and 0.4% of CE, the failure mode observed in transfer results clearly shows how contact is better in the adjacent zones of the squeezed rib.

The DS did not show noticeable differences either in the contact observations through optical microscopy or transfer test results. This may indicate that DS does not have a relevant different in this matter. In this study, however, it does not cover the fact that in commercial formulations, other polymers are added in the formulations such as superplasticizers, air-entrainers and others that may interact with CE. In this situation, further studies of the synergic influence of CEs should be carried out. This could verify other possible impacts of DS, as well of CE content.





## Chapter 7 – Final contributions

### 7.1 Conclusion and perspectives

This thesis offers innovations and further knowledge to the scientific and industrial community. New approaches to understand mortar skin formation were used, offering a deeper comprehension of the issue. Cellulose ether content and type's impact on adhesive properties of adhesive mortars was approached with different techniques in each chapter, offering a broad view.

Contact generation has shown to be related to bulk and skin rheological properties. In Chapter 3, bulk property's characterization shows that higher CE content has a lower squeeze force as the waiting time increases. Due to skin formation, tack tests showed lower tack properties for higher CE content, but the pre-test condition was an equal deformation, and a cylindrical sample, which is not comparable with the real application system, enabled the conclusion that low contact and transfer for low CE content is related to small deformation during squeeze.

Oscillatory rheometry tests in Chapter 3 also contributed to explain smaller squeeze force's evolution when CE is increased, since it showed that CE delayed structuring of cement particles over time. Bulk properties of the mortars with high CE content, showed considerably lower  $G'$  evolution, despite the thickening effect of the polymer.

Chapter 4 introduced interfacial rheology applied to granular materials based on classic techniques. Despite many studies that have characterized the chemical and microstructure, their quantitative impact on skin rheological properties is still unknown, and the latter is what defines the contact between mortar and tiles. The properties of formulations with different content and types of CE, as well the environmental conditions, were evaluated. When CE content was evaluated, it was possible to observe the transition from water evaporation to polymer film formation in rheological properties of the skin. When different degrees of substitution CE were evaluated, different inflection times were observed, despite the similar viscosity and water evaporation of the polymers. When environmental conditions were changed, and windy conditions were introduced, it was verified similar behaviors, but with accelerated reactions.

Water transportation has an impact on interfacial properties, and MRI is used to characterize the evolution of water distribution of the mortars with different CE content. The technique showed how CE increase generates a dryer layer at the surface and helps maintain the moisture inside the sample. And the skin grow is decelerated as the CE content is further increased.

In Chapter 5, micro-tomography was used to assess the microstructure of the adhesive mortar system. Results did not indicate an influence of the application method on the microstructure



or the pore distribution for the different formulations. No traces of skin's effect on the microstructure could be observed. However, the system characterization could offer indication of contact generation, which was better in the case of toothed comb application and higher CE content, which helps explain the improved adhesive stress properties as CE content increases. Finally, in Chapter 6, contact generation is investigated with the use of small depth of field optical microscopy and transfer tests. Despite skin formation in the formulations with higher CE content evaluated in the previous chapters, results showed that waiting time of the contact generation improves, with higher CE content since the higher CE content maintains the moisture in the inner volumes and delays structuring, and this fresh material allows proper squeeze, which leads to the mortar being released from the skin and making contact with the tile. For 0.1% CE-A, contact is lost faster despite the degree of wetting being more evenly distributed. The degree of substitution (DS) did not show noticeable differences.

This thesis can bring more attention to the evaluation of interfacial properties of mortars, as well as the importance of studying both bulk and interfacial properties separately, since they can have different properties while at the same time impacting the final performance of the material.

The investigation offered an evaluation of interfacial properties, bulk properties, and squeeze and tack properties, as well as microstructure and contact generation. It also created a focused study on cellulose ether impact on adhesive mortars.

Skin formation, in some formulations, can still be an issue despite these thesis findings. In the industry, formulations are more complex with a greater variety of additions and additives. In this research, despite the skin rigidity, the materials' properties were able to break and release a fresh material from the inside the ribs. This brittle property however, could not possibly occur in other conditions, and the skin could show high extension rheological behavior with a high elongation limit. Tests to verify this type of behavior of the interface should be conducted to verify this hypothesis.



## Bibliography

- [1] A. Jenni, L. Holzer, R. Zurbriggen, M. Herwegh, Influence of polymers on microstructure and adhesive strength of cementitious tile adhesive mortars, *Cem. Concr. Res.* 35 (2005) 35–50. doi:10.1016/j.cemconres.2004.06.039.
- [2] T. Bühler, R. Zurbriggen, U. Piele, L. Huwiler, R.A. Raso, Dynamics of early skin formation of tiling mortars investigated by microscopy and diffuse reflectance infrared Fourier transformed spectroscopy, *Cem. Concr. Compos.* 37 (2013) 161–170. doi:10.1016/j.cemconcomp.2012.10.008.
- [3] D. Bülchen, J. Kainz, J. Plank, Working mechanism of methyl hydroxyethyl cellulose (MHEC) as water retention agent, *Cem. Concr. Res.* 42 (2012) 953–959. doi:10.1016/j.cemconres.2012.03.016.
- [4] CEN, EN 12004: Adhesives for tiles — Definitions and specifications, *Eur. Stand.* 3 (2002).
- [5] CEN, EN 1347: Adhesives for tiles — Determination of wetting Capability, *Eur. Stand.* (2007).
- [6] M.A. Cincotto, *Disciplina PCC 5042 “Ciência dos materiais aplicada aos ligantes inorgânicos,”* (2014).
- [7] P.K. Mehta, P.J.M. Monteiro, *Concrete: microstructure, properties, and materials*, 2006. doi:10.1036/0071462899.
- [8] P. Hewlett, *Lea’s Chemistry of Cement and Concrete*, Elsevier, 1998. doi:10.1016/B978-0-7506-6256-7.X5007-3.
- [9] M. Cappellari, A. Daubresse, M. Chaouche, Influence of organic thickening admixtures on the rheological properties of mortars: Relationship with water-retention, *Constr. Build. Mater.* 38 (2013) 950–961. doi:10.1016/j.conbuildmat.2012.09.055.
- [10] A. Izaguirre, J. Lanas, J.I. Álvarez, Characterization of aerial lime-based mortars modified by the addition of two different water-retaining agents, *Cem. Concr. Compos.* 33 (2011) 309–318. doi:10.1016/j.cemconcomp.2010.09.008.
- [11] M.E. BurnsHans, H. J. Pracht, Cellulose ethers having a low molecular weight and a high degree of methyl substitution, US4048433A, 1977. <https://patents.google.com/patent/US4048433>.
- [12] Dow Chemical Co., *Methocel Cellulose Ethers: Technical Handbook Form No. 192-01062-0902*, 2002.



- [13] Compendium of Analytical Nomenclature, Elsevier, 1978. doi:10.1016/C2013-0-02923-4.
- [14] R.G. Jones, J. Kahovec, R. Stepto, E.S. Wilks, M. Hess, T. Kitayama, et al., Compendium of Polymer Terminology and Nomenclature, Royal Society of Chemistry, Cambridge, 2009. doi:10.1039/9781847559425.
- [15] T. Wüstenberg, Cellulose and Cellulose Derivatives in the Food Industry, Wiley-VCH Verlag GmbH & Co. KGaA, Weinheim, Germany, 2014. doi:10.1002/9783527682935.
- [16] A.M. Stephe, G.O. Phillips, Food Polysaccharides and Their Applications, CRC Press, 2006. doi:10.1201/9781420015164.
- [17] J.P. Schirle-Keller, H.H. Chsng, G.A. Reineccius, Interaction of Flavor Compounds with Microparticulated Proteins, *J. Food Sci.* 57 (1992) 1448–1451. doi:10.1111/j.1365-2621.1992.tb06880.x.
- [18] J.A. Glomski, Ronald L. Davis, Lewis E. Grove, Water soluble hydroxyethyl methyl cellulose ether thickener for latex paint, 3709876A, 1973.
- [19] J.-Y. Petit, E. Wirquin, Evaluation of various cellulose ethers performance in ceramic tile adhesive mortars, *Int. J. Adhes. Adhes.* 40 (2013) 202–209. doi:10.1016/j.ijadhadh.2012.09.007.
- [20] L. Patural, P. Marchal, A. Govin, P. Grosseau, B. Ruot, O. Devès, Cellulose ethers influence on water retention and consistency in cement-based mortars, *Cem. Concr. Res.* 41 (2011) 46–55. doi:10.1016/j.cemconres.2010.09.004.
- [21] M.A. Winnik, A. Yekta, Associative polymers in aqueous solution, *Curr. Opin. Colloid Interface Sci.* 2 (1997) 424–436. doi:10.1016/S1359-0294(97)80088-X.
- [22] C. Chassenieux, T. Nicolai, L. Benyahia, Rheology of associative polymer solutions, *Curr. Opin. Colloid Interface Sci.* 16 (2011) 18–26. doi:10.1016/j.cocis.2010.07.007.
- [23] M. Cappellari, Influence des éthers de cellulose sur la rhéologie des mortiers projetés, Ecole Normale Supérieure de Cachan, 2013.
- [24] C. Esquenet, Propriétés structurales et dynamiques des solutions de polyélectrolites rigides et semi-rigides et de polysaccharides associatifs, Université Joseph Fourier, 2003.
- [25] K. Balsler, M. Iseringhausen, Cellulose ether, in: E. Bartholomé (Ed.), *Ullmann's Encycl. Ind. Chem.*, 4th Ed, Verlag Chemie, Weinheim, Germany, 1975: pp. 191–212.
- [26] S. Richardson, L. Gorton, Characterisation of the substituent distribution in starch



- and cellulose derivatives, *Anal. Chim. Acta.* (2003) 27–65.
- [27] Dow Chemical Co., Form No. 192-1062-88-JB, 1988.
- [28] A. Kaci, R. Bouras, M. Chaouche, P.A. ani, H. Brossas, Adhesive and rheological properties of mortar joints, *Appl. Rheol.* 19 (2009) 51970.
- [29] M. Wyrzykowski, R. Kiesewetter, J. Kaufmann, R. Baumann, P. Lura, Pore structure of mortars with cellulose ether additions - Mercury intrusion porosimetry study, *Cem. Concr. Compos.* 53 (2014) 25–34. doi:10.1016/j.cemconcomp.2014.06.005.
- [30] K.H. Khayat, Viscosity-enhancing admixtures for cement-based materials — An overview, *Cem. Concr. Compos.* 20 (1998) 171–188. doi:10.1016/S0958-9465(98)80006-1.
- [31] J. Pourchez, Aspects physico-chimiques de l'interaction des éthers de cellulose avec la matrice cimentaire, Ecole Nationale Supérieure des Mines de Saint-Etienne, 2006.
- [32] L. Patural, A. Govin, P. Grosseau, Influence of cellulose ether particle size on water retention on freshly-mixed mortars, *J. Du CEREM.* (2009) 16.
- [33] H.J. Weyer, I. Müller, B. Schmitt, D. Bosbach, A. Putnis, Time-resolved monitoring of cement hydration: Influence of cellulose ethers on hydration kinetics, *Nucl. Instruments Methods Phys. Res. Sect. B Beam Interact. with Mater. Atoms.* 238 (2005) 102–106. doi:10.1016/j.nimb.2005.06.026.
- [34] E.J. Lorand, Cellulose Ethers, *Ind. Eng. Chem.* 30 (1938) 527–530. doi:10.1021/ie50341a011.
- [35] A. Govin, W. Schmidt, M. Bartholin, P. Grosseau, A. Govin, W. Schmidt, et al., Effect of guar gum derivatives combined with superplasticizers on properties of portland cement-pastes To cite this version : HAL Id : hal-01548245 ON PROPERTIES OF PORTLAND CEMENT - PASTES, (2017) 25–26.
- [36] Y. Cheng, K.M. Brown, R.K. Prud'homme, Characterization and intermolecular interactions of hydroxypropyl guar solutions, *Biomacromolecules.* 3 (2002) 456–461. doi:10.1021/bm0156227.
- [37] M.K. Dufficy, S.A. Khan, P.S. Fedkiw, Galactomannan binding agents for silicon anodes in Li-ion batteries, *J. Mater. Chem. A.* 3 (2015) 12023–12030. doi:10.1039/c5ta03126e.
- [38] I. Gordon, Starches from Differing Sources — Supply, Demand, Price Formation, *Starch/Stärke.* 51 (1999) 193–196. doi:10.1002/(SICI)1521-379X(199906)51:6<193::AID-STAR193>3.0.CO;2-#.



- [39] Y. Habibi, L.A. Lucia, eds., *Polysaccharide Building Blocks*, John Wiley & Sons, Inc., Hoboken, NJ, USA, 2012. doi:10.1002/9781118229484.
- [40] A. Buléon, P. Colonna, V. Planchot, S. Ball, Starch granules: Structure and biosynthesis, *Int. J. Biol. Macromol.* 23 (1998) 85–112. doi:10.1016/S0141-8130(98)00040-3.
- [41] J.M. V. BLANSHARD, *Starch: Chemistry and Technology*, 2nd Edition, *Biochem. Soc. Trans.* 14 (1986) 178.2-179. doi:10.1042/bst0140178a.
- [42] D.J. Manners, Recent developments in our understanding of amylopectin structure, *Carbohydr. Polym.* 11 (1989) 87–112. doi:10.1016/0144-8617(89)90018-0.
- [43] G.S. Nilsson, L. Gorton, K.-E. Bergquist, U. Nilsson, Determination of the Degree of Branching in Normal and Amylopectin Type Potato Starch with <sup>1</sup>H-NMR Spectroscopy Improved resolution and two-dimensional spectroscopy, *Starch - Starke.* 48 (1996) 352–357. doi:10.1002/star.19960481003.
- [44] A. Peschard, A. Govin, P. Grosseau, B. Guilhot, R. Guyonnet, Effect of polysaccharides on the hydration of cement paste at early ages, *Cem. Concr. Res.* 34 (2004) 2153–2158. doi:10.1016/j.cemconres.2004.04.001.
- [45] M.A. Winnik, Latex film formation, *Curr. Opin. Colloid Interface Sci.* 2 (1997) 192–199. doi:10.1016/S1359-0294(97)80026-X.
- [46] Y.V. Póvoas, Avaliação da Formação de “Película” na Argamassa Colante e sua Influência na Adesão, University of São Paulo, 2005.
- [47] J.W. Vanderhoff, E.B. Bradford, W.K. Carrington, The transport of water through latex films, *J. Polym. Sci. Polym. Symp.* 41 (1973) 155–174. doi:10.1002/polc.5070410116.
- [48] J.A. Lavelle, Acrylic Latex-Modified Portland Cement, *ACI Mater. J.* 85 (1988) 41–48. doi:10.14359/2495.
- [49] S. Chemical, What are redispersible polymer powders?, (n.d.). <http://celluloseether.com> (accessed March 6, 2018).
- [50] Wacker Chemie AG, Dispersible Polymer Powders, (n.d.). [www.wacker.com](http://www.wacker.com) (accessed March 6, 2018).
- [51] G. Beier, J. Heckmaier, N. Eligius, Verfahren zur Herstellung von redispersierbarem Polyvinylchlorid-Pulver, DE1248292 (B), 1967.
- [52] Dow, *Redispersible Powders: Technical Overview and Product Guide*, 2012.
- [53] M.A. Linné, A. Klein, L.H. Sperling, G.D. Wignall, On the structure and conformation



- of polymer chains in latex particles. I. Small-angle neutron scattering characterization of polystyrene latexes of small diameter, *J. Macromol. Sci. Part B.* 27 (1988) 181–216. doi:10.1080/00222348808245762.
- [54] E.S. Daniels, A. Klein, Development of cohesive strength in polymer films from latices: effect of polymer chain interdiffusion and crosslinking, *Prog. Org. Coatings.* 19 (1991) 359–378. doi:10.1016/0033-0655(91)80018-E.
- [55] A. Toussaint, M. De Wilde, F. Molenaar, J. Mulvihill, Calculation of Tg and MFFT depression due to added coalescing agents, *Prog. Org. Coatings.* 30 (1997) 179–184. doi:10.1016/S0300-9440(96)00685-6.
- [56] Y. Ohama, *Handbook of polymer-modified concrete and mortars: properties and process technology*, (1995) 245.
- [57] H.B. Wagner, *Polymer-Modified Hydraulic Cements*, *Ind. Eng. Chem. Prod. Res. Dev.* 4 (1965) 191–196. doi:10.1021/i360015a011.
- [58] S. Baueregger, M. Perello, J. Plank, Influence of anti-caking agent kaolin on film formation of ethylene–vinylacetate and carboxylated styrene–butadiene latex polymers, *Cem. Concr. Res.* 58 (2014) 112–120. doi:10.1016/J.CEMCONRES.2014.01.017.
- [59] A. Wetzel, R. Zurbriggen, M. Herwegh, *Cement & Concrete Composites Spatially resolved evolution of adhesion properties of large porcelain tiles*, 32 (2010) 327–338. doi:10.1016/j.cemconcomp.2010.02.002.
- [60] J. Sieksmeier, R. Oberste-Padtberg, Factors influencing the open time of building mortars, in: F. Leopolder (Ed.), *Drymix Mortar Yearb. 2007*, Nürnberg, Germany, 2007: pp. 44–9.
- [61] Akzonobel, *Open Time Study 2010 - Mechanisms of tile adhesives*, 2012. (n.d.).
- [62] J.Y. Petit, B. Comelli, R. Perrin, E. Wirquin, Effect of formulation parameters on adhesive properties of ANSI 118-15 and 118-11 compliant tile adhesive mortars, *Int. J. Adhes. Adhes.* 66 (2016) 73–80. doi:10.1016/j.ijadhadh.2015.12.011.
- [63] P. Whittingstall, *Measuring The Viscosity Of Non-Newtonian Fluids*, *Handb. Food Anal. Chem.* 2–2 (2005) 375–383. doi:10.1002/0471709085.ch25.
- [64] K.L. Mittal, *Adhesive joints*, 1982. doi:10.1007/978-1-4613-2749-3.
- [65] J.N. Israelachvili, *17-Adhesion and Wetting Phenomena*, in: *Intermol. Surf. Forces*, 2011: pp. 205–222. doi:10.1016/B978-0-12-375182-9.10011-9.
- [66] A. Einstein, *Über die von der molekularkinetischen Theorie der Wärme geforderte*





- Bewegung von in ruhenden Flüssigkeiten suspendierten Teilchen, *Ann. Phys.* 322 (1905) 549–560. doi:10.1002/andp.19053220806.
- [67] M. von Smoluchowski, Zur kinetischen Theorie der Brownschen Molekularbewegung und der Suspensionen, *Ann. Phys.* 326 (1906) 756–780. doi:10.1002/andp.19063261405.
- [68] J. Mewis, N.J. Wagner, *Colloidal Suspension Rheology*, Cambridge University Press, 2012. doi:10.1017/CBO9780511977978.
- [69] H.C. Hamaker, the London--Van Der Waals Attraction Between Spherical Particles, (1937).
- [70] R. Lee-Desautels, Theory of van der Waals Forces as Applied to Particulate Materials, *Mater. Eng.* 27 (2005) 1–8.
- [71] I.R. de Oliveira, A.R. Studart, R.G. Pileggi, V.C. Pandolfelli, *Dispersão e empacotamento de partículas: princípios e aplicações em processamento cerâmico*, Fazendo Arte, 2000.
- [72] N.P. Cheremisinoff, *Encyclopedia of Fluid Mechanics: Slurry flow technology*, Gulf Publishing Company, 1986.
- [73] J.K. Vennard, R.L. Street, *Elementary Fluid Mechanics*, Wiley, 1983.
- [74] D.C.H. Cheng, Yield stress: A time-dependent property and how to measure it, *Rheol. Acta.* 25 (1986) 542–554. doi:10.1007/BF01774406.
- [75] H. Zhu, Y.D. Kim, D. De Kee, Non-Newtonian fluids with a yield stress, *J. Nonnewton. Fluid Mech.* 129 (2005) 177–181. doi:10.1016/j.jnnfm.2005.06.001.
- [76] P.F.G. Banfill, *Rheology of Fresh Cement and Concrete*, Taylor & Francis, 1991. <https://books.google.com/books?id=4YkSmHSmWE4C>.
- [77] R.G. Pileggi, *Ferramentas para o estudo de desenvolvimento de concretos refratários*, Universidade de São Paulo, 2001.
- [78] P.F. Luckham, S. Rossi, Colloidal and rheological properties of bentonite suspensions, *Adv. Colloid Interface Sci.* 82 (1999) 43–92. doi:10.1016/S0001-8686(99)00005-6.
- [79] N.J. Alderman, G.H. Meeten, J.D. Sherwood, Vane rheometry of bentonite gels, *J. Nonnewton. Fluid Mech.* 39 (1991) 291–310. doi:10.1016/0377-0257(91)80019-G.
- [80] R.R. Iyer, D.W. Bousfield, The leveling of coating defects with shear thinning rheology, *Chem. Eng. Sci.* 51 (1996) 4611–4617. doi:10.1016/0009-



2509(96)00318-1.

- [81] C. Prestidge, T. Tadros, Viscoelastic properties of aqueous concentrated polystyrene latex dispersions containing grafted poly(ethylene oxide) chains, *J. Colloid Interface Sci.* 124 (1988) 660–665. doi:10.1016/0021-9797(88)90204-4.
- [82] D.A.R. Jones, B. Leary, D. V. Boger, The rheology of a sterically stabilized suspension at high concentration, *J. Colloid Interface Sci.* 150 (1992) 84–96. doi:10.1016/0021-9797(92)90270-V.
- [83] S. Mueller, E.W. Llewellyn, H.M. Mader, The rheology of suspensions of solid particles, *Proc. R. Soc. A Math. Phys. Eng. Sci.* 39 (1926) 291–300. doi:10.1007/BF01432034.
- [84] J.E. Funk, D.R. Dinger, *Predictive Process Control of Crowded Particulate Suspensions*, Springer US, Boston, MA, 1994. doi:10.1007/978-1-4615-3118-0.
- [85] R.L. Hoffman, Explanations for the cause of shear thickening in concentrated colloidal suspensions, *J. Rheol. (N. Y. N. Y.)*. 42 (1998) 111–123. doi:10.1122/1.550884.
- [86] H. a. Barnes, Shear-Thickening (“Dilatancy”) in Suspensions of Nonaggregating Solid Particles Dispersed in Newtonian Liquids, *J. Rheol. (N. Y. N. Y.)*. 33 (1999) 329. doi:10.1122/1.550017.
- [87] H.H. a. Barnes, a Barnes, Thixotropy - A review, *J. Non-Newtonian Fluid Mech.* 70 (1997) 1–33. doi:10.1016/S0377-0257(97)00004-9.
- [88] P.F.G. Banfill, Rheology of Fresh Cement and Concrete, *Rheol. Rev.* 2006 (2006) 61–130. doi:10.4324/9780203473290.
- [89] BS, BS 5168: Measurement of fluid flow - Evaluation of uncertainties, *Br. Stand. Inst.* (2005).
- [90] J. Mewis, N.J. Wagner, Thixotropy, *Adv. Colloid Interface Sci.* 147–148 (2009) 214–227. doi:10.1016/j.cis.2008.09.005.
- [91] C.M. Neubauer, M. Yang, H.M. Jennings, Interparticle potential and sedimentation behavior of cement suspensions: Effects of admixtures, *Adv. Cem. Based Mater.* 8 (1998) 17–27. doi:10.1016/S1065-7355(98)00005-4.
- [92] H. a Barnes, D. Bell, Controlled-stress rotational rheometry: An historical review, *Korea-Australia Rheol. J.* 15 (2003) 187–196.
- [93] A. Franck, Instrument Inertia Correction during Dynamic Mechanical Testing, *TA Instruments.* (2005).



- [94] T.G. Mezger, *The rheology handbook: for users of rotational and oscillatory rheometers*, 2nd Editio, Vincentz Network, Hannover, 2006.
- [95] T.G. Mezger, D. van Peij, *Modern Rheology Measurements in Today's Coatings Industry*, in: Congr. Pap. ECS Nürn., Vincentz Network, Hannover, 2005.
- [96] N. Roussel, Steady and transient flow behaviour of fresh cement pastes, *Cem. Concr. Res.* 35 (2005) 1656–1664. doi:10.1016/j.cemconres.2004.08.001.
- [97] A. Franck, Understanding rheology of structured fluids, TA Instruments. (2004) 1–11.
- [98] R.E. Wrolstad, *Current Protocols in Food Analytical Chemistry*, John Wiley & Sons, Inc., Hoboken, NJ, USA, 2001. doi:10.1002/0471142913.
- [99] P. Coussot, *Rheometry of Pastes, Suspensions, and Granular Materials*, John Wiley & Sons, Inc., Hoboken, NJ, USA, 2005. doi:10.1002/0471720577.
- [100] Q. Yuan, X. Lu, K.H. Khayat, D. Feys, C. Shi, Small amplitude oscillatory shear technique to evaluate structural build-up of cement paste, *Mater. Struct.* 50 (2017) 112. doi:10.1617/s11527-016-0978-2.
- [101] A.M. Betioli, P.J.P. Gleize, D.A. Silva, V.M. John, R.G. Pileggi, Effect of HMEC on the consolidation of cement pastes: Isothermal calorimetry versus oscillatory rheometry, *Cem. Concr. Res.* 39 (2009) 440–445. doi:10.1016/j.cemconres.2009.02.002.
- [102] S. Gauffinet-Garrault, *The rheology of cement during setting*, Woodhead Publishing Limited, 2011. doi:10.1016/B978-0-85709-028-7.50005-4.
- [103] A.L. Fujii, D. Dos Reis Torres, R.C. De Oliveira Romano, M.A. Cincotto, R.G. Pileggi, Impact of superplasticizer on the hardening of slag Portland cement blended with red mud, *Constr. Build. Mater.* 101 (2015) 432–439. doi:10.1016/j.conbuildmat.2015.10.057.
- [104] D. Szopinski, G.A. Luinstra, Viscoelastic properties of aqueous guar gum derivative solutions under large amplitude oscillatory shear (LAOS), *Carbohydr. Polym.* 153 (2016) 312–319. doi:10.1016/j.carbpol.2016.07.095.
- [105] K. Hyun, M. Wilhelm, C.O. Klein, K.S. Cho, J.G. Nam, K.H. Ahn, et al., A review of nonlinear oscillatory shear tests: Analysis and application of large amplitude oscillatory shear (LAOS), *Prog. Polym. Sci.* 36 (2011) 1697–1753. doi:10.1016/j.progpolymsci.2011.02.002.
- [106] R.H. Ewoldt, C. Clasen, A.E. Hosoi, G.H. McKinley, Rheological fingerprinting of



- gastropod pedal mucus and synthetic complex fluids for biomimicking adhesive locomotion, *Soft Matter*. 3 (2007) 634. doi:10.1039/b615546d.
- [107] P. Ptaszek, A geometrical interpretation of large amplitude oscillatory shear (LAOS) in application to fresh food foams, *J. Food Eng.* 146 (2015) 53–61. doi:10.1016/j.jfoodeng.2014.08.022.
- [108] S. Ozkan, T.W. Gillece, L. Senak, D.J. Moore, Characterization of yield stress and slip behaviour of skin/hair care gels using steady flow and LAOS measurements and their correlation with sensorial attributes, *Int. J. Cosmet. Sci.* 34 (2012) 193–201. doi:10.1111/j.1468-2494.2012.00702.x.
- [109] C.J. Dimitriou, R.H. Ewoldt, G.H. McKinley, Describing and prescribing the constitutive response of yield stress fluids using large amplitude oscillatory shear stress (LAOStress), *J. Rheol. (N. Y. N. Y.)*. 57 (2013) 27–70. doi:10.1122/1.4754023.
- [110] R.H. Ewoldt, Defining nonlinear rheological material functions for oscillatory shear, *J. Rheol. (N. Y. N. Y.)*. 57 (2013) 177–195. doi:10.1122/1.4764498.
- [111] B.C. Blackwell, R.H. Ewoldt, A simple thixotropic-viscoelastic constitutive model produces unique signatures in large-amplitude oscillatory shear (LAOS), *J. Nonnewton. Fluid Mech.* 208–209 (2014) 27–41. doi:10.1016/j.jnnfm.2014.03.006.
- [112] T. Conte, M. Chaouche, Rheological behavior of cement pastes under Large Amplitude Oscillatory Shear, *Cem. Concr. Res.* 89 (2016) 332–344. doi:10.1016/j.cemconres.2016.07.014.
- [113] M.A. Schultz, L.J. Struble, Use of oscillatory shear to study flow behavior of fresh cement paste, *Cem. Concr. Res.* 23 (1993) 273–282. doi:10.1016/0008-8846(93)90092-N.
- [114] L.J. Struble, W.G. Lei, Rheological changes associated with setting of cement paste, *Adv. Cem. Based Mater.* 2 (1995) 224–230. doi:10.1016/1065-7355(95)90041-1.
- [115] L. Holzer, F. Winnefeld, B. Lothenbach, D. Zampini, The early cement hydration: a multi-method approach, *Int. Congr. Chem. Cem. 11th, Durban, South Africa, May 11-16, 2003.* (2003) 236–248.
- [116] L. Nachbaur, J.C. Mutin, A. Nonat, L. Choplin, Dynamic mode rheology of cement and tricalcium silicate pastes from mixing to setting, *Cem. Concr. Res.* 31 (2001) 183–192. doi:10.1016/S0008-8846(00)00464-6.
- [117] M. -C. Yang, L.E. Scriven, C.W. Macosko, Some Rheological Measurements on Magnetic Iron Oxide Suspensions in Silicone Oil, *J. Rheol. (N. Y. N. Y.)*. 30 (1986)



- 1015–1029. doi:10.1122/1.549892.
- [118] H.J. Walls, S.B. Caines, A.M. Sanchez, S.A. Khan, Yield stress and wall slip phenomena in colloidal silica gels, *J. Rheol.* (N. Y. N. Y). 47 (2003) 847–868. doi:10.1122/1.1574023.
- [119] Z. Sun, T. Voigt, S.P. Shah, Rheometric and ultrasonic investigations of viscoelastic properties of fresh Portland cement pastes, *Cem. Concr. Res.* 36 (2006) 278–287. doi:10.1016/j.cemconres.2005.08.007.
- [120] A. Saasen, C. Marken, N. Blomberg, J. Dawson, M. Rogers, Viscoelastic properties of oilfield cement slurries, in: P.F.G. Banfill (Ed.), *Rheol. Fresh Cem. Concr.*, CRC Press, London, 1991: pp. 170–178. doi:doi.org/10.4324/9780203473290.
- [121] Y. Qian, S. Kawashima, Use of creep recovery protocol to measure static yield stress and structural rebuilding of fresh cement pastes, *Cem. Concr. Res.* 90 (2016) 73–79. doi:10.1016/j.cemconres.2016.09.005.
- [122] L.J. Struble, M.A. Schultz, Using creep and recovery to study flow behavior of fresh cement paste, *Cem. Concr. Res.* 23 (1993) 1369–1379. doi:10.1016/0008-8846(93)90074-J.
- [123] H.A. Barnes, Q.D. Nguyen, Rotating vane rheometry — a review, *J. Nonnewton. Fluid Mech.* 98 (2001) 1–14. doi:10.1016/S0377-0257(01)00095-7.
- [124] M. Couette, On a new apparatus for the study of friction of fluids, *Compt. Rend.* 107 (1888) 388–390.
- [125] R. Chaney, G. Richardson, Measurement of Residual/Remolded Vane Shear Strength of Marine Sediments, in: *Vane Shear Strength Test. Soils F. Lab. Stud.*, ASTM International, 100 Barr Harbor Drive, PO Box C700, West Conshohocken, PA 19428-2959, 1988: pp. 166-166–16. doi:10.1520/STP10328S.
- [126] C.F. Ferraris, Measurement of the rheological properties of cement paste: a new approach, in: J.G. Cabrera, R. Rivera-Villarreal (Eds.), *Role Admixtures High Perform. Concr.*, RILEM Publications, Monterrey, 1999: pp. 333–342.
- [127] A. Kaci, R. Bouras, V.T. Phan, P.A. Andréani, M. Chaouche, H. Brossas, Adhesive and rheological properties of fresh fibre-reinforced mortars, *Cem. Concr. Compos.* 33 (2011) 218–224. doi:10.1016/j.cemconcomp.2010.10.009.
- [128] J. Engmann, C. Servais, A.S. Burbidge, Squeeze flow theory and applications to rheometry: A review, *J. Nonnewton. Fluid Mech.* 132 (2005) 1–27. doi:10.1016/j.jnnfm.2005.08.007.



- [129] N. Özkan, C. Oysu, B.J. Briscoe, I. Aydin, Rheological analysis of ceramic pastes, *J. Eur. Ceram. Soc.* 19 (1999) 2883–2891. doi:10.1016/S0955-2219(99)00054-0.
- [130] N. Delhaye, A. Poitou, M. Chaouche, Squeeze flow of highly concentrated suspensions of spheres, *J. Nonnewton. Fluid Mech.* 94 (2000) 67–74. doi:10.1016/S0377-0257(00)00130-0.
- [131] J. Collomb, F. Chaari, M. Chaouche, Squeeze flow of concentrated suspensions of spheres in Newtonian and shear-thinning fluids, *J. Rheol. (N. Y. N. Y.)*. 48 (2004) 405–416. doi:10.1122/1.1645514.
- [132] N. Roussel, C. Lanos, Particle fluid separation in shear flow of dense suspensions: Experimental measurements on squeezed clay pastes, *Appl. Rheol.* 14 (2004) 256–265. doi:10.3933/ApplRheol-14-256.
- [133] F. Cardoso, Método de formulação de argamassas de revestimento baseado em distribuição granulométrica e comportamento reológico, Universidade de São Paulo, 2009.
- [134] R.G. Pileggi, A.M. Betioli, F.A. Cardoso, V.M. John, Extended Rheological Characterization of Cement Pastes: Squeeze Flow Plus Rotational Rheometry, in: 12th Int. Congr. Chem. Cem., Montreal, Canada, 2007.
- [135] B.H. Min, L. Erwin, H.M. Jennings, Rheological behaviour of fresh cement paste as measured by squeeze flow, *J. Mater. Sci.* 29 (1994) 1374–1381. doi:10.1007/BF00975091.
- [136] T.H. Phan, M. Chaouche, Rheology and stability of self-compacting concrete cement pastes, 15 (2005).
- [137] Z. Toutou, N. Roussel, C. Lanos, The squeezing test: A tool to identify firm cement-based material's rheological behaviour and evaluate their extrusion ability, *Cem. Concr. Res.* 35 (2005) 1891–1899. doi:10.1016/j.cemconres.2004.09.007.
- [138] F.A. Cardoso, V.M. John, R.G. Pileggi, Rheological behavior of mortars under different squeezing rates, *Cem. Concr. Res.* 39 (2009) 748–753. doi:10.1016/j.cemconres.2009.05.014.
- [139] F.A. Cardoso, V.M. John, R.G. Pileggi, P.F.G. Banfill, Characterisation of rendering mortars by squeeze-flow and rotational rheometry, *Cem. Concr. Res.* 57 (2014) 79–87. doi:10.1016/j.cemconres.2013.12.009.
- [140] F.A. Cardoso, F.C. Lofrano, V.M. John, R.G. Pileggi, Influence of Experimental Parameters of the Squeeze-flow Test on the Rheological Behaviour and Phase



- Segregation of Cement Mortars, 22 (2014) 79–85.
- [141] R. Hendrickx, The adequate measurement of the workability of masonry mortar, Katholieke Universiteit Leuven, 2009. doi:ISBN: 978 94 6018 136 8.
- [142] F.A.F.A. Cardoso, A.L.A.L. Fujii, R.G.R.G. Pileggi, M. Chaouche, Parallel-plate rotational rheometry of cement paste: Influence of the squeeze velocity during gap positioning, *Cem. Concr. Res.* 75 (2015) 66–74. doi:10.1016/j.cemconres.2015.04.010.
- [143] M.R.M.M. Costa, E. Pereira, R.G. Pileggi, M.A. Cincotto, Study of the influential factors on the rheological behavior of adhesive mortar available in the market, *Ibracon Struct. Mater. J.* 6 (2013) 399–405.
- [144] J.F. Steffe, *Rheological methods in food process engineering*, Second Edi, Freeman Press, East Lansing, USA, 1996.
- [145] G. Winther, K. Almdal, O. Kramer, Determination of polymer melt viscosity by squeezing flow with constant plate velocity, *J. Nonnewton. Fluid Mech.* 39 (1991) 119–136. doi:10.1016/0377-0257(91)80009-9.
- [146] Y.O. Mohamed Abdelhaye, M. Chaouche, H. Van Damme, The tackiness of smectite muds. 1. The dilute regime, *Appl. Clay Sci.* 42 (2008) 163–167. doi:10.1016/j.clay.2008.01.018.
- [147] Y.O. Mohamed Abdelhaye, M. Chaouche, J. Chapuis, E. Charlaix, J. Hinch, S. Roux, et al., Tackiness and cohesive failure of granular pastes: Mechanistic aspects, *Eur. Phys. J. E.* 35 (2012). doi:10.1140/epje/i2012-12045-6.
- [148] R.G. KUDO, E. K; CARDOSO, F. A; PILEGGI, Squeeze Flow aplicado a argamassas colantes: influência de parâmetros experimentais de configuração e taxa de deslocamento., in: *An. Do IV SBTA*, Belo Horizonte, 2011.
- [149] J. Pourchez, P. Grosseau, R. Guyonnet, B. Ruot, HEC influence on cement hydration measured by conductometry, *Cem. Concr. Res.* 36 (2006) 1777–1780. doi:10.1016/j.cemconres.2006.06.002.
- [150] J. Pourchez, P. Grosseau, B. Ruot, Current understanding of cellulose ethers impact on the hydration of C3A and C3A-sulphate systems, *Cem. Concr. Res.* 39 (2009) 664–669. doi:10.1016/j.cemconres.2009.05.009.
- [151] K.H. Khayat, M. Saric-Coric, F. Liotta, Influence of thixotropy on stability characteristics of cement grout and concrete, *ACI Mater. J.* 99 (2002) 234–241. doi:10.14359/11968.





- [152] C. Brumaud, R. Baumann, M. Schmitz, M. Radler, N. Roussel, Cellulose ethers and yield stress of cement pastes, *Cem. Concr. Res.* 55 (2014) 14–21. doi:10.1016/j.cemconres.2013.06.013.
- [153] C. Maltesh, P. Somasundaran, *Polymers as rheology modifiers*, 1992. doi:10.1016/0166-6622(92)80186-6.
- [154] J. Israelachvili, *Intermolecular and Surface Forces*, Third edit, 2011. doi:10.1016/B978-0-12-375182-9.10025-9.
- [155] G.G. Fuller, Rheology of Mobile Interfaces, *Rheol. Rev.* 2003 (2003) 77–123.
- [156] Y. Fan, S. Simon, J. Sjöblom, Interfacial shear rheology of asphaltenes at oil-water interface and its relation to emulsion stability: Influence of concentration, solvent aromaticity and nonionic surfactant, *Colloids Surfaces A Physicochem. Eng. Asp.* 366 (2010) 120–128. doi:10.1016/j.colsurfa.2010.05.034.
- [157] S. Reynaert, C.F. Brooks, P. Moldenaers, J. Vermant, G.G. Fuller, Analysis of the magnetic rod interfacial stress rheometer, *J. Rheol.* (N. Y. N. Y). 52 (2008) 261. doi:10.1122/1.2798238.
- [158] D. Langevin, Surface shear rheology of monolayers at the surface of water, *Adv. Colloid Interface Sci.* 207 (2014) 121–130. doi:10.1016/j.cis.2013.10.030.
- [159] Y.Y. Zuo, R.A.W. Veldhuizen, A.W. Neumann, N.O. Petersen, F. Possmayer, Current perspectives in pulmonary surfactant - Inhibition, enhancement and evaluation, *Biochim. Biophys. Acta - Biomembr.* 1778 (2008) 1947–1977. doi:10.1016/j.bbamem.2008.03.021.
- [160] TA Instruments, AR-G2 AR2000ex AR1500ex Rheometers Operator's Manual, 2010.
- [161] B.M. Dale, M.A. Brown, R.C. Semelka, *MRI Basic Principles and Applications*, John Wiley & Sons, Ltd, Chichester, UK, 2015. doi:10.1002/9781119013068.
- [162] B. Mackiewicz, *Intracranial Boundary Detection and Radio Frequency Correction in Magnetic Resonance Images*, University of British Columbia, 1990.
- [163] M. Fourmentin, P. Faure, S. Rodts, U. Peter, D. Lesueur, D. Daviller, et al., NMR observation of water transfer between a cement paste and a porous medium, *Cem. Concr. Res.* 95 (2017) 56–64. doi:10.1016/j.cemconres.2017.02.027.
- [164] S. Jarny, N. Roussel, S. Rodts, F. Bertrand, R. Le Roy, P. Coussot, Rheological behavior of cement pastes from MRI velocimetry, *Cem. Concr. Res.* 35 (2005) 1873–1881. doi:10.1016/j.cemconres.2005.03.009.



- [165] A.P.A. Faiyas, S.J.F. Erich, H.P. Huinink, O.C.G. Adan, T.G. Nijland, Effect of MHEC on evaporation and hydration characteristics of glue mortar, *Cem. Concr. Res.* 83 (2016) 97–103. doi:10.1016/j.cemconres.2016.01.010.
- [166] L. Patural, A. Govin, P. Grosseau, B. Ruot, O. Devès, The effect of cellulose ethers on water retention in freshly-mixed mortars, in: *11th Int. Conf. Exhib. Eur. Ceram. Soc.* 2009, 2009: pp. 85–87.
- [167] T. Bühler, U. Pielas, A. Wetzel, M. Herwegh, W. Schlachter, L. Huwiler, et al., Dynamics of Skin Formation and Mechanisms of Open Time Performance of Tile Adhesive Mortars, *Fourth Int. Drymix Mortar Conf. Idmmc Four.* (2013).
- [168] M.L. Bouxsein, S.K. Boyd, B.A. Christiansen, R.E. Guldberg, K.J. Jepsen, R. Müller, Guidelines for assessment of bone microstructure in rodents using micro-computed tomography, *J. Bone Miner. Res.* 25 (2010) 1468–1486. doi:10.1002/jbmr.141.
- [169] H. eun Bhang, N. Tsuchiya, P. Sysa-Shah, C.T. Winkelmann, K. Gabrielson, *In Vivo Small Animal Imaging: A Comparison with Gross and Histopathologic Observations in Animal Models*, Third Edit, Elsevier, 2013. doi:10.1016/B978-0-12-415759-0.00009-1.
- [170] M.J. Paulus, S.S. Gleason, S.J. Kennel, P.R. Hunsicker, D.K. Johnson, High Resolution X-ray Computed Tomography: An Emerging Tool for Small Animal Cancer Research, *Neoplasia.* 2 (2000) 62–70. doi:10.1038/sj.neo.7900069.
- [171] D.P. Bentz, C.J. Haecker, M.A. Peltz, K.A. Snyder, X-ray absorption studies of drying of cementitious tile adhesive mortars, *Cem. Concr. Compos.* 30 (2008) 361–373. doi:10.1016/j.cemconcomp.2007.10.007.
- [172] D. Bentz, C. Haecker, X-ray microtomography studies of air-void instability and growth during drying of tile adhesive mortars, U.S. Department of Commerce, 2008.
- [173] W.A. Kalender, X-ray computed tomography, *Phys. Med. Biol.* 51 (2006). doi:10.1088/0031-9155/51/13/R03.
- [174] A. Cantatore, P. Muller, *Introduction to Computed Tomography Technology*, (2011) 1–65.
- [175] J.H. Lambert, E. Anding, *Photometrie: Photometria, sive De mensura et gradibus luminis, colorum et umbrae* (1760), W. Engelmann, 1892. <https://books.google.com/books?id=zmpJAAAAYAAJ>.
- [176] L. Valdés Tamayo, *Comportement mécanique des mortiers et systèmes d'isolation*



thermique par l'extérieur : Apport de la microtomographie aux R.X, École Normale Supérieure de Cachan, 2015.

- [177] E. Neuser, A. Suppes, Visualizing internal 3D structures with submicrometer resolution, in: Int. Symp. Digit. Ind. Radiol. Comput. Tomogr., Lyon, France, 2007: p. 18.
- [178] E.N. Landis, D.T. Keane, X-ray microtomography, Mater. Charact. 61 (2010) 1305–1316. doi:10.1016/j.matchar.2010.09.012.
- [179] CEN, EN 1346: Adhesives for tiles — determination of open time, Eur. Stand. (2007).
- [180] CEN, EN 12004-2: Adhesives for ceramic tiles — Part 2: Test methods, Eur. Stand. (2017) 44.
- [181] R. Zurbriggen, M. Herwegh, U. Pieleles, T. Bühler, L. Huwiler, A new laboratory method to investigate skin formation and Open Time performance, in: Third Int. Drymix Mortar Conf. Idmmc Three, Nürnberg, Germany, 2011: pp. 1–8.
- [182] H. Mavridis, G.D. Bruce, G.J. Vancso, W.G. C, J. Vlachopoulos, Deformation patterns in the compression of polypropylene disks: Experiments and simulation, J. Rheol. (N. Y. N. Y). 36 (1992) 27. doi:10.1122/1.550340.



**Titre :** Les propriétés adhésives et rhéologie interfaciale de mortiers colles

**Mots clés :** mortier colle, rhéologie interfaciale, polymère, adhésion, IRM, microscopie optique

**Résumé :** Les mortiers colles se composent essentiellement de ciment, de sable, de charges minérales et d'une variété d'additifs (éthers de cellulose, entraînant d'air, latex) et sont utilisés pour coller des carreaux céramique (et d'autres pièces comme la pierre, le verre, etc.) aux substrats. Ils sont généralement appliqués dans une grande surface sur le substrat sous la forme de nervures sur lesquelles les carreaux sont mis. Afin d'obtenir une bonne performance, il est important que les propriétés rhéologiques du mortier permettent un bon contact entre les carrelages, même après plusieurs minutes (temps ouvert) d'exposition aux conditions ambiantes, soit à l'intérieur soit à l'extérieur des bâtiments. A cet effet, il est nécessaire d'éviter la formation d'une couche rigide et/ou sèche à l'interface mortier-air, qui peut être difficile à déformer ou à humidifier correctement la surface de la dalle. Comme le contact initial entre le mortier et le carrelage est la première étape pour le développement des propriétés

adhésives développement des propriétés adhésives entre les matériaux, une bonne compréhension de l'évolution des propriétés rhéologiques à l'interface air-mortier est d'une grande importance pour les producteurs de mortier et les utilisateurs. Dans ce contexte, cette thèse a d'abord développé des méthodes d'évaluation des propriétés interfaciales et une technique microscopique pour visualiser le contact. Ensuite, ces techniques combinées à des essais de tack test/ squeeze et à des procédés rhéologiques déjà existants peuvent être utilisé pour évaluer comment des additifs polymères tels que l'éther de cellulose influent sur les propriétés rhéologiques du mortier adhésif dans le volume et à l'interface pour mieux comprendre les propriétés adhésives. Et enfin, avec l'utilisation de la RMN, ces propriétés pourraient être corrélées avec l'évolution de la distribution de l'eau.

**Title :** Adhesive properties and interfacial rheology of adhesive mortars

**Keywords :** adhesive mortar, interfacial rheology, polymer, adhesion, MRI, optical microscopy

**Abstract :** Adhesive mortars consist basically of cement, sand, mineral fillers and a variety of additives (cellulose ethers, air-entraining, latex) and are used to glue ceramic tiles (and other pieces like stone, glass etc) to substrates. They are usually applied in a large surface on the substrate in the form of ribs on which tiles are put. In order to obtain a good performance, it is important that when the tile is installed, the mortar rheological properties allow for good contact between them, even after several minutes (open time) of exposure to ambient conditions either at internal or external building areas. For this purpose, it is necessary to avoid the formation of a rigid and/or dry layer at the mortar-air interface, which may be difficult to be deformed or wet the tile surface properly. As the initial contact between mortar and tile is the first step for the development of adhesive

properties between the materials, a good comprehension of the rheological properties evolution at the air-mortar interface is of great importance for mortar producers and users. In this context, this thesis firstly developed methods to evaluate interfacial properties and a microscopical technique to visualize the contact. Then, those techniques combined with already existent squeeze flow/tack test and rheological methods can be used to evaluate how polymer additives such as cellulose ether influence the adhesive mortar rheological properties in the volume and at interface to further understand the adhesive properties. And finally, with the use of NMR, those properties could be correlated with water distribution evolution.

